Time-dependent topology of electron density in molecules : A theoretical perspective

Gabriel Breuil

THÈSE POUR OBTENIR LE GRADE DE DOCTEUR DE L'UNIVERSITÉ DE MONTPELLIER

En Chimie et Physico-Chimie des Matériaux

École doctorale Sciences Chimiques Balard

Unité de recherche Institut Charles Gerhardt Montpellier

Topologie dépendante du temps de la densité électronique moléculaire : une approche théorique

Présentée par Gabriel BREUIL
Le 21 octobre 2021

Sous la direction de Benjamin LASORNE et Thibaud ETIENNE

Devant le jury composé de

Isabelle DIXON, Chargée de Recherche, Université de Toulouse, LCPQ	Rapporteure
Valérie BRENNER, Directrice de Recherche, CEA Saclay, IRAMIS	Rapporteure
Morgane VACHER, Chargée de Recherche, Université de Nantes, CEISAM	Examinatrice
Roberto MARQUARDT, Professeur, Université de Strasbourg, LCQ	Examinateur
Christophe IUNG, Professeur, Université de Montpellier, ICGM	Examinateur
Benjamin LASORNE, Chargé de Recherche, Université de Montpellier, ICGM	Directeur de Thèse
Thibaud ETIENNE, Maître de Conférence, Université de Montpellier, ICGM	Co-encadrant de Thèse

UNIVERSITÉ DE MONTPELLIER

This thesis is dedicated to my beloved mother

Acknowledgements

Je tiens tout d'abord à remercier les Dr. Isabelle Dixon, Dr. Valérie Brenner, Dr. Morgane Vacher, Pr. Roberto Marquardt et Pr. Christophe Iung qui ont accepté de juger ces travaux de thèse et d'être présent pour ma soutenance.

Je voudrais remercier l'Université de Montpellier et l'école doctoral des sciences chimiques Balard (EDSCB) et le Ministère de l'Enseignement Supérieur et de la Recherche pour avoir financé ces travaux de thèse sous la forme d'un contrat doctoral.

Benjamin Lasorne, je voudrais te remercier grandement pour la confiance que tu m'as accordé pour porter à bien ces travaux de thèse. Je te remercie pour ta patience mais aussi pour l'autonomie et la liberté dont j'ai pu bénéficier. Merci également pour les discussions personnelles que l'on a pu avoir sur la vie, la famille et la musique.

Thibaud Etienne, je voudrais également te remercier pour la confiance et la patience que tu m'as accordé. C'est avec un grand plaisir que j'ai pu échanger avec toi professionnellement et personnellement durant ces années de thèse. Je souhaite que ta nouvelle aventure à Nancy se passe bien.

Roberto, je tiens à te remercier une seconde fois. Non pour le fait d'avoir accepté de faire parti de mon jury mais pour m'avoir initié à l'univers de la chimie quantique, de la dynamique et de la spectroscopie. Je suis très heureux d'avoir eu l'opportunité de faire six mois de stages il y a quelques années car c'est à la suite de ce stage que j'ai décidé de faire une thèse en chimie quantique.

Emmanuel Fromager, je souhaite également à te remercier. En effet, c'est à la suite de ces quelques heures de mécanique quantiques à l'ECPM que j'ai décidé de te contacter afin de pouvoir faire un stage au laboratoire de chimie quantique de Strasbourg. C'est la qualité de ton enseignement mais également ta pédagogie qui ont, sans aucun doute, éveillé ma curiosité dans ce domaine. Je tiens également à te remercier d'un point de vue personnel, pour les discussions que nous avons pu avoir mais également pour les conseils que tu as pu me donner.

Aurélie, Arthur, Alexandre et Béata, je ne vous remercierai jamais assez pour la bonne ambiance, les conseils et les longues discussions sur nos vies respectives que nous avons pu partager ensemble.

Un grand merci à toute l'équipe CPTM, Marie, Jean-Seb, Christophe, Bruno, Joachim, Clara, Fabrice, Frédéric, Maxime, Mouna et Matthieu pour votre soutien et les discussions scientifiques que nous avons pu avoir durant ces trois années.

Je tiens à remercier du fond du coeur tout mes amis. Allant de Strasbourg à Paris, passant par Bordeaux, Lyon, Oslo, Bruxelles, Edimbourg Saint-Brieuc, Barcelone, Roscoff et Aveiro. Merci à Paul, Cécile, Marion, Charlotte, Quentin, Augustin, Clara, Joris, Karo, Laurène, Martin, Thiebault, Louis-Guilhem, Romane, Simon, Nina et Fuad d'avoir été là dans des moment de joies et de peines et de m'avoir fait rigoler à en pleurer. Merci à toi Clément, c'est avec toi que j'ai fait mon premier stage en quantique, on ne s'est jamais perdu de vue jusqu'à notre thèse. Merci pour discussions scientifiques extrêmement enrichissantes, pour les discussions personnelles mais également pour tout les plans sur la comète que nous faisons ensemble d'un point de vue scientifique que personnel. Merci à mes amis de Montpellier, Léa, Manon, Gary et Perle pour tout ces verres bu ensemble, discussions et rigolades que nous avons pu partager. Théo, Maël, Daniel et Julia, merci à vous d'avoir été mes colocs durant ces trois années, merci d'avoir été tout simplement là avec moi pour partager des moments inoubliables. Encore une fois, merci à vous tous car sans vous ces trois ans n'auraient jamais été si importants pour moi.

Clotilde et Apolline, je vous dis un immense merci pour votre présence, soutien, écoute et aide durant les moments plaisants et difficiles que j'ai vécu durant ces années.

Et enfin je tiens à remercier sincèrement mon père et Florence pour leurs conseils et leur accueil chaleureux à Nîmes.

A vous tous que je viens de remercier, tout simplement, restez comme vous êtes, c'est pour ça que je vous aime.

Abstract

0.1 Abstract in English

Phenylene-ethynylene dendrimers show astonishing properties and are systems to be likely used in opto-electronic devices such as light emitting diodes and conductive molecular wires. They are in the spotlight because they show excellent photostability and high excitation energy transfer efficiency. The excitation energy transfer in phenylene-ethynylene dendrimers is ultrafast and unidirectional. It occurs from the periphery of the molecular system to the core thanks to an excitation energy gradient that extends along the system.

During this PhD, phenylene-ethynylene dendrimers have been studied through a pseudo-fragmentation scheme in which the phenylene-ethynylene dendrimers is decomposed in various subsystems (pseudofragments). The phenylene-ethynylene dendrimers behaves as if the pseudo-fragments (*oligo*phenylene-ethynylene) were weakly interacting together.

Two isomers (the single-trans isomer and the cumulenic isomer) of *oligo*phenylene-ethynylene co-exist in their first adiabatic electronic excited states.

Two diabatic excited states are then considered for each *oligo*phenylene-ethynylene, the ones which are associated to the Lewis structures of the isomers. The potential energy surfaces of phenylene-ethynylene dendrimers and their conical intersections have been rationalised in terms of diabatic states localised on the pseudoframgments.

I have used density-based descriptors that are built from the attachment and detachment densities involved in the electronic transitions. Such descriptors are used to characterise the electronic excited states that are involved in the pseudofragmentation scheme of phenylene-ethynylene dendrimers .

This global strategy allowed us to suggest an alternative excitation energy transfer mechanism that involves both trans-bending and cumulenic-streching deformations on each of the pseudofragments of a phenylene-ethynylene dendrimers .

0.2 Abstract in French

Les dendrimères de phénylène-ethynylène possèdent des propriétés photo-induites remarquables et ils peuvent être utilisés en tant que composants opto-électroniques tels que les diodes électro-luminescentes et les fils conducteurs moléculaires. Les dendrimères de phénylène-ethynylène présentent une photo-stabilité importante et un transfert d'énergie d'excitation ultra-rapide et unidirectionnel. Il va de la périphérie du système moléculaire vers son centre grâce à un gradient d'énergie d'excitation qui s'étend le long du système.

Durant cette thèse, les dendrimères de phénylène-ethynylène ont été étudiés à l'aide d'un schéma de pseudo-fragmentation dans lequel les dendrimères de phénylène-ethynylène sont décomposés en différents sous-systèmes (pseudofragments). Les dendrimères de phénylène-ethynylène se comportent comme si les pseudofragments (*oligo*phénylène-éthynylènes) étaient en faible interaction.

Deux isomères (le simple-trans et le cumulénique) des *oligo*phénylène-éthynylènes co-existent dans leur premier état adiabatique électronique excité.

Deux états diabatiques excités sont alors considérés pour chaque *oligo*phénylène-éthynylènes, ceux qui sont associés à la structure de Lewis des isomères. Les surfaces d'énergie potentielle des dendrimères de phénylène-ethynylène et leur intersections coniques ont été rationalisées à l'aide des états diabatiques localisés sur les pseudofragments.

J'ai utilisé des descripteurs basés sur la densité électronique qui sont construits depuis la densité d'attachement et de détachment impliqués dans les transitions électroniques. Ces descripteurs sont utilisés pour caractériser les états électroniques excités qui sont impliqués dans le schéma de pseudofragmentation des dendrimères de phénylène-ethynylène .

Cette stratégie globale nous a permis de suggérer un mécanisme alternatif du transfert d'énergie d'excitation qui implique à la fois une déformation par un pliage trans et par un étirement cumulénique sur chacun des pseudofragments d'un dendrimères de phénylène-ethynylène .

Table of Contents

List of Figures

List of Tables

Introduction

0.3 Introduction in English

Photoinduced processes in molecules play a crucial role in the case of biological and chemical reactivity, and properties concerning either natural and synthetic systems. One can easily name the natural photosynthesis that concerns living species (chlorophyll-bearing plants), chemical reactions that are induced from a photoexcitation, and the use of artificial photosynthesis in devices such that dye sensitized solar cells and organic light-emitting diodes [3–6].

Amongst various photoinduced processes, the light-harvesting (LH) properties of macro- or supramolecular systems hold our attention in this work. Natural and synthetic systems may show LH properties [7–22]. Studies have been made on the link between the structure of the systems and the excitation energy transfer (EET) process [23–29]. Concerning natural systems, one can name the case of LH properties that arises from photosynthetic abilities of pigment-protein complexes [7–11].

The systems mentioned in the previous refs [7–11] are pigment-protein complexes of the purple bacteria. It is one of the first studied systems that show LH properties but it is not the only one. The complexes have a crystal structure which are an assembly of proteins that surround pigment molecules. The light energy is absorbed by protein-pigment pairs and the excitation energy is transferred to the chemical reaction center of the bacteria which is the junction center of the protein-pigment pairs. The global EET process that occurs through the entire system lasts about 100 ps with a quantum yield (ratio of emitted photons over absorbed photons) of 95% while the EET from a unique protein-pigment pair to the chemical reaction center occurs within the subpicosecond time range. [30, 31].

The term of "LH complexes" has been chosen, for the latter exemple, to characterise the complexes of purple bacteria as the excitation energy is captured on several specific locations on the system (the pigment-protein pairs) and is driven to a unique point of the species (the chemical reaction center).

Organic compounds that have such LH properties give rise to a significant set of applications

within biomedical uses for instance: photodynamical therapy [32,33] and within opto-electronic applications for organic photovoltaic technologies [22,34–36].

The highly efficient and ultrafast EET process is an incentive for designing artificial molecules that show similar LH properties.

Dendrimers are highly structured LH artificial systems, they are promising with respect to their efficient EET properties. [22,35–37] The word *dendrimer* refers to a tree-shaped-like molecular system. It is composed of a major branch that can be viewed as a trunk. At the edge of this trunk, branches (building blocks) are linked to a common node that allows to connect them together. At the edge of these first building blocks, others branches are again linked to each other and so on. Such building blocks can then be associated to the picture of the branches of a tree. The size of branches can be the same or different. There are two types of dendrimers: *compact* dendrimers and *extended* dendrimers. The two classes of dendrimers are depicted in fig. 1.

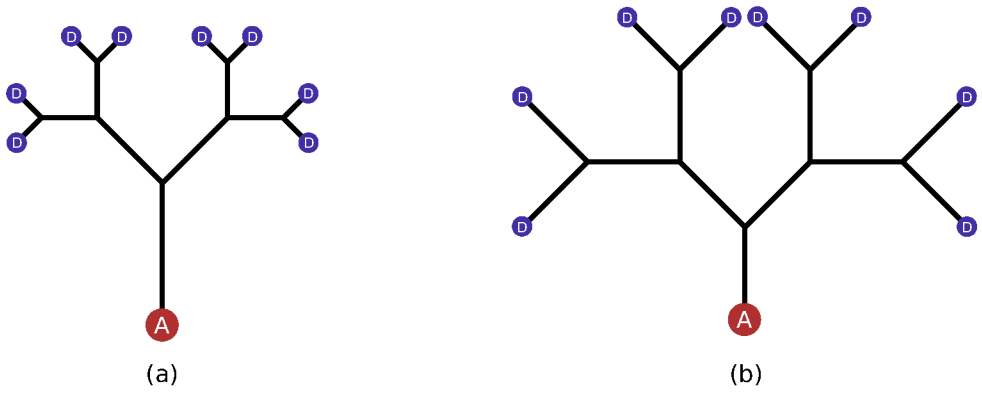

Figure 1: Schematic representation of an extended dendrimer (a) and of a compact dendrimer (b).

The schematic representation of an extended dendrimer is labelled (a) on the left of fig. 1. The length of branches increases from the periphery to the core of the dendrimer. The compact dendrimer is labelled (b) on the right on the same figure. The length of the branches is the same. Concerning the class of extended dendrimers, the EET goes from the periphery to the core of the dendrimer because of energy. It goes from the center toward the periphery in the compact dendrimer class because of entropy. Moreover a dendrimer can be functionalized with electron donor (D, blue disk in fig. 1) and acceptor (A, red disk in fig. 1) groups. The donor groups are fixed at the periphery of the system while the acceptor group is fixed to the trunk of the dendrimer to increase the amount of energy that is absorbed and transferred [34,38]. According

to fig. 1, the EET for the class of compact dendrimers now also goes from the periphery to the core of the system.

In this thesis we are focused on the study of extended phenylene-ethynylene dendrimers (*e*PE-D) that are highly π-conjugated systems. The building blocks are *oligo*(phenylene-ethynylene)s (*o*PE) of various sizes. One of the most famous *e*PE-D is the *nanostar* (see fig. 2).

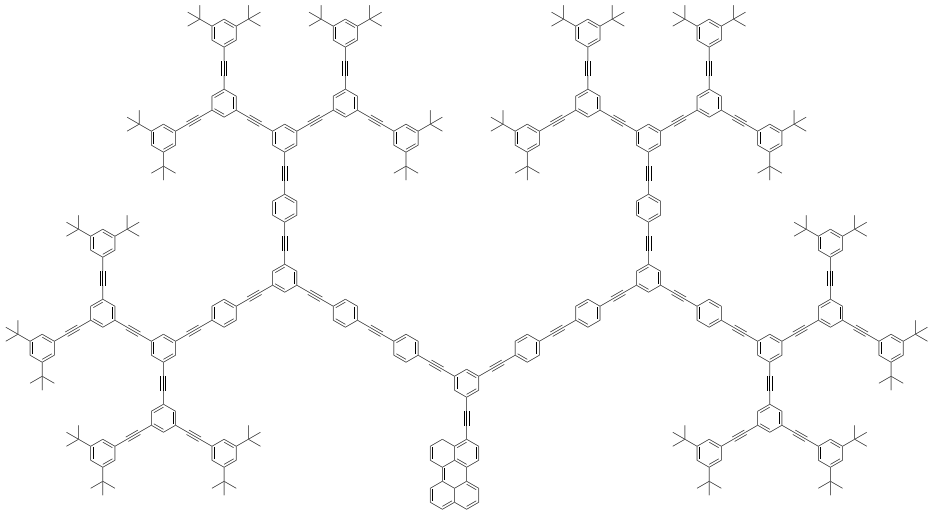

Figure 2: The nanostar.

The nanostar shows astonishing EET properties. Around 99% of the excitation energy is tranferred and the EET is unidirectional (from the peripherical branches to the perylene group) and almost ultrafast (270 ps along the system). [39–41] The consecutive building blocks of 2, 3 and 4 phenylene rings give the peculiar structure of the nanostar and are responsible of the presence of an energy gradient which allows the LH properties and the highly efficient intramolecular energy funneling mechanism. The perylene group can eventually emit. [42]

It has been shown in [40] that steady-state absorption and emission spectra of the nanostar are matching with the superposition of the steady-state spectra of the phenylene-ethynylene building blocks that are the branches of the system. An LH dendritic molecule is then viewed as an array of weakly coupled chromophores (in our case, phenylene-ethynylene building blocks of various sizes). The system absorbs light at wavelengths that depend on the structural properties of the branches. [42]

The *meta*-position of building blocks on common phenylene nodes breaks the π-conjugation from one *o*PE to another. The electronic properties of the nanostar, and more generally of extended dendrimers, is governed by the electronic properties of its building blocks. The EET ability

is defined by the properties of its chromophores.

Such a hierarchical description motivates us to apply a multiscale method that is based on a pseudofragmentation scheme [43]. In such a method, all the pseudofragments are the *o*PE branches of the PE dendrimers. The shared phenylene group between two *o*PE branches is then taken into account twice and so it is not possible to consider the *o*PE branches as real fragments.

The *e*PE-D behave almost as if their pseudofragments were weakly interacting together. Since an *e*PE-D has similar electronic properties as its pseudofragments, the potential energy surfaces of *e*PE-D are studied in this thesis within the pseudofragmentation scheme, in which the potential energy surfaces are rationalised with respect to the ones of the *o*PE branches. This pseudofragmentation scheme, summarised below (fig. 4), has been explicitly explained for 1,3-*bis*(phenylethynyl)benzene (*m*-BPEB, see fig. 3) in ref. [43]

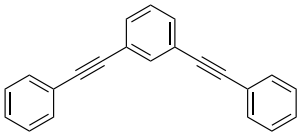

Figure 3: 1,3-*bis*(phenylethynyl)benzene (*m*-BPEB).

The energy minimum in the ground state of *m*-BPEB belongs to the $\mathcal{C}_{2v}$ point group. The Franck-Condon (FC) point (the first optically active state at the ground state equilibrium geometry) lies around $4-5$ eV. The four frontier orbitals of *m*-BPEB at the FC point are gathered in the middle of fig. 4.

The four frontier orbitals are delocalised over all the molecular system. The π orbitals that lie on the two ethynylene groups and on the two peripherical phenylene groups are similar up to a phase considering the HOMO-1/HOMO and LUMO/LUMO+1 pairs while the central phenylene group of each four frontier orbital differs. The pairs of delocalised HOMO-1/HOMO and LUMO/LUMO+1 are quasi degenerate. The "sum" combination of the two non-degenerate HOMO-1/HOMO gives a localised HOMO orbital on the left branch of *m*-BPEB and the "sum" combination of the two LUMO/LUMO+1 gives a localised LUMO orbital on the left branch of *m*-BPEB as well. In contrast, the "difference" combination of the delocalised orbitals gives localised orbitals on the right banch of *m*-BPEB. The localised HOMO orbitals are degenerate and so are the localised LUMO orbitals. The localised orbitals on the right and on the left branch of *m*-BPEB involve a different set of atoms (left and right part) and share a common set of atoms (the phenylene ring) and this is the actual reason why we called the branches of an *e*PE-D,

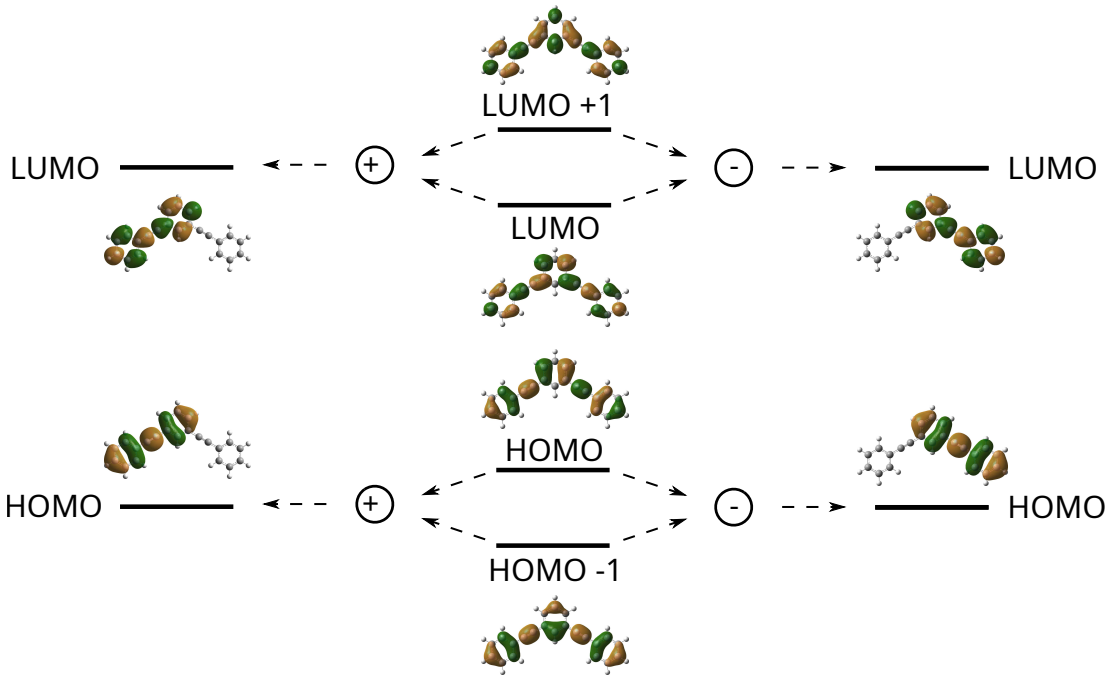

Figure 4: Localised molecular orbitals resulting of the sum and the difference of the frontier molecular orbitals *m*-BPEB.

pseudofragments. The four delocalised frontier orbitals of *m*-BPEB are then non-degenerate due to the weak interactions between the two pseudofragments that is related to the overlap between the two localised orbitals of the pseudofragment. In other words, the larger the overlap is, the stronger would be the interaction between the pseudofragments. *meta*-diphenylethynylphenylene behaves almost as two diphenylene-acetylene weakly interacting together.

Adiabatic and diabatic states are defined such that: the adiabatic electronic states are eigenvectors of the electronic Hamiltonian while the diabatic electronic states are not eigenvectors of the electronic Hamiltonian and there is no nuclear kinetic coupling between them. The diabatic states can be pictured as if they characterised some electronic properties of the system. More details are given on the interpretation of adiabatic and diabatic electronic states in chapters 1 and 2. We define then, in this context, diabatic states that are related to the localised frontier orbitals on the pseudofragments. The diabatic localised-on-the-pseudofragments states of an *e*PE-D match then with the adiabatic delocalised states of the isolated pseudofragment.

Within this thesis, 1,3-*bis*(phenylethynyl)-3-(1,4-bis(phenylethynyl)benzene)benzene *mb*-DPABPEB is studied and analysed within the framework of the pseudofragmentation scheme. Three pseudofragmentation schemes are considered. They are (see fig. 5):

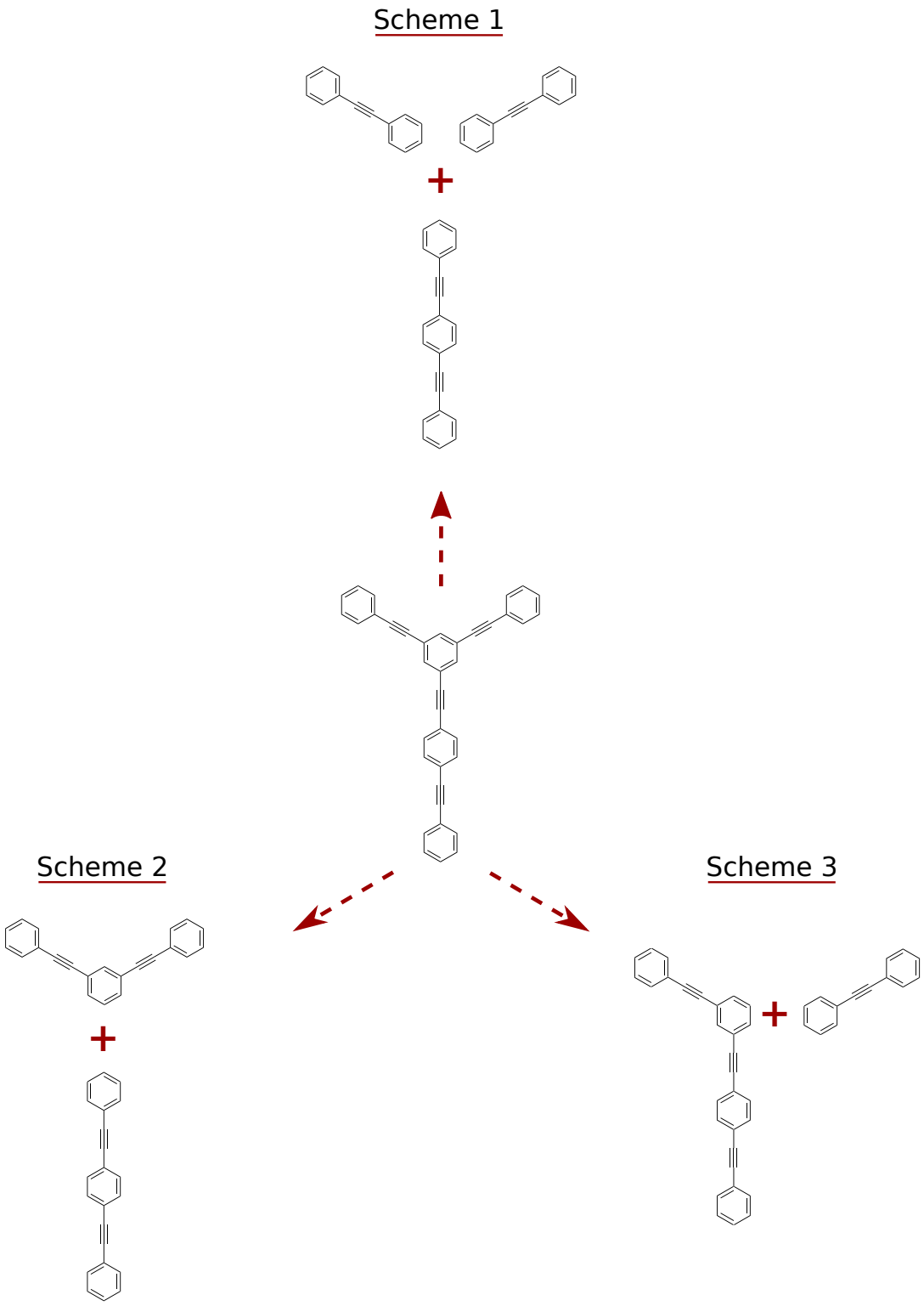

Figure 5: The pseudofragmentation scheme of *mb*-DPABPEB.

- Scheme 1: Two diphenylene-acetylenes (DPA) and one 1,4-bis(phenylethynyl)benzene (BPEB) weakly interacting together;
- Scheme 2: One *m*-BPEB and one BPEB weakly interacting together;
- Scheme 3: One 1-(phenylethynyl)-3-(1,4-bis(phenylethynyl)benzene)benzene (*m*-DPABPEB) and one DPA.

Refs. [39–47] suggest that the EET within an *e*PE-D involves only the first optically active electronic state (S_{act}) of each pseudofragment and streching modes that are localised on the ethynylene groups. In figure 6 is represented an *o*PE that can be pseudofragmented in three pseudofragments: DPA, BPEB and *m*-DPABPEB. The adiabatic potential energy of the *o*PE is schematically represented in plain line and the diabatic localised-on-the-pseudofragments states are represented in dashed colored lines (green: DPA, purple: BPEB, and yellow: *m*-DPABPEB). If the wavepacket is initially localised on the localised-on-DPA diabatic state, some EET will occur from the latter diabatic state toward the localised-on-BPEB diabatic state then to the localised-on-*m*-DPABPEB diabatic state via internal conversion (IC) through conical intersections between electronic states.

In this thesis, a second EET mechanism is suggested. We proposed that the transfer mechanism involve optically inactive states in addition to optically active states. Indeed, close in energy to the first optically active state there is an optically inactive state which involves a *trans*-stilbene-shape-like geometry for linear *o*PE on a unique ethynylene group. These two states for both systems have been accurately studied for DPA and BPEB. [48–53] The ground state (GS) of DPA and of BPEB belong to the $\mathcal{D}_{2h}$ point group (PG). The equilibrium geometries are planar and the phenyl groups are separated from each other by single-triple-single bonds (see fig. 5) in the GS. In the $\mathcal{D}_{2h}$ PG, the minimum in the first optically active state is characterised by a cumulenic structure for both systems: the phenyl groups are quinoidal and are separated from each other by three double bonds (see fig. 7).

The first optically active states for DPA and BPEB are of B_{1u} symmetry (using Mulliken's convention with z along the long axis). C. Robertson and G. A. Worth [51] have shown that, according to the level theory of the electronic structure calculations, S_{act} may not be the first electronic excited state but it is among the first three. The cumulenic minimum is associated to

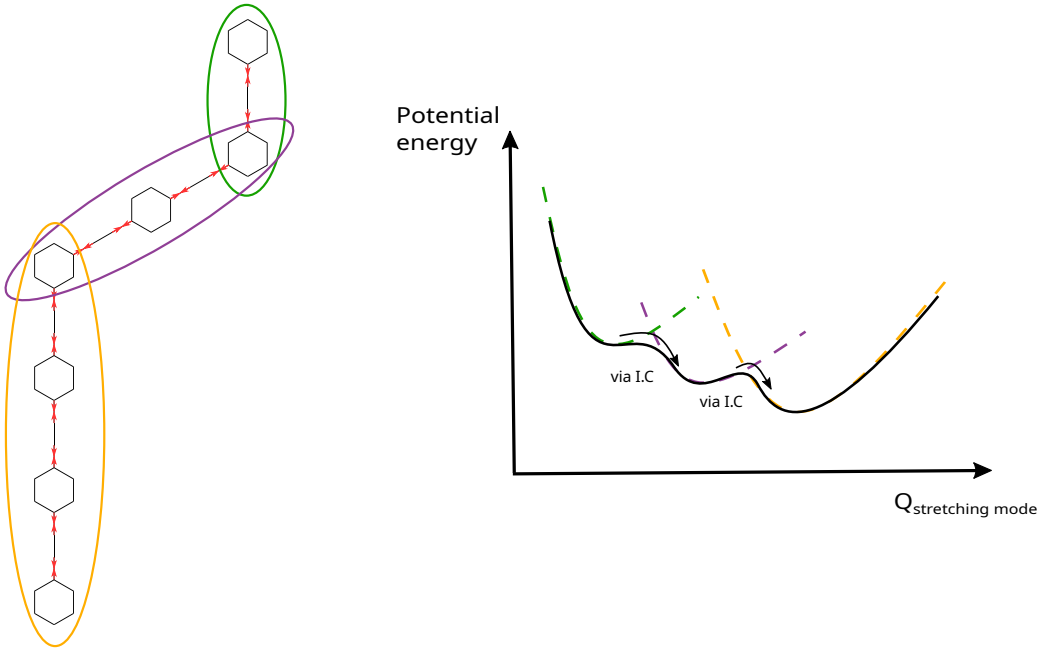

Figure 6: Schematic representation of the EET on a *e*PE-D branch along a stretching mode of the ethynylene groups of the three pseudofragments: DPA, BPEB and DPABPEB.

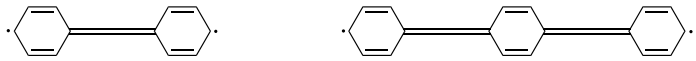

Figure 7: cumulenic isomer of DPA (on the left) and of BPEB (on the right).

a $\pi\pi^*$ single excitation.

The cumulenic structure is not a unique equilibrium geometry in the first excited adiabatic electronic state. The *optically inactive* states which minima correspond to the *trans* structures (see fig. 8) belong to the $\mathcal{C}_{2h}$ PG and are of A_u symmetry (for DPA) and to the $\mathcal{C}_s$ PG and are of A' symmetry (for BPEB). The *trans* structure is associated to a $\pi\sigma^*$ single excitation, the antibonding orbital is localised on the acetylenic bond and corresponds to the in-plane π-system. The *trans* isomer of DPA is lower in energy than the cumulenic one and the energy barrier between them is of hundreds of cm^{-1} [48–51] while the *trans* isomer of BPEB is higher in energy than the cumulenic one and the energy barrier is of 5 000 cm^{-1}. [52, 53]

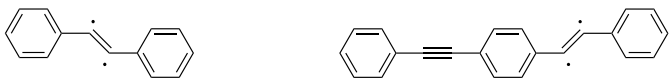

Figure 8: *trans* isomer of DPA (on the left) and *trans* isomer of BPEB (on the right)

No experimental information has been found on the *trans* isomer of BPEB but the *trans*

isomer of DPA has been characterised experimentally [54–61]. A photoisomerization process that involves the optically active and inactive states has been suggested and experimentally characterised by Hirata *et al.* [54]

The photoinduced isomerization process is: $S_0 \xrightarrow{h\nu} X \rightarrow Y \rightarrow T_1$ according to Hirata *et al.*. notations. In this scheme, the state denoted S_0 is the ground state. The state X is a transient short-lived optically active state ($\tau = 8$ ps and $\lambda_{\text{tr}} = 500$ nm, where τ is the species lifetime and λ_{tr} is the transient wavelength). This optically active state intersects the optically inactive state Y which equilibrium geometry is the *trans* isomer. The optically inactive state is a transient long-lived state ($\tau = 200$ ps and $\lambda_{\text{tr}} = 435$ nm and 700 nm). T_1 is the lowest triplet state that interacts with Y.

When the degeneracy between two adiabatic electronic states (*i.e.* they have the same energy) is lifted up, the crossing between both potential energy surfaces has the shape of a cone. Such a topological feature is called a conical intersection (CoIn). In the case of a two-states crossing, only two directions lift the degeneracy. They are called the Gradient Difference (GD) and the Derivative Coupling (DC) and they constitute together a plane that is called the branching space (BS). They play a crucial role [39,62–68] in photoisomerisation processes. More details are given on CoIn, the effect of crossing between two electronic states, and on the DC and GD in chapter 2.

Hirata *et al.* [54] explain that the population transfer between the optically active and inactive states is radiationless and so it includes at least a CoIn. Having access to the CoIn of *mb*-DPABPEB that involve optically active and inactive localised-on-the-pseudofragments diabatic states and characterizing them is one of the major interests of this thesis.

Several methods exist to get access to the geometry of the system for which there is a CoIn between two states [2, 69–74]. Many of them use algorithms that are based on Lagrange multipliers. Refs. [70–73] use analytic gradient methods that are constrained by Lagrange multipliers and ref. [74] uses an algorithm that needs to compute the Hessian of the Lagrange multipliers which involves a second constraint.

The program developed by Harvey *et al.* in [2] based on the work of Bearpark *et al* in [69] was used in this work. It is a method based on analytical energy gradients to determine the locus of the minimum energy of the crossing seam of two adiabatic potential energy surfaces. In our case the non-interacting surfaces correspond to two surfaces of states of different symmetry. However, this method is not as accurate as it could be if one has to find a CoIn that involves two

electronic states of same symmetry. To do so, an extension to this program has been developed during this thesis which involves the numerical energy gradients in the branching space. The numerical calculation of the two vectors of the branching space is determined by the use of the approach developed by Gonon *et al* in [75].

The conical intersections that have been studied in this thesis occur among electronic excited states. Excited states for a molecular system can be characterised as a first approximation by the occupied and virtual molecular orbitals involved in the transition: for exemple $n\pi^*$ transitions, $\pi\pi^*$ transitions etc. However, the electronic excitation for periodic systems are viewed as a quasi-particle, an exciton, which is often represented by the hole-electron model. *e*PE-D are large π-conjugated molecular systems and so they can be described in between the "molecular" picture and the "solid state" picture. Several studies have been performed to understand the LH properties of dendrimers by the use of excitons [76–78] and by characterizing the electronic properties of the excited states by determining the local character of the electronic excitation. [39]

Two types of electronic excited states can be involved in the EET [39]: a charge-transfer (CT) state and a locally-excited (LE) state. A CT state is a covalent state with apparent charges that are created afer the photoexcitation. An LE state is characterised by a biradicaloid property. [79–83] One needs to evaluate quantitatively and qualitatively the nature of the electronic excited states that are involved in the EET. To do so, several methods have been developed in the past decades to design computational tools in order to characterise the electronic properties with "indices" taking characteristic values. Guido *et al.* have defined an index that is based on the charge centroids of the natural transition orbital pairs. [84] Plasser *et al.* have generalized a theory based on natural orbitals to characterise excited states. [85–88] Ciofini *et al.* have built an index D_{CT} that is calculated from the difference density matrix. This index provides the spatial distance between the center of charges of the density distribution. [89–92] In this thesis, descriptors that are derived from the attachement and detachment density matrices have been used. They give a measure of the overlap between the attachement and detachment density functions and the effective amount of net charge transferred in the electronic transition.

Such tools to characterise adiabatic electronic excited states (*i.e.* density based descriptors and the software to determine conical intersections) are used to get a better understanding of the EET in PE-D.

In the case of the wavepacket is localised onto the cumulenic localised-on-the-DPA pseudofragment diabatic state of *mb*-DPABPEB, the cumulenic localised-on-the-BPEB pseudofragment

diabatic state can be easily populated. However, we suggest in this thesis that the wavepacket can be propagated at first from the the cumulenic localised-on-the-DPA pseudofragment diabatic state toward the *trans* localised-on-the-DPA pseudofragment diabatic state then from the *trans* localised-on-the-DPA pseudofragment diabatic state toward the cumulenic localised-on-the-BPEB pseudofragment diabatic state (see fig. 9). A specific study of the diabatic states of the *o*-PE and of the diabatic states of PE-D is carried out.

Theoretical details are given in the first chapter on adiabatic electronic excited states and

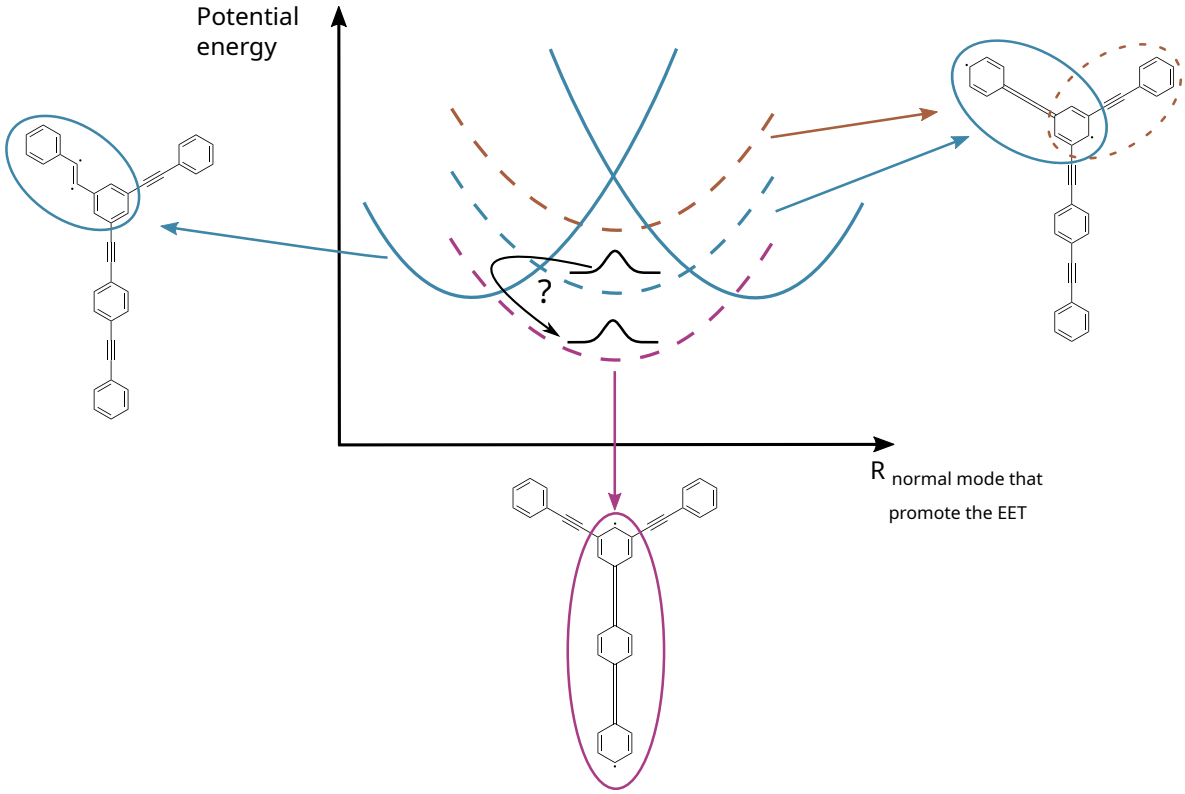

Figure 9: New pathway that could be used by the wavepacket during the EET in a PE-D after a photo-excitation

on approximations that are made. Then the second chapter is addressing on conical intersections, when two adiabatic electronic states are degenerate. The third chapter develops the concept of the electron density and density-based descriptors that are used to characterise adiabatic electronic excited states and conical intersections. In the fourth chapter, the computational method to determine the density-based descriptors is validated, the determination of a conical intersection and the behavior of the density-based descriptors in the vicinity of the conical intersection is studied. Finally, in the last chapter, an alternative mechanism of EET is suggested. To do so,

the first optically active and inactive electronic states of the pseudofragments of *mb*-DPABPEB and of the molecule itself are studied by the use of peudofragmentation scheme. In the general conclusion, an alternative excitation energy transfer mechanism, involving dark states, compared to the received mechanism in the literature is suggested for the nanostar.

0.4 Introduction in French

Dans les systèmes moléculaires naturels et artificiels, les processus photo-induits jouent un rôle crucial en ce qui concernent leur réactivité chimique et biologique. On peut citer par exemple : les réactions chimiques qui sont induites par une photo-excitation, la photo-synthèse dite "naturelle" pour les végétaux chlorophylliens mais aussi la photo-synthèse dite "artificielle" dans le cas des cellules solaires et des diodes organiques électro-luminescentes [3–6].

Parmi les divers processus photo-induits existant dans les systèmes supra- et macro-moléculaire. Nous nous sommes intéressés aux propriétés collectrices de lumière dans ce travail. Les propriétés collectrices de lumière sont présentes à la fois pour des sytèmes naturels et pour des systèmes artificiels [7–22]. Des études ont montré le lien entre la structure des systèmes et le processus de transfert d'énergie d'excitation (TEE) [23–29]. En ce qui concerne les propriétés collectrices de lumière pour des systèmes naturels, on peut citer par exemple les complexes de pigments-protéines [7–11].

Les systèmes présentés dans les références [7–11] sont des complexes pigments-protéines de la bactérie pourpre. Il s'agit là d'un des premiers systèmes moléculaires qui a été étudié pour ses propriétés collectrices de lumière. Cependant, ces complexes-ci ne sont pas un unique exemple de systèmes moléculaires présentant de telles propriétés.

La lumière est absorbée par la paire pigment-protéine et l'énergie d'excitation est transférée vers le centre de la bactérie où a lieu une réaction chimique. Ce lieu est la jonction entre l'ensemble des paires de pigments-protéines. Le TEE global s'étend sur toute la bactérie durant une période de 100 ps avec un rendement quantique de 95%, le rendement quantique étant défini comme le rapport entre la quantité de photons émis et la quantité de photons absorbés. Le TEE d'une unique paire pigment-protéine vers le centre de la bactérie est quant à lui en dessous de l'échelle de temps de la picoseconde. [30, 31].

Le terme de complexes "collecteurs de lumière" a été choisi, pour l'exemple précédent, afin de caractériser les complexes de la bactérie pourpre. En effet, l'énergie d'excitation est capturée sur différents sites spécifiques (les paires pigment-protéine) et est redirigée vers un point unique du système moléculaire (le centre de réaction chimique).

Les composés organiques qui possèdent une telle propriété que de collecter la lumière puis de la transférer ont permis de donner lieu à des applications telles que les thérapies photo-dynamiques dans la biomédecine [32, 33] mais aussi dans les technologies photovoltaïques orga-

niques pour des applications opto-électroniques [22, 34–36].

Les processus de TEE ultra-rapides et hautement efficaces sont alors des conditions nécessaires dans la recherche de nouvelles de molécules artificielles qui présentent des propriétés collectrices de lumière.

Les dendrimères sont des systèmes moléculaires très structurés; ils sont prometteurs afin d'être utilisés comme antennes collectrices de lumière. [22, 35–37] Le mot **dendrimère** fait référence au fait que le système moléculaire a une structure similaire à celle d'un arbre. Un dendrimère est composé d'une branche principale que l'on peut comparer à un tronc. A l'extrémité de cette branche principale, des branches secondaires, plus petites, sont reliées ensemble à un noeud commun afin de connecter la branche principale aux secondaires. De même, à l'extrémité de ces branches secondaires, d'autres branches, plus petites encore, y sont reliées et ainsi de suite. Ces différentes branches (primaire, secondaire, etc.) sont appelées "blocs de construction". Ces blocs de contruction peuvent donc être comparés aux branches d'un arbre. Ces blocs peuvent être de taille similaire ou différente. Il existe ainsi deux types de dendrimères : les dendrimères *compacts* et les dendrimères *étendus*. Les deux types de dendrimères sont réunis dans la figure 10.

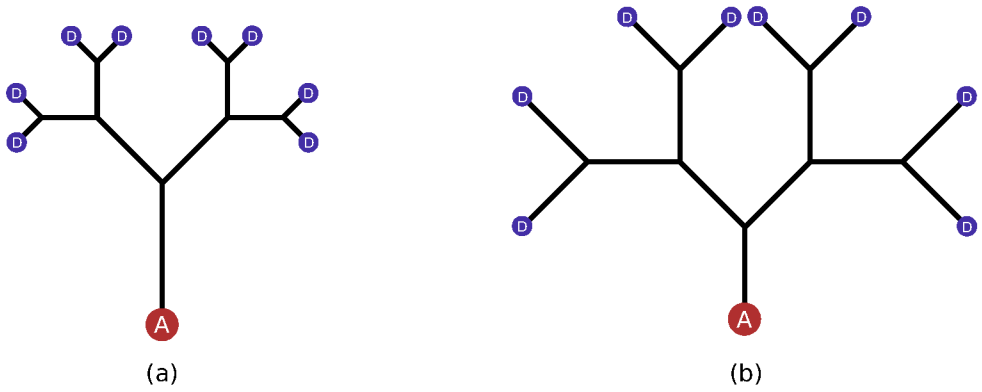

Figure 10: Représentation schématique d'un dendrimère étendu (a) et d'un dendrimère compact (b).

La représentation schématique d'un dendrimère étendu est appelée (a) à gauche de la figure 10. La longueur des des blocs de construction augmente de la périphérie au centre du système. Le dendrimère compact est appelé (b) à droite de la même figure. Les blocs de construction sont tous de même longueur. Concernant les dendrimères étendus, le TEE va de la périphérie au centre du système grâce à un gradient d'énergie, alors que le transfert se fait de manière inverse pour un dendrimère compact: du centre du système à la périphérie à cause de l'entropie. De

plus, un dendrimère peut être fonctionnalisé à l'aide de groupes donneurs d'électrons (D, disque bleu sur la figure 10) et de groupes accepteurs d'électrons (A, disque rouge sur la figure 10). Les groupes donneurs sont fixés à la périphérie du système tandis que le groupe accepteur est fixé au centre du dendrimère. Ainsi, la quantité d'énergie qui est absorbée puis transférée est augmentée [34, 38]. D'après le schéma représentatif d'un dendrimère compact dans la figure 10, le TEE est alors dirigé de la périphérie vers le centre.

Dans cette thèse, nous nous sommes intéressés à l'étude de dendrimères étendus de phénylène-ethynylène (D*e*-PE) qui sont des systèmes π conjugués. Les blocs de construction sont alors des *oligo*(phénylène-ethynylène)s (*o*PE). L'un des dendrimères des plus connu de cette classe-ci est la nanostar. Elle est représentée sur la figure 11.

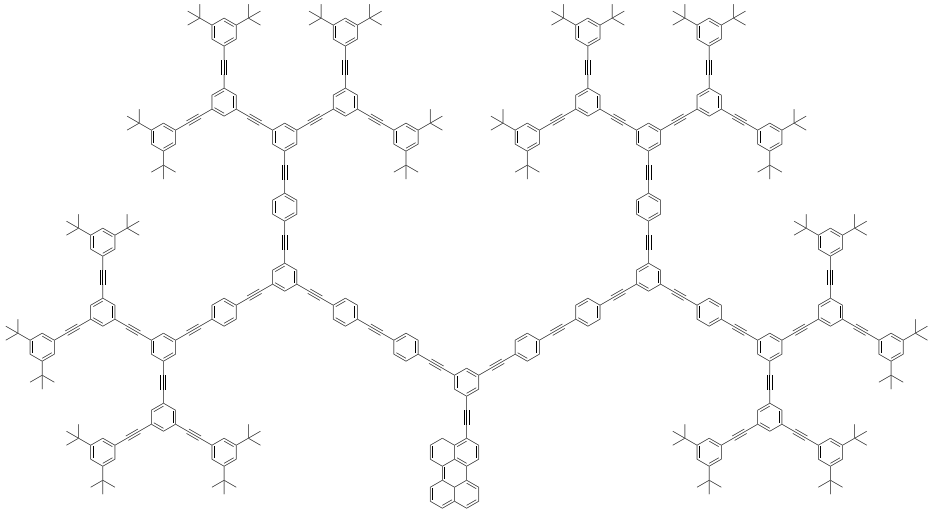

Figure 11: La nanostar

La nanostar présente des propriétés de TEE remarquables. Environ 99% de l'énergie d'excitation est transférée. Le TEE est unidirectionnel (de la périphérie de la nanostar vers le groupe pérylène en son centre) et est quasi ultrarapide (270 ps le long du système) [39–41]. Le groupe pérylène émet la lumière absorbée. Les blocs de construction de deux, trois et quatre phényles donnent une structure particulière à la nanostar et sont responsables de la présence d'un gradient d'énergie d'excitation qui donne lieu aux propriétés collectrices de lumière et au TEE. [42]

Il a été montré dans l'article [40] que les spectres stationnaires d'absorption et d'émission de la nanostar correspondent à la superposition des spectres stationnaires de ses blocs de construction. Une molécule dendritique collectrice de lumière présente alors les propriétés opto-électroniques de chromophores faiblement couplés (dans notre cas, les blocs de construction de

tailles différentes). Le système absorbe la lumière à des longueurs d'onde qui dépendent des propriétés structurales de ses branches. [42]

La position en *meta* des blocs de construction sur un même phényle brise la conjugaison π entre un *o*PE et le suivant. Les propriétés électroniques de la nanostar, et plus généralement des dendrimères étendus, sont gouvernées par les propriétés électroniques des blocs de construction. L'aptitude de transférer l'énergie d'excitation est donc définie par les propriétés des chromophores, donc des blocs de constructions, d'un dendrimère.

Une telle description hiérarchisée nous a intéressés afin d'utiliser une méthode multi-échelle qui est basée sur un schéma de pseudofragmentation [43]. Les pseudofragments de cette méthode sont les blocs de construction d'un D*e*-PE. Les phényles en commun entre les différents blocs de construction sont pris en compte plusieurs fois puisqu'ils appartiennent aux différents blocs de construction : c'est pourquoi il n'est pas possible de considérer les branches d'*o*PE, les blocs de construction, comme de véritables fragments.
Les D*e*-PE se comportent comme si les pseudofragments étaient faiblement interagissants. Dans cette thèse, à l'aide de schémas de pseudofragmentation, les surfaces d'énergie potentielle de D*e*-PE sont rationnalisées à l'aide de l'étude de surfaces d'énergie potentielle des pseudofragments.

Un schéma de pseudofragmentation est détaillé ci-dessous (fig. 13). Il a été détaillé pour le 1,3-*bis*(phenylethynyl)benzene (*m*-BPEB, voir fig. 12) dans l'article [43].

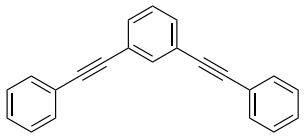

Figure 12: 1,3-*bis*(phényléthynyl)benzène (*m*-BPEB).

Le minimum d'énergie de l'état fondamental du *m*-BPEB appartient au groupe d'espace $\mathcal{C}_{2v}$. Le point Franck-Condon (FC, l'état optiquement actif à la géométrie d'équilibre de l'état fondamental) est vers $4-5$ eV. Les quatre orbitales frontières de *m*-BPEB au point FC sont rassemblées au milieu de la figure 13.

Les quatre orbitales frontières sont délocalisées sur tout le système moléculaire. Les orbitales π qui s'étendent sur les deux groupes éthynylènes et sur les deux phényles périphériques sont similaires à une phase près. Les orbitales moléculaires qui s'étendent sur le phényle central en commun sont toutes différentes. Les paires délocalisées HOMO-1/HOMO et LUMO/LUMO+1 sont ainsi quasiment dégénérées. La "somme" des deux non dégénérées HOMO-1/HOMO donne

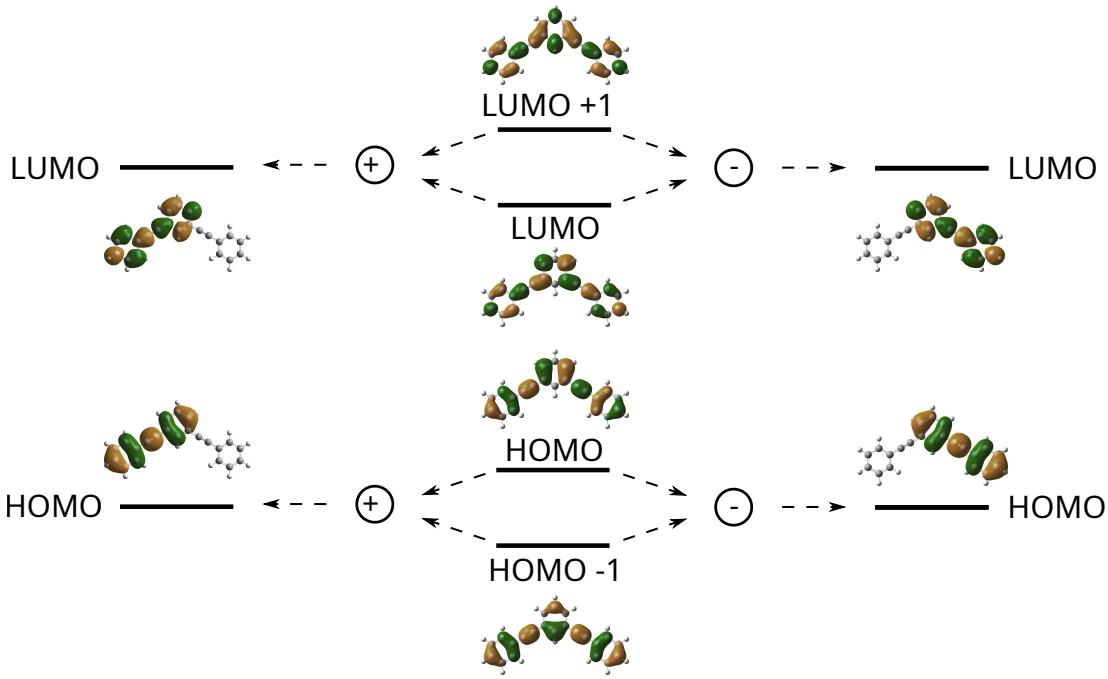

Figure 13: Le schéma de pseudofragmentation de m-BPEB.

une HOMO localisée sur la branche de gauche de m-BPEB et la "somme" des deux non dégénérées LUMO/LUMO+1 donne une LUMO localisée sur la branche de gauche de m-BPEB, de même que la "différence" des paires HOMO-1/HOMO (resp. LUMO/LUMO+1) donne une HOMO (resp. LUMO) localisée sur la branche de droite. Les deux HOMO localisées à gauche ou à droite sont dégénérées, il en est de même concernant les deux LUMO localisées. Les orbitales localisées à gauche ou à droite de m-BPEB impliquent un jeu d'atomes différents (branche de gauche et de droite) et partagent un jeu d'atomes en commun (le phénylène central). C'est justement pour cette raison que l'on appelle les blocs de construction des pseudofragments. En d'autres termes, plus grand est le recouvrement entre les deux orbitales moléculaires localisées, plus grand serait l'interaction entre les deux pseudofragments. m-BPEB se comporte alors comme deux diphényle-acétylènes faiblement interagissant.

Les états électroniques adiabatiques sont définis tels qu'ils sont les vecteurs propres de l'hamiltonien électronique. Les états diabatiques sont quant à eux définis comme n'étant pas des vecteurs propres de l'hamiltonien électronique et comme ayant un couplage cinétique nucléaire nul entre eux. Les états diabatiques peuvent être vus comme s'ils caractérisaient une propriété électronique du système moléculaire. Plus de détails sont donnés sur l'interprétation des états électroniques adiabatiques et diabatiques dans les chapitres 1 et 2. Dans cette thèse,

on détermine un jeu d'états diabatiques tels qu'ils décrivent les orbitales frontières localisées sur les pseudofragments d'un D*e*-PE. Les états diabatiques localisés sur les pseudofragments d'un D*e*-PE correspondent aux états électroniques délocalisés adiabatiques des pseudofragments isolés.

Dans cette thèse, le système 1,3-*bis*(phényléthynyl)-3-(1,4-bis(phényléthynyl)benzène)benzène *mb*-DPABPEB est étudié et est analysé à l'aide de divers schémas de pseudofragmentation. Trois schémas de pseudofragmentation sont étudiés. Ils sont (voir fig. 14) :

- Schéma 1: Deux diphényle-acétylènes (DPA) et un 1,4-bis(phenylethynyl)benzene (BPEB) faiblement interagissants ;
- Schéma 2: Un *m*-BPEB et un BPEB faiblement interagissants ;
- Schéma 3: Un 1-(phényléthynyl)-3-(1,4-*bis*(phényléthynyl)benzène)benzene (*m*-DPABPEB) et un DPA faiblement interagissants.

Les articles [39–47] proposent que seulement le premier état électronique optiquement actif (S_{act}) de chaque pseudofragment est impliqué dans le transfert de l'énergie dans un D*e*-PE. De plus ils suggèrent que le TEE se fasse principalement entre les modes de vibrations d'étirement des groupes éthynylènes. Dans la figure 15 est représenté un *o*PE qui peut être pseudofragmenté en trois pseudofragments : DPA, BPEB et *m*-DPABPEB. L'energie potentielle adiabatique de l'*o*PE total est représentée schématiquement par une courbe pleine et les états diabatiques localisés sur les pseudofragments sont représentés par une courbe en pointillés (vert: DPA, violet: BPEB et jaune: *m*-DPABPEB). Si le paquet d'onde est initialement localisé sur l'état diabatique localisé sur le pseudofragment DPA, un TEE va avoir lieu de cet état diabatique vers l'état diabatique localisé sur le pseudofragment BPEB puis vers l'état diabatique localisé sur le pseudofragment *m*-DPABPEB via conversion interne (CI) à travers des intersections coniques entre états électroniques.

Dans cette thèse, un second mécanisme pour le TEE est proposé. On suggère que le mécanisme de transfert implique des états optiquement inactifs en plus des états optiquement actifs. En effet, proche du premier état optiquement actif des *o*PE, il existe un état optiquement inactif qui implique une géometrie *trans* pour les *o*PE linéaires sur un groupe éthynylène. Ces deux états ont été caractérisés pour DPA et BPEB. [48–53] L'état fondamental de DPA et BPEB appartient au groupe de symétrie $\mathcal{D}_{2h}$. Dans l'état fondamental, les géométries d'équilibre sont linéaires et les phényles sont séparés par une alternance de liaisons simple-triple-simple (voir

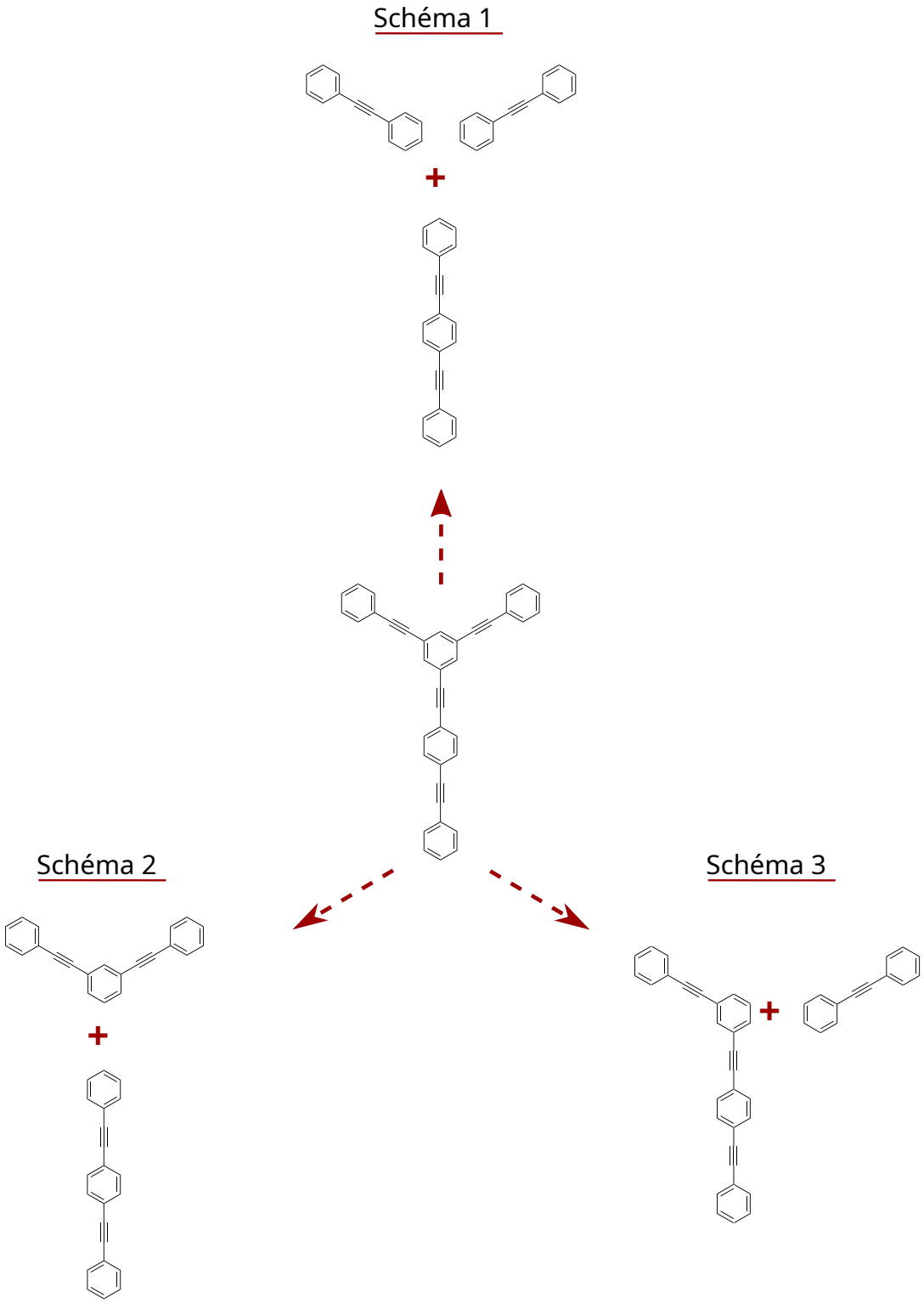

Figure 14: Les schémas de pseudoframentation de *mb*-DPABPEB

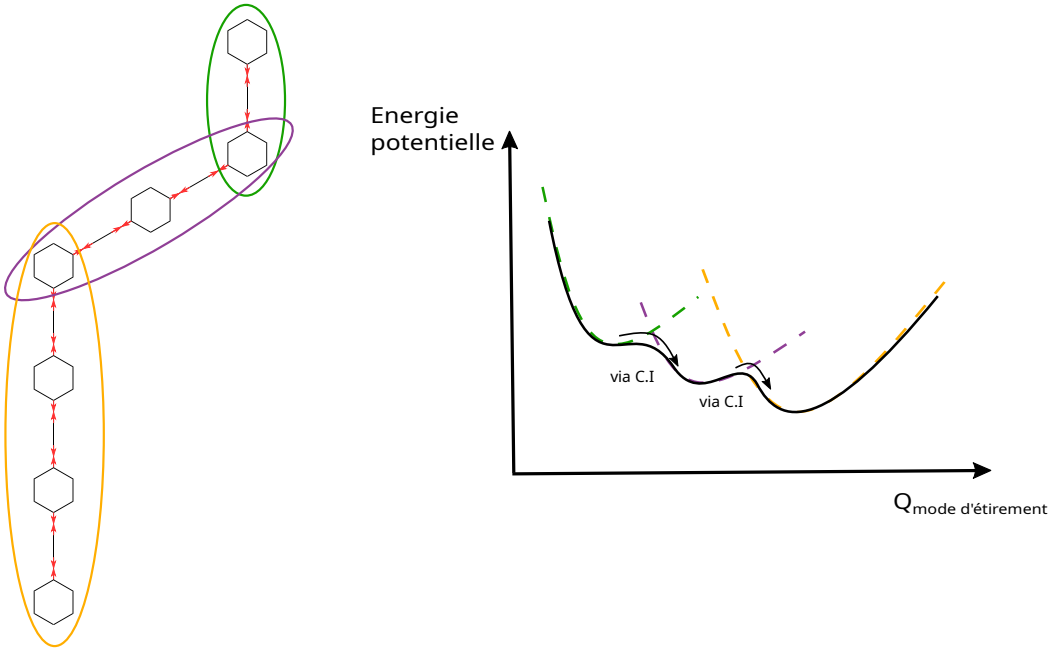

Figure 15: Représentation schématique du transfert d'énergie d'une branche d'un D*e*-PE le long d'un mode d'étirement des groupes éthynylènes des trois pseudofragments : DPA, BPEB, *m*-DPABPEB.

figure 14). Dans le groupe de symétrie $\mathcal{D}_{2h}$ le minimum du premier état optiquement actif est défini par une structure cumulénique pour les deux systèmes : les phényles ont une structure quinoidale et sont séparés par trois liaisons doubles (voir figure 16. Le premier état optiquement

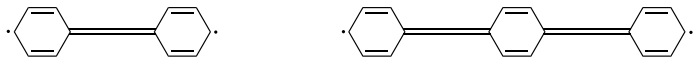

Figure 16: Isomère cumulénique de DPA (à gauche) et de BPEB (à droite).

actif pour DPA et BPEB est 1^1B_{1u} (en utilisant la convention de Muliken avec l'axe z selon le plus grand axe de la molécule).

C. Robertson et G. A. Worth [51] ont montré que selon le niveau de théorie utilisé dans les calculs de structure électronique, S_{act} peut ne pas être le premier état électronique excité mais il fait cependant partie des premiers. Le minimum cumulénique est associé à une excitation $\pi\pi^*$.

Le minimum à la géometrie cumulénique n'est pas un minimum unique. L'état optiquement inactif dont le minimum est associé à une structure *trans* sur un unique groupe ethynylène d'un *o*PE linéaire (voir fig. 17) appartient au groupe de symétrie $\mathcal{C}_{2h}$ et est 1^1A_u pour le DPA, et appartient au groupe de symétrie $\mathcal{C}_s$ et est $1^1A'$ pour le BPEB. Le minimum de cet état optiquement inactif est associé à une excitation $\pi\sigma^*$. L'orbitale anti-liante est localisée sur la liaison

ethynylène et correspond à un système π dans le plan. L'isomère *trans* du DPA est plus bas en énergie que son isomère cumulénique, avec une barrière énergétique de quelques centaines de cm^{-1} [48–51] alors que l'isomère *trans* du BPEB est plus haut en énergie que l'isomère cumulénique avec une barrière énergétique d'environ 5 000 cm^{-1}. [52, 53]

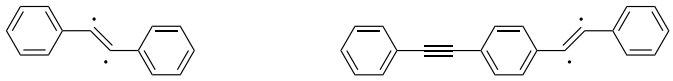

Figure 17: Isomère *trans* de DPA (à gauche) et isomère *trans* de BPEB (à droite).

Aucune donnée expérimentale n'a été trouvée sur l'isomère *trans* de BPEB mais l'isomère *trans* du DPA a été caractérisé expérimentalement [54–61]. Un processus de photoisomérisation qui implique les états optiquement actif et inactif a été proposé et caractérisé expérimentalement par Hirata *et al.* [54]

Le processus d'isomérisation photoinduit est : $S_0 \xrightarrow{h\nu} X \rightarrow Y \rightarrow T_1$ selon les notations de Hirata *et al.* Selon ce processus, l'état S_0 est l'état fondamental, l'état X est un état optiquement actif transitoire de faible durée de vie (τ = 8 ps et λ_{tr} = 500 nm, où τ est la durée de vie de l'espèce et λ_{tr} est la longueur d'onde transitoire). Cet état optiquement actif croise l'état optiquement inactif Y dont la géométrie d'équilibre est celle de l'isomère *trans*. L'état Y est un état transitoire de longue durée de vie (τ = 200 ps et λ_{tr} = 435 nm et 700 nm). T_1 est un état triplet de plus basse énergie qui croise l'état Y dans le groupe de symétrie $\mathcal{C}_{2\text{h}}$

Quand la dégénérescence entre deux états adiabatiques (*i.e.* ils ont la même énergie) est levée, les surfaces d'énergie potentielle des deux états presque dégénérés ont l'apparence d'un cône. Une telle particularité topologique est appelée **intersection conique** (InCo). Seulement deux directions lèvent la dégénérescence : elles sont la différence des gradients (DG) et le couplage dérivatif (CD). Ces deux directions constituent un plan qui est appelé l'espace de branchement. Ces deux directions jouent un rôle crucial [39, 62–68] dans les processus de photoisomérisation. Plus de détails sont donnés sur les InCO, la raison de croisement entre deux états electroniques et sur les directions DG et CD dans le chapitre 2.

Hirata *et al.* [54] expliquent que le transfert de population entre les états optiquement actif et inactif est non radiatif et qu'il implique au moins une InCo. Avoir accès aux InCo de *mb*-DPABPEB qui impliquent les états optiquement actif et inactif des états diabatiques localisés sur les pseudofragments et les caractériser est l'un des intérêts majeurs de cette thèse.

Plusieurs méthodes existent pour avoir accès à la géometrie d'un système pour laquelle il y

a une InCo entre deux états. [2, 69–74] Plusieurs d'entre elles utilisent des algorithmes qui sont basés sur les multiplicateurs de Lagrange. Les articles [70–73] utilisent des méthodes de gradient analytiques qui sont contraints par les multiplicateurs de Lagrange et l'article [74] utilise un algorithme qui a besoin de calculer la hessienne de multiplicateurs de Lagrange, ce qui implique une seconde contrainte.

Le programme développé par Harvey *et al.* dans l'article [2], qui est basé sur le travail de Bearpark *et al.* [69], a été utilisé durant cette thèse. Cette méthode est basée sur l'obtention d'énergies via le calcul de gradients analytiques afin de déterminer la géometrie de la couture de plus basse énergie entre deux surfaces d'énergie potentielle non interagissants. Dans notre cas, les surfaces non interagissantes correspondent à deux surfaces de deux états de symétrie différente. Cependant, cette méthode n'est pas suffisament précise dans le cas d'un croisement entre deux états électroniques de même symétrie. Une extension de ce programme impliquant le calcul d'énergie de gradients numériques dans l'espace de branchement a été développée dans cette thèse. Le calcul numérique des vecteurs de l'espace de branchement est déterminé par l'utilisation d'une approche développée par Gonon *et al* dans [75].

Les InCo qui ont été étudiées dans cette thèse impliquent des états électroniques excités. Les états électroniques excités d'un système moléculaire peuvent être caractérisés en première approximation par les orbitales moléculaires occupées et virtuelles impliquées lors l'excitation : par exemple une excitation $n\pi^*$, une excitation $\pi\pi^*$, etc. Cependant, les excitations électroniques pour les systèmes périodiques peuvent être vues comme une quasi-particule, un exciton, qui est souvent représentées par le modèle trou-particule. De-PE sont de larges systèmes π-conjugués et ils peuvent être donc décrit à la fois par une vision "moléculaire" et une vision "périodique". Plusieurs études ont été faites pour comprendre les propriétés collectrices de lumière des dendrimères avec un modèle excitonique [76–78] et en caractérisant les propriétés des états excités en déterminant le caractère local de l'excitation électronique. [39]

Deux types d'états électroniques excités peuvent être impliqués dans le TEE [39] : un état à transfert de charge et un état localement excité. Un état à transfert de charge est un état covalent avec présence de charges apparentes qui sont crées durant la photoexcitation. Un état localement excité est caractérisé par des propriétés biradicaloides. [79–83] Nous avons besoin d'évaluer quantitativement et qualitativement la nature des états électroniques excités qui sont impliqués dans le TEE. Ainsi, plusieurs méthodes ont été développées durant la dernière décénnie afin de développer des outils computationnels pour caractériser les propriétes électroniques

avec des indices prenant des valeurs caractéristiques. Guido *et al.* ont défini un indice qui est basé sur les centres de charges des paires d'orbitales naturelles de transitions. [84] Plasser *et al.* ont généralisé une théorie basée sur les orbitales naturelles afin de caractériser les états électroniques excités. [85–88] Ciofini *et al.* ont construit un indice D_{CT} qui est calculé à partir de la matrice différence de densité. Cet indice donne la distance entre les centres de charges de la distribution de la densité. [89–92] Dans cette thèse, des descripteurs sont construits à l'aide des matrices de densité d'attachement et de détachement. Ces descripteurs sont utilisés afin de donner une mesure du recouvrement entre les fonctions densité d'attachement et de détachement et la quantité de charge effective qui est transférée durant l'excitation électronique.

De tels outils sont utilisés afin de caractériser les états électroniques adiabatiques excités (*i.e.* descripteurs basés sur la densité électronique et le logiciel de détermination d'intersections coniques) et d'obtenir une meilleure compréhension du TEE dans les D-PE.

Dans le cas où le paquet d'onde est localisé dans l'état diabatique cumulénique localisé sur le pseudoframent de DPA du *mb*-DPABPEB, l'état diabatique cumulénique localisé sur le pseudofragment de BPEB est facilement peuplé. Cependant, nous proposons dans cette thèse que le paquet d'onde peut se propager tout d'abord de l'état diabatique cumulénique localisé sur le pseudoframent de DPA vers l'état diabatique *trans* localisé sur le pseudoframent de DPA puis vers l'état diabatique cumulénique localisé sur le pseudofragment de BPEB (voir figure 18). Une étude précise est donc portée sur les états diabatiques des *o*-PE and des D-PE.

Des détails théoriques sur les états électroniques excités adiabatiques sont donnés dans le premier chapitre. Le second chapitre traite des intersections coniques lorsque deux états adiabatiques sont dégénérés. Le troisième chapitre porte sur le concept de la densité électronique et des descripteurs utilisés pour caractériser les états électroniques. Le quatrième chapitre présente la validation de la méthode computationnelle qui a été utilisée afin de calculer les descripteurs, la détermination d'intersections coniques et du comportement des descripteurs au voisinage d'une intersection conique. Enfin le dernier chapitre suggère un second mécanisme de TEE. Pour ce faire les états optiquement actifs et inactifs de systèmes dendritique et de ses pseudoframgents ont été étudiés.

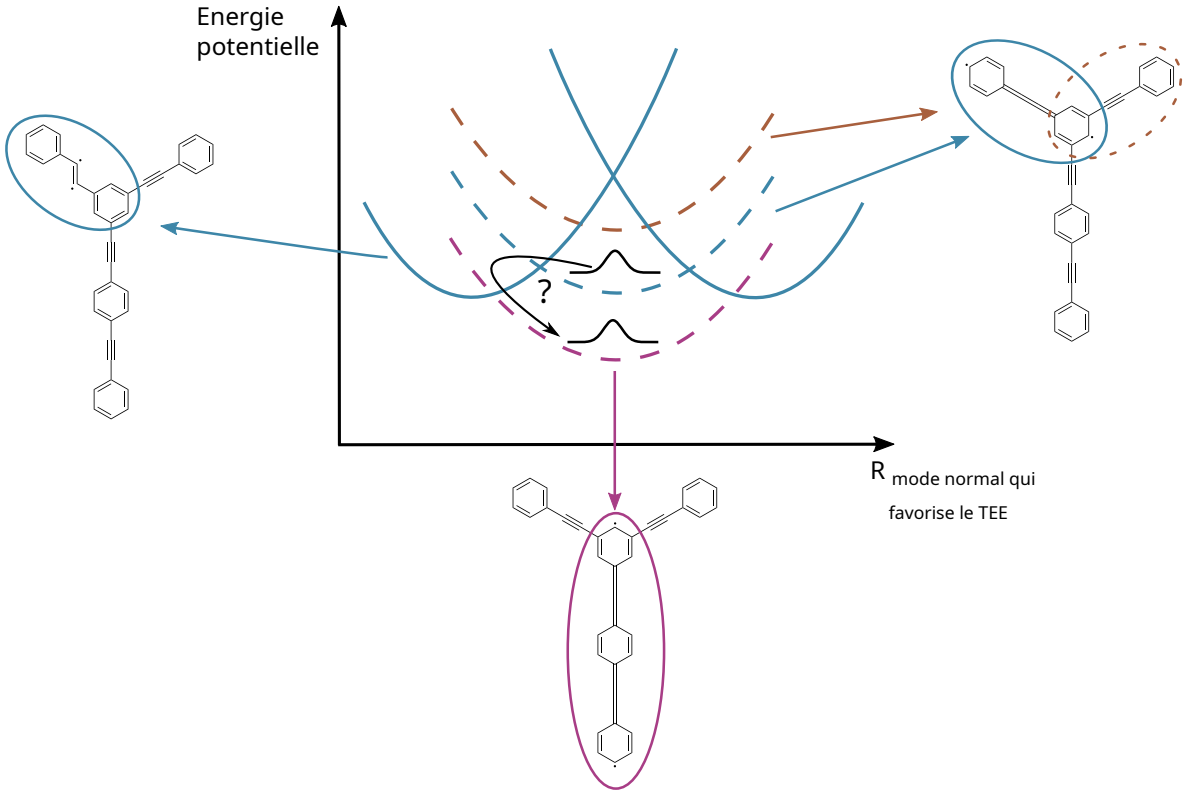

Figure 18: Nouveau chemin potentiel pour le paquet d'onde durant le TEE dans un D-PE après une photo-excitation.

Chapter 1

Electronic states

1.1 Introduction

In quantum mechanics, any system is characterized by what is called a *state*. Its abstract vectorial representation in the Hilbert space is named *ket* and is denoted: $|\Psi(t)\rangle$ at any time. The evolution of a state from its knowledge at $t = 0$ $|\Psi(t = 0)\rangle$ (initial condition) is governed by the time-dependent Schrödinger equation,

$$\hat{H}\,|\Psi(t)\rangle = i\hbar\frac{\partial}{\partial t}\,|\Psi(t)\rangle \tag{1.1}$$

where $\hat{H}$ is the Hamiltonian and $\hbar$ the reduced Planck constant. The time-dependent Schrödinger equation is useful to have access to ultra-fast phenomena such as non-adiabatic processes, photoisomerizations, radiative and non-radiative processes etc. [93–96]

A quantum system is described both as a particle and as a wave. Due to the wave description, when $|\Psi(t)\rangle$ is an eigenstate of eq. 1.1, the state can be stationary: $|\Psi(t)\rangle = \mathrm{e}^{-i\frac{Et}{\hbar}}\,|\Psi\rangle$, and so the time dependency of eq. 1.1 vanishes.

Considering a stationary state, one has the time-independent Schrödinger equation (TISE):

$$\hat{H}\,|\Psi\rangle = E\,|\Psi\rangle \tag{1.2}$$

The energy E is associated to the stationary state.

The two previous equations can only be solved explicitely for very small systems (*e.g.* H_2^+ and H). It is computationally challenging to get an approximate solution for systems made of many particles. Many approximations have been developed to get approached solutions. [97] The three

following chapters present approximations that are made to solve and to compute the TISE (eq. 1.2), the limits of the approximations, and how to analyse the results of the TISE.

1.2 From the molecular Hamiltonian to the electronic Hamiltonian

The systems that have been studied in this thesis are molecular systems that are composed of $\mathrm{N_{e^-}}$ electrons of mass $m_{\mathrm{e^-}}$ (fermions) and of $\mathrm{N_{nu}}$ nuclei (either bosons or fermions), the mass of the I^{th} nucleus is denoted M_I.

The electronic coordinates are $(\mathbf{r}, \boldsymbol{\sigma}_{\mathrm{e^-}}) = \{\mathbf{r}_i, \sigma_i\}_{i \in [\![1;\mathrm{N_{e^-}}]\!]}$, where $\mathbf{r}$ denotes the electronic spatial coordinates such that the i^{th} element $\mathbf{r}_i$ lies in $\mathbb{R}^3$ and $\boldsymbol{\sigma}_{\mathrm{e^-}}$ denotes the electronic spin coordinates such that the i^{th} element σ_i lies in $\Sigma_{\mathrm{e^-}} = \{\alpha, \beta\}$, where α and β are the values associated to a spin up $|\uparrow\rangle$ and a spin down $|\downarrow\rangle$, respectively.

The nuclear coordinates are $(\mathbf{R}, \boldsymbol{\sigma}_{\mathrm{nu}}) = \{\mathbf{R}_I, \sigma_I\}_{I \in [\![1;\mathrm{N_{nu}}]\!]}$, where $\mathbf{R}$ denotes the total nuclear spatial coordinates such as the I^{th} element $\mathbf{R}_I$ lies in $\mathbb{R}^3$ and $\boldsymbol{\sigma}_{\mathrm{nu}}$ denotes the total nuclear spin coordinates.

It may seem difficult to understand the meaning of a ket due to its abstract definition. One can project $|\Psi\rangle$ onto the Hilbert basis vectors related to the position and spin representation. The coordinate representation is related to $|\mathbf{r}, \boldsymbol{\sigma}_{\mathrm{e^-}}, \mathbf{R}, \boldsymbol{\sigma}_{\mathrm{nu}}\rangle$. We have:

$$\langle \mathbf{r}, \boldsymbol{\sigma}_{\mathrm{e^-}}, \mathbf{R}, \boldsymbol{\sigma}_{\mathrm{nu}} | \Psi \rangle = \Psi(\mathbf{r}, \boldsymbol{\sigma}_{\mathrm{e^-}}, \mathbf{R}, \boldsymbol{\sigma}_{\mathrm{nu}}) \tag{1.3}$$

$|\mathbf{r}, \boldsymbol{\sigma}_{\mathrm{e^-}}, \mathbf{R}, \boldsymbol{\sigma}_{\mathrm{nu}}\rangle$ and $|\Psi\rangle$ span the same "abstract" Hilbert space (kets). $\Psi(\mathbf{r}, \boldsymbol{\sigma}_{\mathrm{e^-}}, \mathbf{R}, \boldsymbol{\sigma}_{\mathrm{nu}})$ belongs to the Hilbert space of wavefunctions that are square integrable ($\mathcal{L}^2$) when integration is performed over the coordinates.

Equation 1.3 gives the spatial and spin representation of the state that is called a wavefunction $\Psi(\mathbf{r}, \boldsymbol{\sigma}_{\mathrm{e^-}}, \mathbf{R}, \boldsymbol{\sigma}_{\mathrm{nu}})$. In other words the wave-function is the coordinate representation, which is the projection of the ket $|\Psi\rangle$ onto $|\mathbf{r}, \boldsymbol{\sigma}_{\mathrm{e^-}}, \mathbf{R}, \boldsymbol{\sigma}_{\mathrm{nu}}\rangle$. The meaning of this projection is a probability amplitude and the square of its modulus means a probability density of being at $(\mathbf{r}, \boldsymbol{\sigma}_{\mathrm{e^-}}, \mathbf{R}, \boldsymbol{\sigma}_{\mathrm{nu}})$. The TISE now reads

$$\hat{H}(\mathbf{r}, \boldsymbol{\sigma}_{\mathrm{e^-}}, \mathbf{R}, \boldsymbol{\sigma}_{\mathrm{nu}}) \Psi(\mathbf{r}, \boldsymbol{\sigma}_{\mathrm{e^-}}, \mathbf{R}, \boldsymbol{\sigma}_{\mathrm{nu}}) = E \Psi(\mathbf{r}, \boldsymbol{\sigma}_{\mathrm{e^-}}, \mathbf{R}, \boldsymbol{\sigma}_{\mathrm{nu}}) \tag{1.4}$$

Equation 1.4 is then the coordinate representation of the eigenvalue problem expressed in equation 1.2.

Hereafter, molecular systems will be considered isolated. The interaction between charges is considered as being electrostatic, in other words they interact "instantaneously" together. The particles are considered here as non-relativistic and the molecular Hamiltonian is spin non-dependent. Then, one can solve the TISE within only the spatial coordinates representation $|\mathbf{R}, \mathbf{r}\rangle$ (accounting implicitly for the total spin, in particular of the electrons). Equation 1.4 can be expressed with the total molecular Hamiltonian and the wave-function is then called the *molecular wave-function*.

The molecular wave-function can then be expressed only with electronic and nuclear spatial coordinates such that

$$\langle \mathbf{r}, \mathbf{R} | \Psi_{\text{mol}} \rangle = \Psi_{\text{mol}}(\mathbf{r}, \mathbf{R}) \tag{1.5}$$

The total molecular Hamiltonian operator reads:

$$\begin{aligned} \hat{H}_{\text{mol}} \quad = \quad & \sum_{i<j} \frac{\mathrm{e}^2}{4\pi\epsilon_0 \parallel \mathbf{r}_i - \mathbf{r}_j \parallel} + \sum_{I<J} \frac{\mathrm{e}^2 Z_I Z_J}{4\pi\epsilon_0 \parallel \mathbf{R}_I - \mathbf{R}_J \parallel} - \sum_{i,I} \frac{\mathrm{e}^2 Z_I}{4\pi\epsilon_0 \parallel \mathbf{R}_I - \mathbf{r}_i \parallel} \\ & - \sum_i \frac{\hbar^2 \boldsymbol{\nabla}^2_{\mathbf{r}_i}}{2m_{\mathrm{e}}} - \sum_I \frac{\hbar^2 \boldsymbol{\nabla}^2_{\mathbf{R}_I}}{2M_I} \end{aligned} \tag{1.6}$$

The constitutive terms of the total molecular Hamiltonian are:

- The electrostatic repulsion between the electrons:

$$\hat{V}_{\mathrm{e}^- - \mathrm{e}^-} = \sum_{i<j} \frac{\mathrm{e}^2}{4\pi\epsilon_0 \parallel \mathbf{r}_i - \mathbf{r}_j \parallel}, \tag{1.7}$$

- The electrostatic repulsion between the nuclei:

$$\hat{V}_{\text{nu}-\text{nu}} = \sum_{I<J} \frac{\mathrm{e}^2 Z_I Z_J}{4\pi\epsilon_0 \parallel \mathbf{R}_I - \mathbf{R}_J \parallel}, \tag{1.8}$$

- The electrostatic attraction between the electrons and the nuclei

$$\hat{V}_{\text{nu}-\mathrm{e}^-} = -\sum_i \sum_I \frac{\mathrm{e}^2 Z_I}{4\pi\epsilon_0 \parallel \mathbf{R}_I - \mathbf{r}_i \parallel}, \tag{1.9}$$

- The kinetic energy term for the electrons:

$$\hat{T}_{\mathrm{e}^-} = -\sum_i \frac{\hbar^2 \boldsymbol{\nabla}^2_{\mathbf{r}_i}}{2m_{\mathrm{e}}}, \tag{1.10}$$

- And the kinetic energy term for the nuclei:

$$\hat{T}_{\mathrm{nu}} = -\sum_I \frac{\hbar^2 \boldsymbol{\nabla}^2_{\mathbf{R}_I}}{2M_I} \tag{1.11}$$

respectively, where e is the elementary charge, ϵ_0 the permittivity of vacuum, $\mathbf{r}_i$ the position operator associated to the i^{th} electron spatial coordinate, Z_I the atomic number of the I^{th} nucleus, $\hbar$ the reduced Planck's constant, and $\boldsymbol{\nabla}_{\mathbf{r}_i}$ the Nabla operator associated to the i^{th} electron spatial coordinate.

The expression of the different terms in the total molecular Hamiltonian operator are nuclear coordinate dependent ($\hat{V}_{\mathrm{nu-nu}}$, $\hat{T}_{\mathrm{nu}}$), electronic coordinate dependent ($\hat{V}_{\mathrm{e}^- - \mathrm{e}^-}$, $\hat{T}_{\mathrm{e}^-}$) and depending on both electronic and nuclear coordinates ($\hat{V}_{\mathrm{nu-e}^-}$).

The Hamiltonian cannot be explicitely separated into an electronic part and a nuclear part because of $\hat{V}_{\mathrm{nu-e}^-}$. The total wave-function cannot be expressed then as a single product of a nuclear wave-function and an electronic wave-function. One must find specific approximations to breakdown this co-dependency.

It is possible to re-write the total molecular Hamiltonian operator as the sum of an electronic Hamiltonian operator and a nuclear kinetic operator:

$$\hat{H}_{\mathrm{mol}} = \hat{H}_{\mathrm{e}^-} + \hat{T}_{\mathrm{nu}} \tag{1.12}$$

$$\text{with, } \hat{H}_{\mathrm{e}^-} = \hat{V}_{\mathrm{e}^- - \mathrm{e}^-} + \hat{T}_{\mathrm{e}^-} + \hat{V}_{\mathrm{nu-e}^-} + \hat{V}_{\mathrm{nu-nu}} \tag{1.13}$$

$\hat{H}_{\mathrm{e}^-}$ denotes the electronic Hamiltonian. It is the sum of three local operators ($\hat{V}_{\mathrm{nu-nu}}$, $\hat{V}_{\mathrm{nu-e}^-}$, $\hat{V}_{\mathrm{e}^- - \mathrm{e}^-}$) and of one differential operator ($\hat{T}_{\mathrm{e}^-}$) according to the electronic coordinates. From now

on, the nuclear coordinates $\mathbf{R}$ are viewed as parameters for the electronic Hamiltonian. The total molecular wave-function can be recast as:

$$\begin{aligned} \Psi_{\text{mol}}(\mathbf{r},\mathbf{R}) &= \sum_{i}^{\infty}\sum_{I}^{\infty} C_{I}^{i}\phi_{I}(\mathbf{R})\psi_{i}(\mathbf{r};\mathbf{R}) \\ &= \sum_{i}^{\infty}\Phi_{i}(\mathbf{R})\psi_{i}(\mathbf{r};\mathbf{R}) \end{aligned} \tag{1.14}$$

where $(\psi_{i}(\mathbf{r};\mathbf{R}))_{i\in\mathbb{N}}$ is an infinite orthonormal basis set of electronic wave-functions which depends parametrically of the spatial nuclear coordinates and $(\phi_{I}(\mathbf{R}))_{I\in\mathbb{N}}$ is an infinite orthonormal basis set of nuclear wave-functions and C_{I}^{i} is the expansion coefficient on the i^{th} electronic wave-function of the I^{th} nuclear wave-function. The total molecular state can be represented in the state space but $|\psi_{i}\rangle$ is known for a given set of nuclear spatial coordinates. The nuclear wave-functions cannot be represented in the state space anymore, they are considered as nuclear "factors".

$$\begin{aligned} |\Psi_{\text{mol}}\rangle &= \sum_{i}^{\infty}\sum_{I}^{\infty} C_{I}^{i}\phi_{I}(\mathbf{R})\,|\psi_{i}\rangle \\ &= \sum_{i}^{\infty}\Phi_{i}(\mathbf{R})\,|\psi_{i}\rangle \end{aligned} \tag{1.15}$$

As $|\psi_{i}\rangle$ has a given value for each $\mathbf{R}$, one should write $|\psi_{i};\mathbf{R}\rangle$ or $|\psi_{i}(\mathbf{R})\rangle$ but the generic expression $|\psi_{i}\rangle$ is kept for simplicity. Including eq. 1.15 in eq. 1.4, we get:

$$\sum_{i}^{\infty}\hat{H}_{\text{mol}}\Phi_{i}(\mathbf{R})\,|\psi_{i}\rangle = E_{\text{mol}}\sum_{i}^{\infty}\Phi_{i}(\mathbf{R})\,|\psi_{i}\rangle \tag{1.16}$$

where E_{mol} is the total molecular energy. By multipling on the left by $\langle\psi_{i}|$ eq. 1.16 and since $(\psi_{i}(\mathbf{r};\mathbf{R}))_{i\in\mathbb{N}}$ is an infinite orthonormal basis set, we have:

$$\sum_{j}^{\infty}\langle\psi_{i}|\,\hat{H}_{\text{mol}}\,|\psi_{j}\rangle\,\Phi_{j}(\mathbf{R}) = \delta_{ij}E_{\text{mol}}\Phi_{j}(\mathbf{R}) \tag{1.17}$$

Eq. 1.16 describes the action of the molecular Hamiltonian onto the nuclear factors. To get a better understanding of eq. 1.16 let us consider a system composed of only two electronic states and two corresponding nuclear factors respectively labelled: $|\psi_{1}\rangle$, $|\psi_{2}\rangle$, and $\Phi_{1}(\mathbf{R})$, $\Phi_{2}(\mathbf{R})$ such

that the molecular state reads:

$$|\Psi_{\text{mol}}\rangle = \Phi_1(\mathbf{R})\,|\psi_1\rangle + \Phi_2(\mathbf{R})\,|\psi_2\rangle \tag{1.18}$$

Then, one gets the coupled equations:

$$\begin{cases} \langle\psi_1|\,\hat{H}_{\text{mol}}\,|\psi_1\rangle\,\Phi_1(\mathbf{R}) + \langle\psi_1|\,\hat{H}_{\text{mol}}\,|\psi_2\rangle\,\Phi_2(\mathbf{R}) &= E_{\text{mol}}\Phi_1(\mathbf{R}) \\ \\ \langle\psi_2|\,\hat{H}_{\text{mol}}\,|\psi_1\rangle\,\Phi_1(\mathbf{R}) + \langle\psi_2|\,\hat{H}_{\text{mol}}\,|\psi_2\rangle\,\Phi_2(\mathbf{R}) &= E_{\text{mol}}\Phi_2(\mathbf{R}) \end{cases} \tag{1.19}$$

Eq. 1.19 expresses the action of the molecular Hamiltonian onto the first and the second electronic states: $\langle\psi_1|\,\hat{H}_{\text{mol}}\,|\psi_1\rangle$ and $\langle\psi_2|\,\hat{H}_{\text{mol}}\,|\psi_2\rangle$, and the coupling between the two electronic states: $\langle\psi_1|\,\hat{H}_{\text{mol}}\,|\psi_2\rangle$ and $\langle\psi_2|\,\hat{H}_{\text{mol}}\,|\psi_1\rangle$.

The molecular Hamiltonian is the sum of the electronic Hamiltonian and the nuclear kinetic operator, the action of the two operators onto the electronic kets can be expressed as follows: $\hat{H}_{ij} = \langle\psi_i|\,\hat{H}_{\text{e}^-}\,|\psi_j\rangle$ and $\hat{T}_{ij} = \langle\psi_i|\,\hat{T}_{\text{nu}}\,|\psi_j\rangle$. The electronic wave-functions are often supposed to be real and it is supposed that they are in this work. We have then, $\hat{H}_{ij} = \hat{H}_{ji}$ for $i \neq j$. $\hat{H}_{ij}$ and $\hat{T}_{ij}$ remain operators since they act on the nuclear coordinates.

The total molecular Hamiltonian expressed in the electronic basis set and acting on the nuclear factors is equivalent to write the Hamiltonian operator matrix depending on the nuclear coordinates. We then get the matrices of operators and the corresponding coupled equations as

$$\begin{pmatrix} \hat{H}_{11} + \hat{T}_{11} & \hat{H}_{21} + \hat{T}_{21} \\ \hat{H}_{12} + \hat{T}_{12} & \hat{H}_{22} + \hat{T}_{22} \end{pmatrix} \begin{pmatrix} \Phi_1(\mathbf{R}) \\ \Phi_2(\mathbf{R}) \end{pmatrix} = E_{\text{mol}} \begin{pmatrix} \Phi_1(\mathbf{R}) \\ \Phi_2(\mathbf{R}) \end{pmatrix} \tag{1.20}$$

Until now, no approximation has been performed to separate the nuclear part from the electronic part in the total molecular Hamiltonian. That is why eq. 1.19 gives us coupled equations and a full matrix in eq. 1.20. To have decoupled equations, one should have:

$$\hat{H}_{12} + \hat{T}_{12} = \hat{H}_{21} + \hat{T}_{21} = \hat{0} \tag{1.21}$$

We are going to make several assumptions and approximations in the following sections and discuss on the pros and the cons of the approximations which are not always valid.

1.2.1 Adiabatic basis set

According to previous notations, the matrix representation of the electronic Hamiltonian operator in the electronic basis set $(|\psi_1\rangle, |\psi_2\rangle)$ reads:

$$\mathbf{H}_{\mathrm{e}^-}(\mathbf{R}) = \begin{pmatrix} H_{11}(\mathbf{R}) & H_{21}(\mathbf{R}) \\ H_{12}(\mathbf{R}) & H_{22}(\mathbf{R}) \end{pmatrix} \tag{1.22}$$

Here, the electronic potential elements of the matrix are multiplicative operators and not differential operators as in eq. 1.20. Since the electronic matrix is Hermitian, it can be unitarily diagonalized. Typically, for two real states, there is a unitary matrix (here, orthogonal) $\mathbf{\Theta}$ such as:

$$\mathbf{\Theta}^{\dagger}(\mathbf{R})\mathbf{H}_{\mathrm{e}^-}(\mathbf{R})\mathbf{\Theta}(\mathbf{R}) = \begin{pmatrix} V_1(\mathbf{R}) & 0 \\ 0 & V_2(\mathbf{R}) \end{pmatrix} \tag{1.23}$$

The unitary matrix $\mathbf{\Theta}$ reads:

$$\mathbf{\Theta} = \begin{pmatrix} \cos\left(\theta(\mathbf{R})\right) & \sin\left(\theta(\mathbf{R})\right) \\ -\sin\left(\theta(\mathbf{R})\right) & \cos\left(\theta(\mathbf{R})\right) \end{pmatrix} , \tag{1.24}$$

where the $\theta(\mathbf{R})$ angle satisfies:

$$\tan\left(2\theta(\mathbf{R})\right) = -\frac{2\langle\psi_1|\hat{H}_{\mathrm{e}^-}|\psi_2\rangle}{\langle\psi_2|\hat{H}_{\mathrm{e}^-}|\psi_2\rangle - \langle\psi_1|\hat{H}_{\mathrm{mol}}|\psi_1\rangle} \tag{1.25}$$

$\tan\left(2\theta(\mathbf{R})\right)$ is not defined when $\langle\psi_2|\hat{H}_{\mathrm{mol}}|\psi_2\rangle = \langle\psi_1|\hat{H}_{\mathrm{mol}}|\psi_1\rangle$. We are going to see in the following sections that it is not possible to define the angle $\theta(\mathbf{R})$ when two electronic states are degenerate. Further details are given in the end of this chapter.

The two electronic states that are eigenvectors of $\mathbf{H}_{\mathrm{e}^-}(\mathbf{R})$ are commonly called *adiabatic electronic states* ($\left|\psi_1^{\mathrm{ad}}\right\rangle, \left|\psi_2^{\mathrm{ad}}\right\rangle$) such that

$$\begin{cases} \left|\psi_1^{\mathrm{ad}}\right\rangle = \cos\left(\theta(\mathbf{R})\right)|\psi_1\rangle + \sin\left(\theta(\mathbf{R})\right)|\psi_2\rangle \\ \left|\psi_2^{\mathrm{ad}}\right\rangle = -\sin\left(\theta(\mathbf{R})\right)|\psi_1\rangle + \cos\left(\theta(\mathbf{R})\right)|\psi_2\rangle \end{cases} \tag{1.26}$$

The adiabatic electronic states are the eigenvectors of the eigenvalue problem of the electronic Hamiltonian operator:

$$\hat{\mathrm{H}}_{\mathrm{e}^-}(\mathbf{R})\left|\psi_{1,2}^{\mathrm{ad}}\right\rangle = V_{1,2}(\mathbf{R})\left|\psi_{1,2}^{\mathrm{ad}}\right\rangle \tag{1.27}$$

The "*adiabatic*" term is referred in the superscript "$^{\mathrm{ad}}$". The *adiabatic* word is used because in an adiabatic transformation or during an adiabatic evolution, the transformation is considered infinitesimally slow. Here the nuclear spatial coordinates are viewed as parameters for the electronic Hamiltonian and for the electronic wave-functions (*i.e.*, the nuclei are moving infinitesimally slowly) and so the electronic system adapts immediately. For each nuclear spatial coordinate, one can determine distinct adiabatic electronic states with respect to the validity of eq. 1.25.

Even though the electronic potential coupling is zero for an adiabatic electronic basis, the coupled equations in eq. 1.19 remain coupled through the adiabatic nuclear kinetic coupling operator: $\hat{T}_{12}^{\mathrm{ad}} = \left\langle \psi_1^{\mathrm{ad}} \right| \hat{T}_{\mathrm{nu}} \left| \psi_2^{\mathrm{ad}} \right\rangle \neq 0$ and $\hat{T}_{21}^{\mathrm{ad}} = \left\langle \psi_2^{\mathrm{ad}} \right| \hat{T}_{\mathrm{nu}} \left| \psi_1^{\mathrm{ad}} \right\rangle \neq 0$.

The coupled equations give:

$$\begin{cases} (\hat{V}_1 + \hat{T}_{11}^{\mathrm{ad}})\Phi_1(\mathbf{R}) + \hat{T}_{21}^{\mathrm{ad}}\Phi_2^{\mathrm{ad}}(\mathbf{R}) = E_{\mathrm{mol}}\Phi_1^{\mathrm{ad}}(\mathbf{R}) \\ \\ \hat{T}_{12}^{\mathrm{ad}}\Phi_1(\mathbf{R}) + (\hat{V}_2 + \hat{T}_{22}^{\mathrm{ad}})\Phi_2^{\mathrm{ad}}(\mathbf{R}) = E_{\mathrm{mol}}\Phi_2^{\mathrm{ad}}(\mathbf{R}) \end{cases} \tag{1.28}$$

The full operator matrix in eq. 1.20 written in an electronic adiabatic basis set reads now:

$$\begin{pmatrix} \hat{V}_1 + \hat{T}_{11}^{\mathrm{ad}} & \hat{T}_{21}^{\mathrm{ad}} \\ \hat{T}_{12}^{\mathrm{ad}} & \hat{V}_2 + \hat{T}_{22}^{\mathrm{ad}} \end{pmatrix} \begin{pmatrix} \Phi_1^{\mathrm{ad}}(\mathbf{R}) \\ \Phi_2^{\mathrm{ad}}(\mathbf{R}) \end{pmatrix} = E_{\mathrm{mol}} \begin{pmatrix} \Phi_1^{\mathrm{ad}}(\mathbf{R}) \\ \Phi_2^{\mathrm{ad}}(\mathbf{R}) \end{pmatrix} \tag{1.29}$$

In the next section, we are going to see under what circumstances one can neglect the adiabatic nuclear kinetic coupling terms within the adiabatic point of view.

1.2.2 The Born-Oppenheimer Approximation

The Born-Oppenheimer approximation (BOA) is one of the most famous approximations used in quantum chemistry calculations: we assume that the nuclear masses tend to infinity.

Such an approximation is consistent with the physical picture of an atom in a molecular system which mass is almost equal to the mass of the nuclei. In this thesis we studied systems

based on carbon and hydrogen and so we have $\frac{m_e}{M_{nu(C)}} = 5.0\,10^{-5}$ and $\frac{m_e}{M_{nu(H)}} = 5.0\,10^{-4}$. In this subsection, we are going to study the effect of the BOA on the coupled equations in eq. 1.19.

The nuclear masses occur in the nuclear kinetic operator (see eq. 1.11). For a two-electronic-state approximation, the effect of the nuclear kinetic operator over the total molecular ket expressed in an adiabatic electronic basis gives:

$$\hat{T}_{\mathrm{nu}} \left|\Psi_{\mathrm{mol}}\right\rangle = \sum_I -\frac{\hbar}{2M_I}\hat{\nabla}^2_{\mathbf{R}_I}\left[\Phi_1^{\mathrm{ad}}(\mathbf{R})\left|\psi_1^{\mathrm{ad}}\right\rangle + \Phi_2^{\mathrm{ad}}(\mathbf{R})\left|\Phi_2^{\mathrm{ad}}\right\rangle\right] \tag{1.30}$$

The adiabatic picture is such that for each spatial nuclear coordinates $\Phi_1^{\mathrm{ad}}(\mathbf{R})\left|\psi_1^{\mathrm{ad}}\right\rangle$ and $\Phi_2^{\mathrm{ad}}(\mathbf{R})\left|\psi_2^{\mathrm{ad}}\right\rangle$ are continuous and vary smoothly, except around crossings.

Mathematically speaking the first and the second derivative terms of the nuclear factors and of the adiabatic wave-function are significantly lower than the nuclear masses and so we can approximate the action of the nuclear kinetic operator over the molecular wave-function as acting only on the uncoupled nuclear factors ($\hat{T}_{nu}\Phi_i^{\mathrm{ad}}(\mathbf{R})$).

Chemically speaking the nuclei are "viewed" as being static according to the electrons. For each coordinate there is a unique electronic and nuclear state that characterizes a molecular state.

The coupled equations (see eq. 1.28) become uncoupled and read:

$$\begin{aligned}
\left\langle\psi_1^{\mathrm{ad,BOA}}\right|\hat{H}_{\mathrm{mol}}\left|\psi_1^{\mathrm{ad,BOA}}\right\rangle\Phi_1^{\mathrm{ad,BOA}}(\mathbf{R}) &= E_{\mathrm{mol}}^{\mathrm{BOA}}\Phi_1^{\mathrm{ad,BOA}}(\mathbf{R}) \\
\left\langle\psi_2^{\mathrm{ad,BOA}}\right|\hat{H}_{\mathrm{mol}}\left|\psi_2^{\mathrm{ad,BOA}}\right\rangle\Phi_2^{\mathrm{ad,BOA}}(\mathbf{R}) &= E_{\mathrm{mol}}^{\mathrm{BOA}}\Phi_2^{\mathrm{ad,BOA}}(\mathbf{R})
\end{aligned} \tag{1.31}$$

Using the operator matrix in eq. 1.29 yields

$$\begin{pmatrix} \hat{T}_{11}^{\mathrm{BOA}} + \hat{V}_1^{\mathrm{BOA}} & 0 \\ 0 & \hat{T}_{22}^{\mathrm{BOA}} + \hat{V}_2^{\mathrm{BOA}} \end{pmatrix}\begin{pmatrix} \Phi_1^{\mathrm{ad,BOA}}(\mathbf{R}) \\ \Phi_2^{\mathrm{ad,BOA}}(\mathbf{R}) \end{pmatrix} = E_{\mathrm{mol}}^{\mathrm{BOA}}\begin{pmatrix} \Phi_1^{\mathrm{ad,BOA}}(\mathbf{R}) \\ \Phi_2^{\mathrm{ad,BOA}}(\mathbf{R}) \end{pmatrix} \tag{1.32}$$

The uncoupled equations (eq. 1.31) allow us to determine two single-product molecular states such that

$$\left|\Psi_1^{\mathrm{BOA}}\right\rangle = \Phi_1^{\mathrm{ad,BOA}}(\mathbf{R})\left|\psi_1^{\mathrm{ad,BOA}}\right\rangle \tag{1.33}$$

and

$$\left|\Psi_2^{\mathrm{BOA}}\right\rangle = \Phi_2^{\mathrm{ad,BOA}}(\mathbf{R})\left|\psi_2^{\mathrm{ad,BOA}}\right\rangle \tag{1.34}$$

More generally, the total molecular ket is now reduced to a single product of an adiabatic nuclear wave-function and an adiabatic electronic wave-function:

$$\Psi_{\text{mol}}^{\text{BOA}}(\mathbf{r},\mathbf{R}) = \Phi^{\text{ad,BOA}}(\mathbf{R})\psi^{\text{ad,BOA}}(\mathbf{r};\mathbf{R}) \tag{1.35}$$

which gives in ket representation:

$$\left|\Psi_{\text{mol}}^{\text{ad,BOA}}\right\rangle = \Phi^{\text{ad,BOA}}(\mathbf{R})\left|\psi^{\text{ad,BOA}}\right\rangle \tag{1.36}$$

Such an expression shows that the BOA is an adiabatic approximation.

Thus, within the BOA, $V_i^{\text{BOA}}(\mathbf{R})$ represents a potential energy for the nuclei associated to the i^{th} electronic adiabatic state. Even though the nuclear coordinate vector $\mathbf{R}$ spans in $\mathbb{R}^{3N_{\text{nu}}}$ but the potential energy is invariant along translation and rotation displacement. It maps then, a $3N_{\text{nu}} - 6$-dimensional hypersurface for a non-linear molecular system and a $3N_{\text{nu}} - 5$ for a linear molecular system. Such a hypersurface is called a potential energy surface (PES) for the motion of the nuclei.

1.3 A vibrational point of view in the case of the Born-Oppenheimer approximation

1.3.1 Study of a unique potential energy surface

In this section we consider the i^{th} electronic state as a unique adiabatic electronic state and the Born-Oppenheimer approximation being valid.

As it has been explained in the end of the previous section, the adiabatic electronic energy $V_i^{BOA}(\mathbf{R})$ maps a hypersurface of $3N_{\text{nu}}-6$ dimensions but the nuclear spatial coordinates belong to a space of $3N_{\text{nu}}$ dimensions. In this thesis, we are focused on the exploration of PES and on the characterization of it. In our case it is then useful to reduce the $3N_{\text{nu}}$ nuclear spatial coordinates to a set of $3N_{\text{nu}} - 6$ nuclear spatial coordinates that describes only the "vibrations".

The general nuclear spatial vectors $(\mathbf{R}_I)_{\mathbb{R}^{3N_{\text{nu}}}}$ are chosen without any specific assumption. The reference frame in which the vectors are expressed is assumed to be Galilean and is called *laboratory fixed* (LF). Within the LF frame, the molecular Hamiltonian is explicitly separated within electronic and nuclear spatial coordinates. The first transformation that can be made is to translate the origin of the LF frame at the total molecular center of mass. The center of

mass is often approximated to the nuclear center of mass as the nuclei are much heavier than the electrons. The deviation from the total molecular center of mass to the nuclear center of mass is call the mass polarization.

The orientation of the axes of the LF frame is invariant along this transformation. The new reference frame is called $space-fixed$ (SF). The new nuclear spatial vectors are built such that

$$\mathbf{R}_{I_{SF}} = \mathbf{R}_I - \frac{1}{\sum\limits_J M_J} \sum_K M_K \mathbf{R}_K \tag{1.37}$$

The coordinate transformation can be summarized as

$$(\mathbf{R}_{1_{SF}}, \ldots, \mathbf{R}_{N_{\mathrm{nu}SF}}) \rightarrow (\frac{1}{\sum\limits_J M_J} \sum_K M_K \mathbf{R}_K, \mathbf{R}_2, \ldots, \mathbf{R}_{N_{\mathrm{nu}}}) \tag{1.38}$$

Thanks to the latter transformation, the translational kinetic energy can be separated from the total LF kinetic energy. The molecular Hamiltonian of eq. 1.6 expressed in the SF reference frame is called rovibronic Hamiltonian.

The molecular system is supposed to be in the rotational ground-state $J = 0$ and the electrons are moving adiabatically with respect to the nuclear displacements; there is no Coriolis effect. One can built a third reference frame such that the kinetic energies are invariant according to any rotational displacement of the nuclei. Such a reference frame is called $body-fixed$ (BF). Its origin is also at the total molecular center of mass. The directions of the axes are "attached to the nuclei" via some constraints. The new coordinates read

$$\mathbf{R}_{I_{BF}} = \mathbf{C}\mathbf{R}_{I_{SF}} \tag{1.39}$$

where $\mathbf{C}(\alpha, \beta, \gamma)$ is a rotation matrix that depends on three Euler angles (α, β, γ) and so it depends on three parameters. The BF frame rotates then with the nuclei.
In the BF reference frame we have defined $3N_{\mathrm{nu}} - 6$ internal coordinates where the rotations and translations have been removed. These internal coordinates can be viewed as vibrational coordinates. Then, the associated vectors are called vibrational normal modes and they are defined at an equilibrium geometry.

1.3.2 Photoexcitations

The electronic and vibrational ground state of a molecular system (again, assuming J=0) is the lowest solution of the eigenvalue problem associated to the molecular Hamiltonian. Within the BOA the ground state is characterized by the molecular state:

$$\left|\Psi_0^{\mathrm{BOA}}\right\rangle = \Phi_0^{\mathrm{ad,BOA}} \left|\psi_0^{\mathrm{ad,BOA}}\right\rangle \tag{1.40}$$

and by the ground state adiabatic electronic energy: $E_0^{\mathrm{BOA}}(\mathbf{R})$.

Electronic excited states of a molecular system are then eigenvectors of the electronic Hamiltonian for which the eigenvalues are higher than $E_0^{\mathrm{BOA}}(\mathbf{R})$. Eckart's conditions are supposed to be fulfilled so the nuclear factors can be written as the product of translational, rotational and vibrational contributions. [98] The translational energy can be high compared to the electronic energy but the system potential energy is invariant along a translational displacement. The rotational energies are considered here to be too small to be taken into account. The vibrational nuclear factor $\Phi_\nu(\mathbf{R})$ is then only described by $3N_{\mathrm{nu}} - 6$ vibrational wave-functions within the harmonic approximation.

The excitation from the ground state (or an excited state) toward a higher excited state is governed by the electric dipole moment operator which acts on the electronic and on the vibrational wave-function. The transition dipole moment between $|\Psi'\rangle$ and $|\Psi''\rangle$ is defined as

$$\boldsymbol{\mu}_{tr} = \left\langle \Psi' \right| \hat{\boldsymbol{\mu}} \left| \Psi'' \right\rangle = \left\langle \Psi' \right| \hat{\boldsymbol{\mu}}_{\mathrm{nu}} + \hat{\boldsymbol{\mu}}_{\mathrm{e^-}} \left| \Psi'' \right\rangle \tag{1.41}$$

where $\hat{\boldsymbol{\mu}}$ is the dipole operator, $\hat{\boldsymbol{\mu}}_{\mathrm{nu}}$ the nuclear dipole operator and $\hat{\boldsymbol{\mu}}_{\mathrm{e^-}}$ the electronic dipole operator such as:

$$\hat{\boldsymbol{\mu}} = \hat{\boldsymbol{\mu}}_{\mathrm{nu}} + \hat{\boldsymbol{\mu}}_{\mathrm{e^-}} = \sum_I eZ_I\mathbf{R}_I - \sum_i e\mathbf{r}_i \tag{1.42}$$

Within the BOA, thanks to eqs. 1.36, 1.41 reads:

$$\boldsymbol{\mu}_{tr} = \left\langle \Phi^{\mathrm{BOA}\prime}\psi^{\mathrm{ad,BOA}\prime} \right| \hat{\boldsymbol{\mu}}_{\mathrm{nu}} + \hat{\boldsymbol{\mu}}_{\mathrm{e^-}} \left| \Phi^{\mathrm{BOA}\prime\prime}\psi^{\mathrm{ad,BOA}\prime\prime} \right\rangle \tag{1.43}$$

The term $\left\langle \Phi^{\mathrm{BOA}\prime}\psi^{\mathrm{ad,BOA}\prime}\right| \hat{\boldsymbol{\mu}}_{\mathrm{nu}} \left|\Phi^{\mathrm{BOA}\prime\prime}\psi^{\mathrm{ad,BOA}\prime\prime}\right\rangle$ is equal to zero since two adiabatic electronic states are orthogonal to each other. The second term $\left\langle \Phi^{\mathrm{BOA}\prime}\psi^{\mathrm{ad,BOA}\prime}\right| \hat{\boldsymbol{\mu}}_{\mathrm{e^-}} \left|\Phi^{\mathrm{BOA}\prime\prime}\psi^{\mathrm{ad,BOA}\prime\prime}\right\rangle$ remains. The electronic transition dipole is defined such that:

$$\boldsymbol{\mu}_{tr}^{\mathrm{e}^-} = \left\langle \psi^{\mathrm{ad,BOA}\prime}\right| \hat{\boldsymbol{\mu}}_{\mathrm{e^-}} \left|\psi^{\mathrm{ad,BOA}\prime\prime}\right\rangle \tag{1.44}$$

The total transition dipole moment can then be expressed as

$$\left\langle \Psi^{\prime}\right| \hat{\boldsymbol{\mu}} \left|\Psi^{\prime\prime}\right\rangle = \left\langle \Phi^{\mathrm{BOA}\prime}\right| \hat{\boldsymbol{\mu}}_{tr}^{\mathrm{e}^-} \left|\Phi^{\mathrm{BOA}\prime\prime}\right\rangle \tag{1.45}$$

The analytic formula of $\boldsymbol{\mu}_{tr}^{\mathrm{e}^-}(\mathbf{R})$ is still unkown. The next approximation is called the $Franck-Condon$ approximation (FC approximation). The motivation for introducing a new approximation is that the photoexcitation occurs in such a short time that the transition is "static" for the nuclei. The first step of the FC approximation is to expand the electronic transition dipole moment in a Taylor series, at the equilibrium geometry of the initial adiabatic electronic state:

$$\begin{aligned}
\boldsymbol{\mu}_{tr}^{\mathrm{e}^-}(\mathbf{R}^{\prime}) &= \boldsymbol{\mu}_{tr}^{\mathrm{e}^-}(\mathbf{R}^{\prime}_{eq}) + \sum_I \left(\frac{\partial \boldsymbol{\mu}_{tr}^{\mathrm{e}^-}(\mathbf{R}^{\prime})}{\partial \mathbf{R}^{\prime}_I}\right)_{\mathbf{R}^{\prime}=\mathbf{R}^{\prime}_{eq}} (\mathbf{R}^{\prime}_I - \mathbf{R}^{\prime}_{eq}) \\
&\quad + \tfrac{1}{2}\sum_J\sum_K \left(\frac{\partial^2 \boldsymbol{\mu}_{tr}^{\mathrm{e}^-}(\mathbf{R}^{\prime})}{\partial \mathbf{R}^{\prime}_J \mathbf{R}^{\prime}_K}\right)_{\mathbf{R}^{\prime}=\mathbf{R}^{\prime}_{eq}} (\mathbf{R}^{\prime}_J - \mathbf{R}^{\prime}_{eq})(\mathbf{R}^{\prime}_K - \mathbf{R}^{\prime}_{eq}) \\
&\quad + \dots
\end{aligned} \tag{1.46}$$

The transition dipole moment can then be recast as:

$$\begin{aligned}
\left\langle \Psi^{\prime}\right| \hat{\mu} \left|\Psi^{\prime\prime}\right\rangle &= \boldsymbol{\mu}_{tr}^{e^-}(\mathbf{R}^{\prime}_{eq}) \left\langle \phi_\nu^{\mathrm{BOA}\prime}\right| \left|\phi_\nu^{\mathrm{BOA}\prime\prime}\right\rangle \\
&\quad + \sum_I \left(\frac{\partial \boldsymbol{\mu}_{tr}^{e^-}(\mathbf{R}^{\prime})}{\partial \mathbf{R}^{\prime}_I}\right)_{\mathbf{R}^{\prime}=\mathbf{R}^{\prime}_{eq}} \left\langle \phi_\nu^{\mathrm{BOA}\prime}\right| (\mathbf{R}^{\prime}_I - \mathbf{R}^{\prime}_{eq}) \left|\phi_\nu^{\mathrm{BOA}\prime\prime}\right\rangle \\
&\quad + \tfrac{1}{2}\sum_J\sum_K \left(\frac{\partial^2 \boldsymbol{\mu}_{\mathrm{e}^- tr}(\mathbf{R}^{\prime})}{\partial \mathbf{R}^{\prime}_J \mathbf{R}^{\prime}_K}\right)_{\mathbf{R}^{\prime}=\mathbf{R}^{\prime}_{eq}} \left\langle \phi_\nu^{\mathrm{BOA}\prime}\right| (\mathbf{R}^{\prime}_J - \mathbf{R}^{\prime}_{eq})(\mathbf{R}^{\prime}_K - \mathbf{R}^{\prime}_{eq}) \left|\phi_\nu^{\mathrm{BOA}\prime\prime}\right\rangle \\
&\quad + \dots
\end{aligned} \tag{1.47}$$

The FC approximation corresponds to an expansion of the transition dipole moment limited to the zeroth order term of eq. 1.47. When a transition is said as being fully-allowed, the electronic transition dipole $\boldsymbol{\mu}_{tr}^{e^-}(\mathbf{R}_{eq}^{'})$ is large. The main transition occurs from the initial vibrational nuclear state to the final vibrational nuclear state which overlaps it the most. The overlap between the two vibrational nuclear wave-functions is called the FC integral. The associated FC factors are $|\left\langle \phi_{\nu}^{\mathrm{BOA}\prime}\middle|\phi_{\nu}^{\mathrm{BOA}\prime\prime}\right\rangle|^2$. The transition is then "observed" for large FC factors, the transition is termed allowed.

But if $|\mu_{tr}^{e^-}(\mathbf{R}_{eq}^{'})| \approx 0$ the transition is no longer "observed" anymore and is termed weakly-allowed or even forbidden. For us, in practice, allowed and forbidden transitions, the oscillator strength is actually computed by the software that performs electronic structure calculations. For a zero or close to zero oscillator strength, the state is called an optically forbidden state or a dark state. For a significantly non-zero oscillator strength value, the state is called an optically active state or a bright state. The oscillator strength formula for a transition from the electronic ground state $|\Psi_0\rangle$ to the n^{th} electronic excited state $|\Psi_n\rangle$ is

$$f = \frac{8\pi\tilde{\nu}m_{\mathrm{e}}c}{3h\mathrm{e}} |\langle\Psi_0|\hat{\boldsymbol{\mu}}|\Psi_n\rangle|^2 \tag{1.48}$$

where c is the speed of light, $\tilde{\nu}$ the excitation energy in wavenumber.

1.4 Polarisable continuum model

The polarisable continuum model is a computational method that allows to describe the solvent effects on a molecular system. This method was used in this thesis due to its low computational cost and its qualitative efficiency for non-specific solvant-solute interactions [99–102].

It is based on the determination of a cavity around the molecular system (see fig. 1.1). The molecule is located inside the cavity while the solvent is considered as being continuous outside the cavity and is represented by an external potential $V(\mathbf{r})$.

To determine the external potential, let us consider two charge densities ρ and ρ' of the molecular system. The interaction energy of the two charge densities of the molecule inside the cavity and surrounded by the continuum reads:

$$E_{int}(\rho,\rho') = \int_{\mathbb{R}^3} \rho'(\mathbf{r})V(\mathbf{r})\mathrm{d}\mathbf{r} \tag{1.49}$$

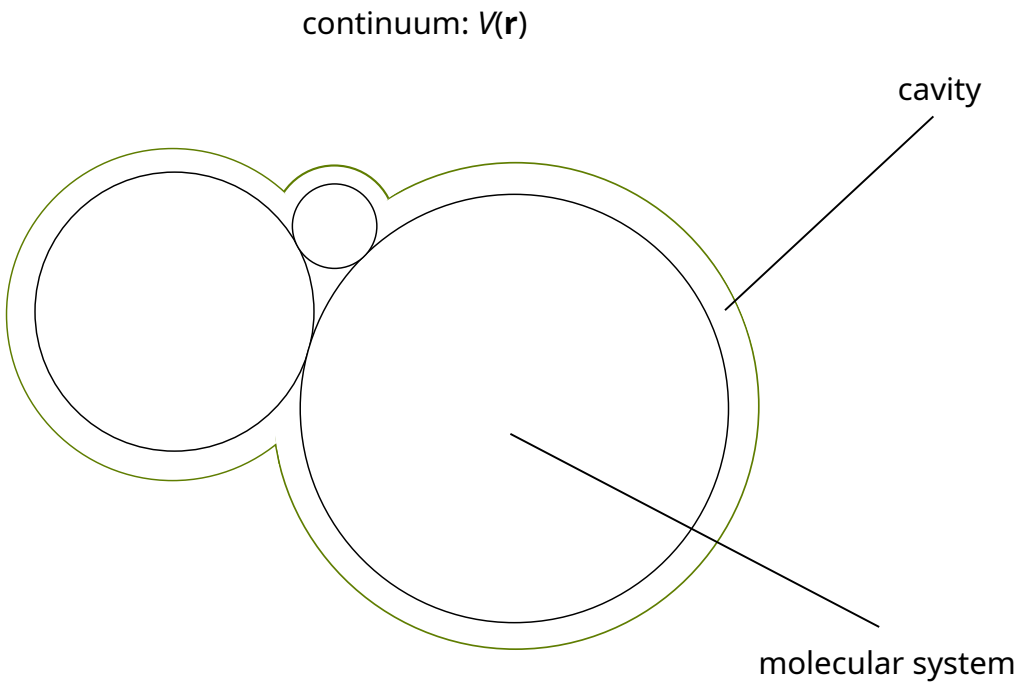

Figure 1.1: Schematic representation of a molecule inside a cavity and surrounded by a solvent that is associated to an external potential.

where $E_{int}(\rho, \rho')$ is the interaction energy.

The external potential $V(\mathbf{r})$ is determined by Poisson's equation:

$$-\nabla\Big[\epsilon(\mathbf{r})\nabla V(\mathbf{r})\Big] = 4\pi\rho(\mathbf{r}) \tag{1.50}$$

where $\epsilon(\mathbf{r})$ is the dielectric constant and we have $\epsilon(\mathbf{r}) = 1$ inside the cavity and $\epsilon(\mathbf{r}) = \epsilon_s$ outside the cavity and is equal to the dielectric constant of the solvant. Solving the Poisson equation we obtain:

• Inside the cavity:

$$-\nabla^2 V(\mathbf{r}) = 4\pi\rho(\mathbf{r}) \tag{1.51}$$

• Outside the cavity:

$$-\epsilon_s\nabla^2 V(\mathbf{r}) = 0 \tag{1.52}$$

Since the solvent creates charge on the surface of the cavity, the electrostatic interaction between

the solvent and the molecule can be rewritten such that:

$$V(\mathbf{r}) = V_s(\mathbf{r}) + V_\sigma(\mathbf{r}) \tag{1.53}$$

where $V_s(\mathbf{r})$ is the electrostatic potential generated by the charge distribution in the molecule and $V_\sigma(\mathbf{r})$ is the electrostatic potential generated by the polarisation of the continous solvent. $V_\sigma(\mathbf{r})$ reads:

$$V_\sigma(\mathbf{r}) = \int_{\mathbb{R}^3} \frac{\sigma(\mathbf{r}')}{\mid \mathbf{r} - \mathbf{r}' \mid} \mathrm{d}^3\mathbf{r}' \tag{1.54}$$

The polarisation continuum method consists in the determination of the surface $\sigma(\mathbf{r}')$ which defines the potential $V_\sigma(\mathbf{r})$. The surface $\sigma(\mathbf{r}')$ reads:

$$\sigma(\mathbf{r}) = \frac{\epsilon_s - 1}{4\pi} \frac{\partial}{\partial \mathbf{n}} \Big[V_s(\mathbf{r}) + V_\sigma(\mathbf{r}) \Big] \tag{1.55}$$

where $\mathbf{n}$ is a unit vector that is applied at the surface of the cavity.

1.5 The limits of the Born-Oppenheimer Approximation

Eq. 1.25 gives us a hint of a problem within the adiabatic representation. There is an issue when two adiabatic electronic states are degenerate.
If we project $\hat{T}_{\mathrm{nu}} \left| \Psi_{\mathrm{mol}} \right\rangle$ onto the adiabatic electronic wave-function basis we get:

$$\begin{aligned} \hat{T}^{\mathrm{ad}}_{ij} \Phi^{\mathrm{ad}}_j(\mathbf{R}) = \sum_I - \frac{\hbar^2}{2M_I} \Big[& \delta_{ij} \hat{\nabla}^2_{\mathbf{R}_I} \Phi^{\mathrm{ad}}_j(\mathbf{R}) \\ & + 2 \left\langle \psi^{\mathrm{ad}}_i \middle| \hat{\nabla}_{\mathbf{R}_I} \psi^{\mathrm{ad}}_j \right\rangle \hat{\nabla}_{\mathbf{R}_I} \Phi^{\mathrm{ad}}_j(\mathbf{R}) \\ & + \left\langle \psi^{\mathrm{ad}}_i \middle| \hat{\nabla}^2_{\mathbf{R}_I} \psi^{\mathrm{ad}}_j \right\rangle \Phi^{\mathrm{ad}}_j(\mathbf{R}) \Big] \end{aligned} \tag{1.56}$$

From this general formula, the sum can be written as three terms:

The zeroth-order term, the kinetic energy that is acting on the nuclear factors:

$$A_{ij}(\mathbf{R}) = \delta_{ij} \hat{\nabla}^2_{\mathbf{R}} \Phi^{\mathrm{ad}}_j(\mathbf{R}) \tag{1.57}$$

The first-order term (first-order non-adiabatic coupling):

$$\mathbf{F}_{ij}(\mathbf{R}) = \left\langle \psi_i^{\mathrm{ad}} \middle| \hat{\nabla}_{\mathbf{R}} \psi_j^{\mathrm{ad}} \right\rangle \tag{1.58}$$

The second-order term (second-order non-adiabatic coupling):

$$G_{ij}(\mathbf{R}) = \left\langle \psi_i^{\mathrm{ad}} \middle| \hat{\nabla}_{\mathbf{R}}^2 \psi_j^{\mathrm{ad}} \right\rangle \tag{1.59}$$

The first and second-order non-adiabatic couplings diverge when two adiabatic electronic states become degenerate.

For the i^{th} and the j^{th} adiabatic electronic state we have:

$$\left\langle \psi_i^{\mathrm{ad}} \right| \hat{H}_{\mathrm{e}^-} \left| \psi_i^{\mathrm{ad}} \right\rangle = V_i(\mathbf{R}), \tag{1.60}$$

and

$$\left\langle \psi_j^{\mathrm{ad}} \right| \hat{H}_{\mathrm{e}^-} \left| \psi_i^{\mathrm{ad}} \right\rangle = \left\langle \psi_i^{\mathrm{ad}} \right| \hat{H}_{\mathrm{e}^-} \left| \psi_j^{\mathrm{ad}} \right\rangle = 0 \tag{1.61}$$

for $i \neq j$.

As the electronic coupling terms are equal to zero for every nuclear spatial coordinates, the gradient of it $\nabla_{\mathbf{R}} \Big(\left\langle \psi_j^{\mathrm{ad}} \right| \hat{H}_{\mathrm{e}^-} \left| \psi_i^{\mathrm{ad}} \right\rangle \Big)$ is equal to zero as well. We have:

$$\left\langle \hat{\nabla}_{\mathbf{R}} \psi_j^{\mathrm{ad}} \right| \hat{H}_{\mathrm{e}^-} \left| \psi_i^{\mathrm{ad}} \right\rangle + \left\langle \psi_j^{\mathrm{ad}} \right| \hat{\nabla}_{\mathbf{R}} \hat{H}_{\mathrm{e}^-} \left| \psi_i^{\mathrm{ad}} \right\rangle + \left\langle \psi_j^{\mathrm{ad}} \right| \hat{H}_{\mathrm{e}^-} \left| \hat{\nabla}_{\mathbf{R}} \psi_i^{\mathrm{ad}} \right\rangle = 0 \tag{1.62}$$

Since $\left|\psi_i^{\mathrm{ad}}\right\rangle$ and $\left|\psi_j^{\mathrm{ad}}\right\rangle$ are eigenvectors of the electronic Hamiltonian, we get:

$$V_i(\mathbf{R}) \left\langle \hat{\nabla}_{\mathbf{R}} \psi_j^{\mathrm{ad}} \middle| \psi_i^{\mathrm{ad}} \right\rangle + \left\langle \psi_j^{\mathrm{ad}} \right| \hat{\nabla}_{\mathbf{R}} \hat{H}_{\mathrm{e}^-} \left| \psi_i^{\mathrm{ad}} \right\rangle + V_j(\mathbf{R}) \left\langle \psi_j^{\mathrm{ad}} \middle| \hat{\nabla}_{\mathbf{R}} \psi_i^{\mathrm{ad}} \right\rangle = 0 \tag{1.63}$$

The adiabatic electronic wave-functions are orthonormal to each other, we can write that:

$$0 = \hat{\nabla}_{\mathbf{R}} \left\langle \psi_j^{\mathrm{ad}} \middle| \psi_i^{\mathrm{ad}} \right\rangle = \left\langle \hat{\nabla}_{\mathbf{R}} \psi_j^{\mathrm{ad}} \middle| \psi_i^{\mathrm{ad}} \right\rangle + \left\langle \psi_j^{\mathrm{ad}} \middle| \hat{\nabla}_{\mathbf{R}} \psi_i^{\mathrm{ad}} \right\rangle \tag{1.64}$$

That is to say:

$$\left\langle \hat{\nabla}_{\mathbf{R}} \psi_j^{\mathrm{ad}} \middle| \psi_i^{\mathrm{ad}} \right\rangle = - \left\langle \psi_j^{\mathrm{ad}} \middle| \hat{\nabla}_{\mathbf{R}} \psi_i^{\mathrm{ad}} \right\rangle \tag{1.65}$$

This allows us to write eq. 1.63 as:

$$(V_j(\mathbf{R}) - V_i(\mathbf{R})) \left\langle \psi_j^{\text{ad}} \middle| \hat{\nabla}_{\mathbf{R}} \psi_i^{\text{ad}} \right\rangle + \left\langle \psi_j^{\text{ad}} \middle| \hat{\nabla}_{\mathbf{R}} \hat{H}_{\text{e}^-} \middle| \psi_i^{\text{ad}} \right\rangle = 0 \tag{1.66}$$

We recognize the first-order non-adiabatic coupling in the previous equation ($\mathbf{F}_{ij}(\mathbf{R}) = \left\langle \psi_j^{\text{ad}} \middle| \hat{\nabla}_{\mathbf{R}} \psi_i^{\text{ad}} \right\rangle$). The latter equation provides the expression for the first-order non-adiabatic coupling which is also called the $Off - diagonal\ Hellmann - Feynman\ theorem$:

$$\mathbf{F}_{ij}(\mathbf{R}) = \frac{\left\langle \psi_i^{\text{ad}} \middle| \hat{\nabla}_{\mathbf{R}} \hat{H}_{\text{e}^-} \middle| \psi_j^{\text{ad}} \right\rangle}{V_j(\mathbf{R}) - V_i(\mathbf{R})} \tag{1.67}$$

As it can be deduced from the off-diagonal Hellmann-Feynman theorem, the first-order non-adiabatic coupling diverges when two adiabatic electronic states are close to each other in terms of energy. In conclusion, the BOA is valid and so the kinetic coupling terms can be neglected as long as the adiabatic electronic states are "far from each other": as long as $V_i(\mathbf{R}) \neq V_j(\mathbf{R})$ significantly. We get back to the adiabatic approximation which considers to describe the molecular state with a single product of adiabatic electronic and nuclear states.

When two or more adiabatic states have the same electronic energies, they cross and are degenerate. The locus of a crossing is called a conical intersection. The behavior of adiabatic electronic energies in the vicinity of a conical intersection will be explained in chapter 2.

Chapter 2

Conical intersections

2.1 Introduction

The present chapter is based on materials presented in several books. [93, 103–105]

Within the Born Oppenheimer approximation (BOA), the nuclear spatial coordinates are considered to be parameters of the molecular system. Minima on PES are associated to equilibrium molecular geometries while saddle points of various order are associated to unstable stationary geometries (a 1^{st}-order saddle point is commonly called a transition state). From the adiabatic representation arises transition state theory to describe reaction mechanisms in the ground state. Transition state theory "allows us" to determine the pathway that connects reactants to products passing by on transition states. Such reactions are called *thermally activated*: temperature supplies enough kinetic energy to cross the energy barrier of the transition state. [106–108].

Transition state theory is valid in the study of adiabatic chemical processes, when a unique adiabatic state is involved. However, non-adiabatic effects can be involved in a chemical process and transition state theory is not valid. Non-adiabatic effects have to be taken into account when the BOA reaches its limit. The limitations of the BOA have been noticed for fast chemical reactions [109, 110] but also for photoinduced processes such as photoisomerizations. [62]

In this thesis, we are focused on photoexcited molecular systems. They can de-excite by emitting light toward the singlet ground state either by fluorescence if the excited electronic state is a singlet or by phosphorescence if the excited state is not a singlet. The light-emitting response from a photoexcitation can vanish if there has been some nuclear reorganization and electronic such that the molecular wave-packet has relaxed radiationlessly to the ground state. Bright and dark states can be involved in the relaxation of the molecular wave-packet. To relax efficiently from one state to another, the adiabatic states have to be close in energy and to be degenerate

or almost at some point - the PES have to cross and the BOA is not valid anymore. The adiabatic representation (when the electronic states are eigenvectors of the electronic Hamiltonian) and the diabatic representation (when the electronic states are not kinetically coupled and they are defined according to a peculiar electronic property that is conserved) are then useful to understand the topology of the PES and what are the pathways that link one electronic state to another.

When two adiabatic electronic states are degenerate, the PES cross along $3N_{\text{nu}} - 8$ directions and the degeneracy is lifted to first orderalong two directions. The shape of the PES is a *double cone* and the locus of a crossing is the apex of the double cone. The crossing of two PES is called a *conical intersection* (CoIn) and the two-dimensional space that lifts the degeneracy to first order is called the branching space (see fig. 2.1).

Different types of CoIn can be classified as:

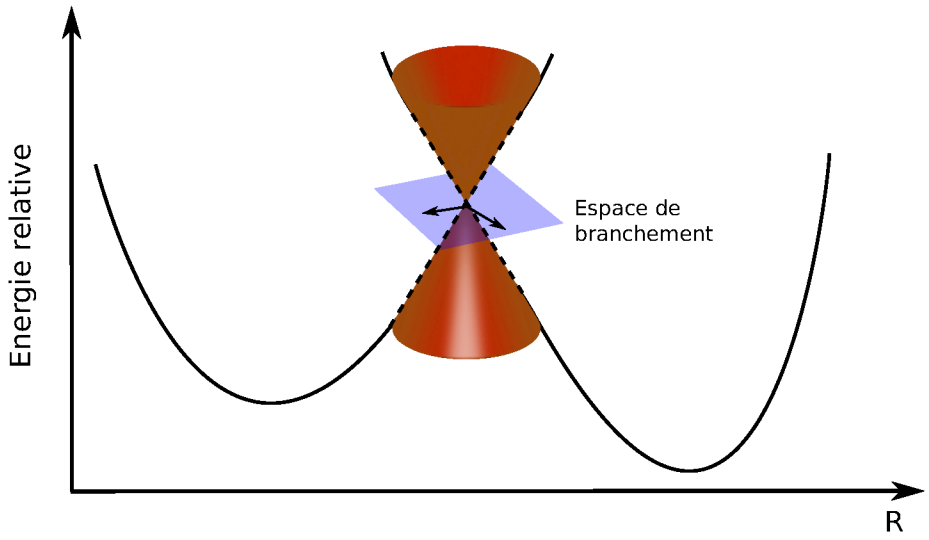

Figure 2.1: Schematic representation of a CoIn between two adiabatic electronic states along a vibrational mode (**R**) that allows the relaxation of the molecular wave-packet

– Specific case: **The non-Abelian groups intersections** due to the Jahn-Teller effect involving two degenerate states of the same symmetry and a degenerate pair of non-totally symmetric displacements that lifts the degeneracy and lowers the point group of the molecular system (in a two- or three-dimensional irreductible representation). [111] We can mention the benzene cation which states ${}^2E_{1\text{g}}$ (or ${}^2E_{2\text{g}}$) are degenerate in the $\mathcal{D}_{6h}$ point group. [112]

– Specific case: **The Abelian groups intersections** where two electronic states of different symmetry cross (in one-dimensional irreductible representation). For exemple in article [43] the crossing $1^1A_1/1^1B_2$ of *meta*-di(phenylethynyl)phenylene has been studied.

– General case: **The accidental intersections**. Two electronic states of same symmetry can cross. For exemple, the crossing between two singlet states $1^1A"/2^1A"$ for H_2S or the crossing between two triplet states $2^3A"/3^3A"$ for CH_2. [113]

2.2 Non-adiabatic couplings and conical intersections

For simplicity reasons, in this chapter the adiabatic electronic states are labelled, within the two-state approximation $|\psi_1\rangle$ and $|\psi_2\rangle$, and their relatives energies are $V_1(\mathbf{R})$ and $V_2(\mathbf{R})$. We suppose that $V_2(\mathbf{R}) \geq V_1(\mathbf{R})$. In this chapter we are going to study the critical case when $V_2(\mathbf{R}) = V_1(\mathbf{R})$. The two adiabatic electronic states are supposed to be singlet states. The case in which two adiabatic electronic states have different spin multiplicities has not been studied in this thesis.
With these new notations, the 1^{st} order non-adiabatic coupling reads:

$$F_{12}(\mathbf{R}) \quad = \quad \langle\psi_1|\nabla_{\mathbf{R}}\psi_2\rangle \quad = \quad \frac{\langle\psi_1|\,\nabla_{\mathbf{R}}\hat{H}_{e^-}\,|\psi_2\rangle}{V_2(\mathbf{R}) - V_1(\mathbf{R})} \tag{2.1}$$

Similarly as in chapter 1, the 1^{st}-order non-adiabatic coupling diverges when $V_2(\mathbf{R}) = V_1(\mathbf{R})$.

The electronic Hamiltonian matrix in eq. 1.23 can be written as the sum of two diagonal matrices such that:

$$\mathbf{H}_{e^-}(\mathbf{R}) \quad = \quad \begin{pmatrix} \frac{V_1(\mathbf{R})+V_2(\mathbf{R})}{2} & 0 \\ 0 & \frac{V_1(\mathbf{R})+V_2(\mathbf{R})}{2} \end{pmatrix} + \begin{pmatrix} \frac{V_1(\mathbf{R})-V_2(\mathbf{R})}{2} & 0 \\ 0 & \frac{V_2(\mathbf{R})-V_1(\mathbf{R})}{2} \end{pmatrix} \tag{2.2}$$

To simplify the previous equation, we determine two functions of $\mathbf{R}$, Δ and Σ, such that:

$$\Delta(\mathbf{R}) = \frac{V_2(\mathbf{R}) - V_1(\mathbf{R})}{2} \tag{2.3}$$

and

$$\Sigma(\mathbf{R}) = \frac{V_1(\mathbf{R}) + V_2(\mathbf{R})}{2} \tag{2.4}$$

Then eq. 2.2 reads:

$$\mathbf{H}_{\mathrm{e}^-}(\mathbf{R}) = \begin{pmatrix} \Sigma(\mathbf{R}) & 0 \\ 0 & \Sigma(\mathbf{R}) \end{pmatrix} + \begin{pmatrix} -\Delta(\mathbf{R}) & 0 \\ 0 & \Delta(\mathbf{R}) \end{pmatrix} \tag{2.5}$$

The second term on the right-hand side of eq. 2.5 is traceless.

Let $\left|\tilde{\psi}_1\right\rangle$ and $\left|\tilde{\psi}_2\right\rangle$ be two non-adiabatic electronic states. $(|\psi_1\rangle, |\psi_2\rangle)$ and $(\left|\tilde{\psi}_1\right\rangle, \left|\tilde{\psi}_2\right\rangle)$ span the same Hilbert space. The non-adiabatic electronic Hamiltonian matrix reads:

$$\tilde{\mathbf{H}}_{\mathrm{e}^-}(\mathbf{R}) = \begin{pmatrix} \tilde{H}_{11}(\mathbf{R}) & \tilde{H}_{12}(\mathbf{R}) \\ \tilde{H}_{21}(\mathbf{R}) & \tilde{H}_{22}(\mathbf{R}) \end{pmatrix} \tag{2.6}$$

$(|\psi_1\rangle, |\psi_2\rangle)$ is the basis in which the electronic Hamiltonian matrix is diagonal. There exists a rotation matrix $\mathbf{\Theta}(\mathbf{R})$ (for real-valued states or unitary matrix in the more general case) such that:

$$\mathbf{H}_{\mathrm{e}^-}(\mathbf{R}) = \mathbf{\Theta}^{\mathsf{T}}(\mathbf{R})\tilde{\mathbf{H}}_{\mathrm{e}^-}(\mathbf{R})\mathbf{\Theta}(\mathbf{R}) \tag{2.7}$$

The analytic expression of the rotation matrix and of $\vartheta(\mathbf{R})$ is given in eqs. 1.24 and 1.25 in chapter 1. The rotation matrix allows us to rotate the electronic basis $(\left|\tilde{\psi}_1\right\rangle, \left|\tilde{\psi}_2\right\rangle)$ to $(|\psi_1\rangle, |\psi_2\rangle)$ such that:

$$\begin{aligned} |\psi_1\rangle &= \cos(\theta(\mathbf{R}))\left|\tilde{\psi}_1\right\rangle + \sin(\theta(\mathbf{R}))\left|\tilde{\psi}_2\right\rangle \\ |\psi_2\rangle &= -\sin(\theta(\mathbf{R}))\left|\tilde{\psi}_1\right\rangle + \cos(\theta(\mathbf{R}))\left|\tilde{\psi}_2\right\rangle \end{aligned} \tag{2.8}$$

As in eq. 2.5 one can write the Hamiltonian matrix of eq. 2.6 as the sum of two matrices:

$$\tilde{\mathbf{H}}_{\mathrm{e}^-}(\mathbf{R}) = \begin{pmatrix} \tilde{\Sigma}(\mathbf{R}) & 0 \\ 0 & \tilde{\Sigma}(\mathbf{R}) \end{pmatrix} + \begin{pmatrix} -\tilde{\Delta}(\mathbf{R}) & \tilde{H}_{12}(\mathbf{R}) \\ \tilde{H}_{21}(\mathbf{R}) & \tilde{\Delta}(\mathbf{R}) \end{pmatrix} \tag{2.9}$$

where $\tilde{\Delta}$ and $\tilde{\Sigma}$ are:

$$\tilde{\Delta}(\mathbf{R}) = \frac{\tilde{H}_{22}(\mathbf{R}) - \tilde{H}_{11}(\mathbf{R})}{2} \tag{2.10}$$

and

$$\tilde{\Sigma}(\mathbf{R}) = \frac{\tilde{H}_{11}(\mathbf{R}) + \tilde{H}_{22}(\mathbf{R})}{2} \tag{2.11}$$

Again, the second matrix on the right-hand side is traceless. The trace is conserved for a unitary transformation, so we have:

$$\tilde{H}_{22}(\mathbf{R}) + \tilde{H}_{11}(\mathbf{R}) = V_1(\mathbf{R}) + V_2(\mathbf{R}) \tag{2.12}$$

which leads to

$$\begin{pmatrix} \Sigma(\mathbf{R}) & 0 \\ 0 & \Sigma(\mathbf{R}) \end{pmatrix} = \begin{pmatrix} \tilde{\Sigma}(\mathbf{R}) & 0 \\ 0 & \tilde{\Sigma}(\mathbf{R}) \end{pmatrix} \tag{2.13}$$

and

$$\begin{pmatrix} \Delta(\mathbf{R}) & 0 \\ 0 & \Delta(\mathbf{R}) \end{pmatrix} = \mathbf{\Theta}^{\mathsf{T}}(\mathbf{R}) \begin{pmatrix} \tilde{\Delta}(\mathbf{R}) & \tilde{H}_{12}(\mathbf{R}) \\ \tilde{H}_{12}(\mathbf{R}) & \tilde{\Delta}(\mathbf{R}) \end{pmatrix} \mathbf{\Theta}(\mathbf{R}) \tag{2.14}$$

Eq. 2.14 leads to the following coupled equations:

$$\begin{cases} \Delta(\mathbf{R}) &= \tilde{\Delta}(\mathbf{R}) \cos\left(2\theta(\mathbf{R})\right) + \tilde{H}_{12}(\mathbf{R}) \sin\left(2\theta(\mathbf{R})\right) \\ 0 &= -\tilde{\Delta}(\mathbf{R}) \sin\left(2\theta(\mathbf{R})\right) + \tilde{H}_{12}(\mathbf{R}) \cos\left(2\theta(\mathbf{R})\right) \end{cases} \tag{2.15}$$

We can deduce analytic formulae of $\cos\left(2\theta(\mathbf{R})\right), \sin\left(2\theta(\mathbf{R})\right)$, and $\tan\left(2\theta(\mathbf{R})\right)$ such that:

$$\begin{aligned} \bullet \quad \cos\left(2\theta(\mathbf{R})\right) &= \frac{\tilde{\Delta}(\mathbf{R})}{\Delta(\mathbf{R})} \\ \bullet \quad \sin\left(2\theta(\mathbf{R})\right) &= -\frac{\tilde{H}_{12}(\mathbf{R})}{\Delta(\mathbf{R})} \\ \bullet \quad \tan\left(2\theta(\mathbf{R})\right) &= -\frac{\tilde{H}_{12}(\mathbf{R})}{\tilde{\Delta}(\mathbf{R})} \end{aligned} \tag{2.16}$$

with signs consistent with assuming $\Delta(\mathbf{R}) \geq 0$.

As the sum of the square of cos and of the square of sin is equal to 1 we have:

$$\Delta(\mathbf{R}) = \sqrt{\tilde{\Delta}(\mathbf{R})^2 + \tilde{H}_{12}(\mathbf{R})^2} \tag{2.17}$$

According to the definition of $\Delta(\mathbf{R})$ (see eq. 2.3), if two adiabatic electronic states are degenerate at $\mathbf{R} = \mathbf{R}_{CoIn}$ then $\Delta(\mathbf{R}_{CoIn}) = 0$. The domain of the square root function is $\mathbb{R}^+$. $\tilde{\Delta}(\mathbf{R})$

and $\tilde{H}_{12}(\mathbf{R})$ are both real. To fulfill $\Delta(\mathbf{R}_{CoIn}) = 0$, the only possibility is to have simultaneously:

$$\begin{aligned} \tilde{H}_{11}(\mathbf{R}_{CoIn}) &= \tilde{H}_{22}(\mathbf{R}_{CoIn}) \\ \tilde{H}_{12}(\mathbf{R}_{CoIn}) &= 0 \end{aligned} \tag{2.18}$$

To first order, the function $\Delta(\mathbf{R})$ behaves as the generic function: $f : (x, y) \mapsto \sqrt{(ax)^2 + (by)^2}$, where a, b, x, y are real numbers. The local derivatives are not continuous at $x = 0$ and $y = 0$:

$$\lim_{x \to 0^+} \frac{f(x,0) - f(0,0)}{x} = |a| \tag{2.19}$$

$$\lim_{x \to 0^-} \frac{f(x,0) - f(0,0)}{x} = -|a| \tag{2.20}$$

and

$$\lim_{y \to 0^+} \frac{f(0,y) - f(0,0)}{y} = |b| \tag{2.21}$$

$$\lim_{y \to 0^-} \frac{f(0,y) - f(0,0)}{y} = -|b| \tag{2.22}$$

Both local derivatives are ill-defined at (0,0), and so are the local derivatives of the function $\Delta(\mathbf{R})$ when the conditions in eq. 2.18 are fulfilled. However the functions $\Sigma(\mathbf{R})$ and $\tilde{\Sigma}(\mathbf{R})$ are well defined and continuous, their first local derivatives are as well.

Due to the behavior of $\Delta(\mathbf{R})$ in the vicinity of $\mathbf{R}_{CoIn}$, the two PES are characterized by a two-dimensional cusp (the apex of a double cone).

There are then two specific directions that characterize a CoIn: the direction that allows $\tilde{H}_{12}(\mathbf{R})$ to have a non-zero value, the direction that couples the two adiabatic electronic states and the direction that allows $\tilde{H}_{11}(\mathbf{R}) - \tilde{H}_{22}(\mathbf{R}) \neq 0$. As a PES is an hypersurface of $3N_{\text{nu}} - 6$ dimensions, two PES can intersect along $3N_{\text{nu}} - 8$ directions. It is call a *seam*. There are two directions that lift the degeneracy to first order at $\mathbf{R} = \mathbf{R}_{CoIn}$: the *derivative coupling* (DC) and the *gradient difference* (GD).

$$\overrightarrow{GD} = \frac{1}{2}\left(\left\langle \tilde{\psi}_2 \right| \hat{\nabla}_{\mathbf{R}=\mathbf{R}_{CoIn}} \tilde{H}_{\text{e}^-} \left| \tilde{\psi}_2 \right\rangle - \langle \tilde{\varphi}_1 | \, \hat{\nabla}_{\mathbf{R}=\mathbf{R}_{CoIn}} \tilde{H}_{\text{e}^-} \, | \tilde{\varphi}_1 \rangle \right) \tag{2.23}$$

$$\overrightarrow{DC} = \langle \tilde{\varphi}_1 | \, \hat{\nabla}_{\mathbf{R}=\mathbf{R}_{CoIn}} \tilde{H}_{\text{e}^-} \, | \tilde{\varphi}_2 \rangle \tag{2.24}$$

The two vectors result from the action of the Nabla operator on $\tilde{\Delta}(\mathbf{R})$ and on $\tilde{H}_{12}(\mathbf{R})$ at $\mathbf{R} = \mathbf{R}_{CoIn}$ thus the two vectors lift the degeneracy at the first-order only. They span a two-

dimensional-space which is called the *branching space*.

The two vectors have been determined for an arbitrary pair of degenerate adiabatic electronic states $\left(|\tilde{\varphi}_1\rangle , |\tilde{\varphi}_2\rangle \right)$. The two adiabatic states can be mixed together to form another pair of degenerate adiabatic states $\left(|\tilde{\varphi}_{mix,1}\rangle , |\tilde{\varphi}_{mix,2}\rangle \right)$ with a mixing angle $\tilde{\vartheta}_{mix}$.

$$\begin{pmatrix} \tilde{\varphi}_{mix,1}(\mathbf{R}_{CoIn}) \\ \tilde{\varphi}_{mix,2}(\mathbf{R}_{CoIn}) \end{pmatrix} = \begin{pmatrix} \cos\tilde{\vartheta}_{mix} & \sin\tilde{\vartheta}_{mix} \\ -\sin\tilde{\vartheta}_{mix} & \cos\tilde{\vartheta}_{mix} \end{pmatrix} \begin{pmatrix} \tilde{\varphi}_1(\mathbf{R}_{CoIn}) \\ \tilde{\varphi}_2(\mathbf{R}_{CoIn}) \end{pmatrix} \tag{2.25}$$

The vectors of the branching space associated to the new pair of degenerate adiabatic electronic states are:

$$\begin{aligned} \overrightarrow{DC}_{mix} &= \cos 2\tilde{\vartheta}_{mix}\overrightarrow{DC} + \sin 2\tilde{\vartheta}_{mix}\overrightarrow{GD} \\ \overrightarrow{GD}_{mix} &= -\sin 2\tilde{\vartheta}_{mix}\overrightarrow{DC} + \cos 2\tilde{\vartheta}_{mix}\overrightarrow{GD} \end{aligned} \tag{2.26}$$

One notices that the vectors of the branching space rotate twice faster than the electronic states. If the mixing angle is $\vartheta_{mix} = \frac{\pi}{4}[\pi]$, the derivative coupling vector $\overrightarrow{DC}_{mix} = \overrightarrow{GD}$ and the gradient difference $\overrightarrow{GD}_{mix} = \overrightarrow{DC}$.

Choosing the working basis of diabatic states can be tedious because one does not know the diabatic states everywhere. We only get adiabatic electronic states from quantum calculations at a conical intersection. Let us consider a pair of adiabatic electronic states $\left(|\varphi_{CoIn,1}\rangle , |\psi_{CoIn,2}\rangle \right)$ and a working basis of diabatic set $\left(\left|\tilde{\psi}_{CoIn,1}\right\rangle , \left|\tilde{\psi}_{CoIn,2}\right\rangle \right)$ at $\mathbf{R} = \mathbf{R}_{CoIn}$ such that the condition in eq. 2.18 are fulfilled then get:

$$\left|\tilde{\psi}_{CoIn,1}\right\rangle = |\varphi_{CoIn,1}\rangle \tag{2.27}$$

and

$$\left|\tilde{\psi}_{CoIn,2}\right\rangle = |\varphi_{CoIn,2}\rangle \tag{2.28}$$

The two diabatic electronic states are then eigenvectors at the apex of the conical intersection but they are not necessarily eigenvectors for other values of $\mathbf{R}$. But as they are diabatic states, they vary smoothly around $\mathbf{R}_{CoIn}$. Around the apex at $\mathbf{R} = \mathbf{R}_{CoIn} + \delta\mathbf{R}$ where $\delta\mathbf{R}$ is an infinitesimal variation of the nuclear spatial coordinates we assume that the working basis of diabatic states do not vary, so that:

$$|\tilde{\varphi}_{CoIn+\delta\mathbf{R},1}\rangle = |\tilde{\varphi}_{CoIn,1}\rangle \tag{2.29}$$

and

$$|\tilde{\varphi}_{CoIn+\delta\mathbf{R},2}\rangle = |\tilde{\varphi}_{CoIn,2}\rangle \tag{2.30}$$

Such diabatic states are called *crude adiabatic* states, they are adiabatic states at the apex of the cone and do not vary at first-order around it.

Chapter 3

Electron density

The present chapter is based on a selection of seminal references [97, 114–118]. As it has been explained in chapter 1, for a given geometry the adiabatic electronic wave-function within the BOA holds information of an adiabatic electronic state. The adiabatic electronic properties can be described by the use of adiabatic electronic wave-function. However, to have access to the adiabatic electronic wave-functions is not an easy task. The Hartree Fock (HF) method is the simplest quantum-chemical methods to find an approximate solution to the electronic problem. This method is the basis of most of quantum wave-function based methods. In the HF method, the electronic wave-function (depending on the number of electrons, N_{e^-}) is approximated to an antisymmetrized product of N_{e^-} single-particle functions (spin-orbitals). Such a wave-function is a single determinant (called a Slater determinant). The approximate wave-function is the exact solution of a system composed of N_{e^-} non-interacting particles (or interacting via mean fields). As the total energy is not exact, the deviation between the exact energy E_{exact} and the energy E_{HF} is called the correlation energy E_{corr} and is defined such that $E_{\mathrm{corr}} = E_{\mathrm{exact}} - E_{HF}$.

In order to calculate an approximate correlation energy, one can build a multi-determinantal wave-function. Post-Hartree Fock methods are based on the results of the mono-determinantal wave function from HF calculations and additionnal determinants are added to the initial mono-determinantal wave-function. One can list configuration interaction methods, perturbative methods, coupled-cluster methods etc. In any case the electronic wave-function that is computed depends on N_{e^-} electrons and each electron is associated to three spatial coordinates and one spin coordinate. [97, 118] The number of basis functions that are necessary to compute a multi-determinantal wave-function to have good accuracy can become huge for large molecular system. That is why we have studied our systems with density functional theory (DFT) and its time-dependent extension (TDDFT) that are based on the one electron density function. It depends

on only three spatial coordinates. Moreover the electronic wave-function is not an observable while electron density profiles can be measured. [119–122]

The square modulus of the electronic wave-function is a probability distribution function. Due to the laws of quantum physics, it is only possible to describe the system probabilistically. The electron density is defined for N_{e^-} electrons but it is computationally challenging to obtain it because one does not know the analytical expression of the N_{e^-} particle density and it depends on too many variables. An alternative is too use the one particle reduced density, even if the analytical formulation is not known, it depends on only two variables, the spatial and spin coordinates of one electron. It contains enough information to describe the system adequately.

3.1 From the N_{e^-}-particle density operators to the one-particle density function

The words "*density*" or "*electron density*" are commonly used as generic terms for electron density matrices, electron density functions, N-body density functions, the one-body reduced density functions etc. In this subsection, an explanation will be given on the considerations used to manipulate electron density entities and the link between them.

The system is treated under the same assumptions regarding the N_{nu} nuclei and N_{e^-} electrons as in chapter 1. The ket of the n^{th} electronic adiabatic state denoted $\left|\psi_n^{\mathrm{ad,BOA}}\right\rangle$ is now abbreviated $|\psi_n\rangle$ unless otherwise stated. As in chapter 1, the electronic coordinates are $(\mathbf{r},\boldsymbol{\sigma}_{\mathrm{e}^-})=\{\mathbf{r}_i,\boldsymbol{\sigma}_i\}_{[\![1;N_{\mathrm{e}^-}]\!]}$, where the i^{th} coordinate of the i^{th} electron is denoted $\mathbf{q}_i = (\mathbf{r}_i,\boldsymbol{\sigma}_i)$, where $\mathbf{r}_i$ is the spatial vector of the i^{th} particle and $\boldsymbol{\sigma}_i$ its spin coordinate. Within the coordinate representation, we have $\langle\mathbf{r}_i|\mathbf{r}'_i\rangle = \delta(\mathbf{r}_i - \mathbf{r}'_i)$ where $\delta(\mathbf{r}_i - \mathbf{r}'_i)$ is the Dirac distribution and $\langle\boldsymbol{\sigma}_i|\boldsymbol{\sigma}'_i\rangle = \delta_{\sigma_i\sigma'_i}$ where $\delta_{\sigma_i\sigma'_i}$ is the Kronecker symbol.

The N_{e^-}-particle electron density operator of the n^{th} electronic adiabatic state is defined as:

$$\hat{\Gamma}_n^{(N_{\mathrm{e}^-})} = |\psi_n\rangle\langle\psi_n| \tag{3.1}$$

The N_{e^-}-dimensional kernel of the N_{e^-}-particle electronic operator is defined as (in the case of real values wave-functions):

$$\begin{aligned}\Gamma_n^{(N_{\mathrm{e}^-})}(\mathbf{q} \mid \mathbf{q}') &= \langle \mathbf{r}, \boldsymbol{\sigma}_{\mathrm{e}^-} | \psi_n \rangle \langle \psi_n | \mathbf{r}', \boldsymbol{\sigma}'_{\mathrm{e}^-} \rangle \\ &= \psi(\mathbf{r}, \boldsymbol{\sigma}_{\mathrm{e}^-}) \psi(\mathbf{r}', \boldsymbol{\sigma}'_{\mathrm{e}^-})\end{aligned} \tag{3.2}$$

The expectation value of an N_{e^-}-particles operator $\hat{\mathrm{A}}$ acting on a N_{e^-}-particle state is defined by :

$$\begin{aligned}\langle \hat{\mathrm{A}} \rangle_n &= \langle \psi_n | \, \hat{\mathrm{A}} \, | \psi_n \rangle \\ &= \sum_{\boldsymbol{\sigma}_1 \cdots \boldsymbol{\sigma}_{N_{\mathrm{e}^-}}} \int \\ &\quad \left[\hat{\mathrm{A}} \Gamma_n{}^{(N_{\mathrm{e}^-})}(\mathbf{r}_1, \boldsymbol{\sigma}_1 \ldots \mathbf{r}_{N_{\mathrm{e}^-}}, \boldsymbol{\sigma}_{N_{\mathrm{e}^-}} \mid \mathbf{r}'_1, \boldsymbol{\sigma}'_1 \ldots \mathbf{r}'_{N_{\mathrm{e}^-}}, \boldsymbol{\sigma}'_{N_{\mathrm{e}^-}}) \right]_{\mathbf{r}=\mathbf{r}', \boldsymbol{\sigma}_{\mathrm{e}^-}=\boldsymbol{\sigma}'_{\mathrm{e}^-}} \mathrm{d}\mathbf{r}_{1-N_{\mathrm{e}^-}}\end{aligned} \tag{3.3}$$

Where $\mathrm{d}\mathbf{r}_{1-N_{\mathrm{e}^-}} = \mathrm{d}\mathbf{r}_1 \cdots \mathrm{d}\mathbf{r}_{N_{\mathrm{e}^-}}$. The issue of computing eq. 3.3 is that the N_{e^-}-particle density matrix or the kernel of the N_{e^-}-particle density operator is in general impossible to obtain due to the large amount of variables. But the operators we are dealing with are the five operators that compose the molecular Hamiltonian: $\hat{H}_{\mathrm{mol}} = \hat{V}_{\mathrm{e}^- - \mathrm{e}^-} + \hat{T}_{\mathrm{e}^-} + \hat{V}_{\mathrm{nu-nu}} + \hat{V}_{\mathrm{nu}-\mathrm{e}^-} + \hat{T}_{\mathrm{nu}}$. Among them, the operators $\hat{V}_{\mathrm{nu-nu}}$ and $\hat{T}_{\mathrm{nu}}$ do not depend on the electronic coordinates, they are called zero-electron operators. The action of the operator $\hat{V}_{\mathrm{nu-nu}}$ on the electronic wave-function is reduced to a simple product but it is not the case of the nuclear kinetic energy operator which deserves a specific treatement within the nonadiabatic context, *i.e.*, when we want to go beyond the Born-Oppenheimer approximation. The operators $\hat{T}_{\mathrm{e}^-}$ and $\hat{V}_{\mathrm{nu}-\mathrm{e}^-}$ depend on the coordinate of one electron, they are called one-electron operators. The last operator is $\hat{V}_{\mathrm{e}^- - \mathrm{e}^-}$ which depends on the distances between any two electrons, is a two-electron operator.

The one-particle reduced density kernel (1-RDK) $\gamma_n(\mathbf{q}_1 \mid \mathbf{q}'_1)$ is defined as:

$$\gamma_n(\mathbf{q}_1 \mid \mathbf{q}'_1) = N_{\mathrm{e}^-} \sum_{\boldsymbol{\sigma}_2 \cdots \boldsymbol{\sigma}_{N_{\mathrm{e}^-}}} \int \psi_n(\mathbf{r}_1, \boldsymbol{\sigma}_1 \ldots \mathbf{r}_{N_{\mathrm{e}^-}}, \boldsymbol{\sigma}_{N_{\mathrm{e}^-}}) \psi_n(\mathbf{r}'_1, \boldsymbol{\sigma}'_1 \ldots \mathbf{r}_{N_{\mathrm{e}^-}}, \boldsymbol{\sigma}_{N_{\mathrm{e}^-}}) \mathrm{d}\mathbf{r}_{2-N_{\mathrm{e}^-}} \tag{3.4}$$

where $\mathrm{d}\mathbf{r}_{2-N_{\mathrm{e}^-}} = \mathrm{d}\mathbf{r}_2 \cdots \mathrm{d}\mathbf{r}_{N_{\mathrm{e}^-}}$

The 1-RDK of eq. 3.4 is defined for computing one electron properties/quantities. It has been arbitrarily chosen that the 1-RDK (and later the one-particle reduced density matrix) have

been built by fixing the coordinates to the electron labelled "1". One could have defined the 1-RDK such that $\gamma_n : (\mathbf{r}_i, \sigma_i) \rightarrow \gamma_n(\mathbf{r}_i, \sigma_i \mid \mathbf{r}'_i, \sigma'_i)$ for instance. Electrons are undistinguishable so the 1-particle reduced density object are well-defined for every electron.

The 1-RDK is defined as the continuous trace over $N-1$ particles of the N_{e^-} dimensional kernel of the N_{e^-}-particle electronic operator.

One can define the one-particle reduced density matrix (1-RDM). Let $(|\varphi_i\rangle)_{i\in\mathbb{N}}$ be a single-particle real function basis. It is defined as: $\varphi_i(\mathbf{q}_j) = \chi_i(\mathbf{r}_j)\xi_i(\sigma_j)$ where χ_i is the i^{th} spatial orbital, ξ_i the spin function of the i^{th} orbital such that $\xi_i = \alpha$ or β and $\mathbf{q}_j$ refers to the coordinate of the j^{th} electron. If two spin-orbitals are said to be orthogonal to each other, they have to be orthogonal according to the orbital and the spin function simultaneously: $\langle\varphi_i|\varphi_j\rangle = \delta_{\chi_i\chi_j}\delta_{\xi_i\xi_j}$.

The formula of ij^{th} element of the 1-RDM:

$$(\boldsymbol{\gamma}_n)_{ij} = \sum_{\boldsymbol{\sigma}_1}\int_{\mathbb{R}^3}\int_{\mathbb{R}^3}\varphi_i(\mathbf{r}_1)\gamma_n(\mathbf{r}_1, \boldsymbol{\sigma}_1 \mid \mathbf{r}'_1, \boldsymbol{\sigma}'_1)\varphi_j(\mathbf{r}'_1)\mathrm{d}\mathbf{r}_1\mathrm{d}\mathbf{r}'_1 \tag{3.5}$$

In the previous equation the symbol * is not written on the spin-orbital φ_j because the spin-orbitals are real here. So the 1-RDK and the 1-RDM are symmetric: $\gamma_n(\mathbf{q}_1 \mid \mathbf{q}'_1) = \gamma_n(\mathbf{q}'_1 \mid \mathbf{q}_1)$ and $(\boldsymbol{\gamma}_n)_{ij} = (\boldsymbol{\gamma}_n)_{ji}$.

The elements of the 1-RDK and the 1-RDM have physical meanings. The diagonal elements $\gamma_{n_{ii}}$ means the probability of finding the particle within the i^{th} spin-orbital when all of the other particles occupy the remaining spin-orbitals and the product $\gamma_n(\mathbf{q}_1 \mid \mathbf{q}_1) \times \mathrm{d}\tau_1$ where $\mathrm{d}\tau_1$ is an elementary volume in $\mathbb{R}^3 \times \sum_{\mathrm{e}^-}$, where $\sum_{\mathrm{e}^-}$ is the electron spin space, means the probability of finding one electron within the elementary volume $\mathrm{d}\tau$ in the vicinity of $\mathbf{q}_1$.

The spin-orbitals in which the matrix representation of the reduced density operator is diagonal are called natural spin-orbitals. The density matrix is symmetric, so it is possible to find an orthonormal single-particle function basis set $\{\mu_i(\mathbf{q})\}$ and an orthogonal matrix $\mathbf{U}$ such that:

$$\begin{aligned}\varphi_i(\mathbf{q}) &= \sum_k U_{ik}\mu_k(\mathbf{q}) \\ \mu_i(\mathbf{q}) &= \sum_k U_{ki}\varphi_k(\mathbf{q})\end{aligned} \tag{3.6}$$

Let us write the i^{th} eigenvalue of the 1-RDM: λ_i and $\Lambda = \mathrm{diag}(\lambda_1, \cdots, \lambda_N)$. We have:

$$\mathbf{U}^{\mathsf{T}}\boldsymbol{\gamma}\mathbf{U} = \boldsymbol{\Lambda} \tag{3.7}$$

The new set of one-particle functions in which the matrix representation of the reduced density operator is diagonal are then the **natural one-particle functions**. The eigenvalues can be viewed as an occupation number and their sum is equal to the total number of electrons in the system.

$$\sum_{\boldsymbol{\sigma}_1} \int_{\mathbb{R}^3} \gamma_n(\mathbf{r}_1, \boldsymbol{\sigma}_1 \mid \mathbf{r}_1, \boldsymbol{\sigma}_1) \mathrm{d}\mathbf{r}_1 \quad = \quad \sum_{i=1}^{N} \gamma_{n_{ii}} \quad = \quad N_{\mathrm{e}^-} \tag{3.8}$$

Then the electron density function is defined such that:

$$n(\mathbf{r}_1) = \sum_{\boldsymbol{\sigma}_1} \gamma_n(\mathbf{r}_1, \boldsymbol{\sigma}_1 \mid \mathbf{r}_1, \boldsymbol{\sigma}_1) \tag{3.9}$$

3.1.1 The electronic transition density kernel

In the same way, it is possible to define the N_{e^-}-particles transition density operator between the n^{th} and the m^{th} electronic adiabatic state:

$$\hat{\Gamma}^{(N_{\mathrm{e}^-})}_{(n\to m)} = |\Psi_m\rangle \langle\Psi_n| \tag{3.10}$$

The 1-particle transition density kernel (1-TDK) reads:

$$\gamma_{(n\to m)}(\mathbf{q}_1 \mid \mathbf{q}'_1) \quad = \quad N_{\mathrm{e}^-} \sum_{\boldsymbol{\sigma}_2 \cdots \boldsymbol{\sigma}_{N_{\mathrm{e}^-}}} \int \psi_n(\mathbf{r}_1, \boldsymbol{\sigma}_1 \ldots \mathbf{r}_{N_{\mathrm{e}^-}}, \boldsymbol{\sigma}_{N_{\mathrm{e}^-}}) \psi_m(\mathbf{r}'_1, \boldsymbol{\sigma}'_1 \ldots \mathbf{r}_{N_{\mathrm{e}^-}}, \boldsymbol{\sigma}_{N_{\mathrm{e}^-}}) \mathrm{d}\mathbf{r}_{2-N_{\mathrm{e}^-}} \tag{3.11}$$

The spin-orbitals in which the matrix representation of the reduced transition density operator is diagonal are called the natural transition spin-orbitals.

3.1.2 Useful and direct applications of the reduced density kernel

In subsection 1.3.2, details are given on the transition dipole moment which depends in our case on the electronic transition dipole moment $\boldsymbol{\mu}^{\mathrm{e}^-}_{(n)}$ (see eq. 1.47). The electronic dipole moment

operator is a local operator (see eq. 1.42). The permanent dipole moment can be expressed by the use of the electron density function:

$$\begin{aligned} \langle \hat{\mu}^{\mathrm{e}^-}_{(n)} \rangle &= \langle \psi_n | \, \hat{\mu}^{\mathrm{e}^-}_{(n)} \, | \psi_n \rangle \\ &= \langle \psi_n | - \mathrm{e} \sum_{i=1}^{N_{\mathrm{e}^-}} \mathbf{r}_i \, | \psi_n \rangle \\ &= -\mathrm{e} \int_{\mathbb{R}^3} \mathbf{r}_1 n(\mathbf{r}_1) \mathrm{d}\mathbf{r}_1 \end{aligned} \tag{3.12}$$

In the same way, it is possible to determine the formula of the transition dipole moment between the n^{th} and the m^{th} electronic state:

$$\begin{aligned} \langle \hat{\mu}^{\mathrm{e}^-} \rangle_{(n \to m)} &= \langle \psi_n | \, \hat{\mu^{\mathrm{e}^-}} \, | \psi_m \rangle \\ &= -\mathrm{e} \sum_{\boldsymbol{\sigma}_1} \int_{\mathbb{R}^3} \mathbf{r}_1 \gamma_{n \to m}(\mathbf{r}_1, \boldsymbol{\sigma}_1 \mid \mathbf{r}_1, \boldsymbol{\sigma}_1) \mathrm{d}\mathbf{r}_1 \end{aligned} \tag{3.13}$$

The expectation values of the contribution to the electronic Hamiltonian (see eq. 1.13) read:

$$\langle \hat{V}_{\mathrm{e}^- - \mathrm{nu}} \rangle = \int_{\mathbb{R}^3} \hat{V}_{\mathrm{e}^- - \mathrm{nu}} n(\mathbf{r}_1) \mathrm{d}\mathbf{r}_1 \tag{3.14}$$

$$\langle \hat{T}_{\mathrm{e}^-} \rangle = \sum_{\boldsymbol{\sigma}_1} \int_{\mathbb{R}^3} \left[\hat{T}_{\mathrm{e}^-} \gamma(\mathbf{r}_1, \boldsymbol{\sigma}_1 \mid \mathbf{r}'_1, \boldsymbol{\sigma}'_1) \right]_{\mathbf{r}_1 = \mathbf{r}'_1, \boldsymbol{\sigma}_1 = \boldsymbol{\sigma}'_1} \mathrm{d}\mathbf{r}_1 \tag{3.15}$$

$$\langle \hat{V}_{\mathrm{e}^- \mathrm{e}^-} \rangle = \sum_{\boldsymbol{\sigma}_1, \boldsymbol{\sigma}_2} \int_{\mathbb{R}^3} \hat{V}_{\mathrm{e}^- \mathrm{e}^-} \Gamma^{(2)}(\mathbf{r}_1, \boldsymbol{\sigma}_1, \mathbf{r}_2, \boldsymbol{\sigma}_2 \mid \mathbf{r}_1, \boldsymbol{\sigma}_1, \mathbf{r}_2, \boldsymbol{\sigma}_2) \mathrm{d}\mathbf{r}_1 \mathrm{d}\mathbf{r}_2 \tag{3.16}$$

3.2 Practical determination of adiabatic electronic energies

This section handles the theory that is used to solve the eigenvalue problem of the electronic Hamiltonian within the Born-Oppenheimer approximation (BOA) by the use of electron density functions. We are going to discuss how the ground state and excited states can be calculated. Unfortunately excited states cannot be computed in the exact same way as the ground state has been obtained. In this thesis, the determination of excited states depends on the accuracy of the

determination of the ground state. The ground state is determined by DFT and excited states by the TDDFT. In the two following subsections, these two methods are briefly described. The reader is kindly referred to refs. [97,116,118] (DFT) and to refs. [123,124] (TDDFT) for further details.

3.2.1 Density functional theory

The DFT principles are based on two theorems that have been proved by Hohenberg and Kohn. [125]

The first theorem stipulates that the interacting many-particle density of the non-degenerate ground state is determined by a unique external potential v induced by the nuclei. The ground state density is a functional of v and v is a unique functional of the ground state density.

The second theorem stipulates that the exact energy of the non-degenerate ground state is a unique functional $E[n_0]$ of the exact ground state density n_0. Such an electron density is the one that minimizes the energy functional $E[n]$. We have:

$$E[n_0] = \min_n E[n] \tag{3.17}$$

The energy of the non-degenerate ground state reads:

$$E[n_0] = \langle \psi_0 | \hat{T}_{\mathrm{e}^-} + \hat{V}_{\mathrm{nu-e}^-} + \hat{V}_{\mathrm{e}^- - \mathrm{e}^-} | \psi_0 \rangle \tag{3.18}$$

$\hat{T}_{\mathrm{e}^-}$ and $\hat{V}_{\mathrm{e}^- - \mathrm{e}^-}$ are said "universal", they depend only on the electron coordinates. But $\hat{V}_{\mathrm{nu-e}^-}$ depends on the nuclear and on the electron coordinates, since it is a multiplicative and a local operator, we have:

$$\langle V_{\mathrm{nu-e}^-} \rangle [n_0] = \int_{\mathbb{R}^3} v(\mathbf{r}_1) n(\mathbf{r}_1) \mathrm{d}\mathbf{r}_1 \tag{3.19}$$

where $\hat{v} = \hat{V}_{\mathrm{nu-e}^-}$ The electronic energy reads:

$$E[n_0] = F[n_0] + \int_{\mathbb{R}^3} v(\mathbf{r}_1) n(\mathbf{r}_1) \mathrm{d}\mathbf{r}_1 \tag{3.20}$$

where $F[n_0]$ is the universal functional such that $F[n_0] = \langle\psi_0|\,\hat{T}_{\mathrm{e}^-} + \hat{V}_{\mathrm{e}^-\mathrm{e}^-}\,|\psi_0\rangle$.

However, the problem is that the universal functional $F[n_0]$ is not know and so the difficulty to find the electron density functions is such that of the electronic ground state is due to the determination of $F[n_0]$.

3.2.2 The Kohn-Sham approach

To simplify the problem, Kohn and Sham proposed that instead of studying a system of N_{e^-} interacting electrons, one can study an auxiliary system of N_{e^-} non-interacting electrons by assuming the following hypothesis to be true: there exists an external potential v for an N_{e^-} non-interacting electron system such that the electron density function gives the same exact energy as the one of a system of N_{e^-} interacting electrons. The spin-orbitals, here, are called the Kohn-Sham orbitals (KS spin-orbitals). The electronic wave-function is a Slater determinant of KS spin-orbitals:

$$\left|\Psi_0^{KS}\right\rangle = \frac{1}{\sqrt{N_{\mathrm{e}^-}!}}\det\Big(\varphi_i^{KS}(\mathbf{r}_j, \boldsymbol{\sigma}_j)\Big)_{(i,j)\in[\![1,N_{\mathrm{e}^-}]\!]^2} \tag{3.21}$$

The electron density function then reads:

$$n(\mathbf{r}_1) = 2\sum_{i=1}^{\frac{N_{\mathrm{e}}^-}{2}} |\ \chi_i^{KS}(\mathbf{r_1})\ |^2 \tag{3.22}$$

We have to keep in mind that the electronic kinetic energy $T_{\mathrm{e}^-}^{KS}[n]$ is exact for a system of N_{e^-} non-interacting electrons and is not equal to the electronic kinetic energy $T_{\mathrm{e}^-}[n]$ which is unkown.

The electronic repulsion potential energy $V_{\mathrm{e}^-\mathrm{e}^-}$ reads in the KS hypothesis:

$$V_{\mathrm{e}^-\mathrm{e}^-}^{KS}[n] = \int \hat{V}_{\mathrm{e}^-\mathrm{e}^-} n(\mathbf{r}_1)\Big(n(\mathbf{r}_2) + \gamma^{xc}(\mathbf{r}_1 \mid \mathbf{r}_2)\Big)\mathrm{d}\mathbf{r}_1\mathrm{d}\mathbf{r}_2 \tag{3.23}$$

where $\gamma^{xc}(\mathbf{r}_1 \mid \mathbf{r}_2)$ is the exchange density function between two electrons. The electronic repulsion potential energy can be written as the sum of a Coulomb and a exchange-correlation functional, $J[n]$ and $K[n]$, such that:

$$J[n] = \int \hat{V}_{\mathrm{e}^-\mathrm{e}^-} n(\mathbf{r}_1)n(\mathbf{r}_2)\mathrm{d}\mathbf{r}_1\mathrm{d}\mathbf{r}_2 \tag{3.24}$$

and

$$K[n] = \int \hat{V}_{\mathrm{e}^- - \mathrm{e}^-} n(\mathbf{r}_1)\gamma^{xc}(\mathbf{r}_1 \mid \mathbf{r}_2)\mathrm{d}\mathbf{r}_1\mathrm{d}\mathbf{r}_2 \tag{3.25}$$

The total energy of a Kohn-Sham approximation remains a density functional:

$$E^{KS}[n] = \int v^{KS}(\mathbf{r}_1)n(\mathbf{r}_1)\mathrm{d}\mathbf{r}_1 + T_{\mathrm{e}^-}^{KS}[n] + J[n] + E_{xc}(n) \tag{3.26}$$

where $E_{xc}[n] = T_{\mathrm{e}^-}[n] - T_{\mathrm{e}^-}^{KS}[n] + K[n]$ is the exchange-correlation functional. This term embraces the remaining kinetic term that is not obtained within $T_{\mathrm{e}^-}^{KS}[n]$ and the exchange-correlation term. $E^{KS}[n]$ is unfortunately not know and is approximated in DFT calculations. Minimizing the exchange-correlation functional allows to get an electron density function close to the exact density of a system of N_{e^-} interacting particles.

As the electronic wave-function is written as a Slater determinant of KS spin-orbitals, one can write a one-electron Hamiltonian $\hat{h}^{KS}$ (the Kohn-Sham operator):

$$\hat{h}^{KS} = \hat{T}_{\mathrm{e}^-} + \hat{v}^{KS} \tag{3.27}$$

with

$$\hat{v}^{KS} = \hat{v} + \hat{v}_H + \hat{v}_{xc} \tag{3.28}$$

where v is the external potential, $v_H = \int \frac{\mathrm{e}^2 n(\mathbf{r}_1)}{4\pi\epsilon_0|\mathbf{r}_1 - \mathbf{r}_2|}\mathrm{d}\mathbf{r}_1$ is the Hartree potential and $v_{xc} = \frac{\delta E_{xc}(n)}{\delta n(\mathbf{r}_1)}$ is the exchange-correlation potential. One can solve the Kohn-Sham equation with a self-consistent method to determine optimal KS spin-orbitals.

To approximate the exchange-correlation potential, various functionals have been developed. We differenciate three type of functionals:

• The functionals obtain from the local density approximation (LDA) for which the electron density is assumed to be uniform and is computed locally.

• The functionals obtain from the generalized gradient approximations (GGA). The electron density is considered non-uniform. The functionals that are built over this approximation are called exchange functionals.

• The last type of functionals are the hybrid exchange-correlation functionals. They are built

such that there is an exchange-correlation part which result from GGA and there is an exchange part which results from the Hartree-Fock method.

3.3 TDDFT

As explained before, the Hohenberg and Kohn theorems are valid only for the non-degenerate ground state. The DFT method does not allow to compute excited state energies in its standard form. This thesis is focused on the understanding of the photoexcitation in molecular systems. Therefore, one needs to compute excited state energies and properties of molecular systems.

To compute excited state with a density-based method, the global idea is to understand how the ground state density reacts when the system is perturbed (*i.e.* when the system is excited).

The response of the ground state to the perturbation has been studied in many ways. In our case, we are focused on the linear response of the ground state to a time dependent perturbation. The linear-response of the DFT is based on two theorems proved by Runge and Gross [126] and by van Leeuwen [127].

Runge and Gross proved that if two external potentials differ only from a time dependent constant there is a correspondence between these potentials and the electron density.

Van Leeuwen proved that if an external potential is applied to a system that is described by a wave-function, there is another external potential applied to another system and that is described by another wave-function such that these two systems have the same electron density.

Let us consider a system of N_{e^-} electrons in its ground state from $t = 0$ to $t = t_0$ described by an electron density function $n_0(\mathbf{r}_1)$ and by an external potential $v_0(\mathbf{r}_1)$. At $t = t_0$, an external interaction is applied such that it leads to an electronic transition. The response of the external potential and the electron density is studied at the first-order, hence, linear-response. We have:

$$v(\mathbf{r}_1, t) = v_0(\mathbf{r}_1) + \delta v(\mathbf{r}_1, t) \tag{3.29}$$

and

$$n(\mathbf{r}_1, t) = n_0(\mathbf{r}_1) + \delta n(\mathbf{r}_1, t) \tag{3.30}$$

where $\delta v(\mathbf{r}_1, t)$ and $\delta n(\mathbf{r}_1, t)$ are defined such that:

$$\delta v(\mathbf{r}_1, t) = \int\int \left.\frac{\delta v(\mathbf{r}_1, t)}{\delta n(\mathbf{r}'_1, t')}\right|_{v=v_0} \delta n(\mathbf{r}'_1, t')\mathrm{d}\mathbf{r}'_1\mathrm{d}t' \tag{3.31}$$

and

$$\delta n(\mathbf{r}_1,t) = \int\int \left.\frac{\delta n(\mathbf{r}_1,t)}{\delta v(\mathbf{r}'_1,t')}\right|_{n=n_0} \delta v(\mathbf{r}'_1,t')\mathrm{d}\mathbf{r}'_1\mathrm{d}t' \tag{3.32}$$

The first-order response of the external potential within the Kohn-Sham approximation reads:

$$v^{KS}(\mathbf{r}_1,t) = v_0^{KS}(\mathbf{r}_1) + \delta v^{KS}(\mathbf{r}_1,t) \tag{3.33}$$

where $v_0^{KS}(\mathbf{r}_1)$ is expressed in eq. 3.28:

$$v_0^{KS}(\mathbf{r}_1) = v_0(\mathbf{r}_1) + \int \frac{\mathrm{e}^2 n_0(\mathbf{r}'_1)}{4\pi\epsilon_0 \mid \mathbf{r}_1 - \mathbf{r}'_1 \mid}\mathrm{d}\mathbf{r}'_1 + \frac{\delta E_{xc}[n_0]}{\delta n_0(\mathbf{r}_1)} \tag{3.34}$$

The first-order term in eq. 3.33 reads:

$$\delta v^{KS}(\mathbf{r}_1,t) = \delta v(\mathbf{r}_1,t) + \delta v_{\mathrm{H}}(\mathbf{r}_1,t) + \delta v_{xc}(\mathbf{r}_1,t) \tag{3.35}$$

where $\delta v(\mathbf{r}_1,t)$ is given in eq. 3.31,

$$\delta v_{\mathrm{H}}(\mathbf{r}_1,t) = \int \frac{\mathrm{e}^2 \delta n(\mathbf{r}_1,t)}{4\pi\epsilon_0 \mid \mathbf{r}_1 - \mathbf{r}'_1 \mid}\mathrm{d}\mathbf{r}'_1 \tag{3.36}$$

and

$$\delta v_{xc}(\mathbf{r}_1,t) = \int\int \frac{\mathrm{e}^2}{4\pi\epsilon_0} f_{xc}(\mathbf{r},\mathbf{r}',t,t')\delta n(\mathbf{r}',t')\mathrm{d}\mathbf{r}'\mathrm{d}t' \tag{3.37}$$

$f_{xc}(\mathbf{r},\mathbf{r}',t,t')$ is the exchange-correlation kernel and reads:

$$f_{xc}(\mathbf{r},\mathbf{r}',t,t') = \left.\frac{\delta^2 E_{xc}[n]}{\delta n(\mathbf{r},t)\delta n(\mathbf{r}',t')}\right|_{n(\mathbf{r}_1,t)=n_0(\mathbf{r}_1)} \tag{3.38}$$

The Fourier transform of $f_{xc}(\mathbf{r},\mathbf{r}',t,t')$ gives:

$$f_{xc}(\mathbf{r},\mathbf{r}',\omega) = \left.\frac{\delta v^{KS}(\mathbf{r}_1,\omega)}{\delta n^{KS}(\mathbf{r}_1,\omega)}\right|_{v^{KS}(\mathbf{r}_1,\omega)=v_0^{KS}(\mathbf{r}_1)} - \left.\frac{\delta v(\mathbf{r}_1,\omega)}{\delta n(\mathbf{r}_1,\omega)}\right|_{v(\mathbf{r}_1,\omega)=v_0(\mathbf{r}_1)} - \frac{1}{\mid \mathbf{r} - \mathbf{r}' \mid} \tag{3.39}$$

where ω is the angular frequency of the Fourier transform. The linear-response theory leads to the following coupled equations that are known in the literature as Casida's equations [124]:

$$\left(\begin{bmatrix} \mathbf{A} & \mathbf{B} \\ \mathbf{B}^* & \mathbf{A}^* \end{bmatrix} - \omega \begin{bmatrix} \mathbf{1} & \mathbf{0} \\ \mathbf{0} & -\mathbf{1} \end{bmatrix} \right) \begin{bmatrix} \mathbf{X} \\ \mathbf{Y} \end{bmatrix} = \mathbf{0} \tag{3.40}$$

where

• The ij^{th} element of the matrix $\mathbf{A}$:

$$A_{ij} = \delta_{ij} \frac{\varepsilon_i - \varepsilon_j}{\hbar} + N_{\mathrm{e}^-} f_{xc}^{ij} \tag{3.41}$$

with δ_{ij} the Kronecker symbol, ε_i the eigenvalue associated to the i^{th} KS spin-orbital and $f_{xc}^{ij} = \int \phi_i^*(\mathbf{r}) \phi_j^*(\mathbf{r}') f_{xc}(\mathbf{r}, \mathbf{r}') \phi_1^*(\mathbf{r}) \phi_1^*(\mathbf{r}') \mathrm{d}\mathbf{r}\mathrm{d}\mathbf{r}'$.

• The ij^{th} element of the matrix $\mathbf{B}$:

$$B_{ij} = N_{\mathrm{e}^-} f_{xc}^{ij} \tag{3.42}$$

• The i^{th} element of the column matrix $\mathbf{X}$:

$$X_i = -\frac{\langle \phi_i | \hat{V}_{ext} | \phi_1 \rangle}{2(\varepsilon_i - \varepsilon_0) - 2\hbar\omega} \tag{3.43}$$

• The i^{th} element of the column matrix $\mathbf{Y}$:

$$Y_i = -\frac{\langle \phi_1 | \hat{V}_{ext} | \phi_i \rangle}{2(\varepsilon_i - \varepsilon_0) + 2\hbar\omega} \tag{3.44}$$

TDDFT calculations are then based on the resolution of Casida's equations and the evaluation of the elements of the matrices $\mathbf{X}$ and $\mathbf{Y}$.The ij^{th} element X_{ij} corresponds to the coefficient associated to the single excitation from the spin-orbital ϕ_i toward the spin-orbital ϕ_j and the ij^{th} element Y_{ij} correspond to the coefficient associated to the single deexcitation from the spin-orbital ϕ_i to the spin-orbital ϕ_j.

3.4 Characterization of electronic adiabatic states

As it has been explained in the previous sections an electronic state can be characterized by two kinds of representations. The adiabatic representation is based on electronic states that are

eigensolutions of the electronic Schrödinger equation and the diabatic representation for which electronic states are labelled according to their chemical "nature". If the electronic states are energetically far from each other we might suppose that the adiabatic states match with the diabatic ones. Finding diabatic states can then help to get a better description of the system.

The usual representation is the adiabatic one. It is labelled according to an energy classification. The adiabatic states are what one gets from quantum chemistry calculations. It is less direct to get a diabatic picture of the system because it can be difficult to find an appropriate electronic nature classification. One can use the symmetry, the oscillator strength, molecular orbitals, natural transition orbitals etc. to sort diabatic states. However these characteristics are not universal; the electronic states might have the same symmetry, they might have a null oscillator strength, they might result from a strong mixing between molecular orbitals, they might be coupled to each other and the natural transition orbitals can then differ. A diabatic wave-function is almost constant with respect to variations of the geometry (nuclear coordinates) and so is the electron density. Here, a method based on electron density based descriptors to characterize electronic adiabatic states is explained.

3.4.1 Attachment and Detachment density matrices

Let $\{\varphi_i\}_{i\in[\![1;N_t]\!]}$ be a complete basis set of spin-orbitals. In the case of a single determinant, the complete spin-orbital basis set can be decomposed into two subsets of spin-orbitals: one called *occupied* and the other *virtual*. $\{\varphi_i\}_{i\in[\![1;N_o]\!]}$ being the *occupied* subset and $\{\varphi_l\}_{l\in[\![N_o+1;N_t]\!]}$ being the *virtual* subset.

As said in the previous subsection, the 1-RDM of the n^{th} electronic adiabatic state is defined as follows:

$$\gamma^n_{ij} = \sum_{\boldsymbol{\sigma}_1}\int_{\mathbb{R}^3}\int_{\mathbb{R}^3}\varphi_i(\mathbf{r}_1,\boldsymbol{\sigma}_1)\gamma^n(\mathbf{r}_1,\boldsymbol{\sigma}_1 \mid \mathbf{r}'_1,\boldsymbol{\sigma}'_1)\varphi_j(\mathbf{r}'_1,\boldsymbol{\sigma}'_1)\mathrm{d}\mathbf{r}_1\mathrm{d}\mathbf{r}'_1 \tag{3.45}$$

The one-particle reduced difference density matrix 1-RDDM is defined as being the difference of the 1-RDM of the n^{th} state and the 1-RDM of the ground state:

$$\boldsymbol{\gamma}^\Delta = \boldsymbol{\gamma}^n - \boldsymbol{\gamma}^0 \tag{3.46}$$

The 1-RDDM is a symmetric matrix due to the fact that $\boldsymbol{\gamma}^n$ and $\boldsymbol{\gamma}^0$ are symmetric. It is always possible to find a orthogonal matrix $\mathbf{U}$ which diagonalizes the 1-RDDM. The basis set which

diagonalizes $\boldsymbol{\gamma}^{\Delta}$ is then made of **natural difference orbitals**. We have:

$$\mathbf{U}^{\mathsf{T}}\boldsymbol{\gamma}^{\Delta}\mathbf{U} = \boldsymbol{\Lambda} \tag{3.47}$$

where $\boldsymbol{\Lambda}$=diag$(\lambda_1, \cdots, \lambda_{N_t})$. We now define $\boldsymbol{\Lambda}_-$ and $\boldsymbol{\Lambda}_+$:

$$\begin{aligned} \boldsymbol{\Lambda}_- &= \tfrac{1}{2}(\sqrt{\boldsymbol{\Lambda}^2} - \boldsymbol{\Lambda}) \\ \boldsymbol{\Lambda}_+ &= \tfrac{1}{2}(\sqrt{\boldsymbol{\Lambda}^2} + \boldsymbol{\Lambda}) \end{aligned} \tag{3.48}$$

The two matrices $\boldsymbol{\Lambda}_-$ and $\boldsymbol{\Lambda}_+$ are positive semi-definite and are associated to the negative and the positive eigenvalues of the 1-RDDM, respectively.

These two diagonal matrices are backtransformed in the basis set of spin-orbitals in which $\boldsymbol{\gamma}^{\Delta}$ has been written, leading to two square matrices which are called *attachment* and *detachment* matrices:

$$\begin{aligned} \boldsymbol{\gamma}^{d} &= \mathbf{U}\boldsymbol{\Lambda}_-\mathbf{U}^{\mathsf{T}} \\ \boldsymbol{\gamma}^{a} &= \mathbf{U}\boldsymbol{\Lambda}_+\mathbf{U}^{\mathsf{T}} \end{aligned} \tag{3.49}$$

The previous equations can be expressed in terms of electron density functions,

$$\begin{aligned} n^{\Delta}(\mathbf{r}) &= \sum_i \sum_j \left(\boldsymbol{\gamma}^{\Delta}\right)_{ij} \varphi_i(\mathbf{r})\varphi_j(\mathbf{r}) \\ &= \sum_i \sum_j \left(\boldsymbol{\gamma}^{n} - \boldsymbol{\gamma}^{0}\right)_{ij} \varphi_i(\mathbf{r})\varphi_j(\mathbf{r}) \\ &= n^n(\mathbf{r}) - n^0(\mathbf{r}) \\ &= n^a(\mathbf{r}) - n^d(\mathbf{r}) \end{aligned} \tag{3.50}$$

with

$$n^a(\mathbf{r}) = \sum_i^{N_t} \sum_j^{N_t} \left(\boldsymbol{\gamma}^{a}\right)_{ij} \varphi_i(\mathbf{r})\varphi_j(\mathbf{r}) \tag{3.51}$$

$$n^d(\mathbf{r}) = \sum_i^{N_t} \sum_j^{N_t} \left(\boldsymbol{\gamma}^{d}\right)_{ij} \varphi_i(\mathbf{r})\varphi_j(\mathbf{r}) \tag{3.52}$$

$n^{\Delta}(\mathbf{r})$ corresponds to the net change of density due to the photoexcitation between the density of the excited state from the density of the ground state.

3.5 Density based descriptors

The *attachment detachment* picture can be viewed as the rearangment of electron density that occurs dues to the photoexcitation. The attachment (resp. detachment) space is defined as being the space built on the subset of spin-orbitals in which the $\mathbf{\Lambda}_+$ (resp. $\mathbf{\Lambda}_-$) matrix has non-zero value. As there is conservation of the charge during the photoexcitation, one can thus write the following equality:

$$\vartheta = \int_{\mathbb{R}^3} n^a(\mathbf{r})\mathrm{d}\mathbf{r} = \int_{\mathbb{R}^3} n^d(\mathbf{r})\mathrm{d}\mathbf{r} \tag{3.53}$$

Two density-based numbers can then be defined to get information on the charge displacement during the photoexcitation. The first one is labelled ϕ_{S}. It is the overlap between the attachment and the detachment densities. The second one is labelled χ and characterizes the amplitude of the charge transferred within the detachment-attachment space:

$$\phi_{\mathrm{S}} = \vartheta^{-1}\int_{\mathbb{R}^3}\sqrt{n^a(\mathbf{r})n^d(\mathbf{r})}d\mathbf{r} \tag{3.54}$$

$$\chi = \frac{1}{2}\int_{\mathbb{R}^3} \mid n^{\Delta}(\mathbf{r}) \mid d\mathbf{r} \tag{3.55}$$

The two descriptors are dimensionless and their values lie between zero and one. If ϕ_{S} is close to one that means the detachment and the attachment densities are similar and so the electronic excited adiabatic state is considered to be locally excited while a ϕ_{S} value close to zero means the two densities do not overlap and so the electronic excited adiabatic state is considered to be a charge transfer state. In the same way, if χ is close to one it means that a net charge is moved in space during the photoexcitation.

3.5.1 Evaluation of the *attachment* and *detachment* density matrices in TD-DFT calculations

In the case of TD-DFT calculations (as in this work), it is actually not necessary to diagonalize the entire 1-DDM to obtain the *attachment* and the *detachment* density matrices. It is possible to obtain the latter two density matrices by the use of elements of the transition density matrix.

The TD-DFT method is a single reference method and thanks to Casida's equations, one can write the 1-TDM between the ground state and the n^{th} electronic adiabatic excited state as:

$$\boldsymbol{\gamma}_{0\to n} = \begin{pmatrix} \mathbf{0}_o & \mathbf{Y} \\ \mathbf{X}^\mathsf{T} & \mathbf{0}_v \end{pmatrix} \tag{3.56}$$

Grossly speaking, he $\mathbf{X}$ can be viewed as the coefficient matrix of single excitations where its il^{th} element is seen as the single excitation from the i^{th} spin-orbital toward the l^{th} spin-orbital, while the $\mathbf{Y}$ is the coefficient matrix of single deexcitations and so its il^{th} elements is the single deexcitation from the l^{th} spin-orbital toward the i^{th} spin-orbital. Moreover $\mathbf{X}$ is a rectangular matrix of size $N_o \times (N_t - N_o)$ and $\mathbf{Y}$ is a rectangular matrix of size $(N_t - N_o) \times N_o$. $\boldsymbol{\gamma}_{0\to n}$ is composed of two other blocks filled with zeros of size $N_o \times N_o$ ($\mathbf{0}_o$ matrix) and $(N_t - N_o) \times (N_t - N_o)$ ($\mathbf{0}_v$ matrix). Reference [128] demonstrates how to link the difference density matrix to the two rectangular matrices $\mathbf{X}$ and $\mathbf{Y}$ by the use of Wick's theorem. Only the main result is written here:

$$\boldsymbol{\gamma}^\Delta = \begin{pmatrix} -(\mathbf{X}\mathbf{X}^\mathsf{T} + \mathbf{Y}\mathbf{Y}^\mathsf{T}) & \mathbf{0}_{ot} \\ \mathbf{0}_{to} & (\mathbf{X}^\mathsf{T}\mathbf{X} + \mathbf{Y}^\mathsf{T}\mathbf{Y}) \end{pmatrix} \tag{3.57}$$

We know from before that:

$$\boldsymbol{\gamma}^\Delta = \mathbf{U}\boldsymbol{\Lambda}\mathbf{U}^\mathsf{T} = \mathbf{U}\boldsymbol{\Lambda}_+\mathbf{U}^\mathsf{T} - \mathbf{U}\boldsymbol{\Lambda}_-\mathbf{U}^\mathsf{T} = \boldsymbol{\gamma}^a - \boldsymbol{\gamma}^d \tag{3.58}$$

The $\boldsymbol{\Lambda}_+$ matrix is built such as its diagonal elements are greater or equal to zero and the $\boldsymbol{\Lambda}_-$ matrix is built such as its diagonal elements are greater or equal to zero. Moreover, it is possible to organize the eigenvectors such as the diagonal of $\boldsymbol{\Lambda}_+$ is at first filled with zeros and then non-zero elements. If so, the diagonal of $\boldsymbol{\Lambda}_-$ is at first filled with non-zero elements and then zeros. The two matrices read:

$$\boldsymbol{\Lambda}_+ = \frac{1}{2}(\sqrt{\boldsymbol{\Lambda}^2} + \boldsymbol{\Lambda}) \tag{3.59}$$

and

$$\boldsymbol{\Lambda}_- = \frac{1}{2}(\sqrt{\boldsymbol{\Lambda}^2} - \boldsymbol{\Lambda}) \tag{3.60}$$

The *attachment* and *detachment* density matrices have then the following shape:

$$\boldsymbol{\gamma}^a = \begin{pmatrix} \mathbf{0}_o & \mathbf{0}_{ot} \\ \mathbf{0}_{to} & \mathbf{A} \end{pmatrix} \qquad \boldsymbol{\gamma}^d = \begin{pmatrix} \mathbf{D} & \mathbf{0}_{ot} \\ \mathbf{0}_{to} & \mathbf{0}_t \end{pmatrix} \tag{3.61}$$

As $\boldsymbol{\gamma}^\Delta = \boldsymbol{\gamma}^a - \boldsymbol{\gamma}^d$ we must have that:

$$\boldsymbol{\gamma}^a = \begin{pmatrix} \mathbf{0}_o & \mathbf{0}_{ot} \\ \mathbf{0}_{to} & (\mathbf{X}^\mathsf{T}\mathbf{X} + \mathbf{Y}^\mathsf{T}\mathbf{Y}) \end{pmatrix} \qquad \boldsymbol{\gamma}^d = \begin{pmatrix} (\mathbf{X}\mathbf{X}^\mathsf{T} + \mathbf{Y}\mathbf{Y}^\mathsf{T}) & \mathbf{0}_{ot} \\ \mathbf{0}_{to} & \mathbf{0}_t \end{pmatrix} \tag{3.62}$$

Only the matrix elements of $\mathbf{X}$ and $\mathbf{Y}$ have to be calculated to obtain the attachment and the detachment matrices.

Chapter 4

Computational details

In this thesis, electronic structure calculation were performed with the functional CAM-B3LYP which is a hybrid exchange-correlation functional [129]. Such a functionnal has been considered because it takes into account the qualities of the functionnal B3LYP and long-range corrections that allow to compute accurately Rydberg states and charge transfer excitations. The 6-31+G∗ basis was used. The choice of such a level of theory is based on previous articles [61,130] in which vibrationnaly resolved absorption spectra of *oligo*phenylene ethynylene have been computed and compared to experimental absorption spectra. Theoretical absorption spectra are in good agreement with the experimental ones and so one can assume that DFT and TDDFT calculation with CAM-B3LYP/6-31+G∗ reproduce efficiently the experimental data. Electronic structure calculations were performed with the Gaussian16 (revision A.03) package [131].

The vibrational normal modes have been determined in this thesis by the use of the software Gaussian16 within the harmonic approximation at the equilibrium geometry of the ground state and at all stationary points previously optimised.

Another aspect that deserves specific attention regarding computational settings is the calculation of descriptors (see their definitions in chapter 3). Attachment and detachment densities were computed with a numerical integration. That is to say, the space is discretised and the electron density are computed on a grid. The numerical integration was performed on a Cartesian grid by the Cubegen utility from the Gaussian16 package. The thickness of the Cartesian grid has been evaluated since the efficiency of the spatial discretisation depends of the latter thickness. Then, the Cartesian grid was chosen built such that 6 points/bohr are considered.

The density-based descriptors were computed with the Mesra software that has been developed by T. Etienne [132].

In figure 4.1 is represented a flowchart of the hierarchy of the various calculations that were

performed in this work. At first, minima, saddle points and conical intersections were determined by the use of electronic structure calculations then, in the case of minima: vibrationally resolved absorption and emission spectra were obtained wihtin the Franck-Condon approximation with the FCHT module of Gaussian 16 [133] and in the case of conical intersections: the branching space (BS) vectors were determined with the approach presented in ref. [75]. The last calculations were the attachment and detachment densities and density-based descriptors calculations at minima, saddle points and conical intersections.

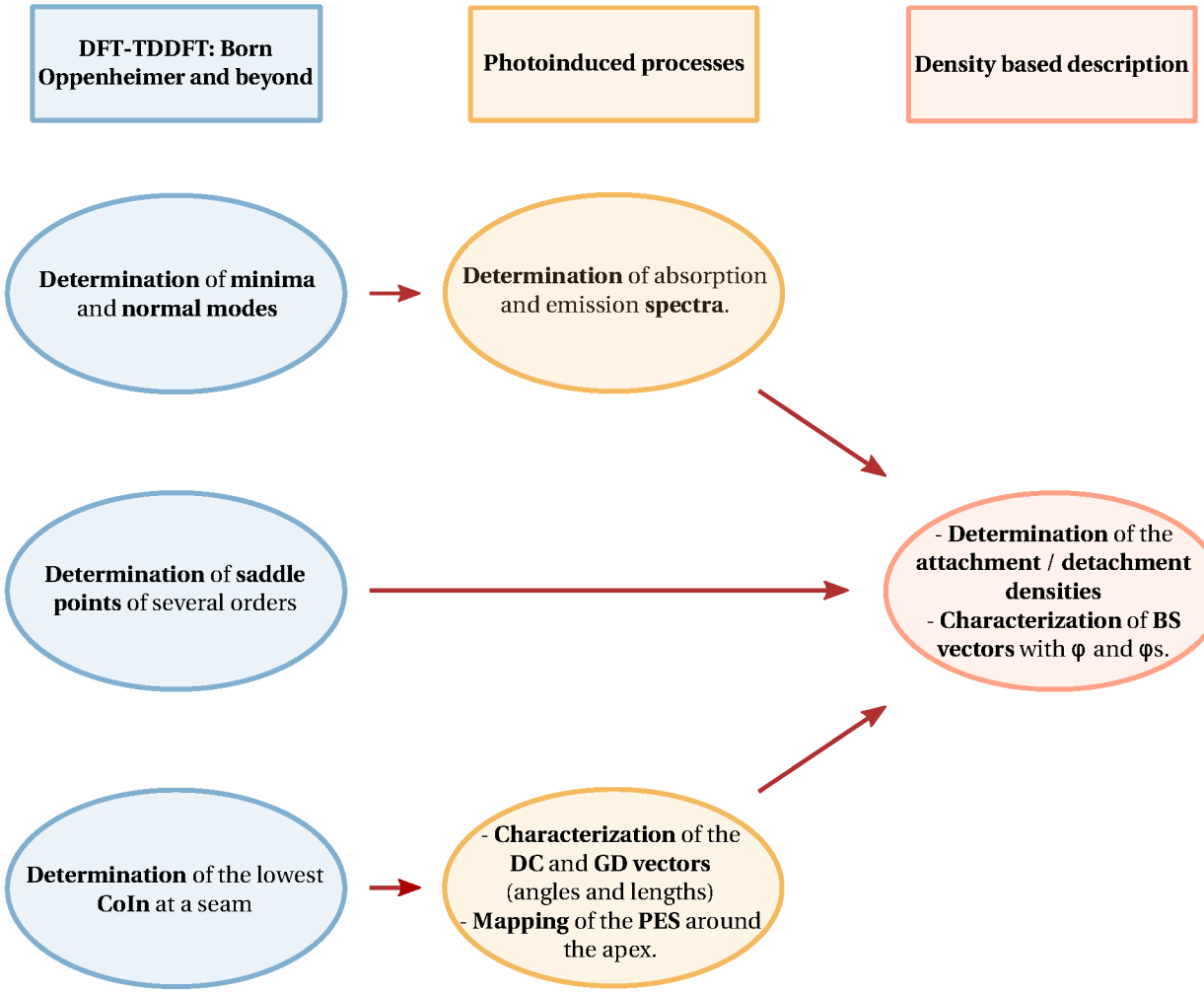

Figure 4.1: Flowchart of calculation hierarchy

Chapter 5

Development of numerical tools

5.1 Evaluation of two computational methods for describing the densities of electronic excited states

The analytic formulae of the two electron density-based descriptors that we have been focused on ($\chi(\mathbf{R})$ and $\phi_S(\mathbf{R})$) are given in eqs. 3.54 and 3.55. The nuclear spatial dependence is explicitely written as we study in this section the variation of the two descriptors along $\mathbf{R}$. Both descriptors involve the integration of electron spatial coordinates over the Euclidean space. The attachment and detachment matrix elements are known but we do not know the primitives of the electron attachment and detachment functions nor the primitives of the electron density functions. Unfortunately, the two descriptors are based on these functions. Two computational approaches are compared in this section to calculate the two descriptors at any geometry: the numerical integration (NI) and the population analysis (PA) methods.

The NI method, that is based on the projection of the 1-RDM in the Euclidean space by using a Cartesian grid, is supposed to be exact in the condition that the grid is fine enough in infinite dimensions. The issue of this method is that it is computationally expensive. An alternative is then to use another method, the PA method. We want to know if this method, which is less computationally expensive, is a good approximation and if the results are in adequation with the chemical and physical properties of various molecular systems.

An extended set of various molecules is used (see fig. 5.1). The set of molecules have not been chosen arbitrarily: We want to evaluate the influence of the size of the system (S1, S2, S3, S10, S11), the nature of the excited state: long-range charge transfer or locally excited (S1, S2, S9), the basis set (S1, S2, S3) and the functional (S3, S4, S5, S6, S7, S8, S9, S10) on the descriptor values. In reference [134], the set of molecules S1 have already been used to

characterize the efficiency of the computational methods used to calculate $\chi(\mathbf{R})$ and $\phi_S(\mathbf{R})$. The set of molecules S2 to S10 have already been used in ref. [135] to calculate the overlap between the modulus of occupied and the virtual orbitals and to evaluate the locality of the electronic photo-excitation according to the choice of the basis set and the exchange-correlation functional. For this wide set of molecules, the computational validity of the descriptors has been tested as well on the *oligo*-phenylethynylene (*o*PE) studied in this thesis (set S11). In the first research paper

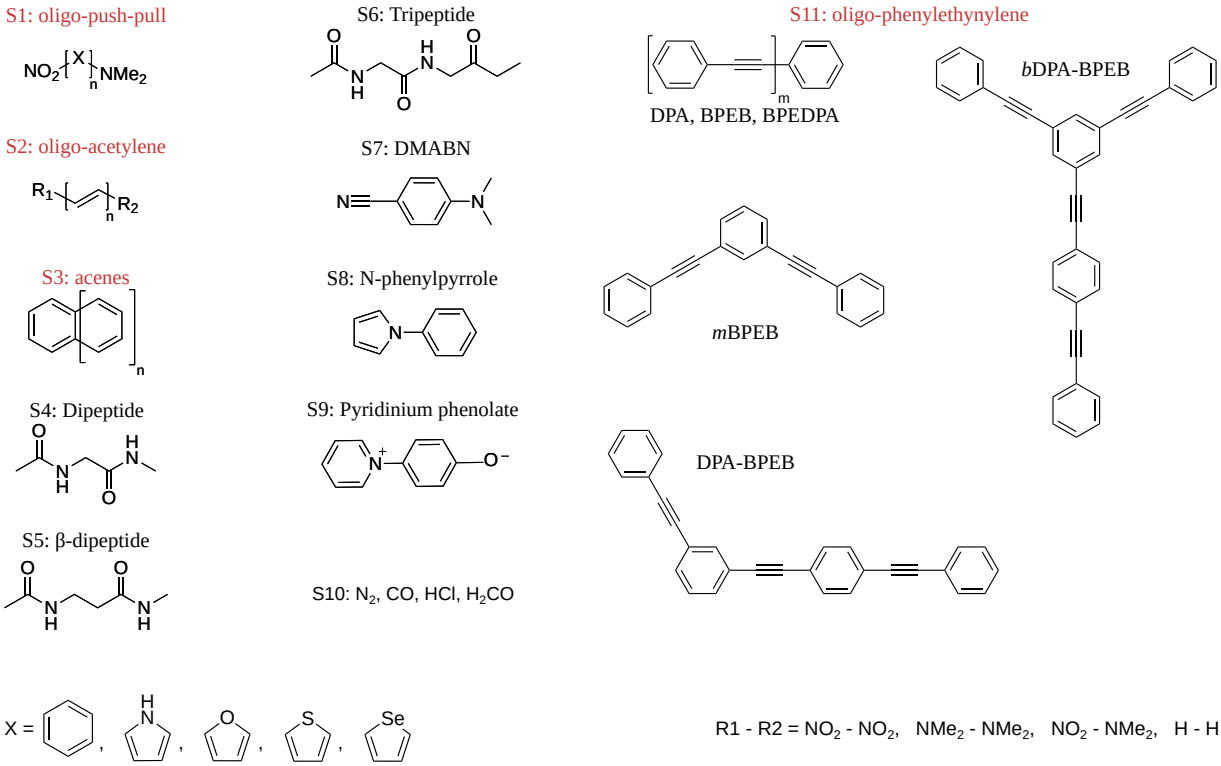

Figure 5.1: Set of molecules used to validate the computational method of the electron density-based descriptors in reference [1], the set written in red is studied in this section.

published in the context of this PhD [1], a precise evaluation of the descriptors according to the previous criteria is explained. The PA method is efficient for medium and large sized molecules. Usually, the values of ϕ_S are trustful if they range between 0.50 and 0.90. If they range under the lower limit or above the higher limit, one needs to compute the descriptors by the use of the NI method. Ref. [1] showed that the size of the basis set does not have an influence on the efficiency on the PA method. The reasoning of this research paper is not developed in the present manuscript and so the reader is kindly referred to this reference for a more exhaustive analysis on the validity of the descriptors. The aim of this thesis holds on the understanding of the potential energy surfaces and the excitation energy transfer within a phenylethynylene dendrimer. Many

*oligo*phenylene-ethynylenes of various size are studied in chapter 6 and their adiabatic electronic excited states are characterized by the use of the density-based descriptors and the attachement the detachment density matrices. Since the size of an *oligo*phenylene-ethynylene can vary from 24 atoms (DPA) to 60 (*b*DPA-BPEB) the validity of the PA method according to the size of the systems will be evaluated here.

5.1.1 The numerical integration

Numerical integration is the reference computational method for the set of molecules in fig. 5.1. It is used to generate density cubes of the attachment and the detachment electron densities n_a and n_d. What is called a density cube is the space discretisation of the electron density on a grid. A discrete sum is then performed to calculate the electron density-based descriptors as approximate integrals.

5.1.2 The population analysis

Population analysis (PA) is based on the decomposition of the electronic density into atomic contributions related to a set of atomic orbitals.
According to the notations in chapter 3, the electron density function for a single Slater determinant reads over occupied spatial orbitals:

$$n(\mathbf{r}_1) = 2 \sum_{i}^{N_{e^-}/2} \mid \chi_i(\mathbf{r}_1) \mid^2 \tag{5.1}$$

where $\chi_i(\mathbf{r}_1)$ is the i^{th} spatial part of the j^{th} canonical occupied spin-orbital. In the basis of atomic orbitals such that $\phi_\alpha(\mathbf{r})$ is the α^{th} atomic orbital, we have:

$$n(\mathbf{r}_1) = \sum_{i}^{N_{e^-}/2} \Big[\sum_{\alpha} (\mathbf{C})_{\alpha i} \phi_\alpha(\mathbf{r}_1) \Big]^2 \tag{5.2}$$

where $(\mathbf{C})_{\alpha i}$ is the linear coefficient of the atomic orbital contribution. By integrating over the space, we have:

$$\int_{\mathbb{R}^3} n(\mathbf{r}_1) \mathrm{d}\mathbf{r}_1 = \mathrm{tr}(\mathbf{PS}) \tag{5.3}$$

where

$$(\mathbf{P})_{\alpha\beta} = 2 \sum_{i}^{N_{e^-}/2} (\mathbf{C})_{\alpha i}(\mathbf{C})_{\beta i} \tag{5.4}$$

and

$$(\mathbf{S})_{\alpha\beta} = \langle \phi_\alpha | \phi_\beta \rangle \tag{5.5}$$

$(\mathbf{P})_{\alpha\beta}$ is 1-RDM element and $(\mathbf{S})_{\alpha\beta}$ is an overlap matrix element between the α^{th} and the β^{th} atomic orbitals. The α^{th} gross orbital population is defined such that

$$m_\alpha = (\mathbf{S}^{1-x}\mathbf{P}\mathbf{S}^{x})_{\alpha\alpha} \tag{5.6}$$

where $x \in [0, 1]$. In the case of $x = 0$ and $x = 1$ the PA is called the Mulliken PA and in the case of $x = \frac{1}{2}$ the PA is called the Löwdin PA and the α^{th} Löwdin gross orbital population is defined such that:

$$l_\alpha = (\mathbf{S}^{1/2}\mathbf{P}\mathbf{S}^{1/2})_{\alpha\alpha} \tag{5.7}$$

It has been demontrated in Appendix C of [1] that the Löwdin PA does not give unphysical values of orbital populations. Other than 0.5 values of x, the gross orbital population can have negative values. Only with Löwdin PA, we have $l_\alpha \in [0, 2]$.

The Löwdin PA applied to the detachment ($n^d(\mathbf{r})$) and the attachment ($n^a(\mathbf{r})$) electron density functions expressed in eqs. 3.54 and 3.55 gives the following alternative expression to the electron density-based descriptors:

$$\phi_{\mathrm{S}}^{PA} = \vartheta^{-1} \sum_{\alpha} \sqrt{\left(\mathbf{S}^{1/2}\gamma^a\mathbf{S}^{1/2}\right)_{\alpha\alpha}\left(\mathbf{S}^{1/2}\gamma^d\mathbf{S}^{1/2}\right)_{\alpha\alpha}} \tag{5.8}$$

and

$$\chi^{PA} = \frac{1}{2} \sum_{\alpha} \mid \left(\mathbf{S}^{1/2}\gamma^a\mathbf{S}^{1/2}\right)_{\alpha\alpha} - \left(\mathbf{S}^{1/2}\gamma^d\mathbf{S}^{1/2}\right)_{\alpha\alpha} \mid \tag{5.9}$$

In practice, ϑ is always strictly greater than zero, $\boldsymbol{\gamma}_a$ and $\boldsymbol{\gamma}_d$ are positive definite. The contribution of the attachment and detachment densities are decomposed on the atomic orbitals. The two formulae look like the expression of the two descriptors in eqs. 3.54 and 3.55 which are suitable for the NI method but here the contributions are taken into account differently.

5.1.3 Results

The descriptor values are presented in tables 5.1, 5.2, 5.3, 5.4 where they are rounded to two decimal places. The values of the two descriptors obtained with the PA method are shown (ϕ_{S}^{PA} and χ^{PA}) and the deviation of the two descriptors to the one obtained by the NI method are labelled $\Delta\phi_{\mathrm{S}}$ and $\Delta\chi$. In the manner of ref. [134] the deviation of the two methods is tolerated if it is lower than 0.05.

The influence of the size of the systems on the deviation between the NI and PA methods is heterogeneous.

n	E-S	ϕ_{S}^{PA}	$\Delta\phi_{\mathrm{S}}$	ϕ_{S}^{PA}	$\Delta\phi_{\mathrm{S}}$	ϕ_{S}^{PA}	$\Delta\phi_{\mathrm{S}}$	ϕ_{S}^{PA}	$\Delta\phi_{\mathrm{S}}$	ϕ_{S}^{PA}	$\Delta\phi_{\mathrm{S}}$
		phenyl		pyrrole		furane		thiophene		selenophene	
1	1	0.55	0.05	0.69	0.02	0.68	0.03	0.70	0.03	0.72	0.04
	2	0.09	0.40	0.48	0.36	0.48	0.36	0.48	0.39	0.48	0.38
	3	0.82	0.02	0.34	0.14	0.52	0.40	0.51	0.41	0.54	0.03
2	1	0.41	0.04	0.57	0.01	0.60	0.03	0.58	0.02	0.68	0.02
	2	0.47	0.03	0.49	0.42	0.48	0.35	0.76	0.25	0.52	0.25
	3	0.74	0.01	0.40	0.03	0.71	0.04	0.72	0.00	0.60	0.12
3	1	0.31	0.02	0.48	0.01	0.53	0.02	0.51	0.02	0.62	0.02
	2	0.54	0.01	0.73	-0.01	0.78	-0.02	0.75	-0.01	0.79	-0.01
	3	0.72	-0.02	0.63	0.01	0.69	0.00	0.70	-0.01	0.74	-0.01
4	1	0.31	0.02	0.39	0.00	0.47	0.02	0.52	0.01	0.57	0.01
	2	0.54	0.01	0.60	0.00	0.77	-0.02	0.75	-0.02	0.78	-0.01
	3	0.72	-0.02	0.71	-0.03	0.66	0.00	0.70	-0.01	0.74	-0.01
5	1	0.23	0.00	0.34	0.01	0.42	0.01	0.47	0.00	0.53	0.00
	2	0.66	-0.03	0.52	0.00	0.75	-0.02	0.73	-0.02	0.76	-0.02
	3	0.68	-0.03	0.71	-0.04	0.65	-0.01	0.68	-0.02	0.72	-0.02

Table 5.1: ϕ_{S}^{PA} values from PA calculations and their deviations from NI calculations: $\Delta\phi_{\mathrm{S}} = \phi_{\mathrm{S}}^{NI} - \phi_{\mathrm{S}}^{PA}$, obtained for the first three electronic excited adiabatic states of the *oligo*-push-pull series S1 with the level of theory PBE0/6-311++G(2d,p).

The first set of molecules is S1, the *oligo*-push-pull (*o*PP) molecules. The *o*PP systems have a nitro-group and a dimethyl-amine group on each side, they are electron acceptor and donor goups, respectively. Such functional groups have been chosen to ensure that a charge transfer

n	E-S	ϕ_S^{PA}	$\Delta\phi_S$	ϕ_S^{PA}	$\Delta\phi_S$	ϕ_S^{PA}	$\Delta\phi_S$	ϕ_S^{PA}	$\Delta\phi_S$
		NO_2-NO_2		NMe_2-NMe_2		NO_2-NMe_2		H-H	
	1	0.04	0.37	0.29	0.06	0.14	0.34	0.01	0.31
1	2	0.04	0.48	0.31	0.01	0.60	0.05	0.16	0.18
	3	0.05	0.49	0.33	-0.03	0.17	0.37	0.92	-0.11
	1	0.08	0.41	0.28	0.09	0.60	0.07	0.94	-0.09
2	2	0.08	0.41	0.21	0.08	0.09	0.40	0.01	0.31
	3	0.09	0.47	0.15	0.13	0.09	0.42	0.04	0.24
	1	0.08	0.40	0.18	0.12	0.62	0.05	0.97	-0.10
3	2	0.08	0.39	0.53	0.02	0.13	0.33	0.01	0.31
	3	0.84	-0.06	0.29	0.05	0.13	0.38	0.02	0.24
	1	0.86	-0.06	0.84	-0.06	0.63	0.05	0.98	-0.11
4	2	0.07	0.39	0.20	0.10	0.06	0.39	0.98	-0.05
	3	0.07	0.39	0.48	0.01	0.63	0.05	0.02	0.24
	1	0.88	-0.08	0.91	-0.08	0.64	0.04	0.98	-0.12
5	2	0.07	0.38	0.27	0.07	0.12	0.33	0.98	-0.05
	3	0.07	0.38	0.29	0.07	0.87	-0.01	0.02	0.24

Table 5.2: ϕ_S^{PA} values from PA calculations and their deviations from NI calculations: $\Delta\phi_S = \phi_S^{NI} - \phi_S^{PA}$, obtained for the first three electronic excited adiabatic states of the *oligo*-acetylene series S2 with the level of theory PBE0/6-311++G(2d,p).

state is involved in the first three electronic excited states. The repetitive units on set S1 can be a phenyl, a pyrrole, a furane, a thiophene and a selenophene group. We see on table 5.1 that for a same amount of repetitive unit the deviation is similar for each system. In the case of $n = 1$ and $n = 2$ we note that the density-based descriptors are very sensitive to the computational method. The deviation is not acceptable if ϕ_S has value under 0.52. Considering the selenophene (third electronic excited state) and thiophene (second electronic excited state) with two repetitive units, we see that ϕ_S^{PA} is equal to 0.60 and 0.76, respectively, and the deviation is not acceptable. But for larger systems ($n = 3$ to $n = 5$) all of the deviations are acceptable. The second set of molecules is S2, the *oligo*-acetylene (*o*A) molecules. The size of *o*A varies and the two functional groups on each side of the *o*A thus it influences the locality of the excited states (NO_2 and NO_2, NO_2 and NMe_2, NMe_2 and NMe_2, H and H). The results on this set differ in some aspects to the results of set S1. The results are gathered in table 5.2. We see

n	E-S	ϕ_{S}^{PA}	$\Delta\phi_{\mathrm{S}}$	χ^{PA}	$\Delta\chi$
	1	0.92	-0.06	0.13	0.14
1	2	0.98	0.00	0.15	0.00
	3	0.88	-0.07	0.21	0.11
	1	0.90	0.08	0.12	0.18
2	2	0.98	-0.01	0.13	0.02
	3	0.91	-0.06	0.18	0.09
	1	0.90	-0.09	0.10	0.18
3	2	0.97	-0.01	0.12	0.03
	3	0.90	-0.06	0.24	0.07
	1	0.90	0.10	0.09	0.19
4	2	0.89	-0.05	0.25	0.05
	3	0.97	-0.01	0.12	0.03
	1	0.90	-0.09	0.09	0.18
5	2	0.90	-0.06	0.27	0.06
	3	0.89	-0.05	0.27	0.09

Table 5.3: Descriptor values from PA calculations and their deviations from NI calculations: $\Delta\phi_{\mathrm{S}} = \phi_{\mathrm{S}}^{NI} - \phi_{\mathrm{S}}^{PA}$ and $\Delta\chi = \chi^{NI} - \chi^{PA}$, obtained for the first three electronic excited adiabatic states of the *oligo*-acenes series S3 with the level of theory B3LYP/cc-pVTZ.

that the deviation is acceptable for every system if the descriptor does not have extreme values: close to one or close to zero. If the ϕ_{S}^{PA} values lie between 0.3 and 0.8 the PA method is in good agreement with the NI method. But in the case of a pure charge transfer state where an effective charge is displaced from one site to another of the molecule, for example, considering two repetitive units ($n = 2$) and for the second excited state (ES= 2) for NO_2 and NMe_2 as functional groups, $\phi_{\mathrm{S}}^{PA} = 0.09$ and the deviation is equal to 0.40. In the same way, in the case of a pure locally excited state where the attachement and detachment densities are localised in the exact same area, the deviation is not acceptable. Indeed in the case of $n = 3$, ES= 1 with H and H as functional group we get $\phi_{\mathrm{S}}^{PA} = 0.97$ and the deviation is -0.10. The third set of molecules S3 is a series of *oligo*-acenes. Due to the high conjugation of the π-system, the excited states are delocalized over the whole system. The results of the set S3 are gathered in table 5.3. No trend is observed within the results of this set. The extreme values of the descriptors (close to 0 or 1) lead to both acceptable and non-acceptable deviations. For example in the case of n=4, $\phi_{\mathrm{S}}^{PA} = 0.90$ and $\Delta\phi_{\mathrm{S}} = 0.10$ for the first electronic excited state while $\phi_{\mathrm{S}}^{PA} = 0.97$ and

n	E-S	ϕ_{S}^{PA}	$\Delta\phi_{\mathrm{S}}$	χ^{PA}	$\Delta\chi$
1	S_1	0.98	-0.12	0.14	0.22
2	S_1	0.99	-0.13	0.12	0.26
3	S_1	0.99	-0.14	0.11	0.28
m-BPEB	S_1	0.98	-0.12	0.14	0.22
m-DPABPEB	S_1	0.99	-0.25	0.12	0.26
m-DPABPEB	S_2	0.98	-0.12	0.14	0.22
bm-DPABPEB	S_1	0.99	-0.13	0.12	0.26
bm-DPABPEB	S_2	0.98	-0.11	0.16	0.20

Table 5.4: Descriptor values from PA calculations and their deviations from NI calculations: $\Delta\phi_{\mathrm{S}} = \phi_{\mathrm{S}}^{NI} - \phi_{\mathrm{S}}^{PA}$ and $\Delta\chi = \chi^{NI} - \chi^{PA}$, obtained for the first electronic excited adiabatic states of the *o*PE series S11 with the level of theory CAM-B3LYP/6-31+G(d).

$\Delta\phi_{\mathrm{S}} = -0.01$ for the third one. Here, the highest value of ϕ_{S}^{PA} leads to the acceptable deviation which is totally different than the study of the S2 set.

In addition to that, the PA method is characterized by similar efficiency on the χ^{PA} values and its deviation. If the deviation is acceptable (or not) for one of the two descriptors, it is for the second. The last set of molecules is the set labelled S11. It is composed of *oligo*-phenylene-ethynylenes (*o*PE) that have been studied in this thesis. The results are gathered in table 5.4. The trend is obvious here: ϕ_{S}^{PA} is overestimated and χ^{PA} is underestimated for to the descriptors calculated by the NI method. The deviation for every system is non-acceptable as it is higher than 0.05 and is around -0.12 for the ϕ_{S} descriptor and is around 0.22 for the χ descriptor.

The population analysis calculation method does not give enough similar qualitative and quantitative results to the one of the numerical integration calculation method. Even though the population analysis method gives acceptable results for the sets S1, S2, S3 if ϕ_{S}^{PA} takes values between 0.50 and 0.80, the population analysis method is not acceptable for the set of *oligo*-phenylene-ethynylene S11. ϕ_{S} is over-estimated and χ is under-estimated. From now on, the calculations of the descriptors will be perfomed with the numerical integration method.

5.2 The behavior of the descriptors in the vicinity of a conical intersection

The two descriptors χ and ϕ_{S} have been developed with the goal of characterizing the nature of electronic excited states and precisely to get a systematic picture of the locality of electronic excitations. Considering a chemical point of view, diabatic states are chosen to be conservative according to electronic properties. It can be the symmetry of electronic excited states, the oscillator strength and descriptors may also be used to characterize diabatic and adiabatic electronic states. In this section, descriptors are then studied as functions of $\mathbf{R}$.

A conical intersection (CoIn) is the locus where two adiabatic electronic states are degenerate and so where the BOA is not valid. The branching space (BS) is the two-dimensional space in which the two adiabatic states are not degenerate to first order. The two BS vectors are the gradient difference (GD) and the derivative coupling (DC) vectors.

Typically, according to an arbitrary choice of diabatic states based on the conservation of an electronic property, the GD vector is the direction that swaps the diabatic assignment of the adiabatic electronic states. The direction of the GD vector is the direction of the maximum preservation of chemical nature. Along this direction there is a swapping of the electronic properties of two states that cross. This is why it is also called the "tuning mode".

The DC vector is the direction along which the two adiabatic electronic states are the most mixed with respect to the diabatic ones. It is also called the "coupling mode".

CoIn are then the locus around which an electronic property can vary significantly to first order. Since χ and ϕ_{S} are functions that characterize the locality of an electronic excitation, we study the variation of the two functions in the vicinity of CoIn.

The two descriptors are studied in the vicinity of two major types of CoIn of this thesis (see fig. 5.2). They are labelled $\mathrm{Qx}_{cu/tr}^{DPA}$ and $\mathrm{Qx}_{pf}^{m-BPEB}$. The first CoIn, $\mathrm{Qx}_{cu/tr}^{DPA}$ is a CoIn for the first two electronic adiabatic excited states of diphenylacetylene (DPA). It involves the first optically active state 1^1B_{u} and the first optically inactive state 1^1A_{u} in the $\mathcal{C}_{2\mathrm{h}}$ point group (PG). The energy minimum of the optically active state is associated to the cumulenic isomer of DPA (see fig. 5.3) and belongs to the $\mathcal{D}_{2\mathrm{h}}$ PG, the state is of $B_{1\mathrm{u}}$ symmetry. The energy minimum of the 1^1A_{u} state is associated to the *trans* isomer of DPA (see fig. 5.3) in the $\mathcal{C}_{2\mathrm{h}}$ PG.

A $B_{3\mathrm{g}}$ deformation from the cumulenic isomer leads to the *trans* isomer (see fig. 5.3). The direction of the GD vector has been chosen such that it conserves the PG and allows the sym-

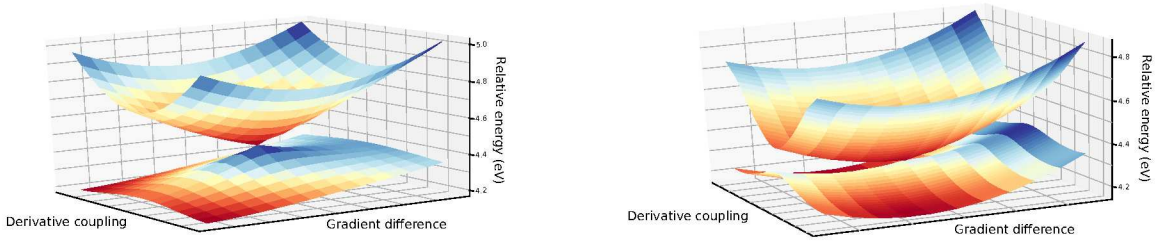

Figure 5.2: Conical intersection $1^1B_u/1^1A_u$ of diphenylacetylene labelled $Qx_{cu/tr}^{DPA}$ (on the left) and conical intersection $1^1A_1/1^1B_2$ of 1,3-*bis*(phenylethynyl)benzene labelled Qx_{pf}^{m-BPEB} (on the right).

metry swapping between the two electronic adiabatic excited states. The GD vector is then of A_g symmetry. Due to symmetry reasons, the DC vector is of B_g symmetry and it is orthogonal to the GD vector. Along the DC vector, the molecular geometry belongs to the $\mathcal{C}_i$ point group and the crossing involves the 1^1A_u and the 2^1A_u states for such distorted, out-of-plane geometries. The second CoIn is Qx_{pf}^{m-BPEB} which involves the first two electronic adiabatic excited

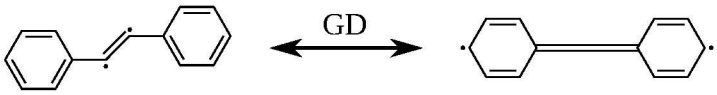

Figure 5.3: *Trans* isomer of DPA (on the left) and cumulenic isomer (on the right).

states of 1,3-*bis*(phenylethynyl)-benzene (*m*BPEB). This crossing has already been deeply studied in the article [43] since it is at the center of the study on the pseudofragmentation scheme of phenylethynylene dendrimers. The CoIn belongs to the $\mathcal{C}_{2v}$ point group and it results from the crossing between the two optically active states 1^1B_2 and 1^1A_1. The two states are delocalized states that can be characterized by single excitations HOMO-1→LUMO and HOMO→LUMO+1. The lowest energy points of these two states within the $\mathcal{C}_{2v}$ point group are two first order saddle points which belong to the PES of the first electronic adiabatic excited state. In addition, this PES shows two minima of same energy (4.12 eV) (see fig. 5.4). These two minima belong to the $1^1A'$ state of the $\mathcal{C}_s$ point group. The GD vector has been chosen such that the crossing involves the first two optically active states 1^1A_1 and 1^1B_2. The GD vector conserves the symmetry of the system and is then A_1. Due to symmetry reasons the DC vector does not preserve the $\mathcal{C}_{2v}$ point group and is orthogonal to the GD vector. The DC vector is determined such that the two electronic adiabatic excited states involved in the crossing are $1^1A'$ and $2^1A'$ in $\mathcal{C}_s$. The relative energy of the first two electronic adiabatic excited states of DPA, the first three electronic adiabatic excited states of *m*BPEB, the associated oscillator strengths, ϕ_S and χ are plotted along

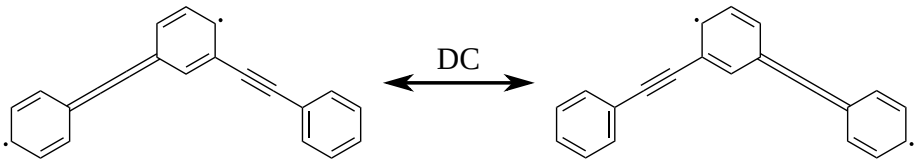

Figure 5.4: Localized cumulenic isomers either on the left or on the right pseudrofragment (on the left and on the right, respectively).

the two vectors of the branching space which have been determined above (see fig. 5.5 and 5.6). Eventhough the CoIn $\mathrm{Qx}_{pf}^{m-BPEB}$ involves only the first two electronic adiabatic excited states, there are two avoided crossings between the second and the third electronic adiabatic excited state and so the three electronic adiabatic excited states have been plotted for clarity. In the plots, the abscissa is dimensionless. The unit x along the abscissa corresponds to a displacement along $x \times a_0 \times 5.0\,10^{-4}$ the branching space vectors to ensure the 1^{st} order lifting of degeneracy. a_0 is the Bohr radius.

The GD vector of the CoIn $\mathrm{Qx}_{cu/tr}^{DPA}$ have been chosen such that it is A_g and it allows the first two singlet states to swap their symmetries. On fig. 5.5 we notice that the first singlet state is 1^1B_u from -7 to 0 and is 1^1A_u from 0 to 7 and the second singlet state is 1^1A_u then 1^1B_u along this coordinate. The 1^1B_u state (1^1B_1u in the $\mathcal{D}_\mathrm{2h}$ point group) is known to be the first bright singlet state and the 1^1A_u state is known to be an optically forbidden state [51]. As the GD vector is the direction that swaps the symmetry between these two states, we observe as well the swapping of the oscillator strength on fig. 5.5.

The DC vector has the direction that mixes the first two electronic adiabatic excited states such that they have the same symmetry along this direction, they are 1^1A_u and 2^1A_u. At 0, at the apex, the adiabatic states are degenerate so undetermined which explains the brutal variation of the oscillator strength while on the right and on the left of the apex, the two states are maximally mixed with each other (normalised sum and difference) and so the oscillator strengths of both states are similar.

Along these two directions, the two density-based descriptors vary in the same way as the oscillator strength according to the arbitrary choice of the diabatic states. Along the GD direction there are abrupt variations of ϕ_S and χ. The first electronic adiabatic excited state is characterized by ϕ_S values around 0.85 and by a χ value around 0.35 when the first electronic adiabatic excited state is of 1^1B_u symmetry and when it is of 1^1A_u symmetry, it is characterized by ϕ_S values around 0.55 and by a χ value around 0.70. At a CoIn, ϕ_S and χ are undetermined

but they have been calculated in the vicinity of the CoIn along the DC vector: the descriptors have values around 0.70 and 0.55 respectively.

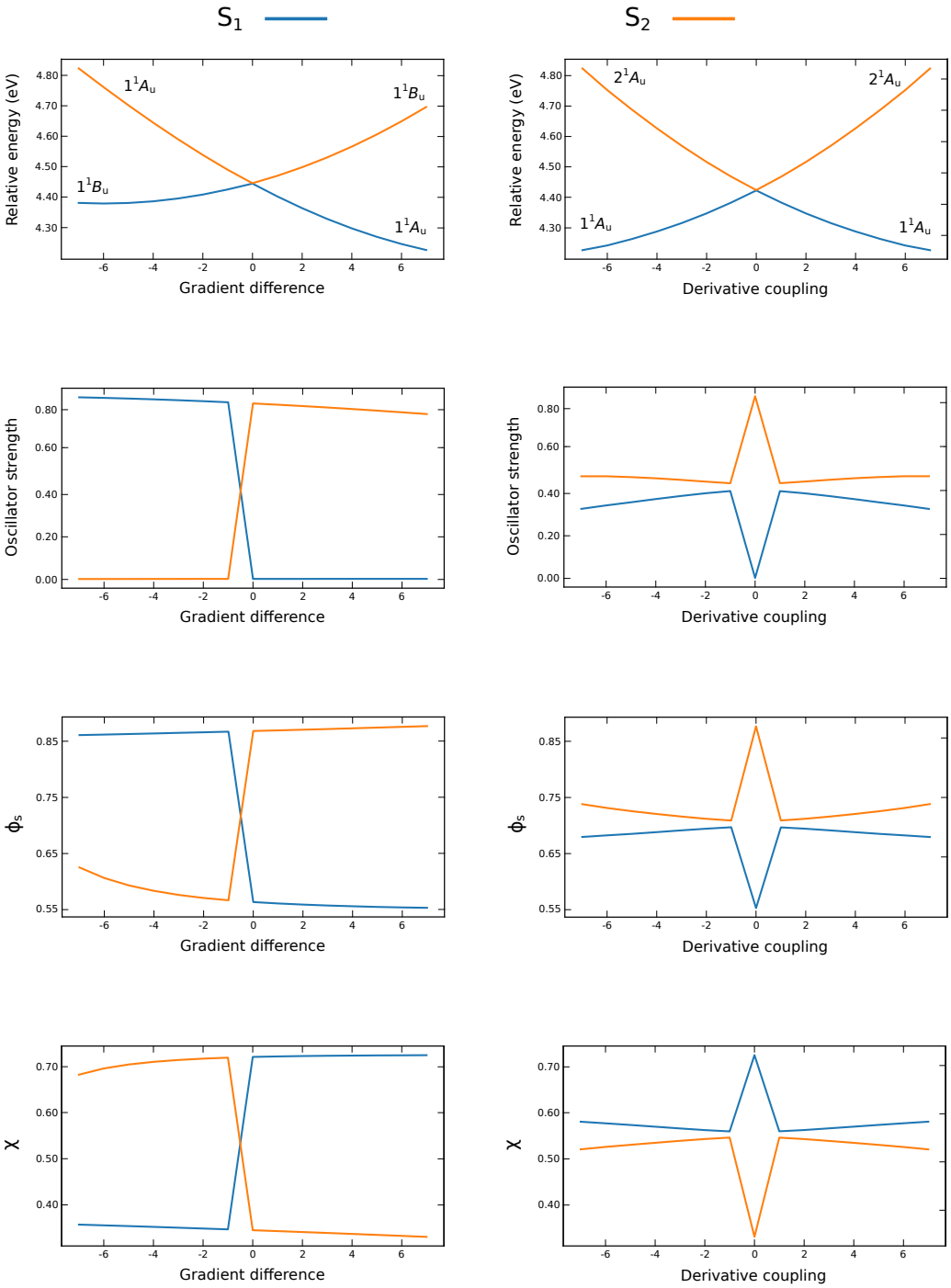

Figure 5.5: Relative energy in eV, oscillator strength, ϕ_S and ϕ are plotted along the two vectors GD and DC in the vicinity of the CoIn $Qx^{DPA}_{cu/tr}$ for the first two electronic adiabatic excited states. The first singlet is plotted with line in blue and the second singlet is plotted with line in orange.

The GD direction of the second CoIn, $\mathrm{Qx}_{pf}^{m-BPEB}$, allows the symmetry swapping between the first two diabatic states: 1^1B_2 and 1^1A_1. Both of these diabatic states are optically active states. The 1^1B_2 state is characterized by an oscillator strength which value is almost constant at 1.70. The values of ϕ_S and χ vary from 0.72 to 0.76 and from 0.39 to 0.34 respectively. The second diabatic state, the 1^1A_1 state, is characterized by oscillator strength values around 0.37. The values of the descriptors are almost constant such that $\phi_\mathrm{S} \approx 0.77$ and $\chi \approx 0.33$. Along this direction, we see that the two descriptors and the oscillator strength evolve in the same way. There is a swapping of the oscillator strengths and descriptors values on the first and the second adiabatic singlet states according to the swapping of the symmetries of the two states. The DC direction is the one that mixes the two adiabatic singlet states $1^1A'$ and $2^1A'$ and on the left and right of this CoIn the two adiabatic states have the same oscillator strength value (around 1.00). Moreover, there are two avoided crossings between the second and the third excited singlet states around -18 and 18 (see fig. 5.6.). The way the oscillator strength varies when considering the second and the third electronic singlet excited states, we observe a variation of its value from 1.00 to 0.00 and so the direction of this DC vector is a direction that swap the oscillator strength between $2^1A'$ and $3^1A'$. The variation of the two descriptors along this direction is more complicated. The drastic variations of ϕ_S and χ from -20 to -10 and from 10 to 20 of the second and third electronic adiabatic excited states match with the avoided crossing. However it not possible to characterize this DC direction as a direction that mixes these two density-based descriptors. Between -5 and 5 we see that the oscillator strength of the first and the second electronic adiabatic excited states are equal to each other and the second electronic adiabatic excited state does not interact significantly with the third electronic adiabatic excited state and so we can consider that within this interval, only the first and the second electronic adiabatic excited states interact with each other. On the right and on the left of the CoIn, ϕ_S of S_1 and S_2 have both similar values (around 0.74) and χ of both states have values around 0.36. They vary as the oscillator strength and so it seems that this DC direction is a direction that mixes the density-based descriptors. However, it is difficult to be certain since the third electronic adiabatic excited state has a strong effect on the variation of the two density-based descriptors. In addition, at the CoIn, along the DC direction the oscillator strength rises or falls drastically according to the first or the second electronic adiabatic excited state. Similar variation is observed on fig. 5.5 on the study of the CoIn $\mathrm{Qx}_{cu/tr}^{DPA}$ considering the oscillator strength, ϕ_S and χ but on the study of the second CoIn $\mathrm{Qx}_{pf}^{m-BPEB}$, the two density-based descriptors do not vary in a similar way.

They both rise drastically.

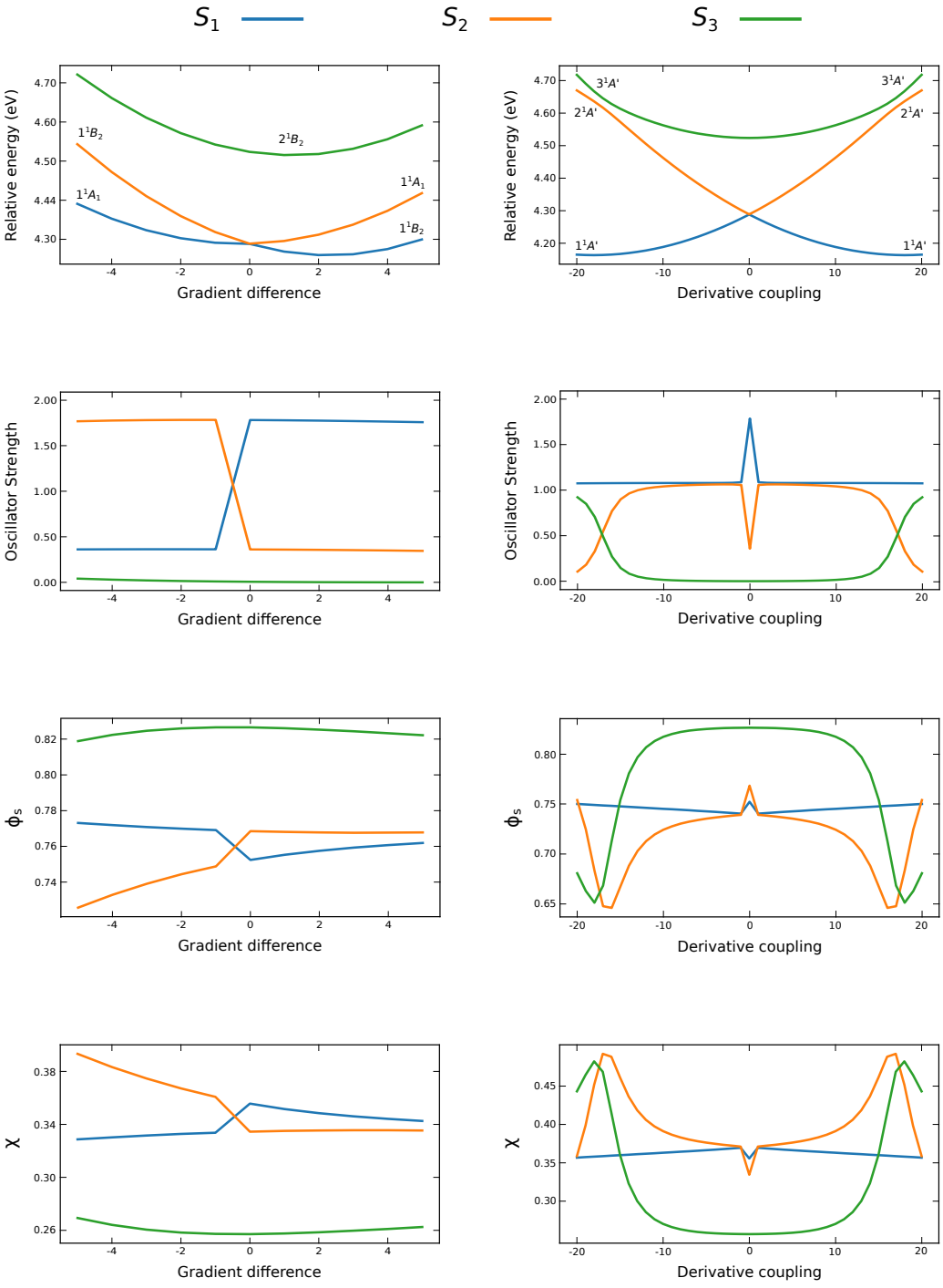

Figure 5.6: The oscillator strength and the two electron density-based descriptors χ and ϕ_S are plotted along the GD vector and the DC vector of the CoIn d22.

To understand why the two density-based descriptors behave oddly in the vicinity of the CoIn $\mathrm{Qx}_{pf}^{m-BPEB}$ while they behave as the oscillator strength in the vicinity of the CoIn $\mathrm{Qx}_{cu/tr}^{DPA}$, one needs to get a writing of the adiabatic descriptors and of the oscillator strength by taking into account diabatic electronic excited states.

For simplicity we consider that the ground state does not cross at all the first adiabatic electronic excited states and that the ground state is approximately diabatic. We supposed that we are in the two-excited-state approximation where $\left|\psi_1^{\mathrm{ad}}\right\rangle$ and $\left|\psi_2^{\mathrm{ad}}\right\rangle$ are two adiabatic electronic excited states and that there is two strictly diabatic states $\left|\psi_1^{\mathrm{dia}}\right\rangle$ and $\left|\psi_2^{\mathrm{dia}}\right\rangle$. In the vicinity of a conical intersections we can rotate from an adiabatic set to a diabatic set:

$$\begin{array}{rcl} \left|\psi_1^{\mathrm{ad}}\right\rangle & = & \cos\left(\theta(\mathbf{R})\right)\left|\psi_1^{\mathrm{dia}}\right\rangle + \sin\left(\theta(\mathbf{R})\right)\left|\psi_2^{\mathrm{dia}}\right\rangle \\ \left|\psi_2^{\mathrm{ad}}\right\rangle & = & -\sin\left(\theta(\mathbf{R})\right)\left|\psi_1^{\mathrm{dia}}\right\rangle + \cos\left(\theta(\mathbf{R})\right)\left|\psi_2^{\mathrm{dia}}\right\rangle \end{array} \tag{5.10}$$

The adiabatic N_{e^-}-particle electron density operators of the first ($\hat{\Gamma}_1^{\mathrm{ad}}$) and the second ($\hat{\Gamma}_2^{\mathrm{ad}}$) adiabatic electronic excited states are defined as:

$$\begin{array}{rcl} \hat{\Gamma}_1^{\mathrm{ad}} & = & \left|\psi_1^{\mathrm{ad}}\right\rangle\left\langle\psi_1^{\mathrm{ad}}\right| \\ \hat{\Gamma}_2^{\mathrm{ad}} & = & \left|\psi_2^{\mathrm{ad}}\right\rangle\left\langle\psi_2^{\mathrm{ad}}\right| \end{array} \tag{5.11}$$

The diabatic N_{e^-}-particle electron density operators are defined similarly. We would get the same equations as 5.11 by substituting the upperscript "ad" by the upperscript "dia". The adiabatic N_{e^-}-particle transition density operators between the first and the second adiabatic electronic excited states, and between the second and the first adiabatic electronic excited states are defined such that:

$$\begin{array}{rcl} \hat{\Gamma}_{12}^{\mathrm{ad}} & = & \left|\psi_1^{\mathrm{ad}}\right\rangle\left\langle\psi_2^{\mathrm{ad}}\right| \\ \hat{\Gamma}_{21}^{\mathrm{ad}} & = & \left|\psi_2^{\mathrm{ad}}\right\rangle\left\langle\psi_1^{\mathrm{ad}}\right| \end{array} \tag{5.12}$$

The diabatic N_{e^-}-particle transition density operators are defined similarly. We would get the same equations as 5.12 by substituting the upperscript "ad" by the upperscript "dia". Eqs. 5.10, 5.11 and 5.12 give then:

$$\hat{\Gamma}_1^{\mathrm{ad}} = \Big(\cos\left(\theta(\mathbf{R})\right)\Big)^2\hat{\Gamma}_1^{\mathrm{dia}} + \Big(\sin\left(\theta(\mathbf{R})\right)\Big)^2\hat{\Gamma}_2^{\mathrm{dia}} + \cos\left(\theta(\mathbf{R})\right)\sin\left(\theta(\mathbf{R})\right)\left(\hat{\Gamma}_{12}^{\mathrm{dia}} + \hat{\Gamma}_{21}^{\mathrm{dia}}\right) \tag{5.13}$$

and

$$\hat{\Gamma}_2^{\mathrm{ad}} = \Big(\sin\big(\theta(\mathbf{R})\big)\Big)^2 \hat{\Gamma}_1^{\mathrm{dia}} + \Big(\cos\big(\theta(\mathbf{R})\big)\Big)^2 \hat{\Gamma}_2^{\mathrm{dia}} - \cos\big(\theta(\mathbf{R})\big)\sin\big(\theta(\mathbf{R})\big)\big(\hat{\Gamma}_{12}^{\mathrm{dia}} + \hat{\Gamma}_{21}^{\mathrm{dia}}\big) \tag{5.14}$$

Since we are working with real wavefunctions, we have $\hat{\Gamma}_{12}^{\mathrm{dia}} = \hat{\Gamma}_{21}^{\mathrm{dia}}$ then:

$$\hat{\Gamma}_1^{\mathrm{ad}} = \Big(\cos\big(\theta(\mathbf{R})\big)\Big)^2 \hat{\Gamma}_1^{\mathrm{dia}} + \Big(\sin\big(\theta(\mathbf{R})\big)\Big)^2 \hat{\Gamma}_2^{\mathrm{dia}} + 2\cos\big(\theta(\mathbf{R})\big)\sin\big(\theta(\mathbf{R})\big)\hat{\Gamma}_{12}^{\mathrm{dia}} \tag{5.15}$$

and

$$\hat{\Gamma}_2^{\mathrm{ad}} = \Big(\sin\big(\theta(\mathbf{R})\big)\Big)^2 \hat{\Gamma}_1^{\mathrm{dia}} + \Big(\cos\big(\theta(\mathbf{R})\big)\Big)^2 \hat{\Gamma}_2^{\mathrm{dia}} - 2\cos\big(\theta(\mathbf{R})\big)\sin\big(\theta(\mathbf{R})\big)\hat{\Gamma}_{12}^{\mathrm{dia}} \tag{5.16}$$

using trigonometric relations, the two previous equations read:

$$\hat{\Gamma}_1^{\mathrm{ad}} = \frac{1}{2}\big(\hat{\Gamma}_1^{\mathrm{dia}} + \hat{\Gamma}_2^{\mathrm{dia}}\big) + \frac{1}{2}\cos\big(2\theta(\mathbf{R})\big)\big(\hat{\Gamma}_1^{\mathrm{dia}} - \hat{\Gamma}_2^{\mathrm{dia}}\big) + \sin\big(2\theta(\mathbf{R})\big)\hat{\Gamma}_{12}^{\mathrm{dia}} \tag{5.17}$$

and

$$\hat{\Gamma}_2^{\mathrm{ad}} = \frac{1}{2}\big(\hat{\Gamma}_1^{\mathrm{dia}} + \hat{\Gamma}_2^{\mathrm{dia}}\big) - \frac{1}{2}\cos\big(2\theta(\mathbf{R})\big)\big(\hat{\Gamma}_1^{\mathrm{dia}} - \hat{\Gamma}_2^{\mathrm{dia}}\big) - \sin\big(2\theta(\mathbf{R})\big)\hat{\Gamma}_{12}^{\mathrm{dia}} \tag{5.18}$$

The latter equations are written for the N_{e^-}-electron densities however, they can be represented in the one-electron space coordinates. Thus it gives us access to the one-particle adiabatic electronic density functions:

$$n(\mathbf{R})_1^{\mathrm{ad}} = \frac{1}{2}\big(n(\mathbf{R})_1^{\mathrm{dia}} + n(\mathbf{R})_2^{\mathrm{dia}}\big) + \frac{1}{2}\cos\big(2\theta(\mathbf{R})\big)\big(n(\mathbf{R})_1^{\mathrm{dia}} - n(\mathbf{R})_2^{\mathrm{dia}}\big) + \sin\big(2\theta(\mathbf{R})\big)\gamma(\mathbf{R})_{12}^{\mathrm{dia}} \tag{5.19}$$

and

$$n(\mathbf{R})_2^{\mathrm{ad}} = \frac{1}{2}\big(n(\mathbf{R})_1^{\mathrm{dia}} + n(\mathbf{R})_2^{\mathrm{dia}}\big) - \frac{1}{2}\cos\big(2\theta(\mathbf{R})\big)\big(n(\mathbf{R})_1^{\mathrm{dia}} - n(\mathbf{R})_2^{\mathrm{dia}}\big) - \sin\big(2\theta(\mathbf{R})\big)\gamma(\mathbf{R})_{12}^{\mathrm{dia}} \tag{5.20}$$

where $n(\mathbf{R})_1^{\mathrm{ad}}$ and $n(\mathbf{R})_1^{\mathrm{ad}}$ are the adiabatic electron density functions of the first and the second adiabatic electronic excited states, $n(\mathbf{R})_1^{\mathrm{dia}}$ and $n(\mathbf{R})_2^{\mathrm{dia}}$ are the diabatic electron density functions of the first and the second diabatic electronic excited states, and $\gamma(\mathbf{R})_{12}^{\mathrm{dia}}$ is the diabatic transition density function between the first and the second diabatic electronic excited states.

The adiabatic density-based descriptors χ and φ depend explicitly of $n(\mathbf{R})_1^{\mathrm{ad}}$ or of $n(\mathbf{R})_2^{\mathrm{ad}}$,

depending if they are obtained for the first or the second adiabatic electronic excited states, because of the difference density function. The adiabatic descriptor ϕ_{S} depends on the attachment and detachment densities function which are obtained from the difference density matrix. The three adiabatic descriptors depend then explicitly or implicitly on the diabatic electron density function ($n(\mathbf{R})_1^{\mathrm{dia}}$ and $n(\mathbf{R})_2^{\mathrm{dia}}$) and on the diabatic transition density function ($\gamma(\mathbf{R})_{12}^{\mathrm{dia}}$) which is related to the coupling between the two diabatic states.

Let us consider an observable that varies little with the nuclear coordinates, for example the electric dipole $\hat{\boldsymbol{\mu}}$. For simplicity, we consider a single vector component and we denote it $\hat{\boldsymbol{\mu}}$. The adiabatic transition dipole moments between the ground state and the first adiabatic electronic excited state, and between the ground state and the second adiabatic electronic excited state are defined as:

$$\mu_{01}^{\mathrm{ad}} = \langle \psi_0 | \, \hat{\mu} \, \left| \psi_1^{\mathrm{ad}} \right\rangle \tag{5.21}$$

$$\mu_{02}^{\mathrm{ad}} = \langle \psi_0 | \, \hat{\mu} \, \left| \psi_2^{\mathrm{ad}} \right\rangle \tag{5.22}$$

The oscillator strength f^{ad} is defined such that is proportional to the square modulus of the adiabatic transition dipole moment. According to the rotation equations of eq. 5.10, we have:

$$\begin{aligned} \boldsymbol{\mu}_{01}^{\mathrm{ad}}(\mathbf{R}) &= \cos\left(\theta(\mathbf{R})\right)\boldsymbol{\mu}_{01}^{\mathrm{dia}} + \sin\left(\theta(\mathbf{R})\right)\boldsymbol{\mu}_{02}^{\mathrm{dia}} \\ \boldsymbol{\mu}_{02}^{\mathrm{ad}}(\mathbf{R}) &= -\sin\left(\theta(\mathbf{R})\right)\boldsymbol{\mu}_{01}^{\mathrm{dia}} + \cos\left(\theta(\mathbf{R})\right)\boldsymbol{\mu}_{02}^{\mathrm{dia}} \end{aligned} \tag{5.23}$$

and

$$\begin{aligned} f_{01}^{\mathrm{ad}}(\mathbf{R}) &= \Big(\cos\left(\theta(\mathbf{R})\right)\Big)^2 f_{01}^{\mathrm{dia}} + \Big(\sin\left(\theta(\mathbf{R})\right)^2\Big) f_{02}^{\mathrm{dia}} + \cos\left(\theta(\mathbf{R})\right)\sin\left(\theta(\mathbf{R})\right)\left(\boldsymbol{\mu}_{01}^{\mathrm{dia}}\boldsymbol{\mu}_{02}^{\mathrm{dia}} + \boldsymbol{\mu}_{02}^{\mathrm{dia}}\boldsymbol{\mu}_{01}^{\mathrm{dia}}\right) \\ f_{02}^{\mathrm{ad}}(\mathbf{R}) &= \Big(\sin\left(\theta(\mathbf{R})\right)\Big)^2 f_{01}^{\mathrm{dia}} + \Big(\cos\left(\theta(\mathbf{R})\right)^2\Big) f_{02}^{\mathrm{dia}} - \cos\left(\theta(\mathbf{R})\right)\sin\left(\theta(\mathbf{R})\right)\left(\boldsymbol{\mu}_{01}^{\mathrm{dia}}\boldsymbol{\mu}_{02}^{\mathrm{dia}} + \boldsymbol{\mu}_{02}^{\mathrm{dia}}\boldsymbol{\mu}_{01}^{\mathrm{dia}}\right) \end{aligned} \tag{5.24}$$

Since $\boldsymbol{\mu}_{01}^{\mathrm{dia}}$ and $\boldsymbol{\mu}_{02}^{\mathrm{dia}}$ are vectors that are here not along the same axes their product is equal to zero. Then we get:

$$\begin{aligned} f_{01}^{\mathrm{ad}}(\mathbf{R}) &= \Big(\cos\left(\theta(\mathbf{R})\right)\Big)^2 f_{01}^{\mathrm{dia}} + \Big(\sin\left(\theta(\mathbf{R})\right)\Big)^2 f_{02}^{\mathrm{dia}} \\ f_{02}^{\mathrm{ad}}(\mathbf{R}) &= \Big(\sin\left(\theta(\mathbf{R})\right)\Big)^2 f_{01}^{\mathrm{dia}} + \Big(\cos\left(\theta(\mathbf{R})\right)\Big)^2 f_{02}^{\mathrm{dia}} \end{aligned} \tag{5.25}$$

Using trigonometric relations, we can get a simplifed writing of eq. 5.26 as we did for eq. 5.12:

$$\begin{aligned} f_{01}^{\mathrm{ad}}(\mathbf{R}) &= \tfrac{1}{2}(f_{01}^{\mathrm{dia}} + f_{02}^{\mathrm{dia}}) + \tfrac{1}{2}\cos\left(2\theta(\mathbf{R})\right)\tfrac{1}{2}(f_{01}^{\mathrm{dia}} - f_{02}^{\mathrm{dia}}) \\ f_{02}^{\mathrm{ad}}(\mathbf{R}) &= \tfrac{1}{2}(f_{01}^{\mathrm{dia}} + f_{02}^{\mathrm{dia}}) - \tfrac{1}{2}\cos\left(2\theta(\mathbf{R})\right)\tfrac{1}{2}(f_{01}^{\mathrm{dia}} - f_{02}^{\mathrm{dia}}) \end{aligned} \tag{5.26}$$

5.2.1 In the vicinity of a conical intersection

Along the GD-type coordinate $\mathbf{R}_i$

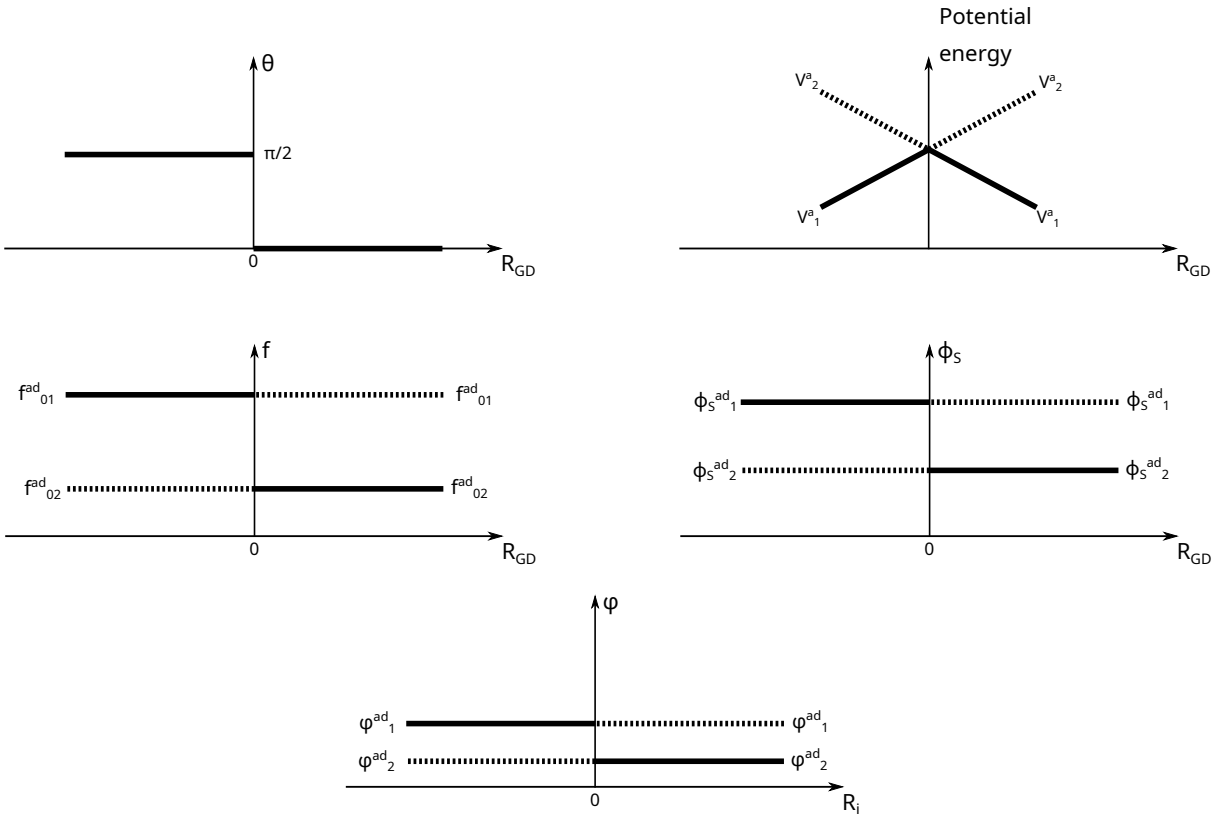

Figure 5.7: Schematic representation of the mixing angle (θ), the adiabatic potential energies (V_1^{ad} and V_2^{ad}), the ϕ_{S} adiabatic descriptors ($\phi_{\mathrm{S}\,1}^{\mathrm{ad}}$ and $\phi_{\mathrm{S}\,2}^{\mathrm{ad}}$), and the φ adiabatic descriptors (φ_1^{ad} and φ^{ad}) along the GD-type coordinate $\mathbf{R}_{\mathrm{GD}}$.

The GD-direction is chosen to be the direction that swaps the diabatic electronic excited states (see fig. 5.7) such that:

For all $\mathbf{R}_{\mathrm{GD}} < 0$ we have $\theta = \frac{\pi}{2}$:

$$\begin{aligned} \left|\psi_1^{\mathrm{ad}}\right\rangle &= \left|\psi_1^{\mathrm{dia}}\right\rangle \\ \left|\psi_2^{\mathrm{ad}}\right\rangle &= \left|\psi_2^{\mathrm{dia}}\right\rangle \end{aligned} \tag{5.27}$$

and for all $\mathbf{R}_{\mathrm{GD}} > 0$ we have $\theta = 0$:

$$\begin{aligned} \left|\psi_1^{\mathrm{ad}}\right\rangle &= \left|\psi_2^{\mathrm{dia}}\right\rangle \\ \left|\psi_2^{\mathrm{ad}}\right\rangle &= \left|\psi_1^{\mathrm{dia}}\right\rangle \end{aligned} \tag{5.28}$$

Along this direction, the adiabatic states are equal to a unique diabatic state, there is then no mixing between diabatic states that could appear in the expression of the adiabatic states and so the density-based descriptors are not affected by the values of the diabatic transition density function.

Along the DC-type coordinate $\mathbf{R}_i$

The DC-direction is chosen to be the direction that mixes the diabatic electronic excited states with each other (see fig. 5.8) such that:
For all $\mathbf{R}_{\mathrm{DC}} < 0$ we have $\theta = \frac{\pi}{4}$:

$$\begin{aligned} \left|\psi_1^{\mathrm{ad}}\right\rangle &= \frac{\left|\psi_1^{\mathrm{dia}}\right\rangle + \left|\psi_2^{\mathrm{dia}}\right\rangle}{\sqrt{2}} \\ \left|\psi_2^{\mathrm{ad}}\right\rangle &= \frac{\left|\psi_2^{\mathrm{dia}}\right\rangle - \left|\psi_1^{\mathrm{dia}}\right\rangle}{\sqrt{2}} \end{aligned} \tag{5.29}$$

and for all $\mathbf{R}_{\mathrm{DC}} > 0$ we have $\theta = \frac{3\pi}{4}$:

$$\begin{aligned} \left|\psi_1^{\mathrm{ad}}\right\rangle &= \frac{\left|\psi_2^{\mathrm{dia}}\right\rangle - \left|\psi_1^{\mathrm{dia}}\right\rangle}{\sqrt{2}} \\ \left|\psi_2^{\mathrm{ad}}\right\rangle &= \frac{\left|\psi_1^{\mathrm{dia}}\right\rangle + \left|\psi_2^{\mathrm{dia}}\right\rangle}{\sqrt{2}} \end{aligned} \tag{5.30}$$

Along this direction, since the diabatic states are mixed with each other and so the diabatic transition density function can indeed affect the behavior of the density-based descriptors in the vicinity of a conical intersection.

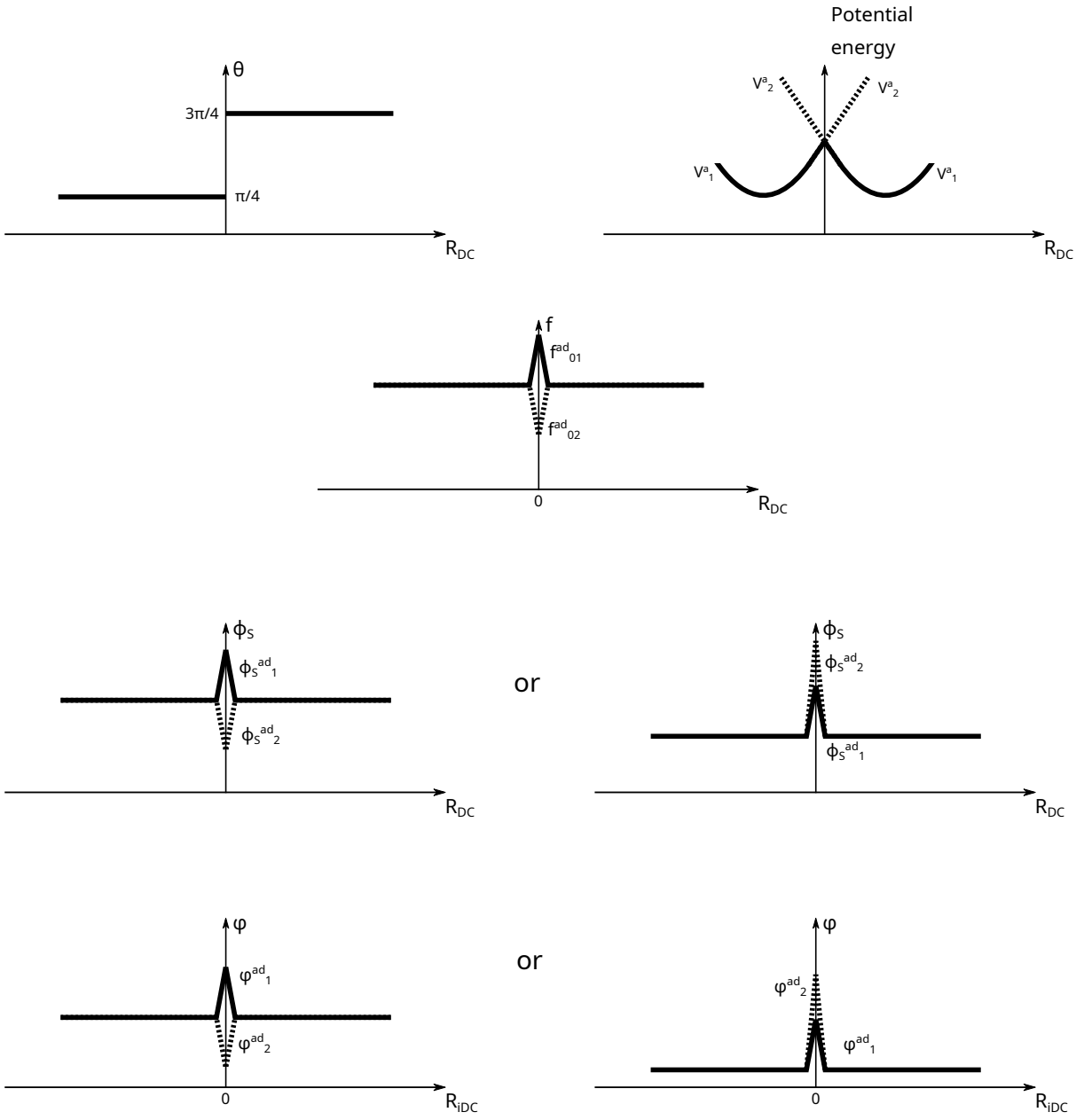

Figure 5.8: Schematic representation of the mixing angle (θ), the adiabatic potential energies (V_1^{ad} and V_2^{ad}), the ψ_{S} adiabatic descriptors ($\phi_{\mathrm{S}\,1}^{\mathrm{ad}}$ and $\psi_{\mathrm{S}\,2}^{\mathrm{ad}}$), and the φ adiabatic descriptors (φ_1^{ad} and φ^{ad}) along the DC-type coordinate $\mathbf{R}_{\mathrm{DC}}$.

A sign study

The density-based descriptors are expressed with a square-root (ϕ_S) or with a modulus (φ and χ). We can then defined six subdomains of $\mathbb{R}^3$: $\mathbb{A}_1$, $\mathbb{B}_1$, $\mathbb{A}_2$, $\mathbb{B}_2$, $\mathbb{E}_1$, $\mathbb{E}_2$ such that:

$$\begin{array}{lcllcl} \mathbb{A}_1 \bigcup \mathbb{B}_1 \bigcup \mathbb{E}_1 & = & \mathbb{R}^3 & \mathbb{A}_2 \bigcup \mathbb{B}_m \bigcup \mathbb{E}_2 & = & \mathbb{R}^3 \\ \mathbb{A}_1 \bigcap \mathbb{B}_1 & = & \varnothing & \mathbb{A}_2 \bigcap \mathbb{B}_m & = & \varnothing \\ & & \text{and} & & & \\ \mathbb{A}_1 \bigcap \mathbb{E}_1 & = & \varnothing & \mathbb{A}_2 \bigcap \mathbb{E}_2 & = & \varnothing \\ \mathbb{B}_1 \bigcap \mathbb{E}_1 & = & \varnothing & \mathbb{B}_m \bigcap \mathbb{E}_2 & = & \varnothing \end{array} \tag{5.31}$$

The adiabatic electronic densities are defined as follows in these sub-domains:

- $\forall \mathbf{r} \in \mathbb{A}_1,\ n_1^{\Delta}(\mathbf{r};\mathbf{R}) < 0$
- $\forall \mathbf{r} \in \mathbb{A}_2,\ n_2^{\Delta}(\mathbf{r};\mathbf{R}) < 0$
- $\forall \mathbf{r} \in \mathbb{B}_1,\ n_1^{\Delta}(\mathbf{r};\mathbf{R}) > 0$
- $\forall \mathbf{r} \in \mathbb{B}_m,\ n_2^{\Delta}(\mathbf{r};\mathbf{R}) > 0$
- $\forall \mathbf{r} \in \mathbb{E}_1,\ n_1^{\Delta}(\mathbf{r};\mathbf{R}) = 0$
- $\forall \mathbf{r} \in \mathbb{E}_2,\ n_2^{\Delta}(\mathbf{r};\mathbf{R}) = 0$

Such domains actually depend on $\mathbf{R}$ and then are different for each coordinate values. $\mathbb{E}_1$ and $\mathbb{E}_2$ must be manifolds of dimension 2 at maximum because in these two domains we have $n_1^{\Delta}(\mathbf{r};\mathbf{R}) = 0$ and $n_2^{\Delta}(\mathbf{r};\mathbf{R}) = 0$. Analytic functions cannot be constant over an open set.

In the subspaces: $\mathbb{E}_1$ and $\mathbb{E}_2$, the density differences $n_1^{\Delta}(\mathbf{r};\mathbf{R}) = 0$ and $n_2^{\Delta}(\mathbf{r};\mathbf{R}) = 0$. The density differences cannot be equal to zero over an open set in $\mathbb{R}^3$. It would mean that $n_1^{\Delta}(\mathbf{r};\mathbf{R}) = n_0(\mathbf{r};\mathbf{R})$ and $n_2^{\Delta}(\mathbf{r};\mathbf{R}) = n_0(\mathbf{r};\mathbf{R})$ for a finite interval of electronic coordinates. In

other words, two states cannot have the same wave functions over a finite-size domain physically. However it is possible that the difference density be equal to zero over manifolds of dimension two or less. Thus the following sub-domains are sets of surfaces at most.: $\mathbb{B}_1 \bigcap \mathbb{E}_2$, $\mathbb{A}_1 \bigcap \mathbb{E}_2$.

In these subdomains, χ can be rewritten such that:

$$\begin{aligned}
\chi_1(\mathbf{R}) &= \tfrac{1}{2} \int\limits_{\mathbb{R}^3} \mid n_1^{\Delta}(\mathbf{r};\mathbf{R}) \mid d\mathbf{r} \\
&= \tfrac{1}{2}\Bigg(- \Bigg(\int\limits_{\mathbb{A}_1 \bigcap \mathbb{A}_2} n_1^{\Delta}(\mathbf{r};\mathbf{R})\mathrm{d}\mathbf{r} + \int\limits_{\mathbb{A}_1 \bigcap \mathbb{E}_2} n_1^{\Delta}(\mathbf{r};\mathbf{R})\mathrm{d}\mathbf{r} + \int\limits_{\mathbb{A}_1 \bigcap \mathbb{B}_m} n_1^{\Delta}(\mathbf{r};\mathbf{R})\mathrm{d}\mathbf{r} \Bigg) \\
&\quad + \int\limits_{\mathbb{B}_1 \bigcap \mathbb{A}_2} n_1^{\Delta}(\mathbf{r};\mathbf{R})\mathrm{d}\mathbf{r} + \int\limits_{\mathbb{B}_1 \bigcap \mathbb{E}_2} n_1^{\Delta}(\mathbf{r};\mathbf{R})\mathrm{d}\mathbf{r} + \int\limits_{\mathbb{B}_1 \bigcap \mathbb{B}_m} n_1^{\Delta}(\mathbf{r};\mathbf{R})\mathrm{d}\mathbf{r} \Bigg)
\end{aligned} \tag{5.32}$$

We see from eq. 5.32 that the signs of the density-based descriptor χ_1 (and to some extent φ, depend on subdomains that are associated to the n^{th} and m^{th} simultaneously. Moreover the subdomains depend on the nuclear coordinates because they are defined according to the positive, negative and null values of the difference density at a certain geometry. It must be stressed out that even the domains $\mathbb{A}_1$, $\mathbb{A}_2$, $\mathbb{B}_1$, $\mathbb{B}_2$ depend on the nuclear coordinates. So it seems quite impossible to establish any systematic relationship. If χ_1 and χ_2 are to be expressed in terms of diabatic contributions, cosine and sine will have erratic signs. The reason why the two density-based descriptors behave oddly in the vicinity of some CoIn is that the square-root and the absolute-value functions somewhat remove the distinct roles of the signs of positive and negative contributions of diabatic densities differences within the adiabatic ones. The diabatic contributions in vicinity of CoIn are then difficult to consider in a systematic manner. Unlike the electronic properties as the oscillator strength, the transformations (see eqs. 1.23, 2.7, 2.8, 2.25, and 2.26) are not linear anymore with respect to expansion coefficients because of the square-root and the absolute-value functions. To treat the descriptors adequately, one needs to study them within various subspaces for each nuclear and electronic coordinates.

5.3 Determination of the minimum energy of a seam

In chapter 2, it has been explained that two adiabatic electronic states can be degenerate along $3N_{\text{nu}} - 8$ directions. The two directions that lift the degeneracy to the 1^{st} order are the $\overrightarrow{GD}$ (gradient difference) and the $\overrightarrow{DC}$ (derivative coupling) vectors, and they span the branching space (BS). The $3N_{\text{nu}} - 8$-dimensional hypersurface is called a seam and the energy value of a seam is not constant and so it has a global minimum see fig. 5.9. To evaluate the efficiency of the population transfer at a conical intersection (CoIn), one has to determine the minimum of the seam, which is the most representative, and characterize it by estimating the non-adiabatic coupling between the two states. Arbitrary choices of vectors of the branching space for two CoIn have been represented in fig. 5.9. One has to keep in mind that they are not well determined at the apex of the CoIn but they are around the CoIn and they "rotate" arbitrarily around the apex of a CoIn. The minimisation of a seam used in the present work is based on the program

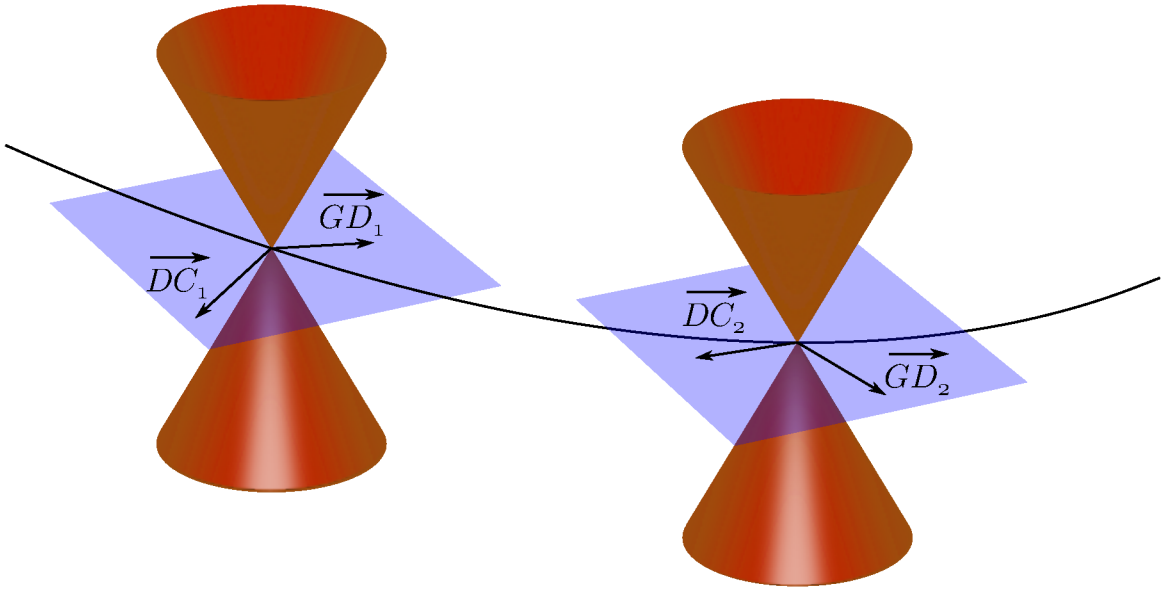

Figure 5.9: Schematic representation of two conical intersections along the seam (black line) and their respective branching space vectors.

developed by Harvey et al [2] which has been inspired by ref. [69].

Harvey *et al* have developed a seam minimization algorithm for states of different spin-multiplicity (see. section 2.1). This algorithm is also adequate for a seam minimisation of states of different symmetry. For a pair of two adiabatic electronic states $\{|\psi_1\rangle, |\psi_2\rangle\}$ of two different symmetries that are implied in the CoIn, the $\overrightarrow{GD}$, that is perpendicular to the seam,

is totally symmetric due to the fact that the gradient of the Hamiltonian is totally symmetric. The Hellman-Feynman expression of the half-difference gradient vector ($\overrightarrow{GD}$) is such that

$$\overrightarrow{GD} = \frac{\langle\psi_2|\,\overrightarrow{\nabla}_{\mathbf{R}}\hat{H}\,|\psi_2\rangle - \langle\psi_1|\,\overrightarrow{\nabla}_{\mathbf{R}}\hat{H}\,|\psi_1\rangle}{2} \tag{5.33}$$

The gradient of the seam ($\overrightarrow{GS}$) is defined as being the projection of the energy gradient of $|\psi_2\rangle$ ($|\psi_1\rangle$) respectively) onto the seam in ref. [69] (in ref. [2] respectively). As $\overrightarrow{GD}$ is orthogonal to $\overrightarrow{GS}$, on does simply defined $\overrightarrow{GS}$ as:

$$\overrightarrow{GS} = \langle\psi_1|\,\overrightarrow{\nabla}_{\mathbf{R}}\hat{H}\,|\psi_1\rangle - \Big[\,\langle\psi_1|\,\overrightarrow{\nabla}_{\mathbf{R}}\hat{H}\,|\psi_1\rangle \cdot \overrightarrow{GD}\Big]\frac{\overrightarrow{GD}}{||\,\overrightarrow{GD}\,||^2} \tag{5.34}$$

The total gradient ($\overrightarrow{TG}$) along which the energy of the seam and the energy difference have to be minimized together is then the weighted sum of the two previous gradients (see fig. 5.11) such that

$$\overrightarrow{TG} = \overrightarrow{GD} + \overrightarrow{GS} \tag{5.35}$$

Similarly to the expression of the $\overrightarrow{GD}$, the $\overrightarrow{DC}$ is defined as

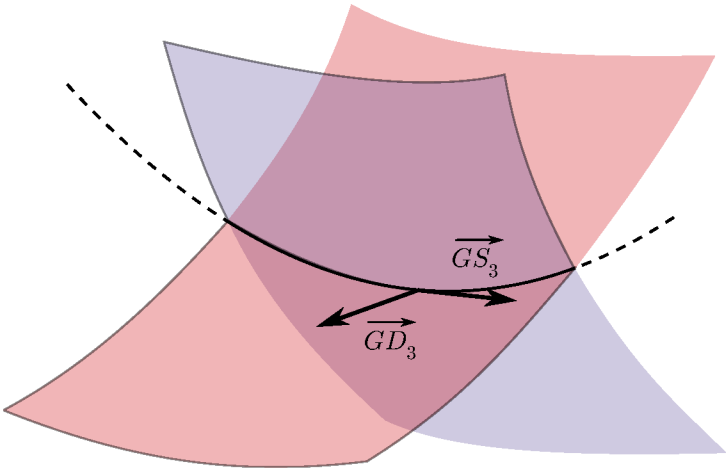

Figure 5.10: Schematic representation of two potential energy surfaces of two different symmetries.

$$\overrightarrow{DC} = \langle\phi_1|\,\overrightarrow{\nabla}_{\mathbf{R}}\hat{H}\,|\phi_2\rangle \tag{5.36}$$

In the case of CoIn where the two states have different symmetry, if the gradient of the seam if totally symmetric, we have the $\overrightarrow{DC}$ orthogonal to the $\overrightarrow{GD}$ and to the $\overrightarrow{GS}$ (see fig. 5.10). The algorithm minimizes then the norm of $\overrightarrow{GD}$ and of $\overrightarrow{DC}$. However in the general case of CoIn, the accidental intersections, the two adiabatic electronic states of same symmetry can cross. The $\overrightarrow{GD}$ and the $\overrightarrow{DC}$ may or may not be orthogonal to each other but can always be made orthogonal to each other if required. However, the $\overrightarrow{DC}$ may or may not be orthogonal to the total gradient but it is orthogonal to the gradient of the seam by definition. The $\overrightarrow{TG}$ is then the sum of the three vectors (see fig. 5.11) such that

$$\overrightarrow{TG} = \alpha\overrightarrow{GD} + \beta\overrightarrow{GS} + \gamma\overrightarrow{DC} \tag{5.37}$$

where $\alpha,\ \beta,\ \gamma$ are coefficients. The actual definition of the 1^{st}-order non-adiabatic coupling

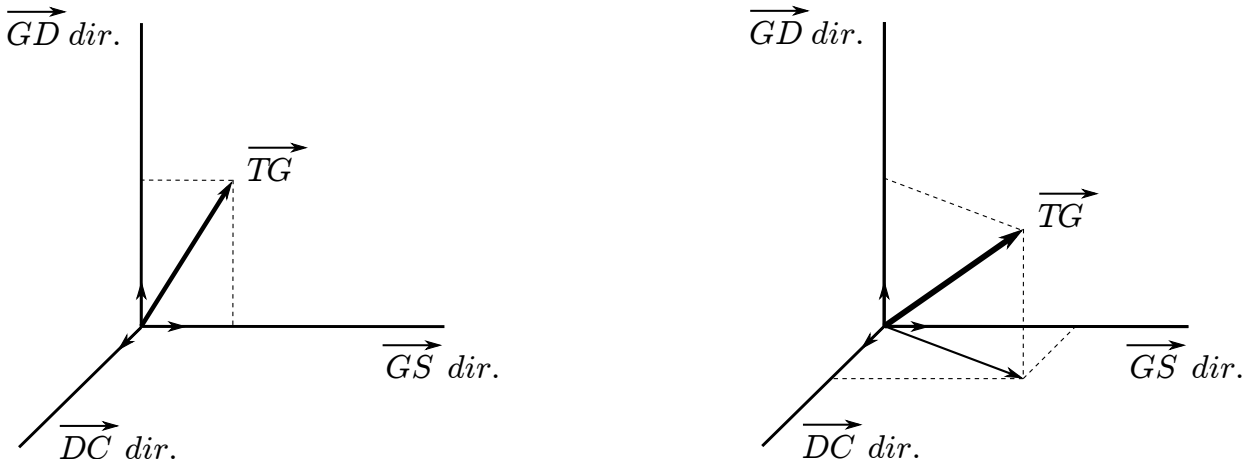

Figure 5.11: Vectorial representation of the total gradient in the case of CoIn where the two states have different symmetry (on the left) and in the case where the two states have the same symmetry (on the right).

(1-NAC) between two states $\{|\phi_1\rangle, |\phi_2\rangle\}$ is

$$\mathbf{F}_{12} = \left\langle \phi_1 \middle| \hat{\nabla}_{\mathbf{R}} \phi_2 \right\rangle \tag{5.38}$$

and its Hellman-Feynman expression is

$$F_{12} = \frac{\langle \phi_1 | \nabla_{\mathbf{R}} \hat{H} | \phi_2 \rangle}{V_2(\mathbf{R}) - V_1(\mathbf{R})} \tag{5.39}$$

The expression of the gradient difference (eq. 5.33) and of the derivative coupling (eq. 5.39) are valid for adiabatic states but they cannot be calculated exactly when we do not know the exact expression of the wave-functions such as here. A numerical method is proposed in ref. [75] to compute branching space vectors which are orthogonal to each other by the use of Hessians. To tackle the fact that $\overrightarrow{TG}$ depends on the $\overrightarrow{DC}$, I have merged the algorithm from ref. [75] and from ref. [2] in order to minimize the energy of the seam along the three directions that compose the total gradient.

To evaluate the efficiency of the merged algorithm on seam minimisation, it has been compared to the algorithm developed by Harvey *et al* [2]. The values obtained by the use of the latter algorithm are considered as being the reference one because this algorithm has already proven its efficiency.

We expect that the two algorithms would give the same relative energies for crossings that involve states of different symmetry since it is not needed to include the $\overrightarrow{DC}$ within the $\overrightarrow{TG}$. For crossings that involve states of same symmetry, we expect that the merged algorithm would give lower relative energy values or at least same relative energy values than the algorithm developed by Harvey *et al.* CoIn have been determined for systems of various size: diphenylacetylene (DPA), 1,4-bis(phenylethynyl) benzene (BPEB), 1,3-*bis*(phenylethynyl) benzene (*m*-BPEB), and 1-(phenylethynyl)-3-(1,4-bis (phenylethynyl) benzene) benzene (DPABPEB) and are gathered in table 5.5: CoIn of DPA, BPEB and *m*-BPEB gathered in table 5.5 involve for each crossing

	DPA	BPEB	*m*-BPEB			*m*-DPABPEB
	$1^1B_{1u}/1^1A_{1u}$	$1^1A'/1^1A$"	$1^1A'/1^1A$"	$1^1A'/1^1A$"	$1^1A_1/1^1B_2$	$1^1A'/2^1A'$
$\Delta(E)$	0.001	-0.002	0.003	-0.005	0.002	0.002
$E_{\text{alg.ref}}$	4.444	4.187	4.440	4.437	4.289	4.291

Table 5.5: Values of the minimized energies from the algorithm from ref. [2] ($E_{\text{alg.ref}}$) and energy difference between the minimized energy with algorithm from ref. [2] and with the merged algorithm ($\Delta(E)$). The energies and energy differences are expressed in eV.

two states of different symmetry. Since they are different symmetry crossings, the algorithm of Harvey *et al* provides us the supposed-minimal energy of the seam according to the level of theory. Since the $\overrightarrow{DC}$ vector is orthogonal to the gradient of the seam, in this case, we should not need to take into consideration the component of $\overrightarrow{TG}$ along $\overrightarrow{DC}$.

As the merged algorithm needs to calculate numerically the Hessians of the two states that cross at each step along the seam, it has a non-negligible computational cost, while the algorithm from ref. [2] needs only to compute the gradient for each step.

CoIn of DPABPEB gathered in table 5.5 is a crossing that involves two adiabatic electronic states of same symmetry ($1^1A'/2^1A'$). Then the total gradient has three components (see fig. 5.11) and the minimization energy algorithm should be more efficient with the merged algorithm. However, the difference between the minimized energy of the two algorithms is low: $\Delta(E) = 0.002$ eV. It is not possible to conclude on the efficiency of the merged algorithm with only one result which shows that the two algorithms give the same value. We would expect that the merged algorithm gives better results (*i.e.* minima of lower energy). DPABPEB is a molecule of 48 atoms and so the gradient that is computed during an electronic structure calculation has 144 elements and the Hessian has 10 440 elements that have to be calculated. The algorithm to compute numerically the coordinates of an orthogonal pair of vectors of the BS has been tested on two smaller molecules: benzene (666 elements in the Hessian) and 3-hydroxychromone (1 485 elements in the Hessian). The algorithm from ref. [2] has been tested on a smaller molecule as well: the phenyl cation (33 elements in the gradient). The minimization of the seam of DPA-BPEB could have been miscalculated due to error accumulation as the amount of matrix elements is higher than these calculated to validate the algorithm.

To conclude this chapter, the two density-based descriptors ϕ_S and χ are computed from now on with the numerical integration method since the population analysis approximation is not good enough to obtain reliable results according to the locality of the electronic photo-excitation for the systems of interest in this study.

Conical intersections are determined with the merged algorithm since it gives similar results than those obtained with the algorithm from ref. [2] and it should improve the energy minimization in the case of a same-symmetry crossing.

Eventhough the two density-based descriptors behave oddly in the vicinity of a conical intersection, this behavior has been rationalised and their use as electronic excited state descriptors is not discarded but they have to be handled carefully.

Chapter 6

Dendrimers and their building blocks

6.1 Introduction

The nanostar dendrimer (see fig. 2) has been tremendously studied in the past decades [40, 45, 46, 68, 78, 136–145]. Phenylene-ethynylene dendrimers (PE-D) show astonishing properties and are systems to be likely used in opto-electronic devices such as organic light emitting diodes (OLED) and conductive molecular wires. The nanostar seems to be one of the best candidate for these devices. If PE-D, and so the nanostar, are in the spotlight for such devices it is because they show an excellent photostability and high energy excitation transfer (EET) efficiency. The EET in PE-D is ultrafast and unidirectional. It occurs from the periphery of the molecular system to the core. Indeed, it is possible to locally excite the peripheral branches of a PE-D and the EET occurs thanks to an excitation energy gradient that extends along the system [41, 45, 46, 68, 78, 136, 138, 139, 142–145].

The EET in PE-D have been studied in various ways: A Förster model has been developed but it has limitations since it neglects dynamical effects and it underestimates the rate of the EET [40, 136, 137]; the local excitations on the various branches have been studied by an exciton model that gives a description of the optical properties of the nanostar and information on the energy transfer within various PE-D [140, 144]; non-adiabatic dynamics have been performed on building blocks of the nanostar and the studies concluded to the fact that the EET implies mainly the stretching of the triple bonds of diphenylacetylene (DPA) [45, 46, 68, 139, 142, 145]; Kirkwood et al [143] have studied the propagation of the exciton density matrix along PE-D, and steady-state and time-resolved spectroscopy [41, 78, 141] have concluded that the EET occurs from branch to branch and does not occur directly from the periphery of PE-D to the core of the system. However, at low temperature ($T = 10$ K) the excitations are localised on the branches

but at higher temperature there is an energy shift to the lower wavelengths which leads to a superposition of the different contributions to the absorption spectra [41, 68].

To supplement these studies, a pseudofragmentation scheme [43] is used in which the PE-D is decomposed in various subsystems (pseudofragments). The PE-D behaves as if the pseudofragments were weakly interacting together. The pseudofragmentation scheme explained in the general introduction (see ch.) and developed by Ho and Lasorne [43] allows to study a PE-D as if its branches (*oligo*phenylene ethynylene − *o*PE) were weakly interacting together. In this chapter, we are going to see how we can build and characterise the potential energy surfaces (PES) of a PE-D by studying the PES of the *o*PE that compose it.

The first section of this chapter will show chacterizations of the first adiabatic electronic excited states of *o*PE by the use of the density-based descriptors, equilibrium geometries, saddle points and conical intersections (CoIn). The second section will handle how two pseudofragments are coupled with each other when they are actually linked together at a common phenylene ring in *meta*-position. Two examples are studied: the case when the two pseudofragments are the same (two DPA), and the case when two pseudofragments are different (one DPA and one BPEB). The third section will explain how we can study and understand the PES of the smallest PE-D, named d223.

6.2 *oligo*phenylene ethynylenes

In this section, three *o*PE are studied as they are the main three branches of the nanostar: DPA, BPEB and DPABPEB. The Lewis structure of the equilibrium geometry for each in their ground state is represented in the left side of fig. 6.1. The three systems are highly π-conjugated, the aromatic phenyl groups are spaced by an alternation of single-triple-single bonds that is an ethynylene group. These three structures belong to the $\mathcal{D}_{2h}$ point group. In this chapter, the convention of Mulliken is used for $\mathcal{D}_{2h}$ such that the z axis is fixed as being the major axis of the molecules, most of atoms are invariant along the C_2 axis, and the x axis is fixed as being orthogonal to the molecular plane (see fig. 6.1). The ground state of the three systems is then 1^1A_g since they are closed shell.

6.2.1 Characteristics of the potential energy surfaces

The first optically active adiabatic electronic excited states of DPA have been experimentally and theoretically characterised [48–51, 54, 58, 60, 61, 146–151]. It has been observed that at the

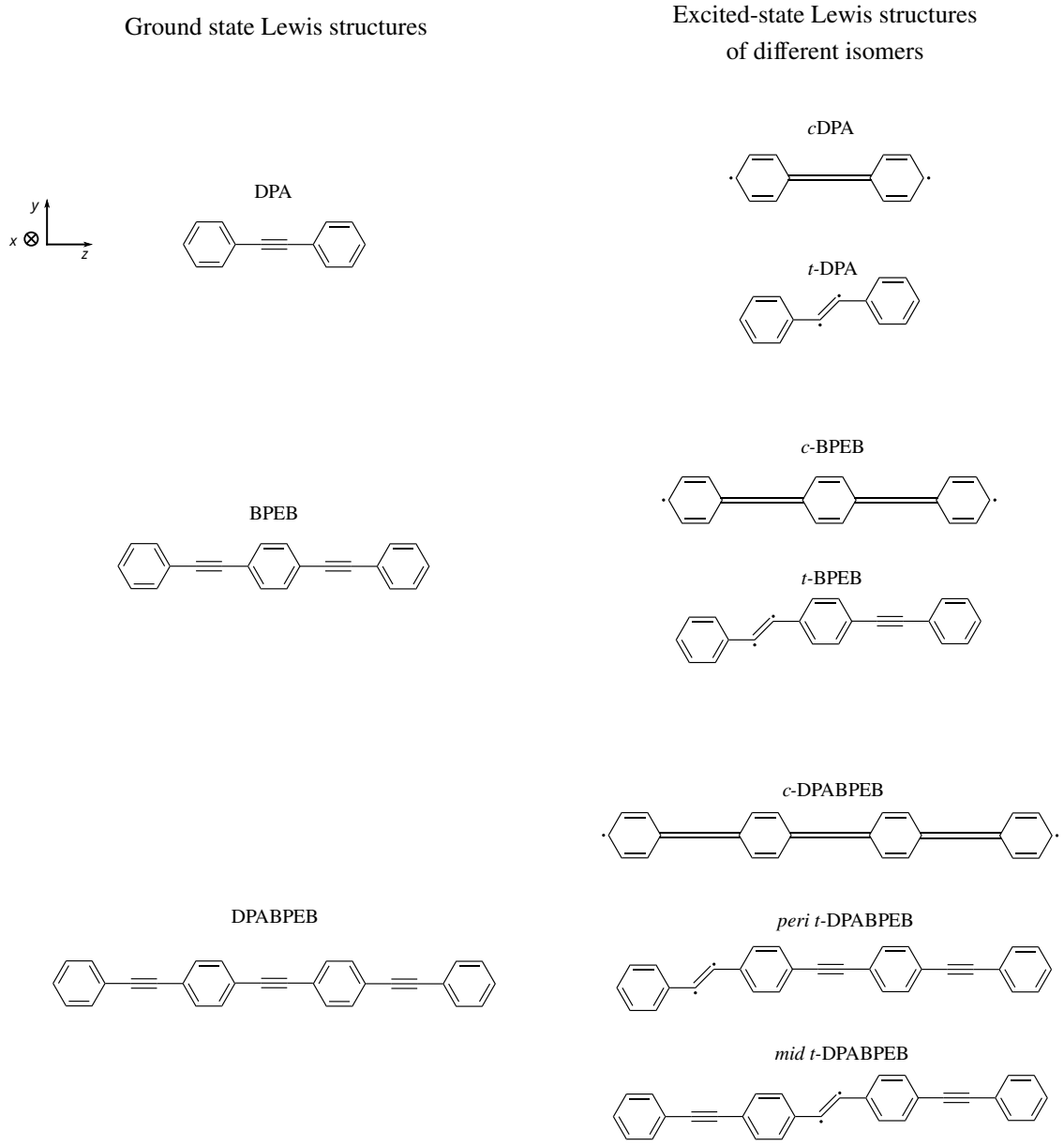

Figure 6.1: Lewis structures of DPA, BPEB and DPABPEB in the ground state and of their isomers in the first adiabatic excited electronic states.

ground state equilibrium geometry (also called the Franck-Condon − FC − geometry), the first optically active state is 1^1B_{1u}. However, there is no consensus on the energy ordering of this state [49,51,58,61,150,151]. This state lies around $4-5$ eV but it might not be the first adiabatic electronic excited state. Within this range of $4-5$ eV, five adiabatic electronic excited states have been noticed (1^1B_{1u}, 1^1B_{2u}, 1^1B_{3g}, 1^1A_u, and 2^1A_g).

The energy minimum of the 1^1B_{1u} state is associated to a cumulenic structure: there are

three double bonds instead of the ethynylene group and the two benzenes have a quinoidal structure (see fig. 6.1). The geometry of the system at the energy minimum of the 1^1B_{1u} state is named as the cumulenic isomer.

This optically active state is the precursor of an optically inactive state which energy minimum is associated to a *trans* structure (see fig. 6.1). One needs to differenciate equilibrium geometries and Lewis structures: equilibrium geometries to which isomers are associated correspond to the nuclei position while Lewis structures correspond to the bonding pattern of the electrons.

From their experiments, Hirata *et al.* [54] have proposed a transfer mechanism that involves the two previous adiabatic electronic excited states and is labelled $S_0 \rightarrow X \rightarrow Y \rightarrow T_1$ in which the state S_0 is the singlet ground state, X is the optically active state, Y is the optically inactive state, and T_1 is the first triplet state.

The optically inactive state which belongs to the $\mathcal{C}_{2h}$ point group has been characterised theoretically as well [48–50, 60, 149]. This state is 1^1A_u and its minimum is lower in energy than the minimum of 1^1B_{1u} in $\mathcal{D}_{2h}$. In the $\mathcal{C}_{2h}$ point group the 1^1B_{1u} state is labelled 1^1B_u. According to the literature [48–51, 60, 149] and depending on the level of theory, the optically inactive state lies between the fifth and the ninth adiabatic electronic excited state at the ground state geometry.

We used the CAM-B3LYP/6-31+G(d) level of theory for *o*PE in this work. The energy are given relative to the energy minimum of the ground state. Considering DPA, the 1^1B_{1u} is the first adiabatic electronic excited state at the FC point and lies at 4.476 eV (see table 6.1). The energy minimum of this optically active state is at 4.144 eV. The 1^1B_{1u} state is characterised by a non-zero oscillator strength value for these two structures: $f = 0.93$ (at the FC point) and $f = 0.96$ (for the equilibrium geometry of the cumulenic structure), see table 6.2 while the minimum of the optically inactive state lies at 3.716 eV and so is lower in energy than the minimum of the 1^1B_{1u} state. Less information is given in the literature on the cumulenic and on the *trans* isomers of BPEB [52,53]. Here we must differenciate two types of *trans* isomers: the single-*trans* isomers that we label *t*-BPEB and which Lewis structure is represented on fig. 6.1, only a single ethynylene group of BPEB is *trans*-bent and the double-*trans* isomer is the molecular system such that the two ethynylene groups of BPEB are *trans*-bent. Moreover, there are two types of double-*trans* isomers: both peripheral phenyls can be on the same side of the central axis of the benzene in the middle of BPEB and the two peripheral phenyls can be on opposite sides.

	FC point	cumulenic isomer	*trans* isomer
DPA	1^1B_{1u} : 4.476	1^1B_{1u} : 4.144	1^1A_u : 3.716
BPEB	1^1B_{1u} : 3.896	1^1B_{1u} : 3.624	1^1A" : 3.685
DPABPEB	1^1B_{1u} : 3.626	1^1B_{1u} : 3.376	1^1A" : 3.687: *peri t*-DPABPEB 1^1A_u : 3.652: *mid t*-DPABPEB

Table 6.1: Relative energies (eV) of the Franck-Condon point, the cumulenic isomer and the *trans* isomer according to the minimum of the ground state of DPA, BPEB and DPABPEB.

We are only focused on single-*trans* isomers because double-*trans* isomers can in fact be viewed as isomers that arise from a doubly-excited electronic state which are not our focus here. Such consideration on the double-*trans* isomer will be explained further in this section.

The cumulenic structure and the FC point belong to $\mathcal{D}_{2h}$ and the single-*trans* structure belongs to $\mathcal{C}_s$. Both references [52, 53] have determined that the minimum of the optically inactive state (1^1A") is higher than the minimum of the optically active state (1^1B_{1u}). Fujiwara *et al.* [52] have found that the energy minimum of 1^1B_{1u} state is at 3.25 eV and the energy minimum of the 1^1A" is at 3.51 eV while Hodecker *et al.* [53] have localised the two minima at 3.90 eV and 4.25 eV, respectively. Our level of theory places the energy minimum of the 1^1B_{1u} state at 3.624 eV and the energy minimum of the 1^1A" state at 3.685 eV (see table 6.1). Eventhough the energy values differ, the three levels of theory (TD-BP86/cc-pVDZ [52], CAM-B3LYP/def2-TZVP [53], and CAM-B3LYP/6-31+G(d) for us) give similar results according to the relative positions of the two minima: the energy minimum of the 1^1A" state is higher than the energy minimum of the 1^1B_{1u} state.

The 1^1B_{1u} is characterised by high oscillator strength values: $f = 2.00$ at its energy minimum, see table 6.1 while the 1^1A" energy minimum has a null-oscillator strength.

	cumulenic structure	*trans*-structure
DPA	0.96	0.00
BPEB	2.00	0.00
DPABPEB	2.94	0.00: *pari t*-DPABPEB 0.00: *mid t*-DPABPEB

Table 6.2: Oscillator strength (f) of the cumulenic and *trans* structures at their energy minima in the first adiabatic electronic excited state.

No data have been found on the isomers within the first adiabatic electronic excited states

of DPABPEB. The equilibrium geometry of the minimum of the ground state energy belongs to $\mathcal{D}_{2h}$ as well and the first singlet state is the optically active state 1^1B_{1u} which lies at 3.626 eV. The equilibrium geometry of the energy minimum to the 1^1B_{1u} state belongs also to $\mathcal{D}_{2h}$ and lies at 3.376 eV. The Lewis structure at the latter equilibrium geometry is represented in fig. 6.1 and the cumulenic isomer is labeled *c*-DPABPEB.

Since there are three ethynylene groups, it may be considered that the single-*trans*, the double-*trans* and the triple-*trans* structures could be associated to equilibrium geometries. However, single-*trans* minima and so single-*trans* isomers exist in the first adiabatic electronic excited states which is consistent with the fact that the double- and triple-*trans* structures correspond in fact to multiple excitations. There are two different single-*trans* isomers: the peripheral-*trans* isomer (*peri t*-DPABPEB) and the middle-*trans* isomer (*mid t*-DPABPEB). Their Lewis structures are gathered in figure 6.1. The geometry of the *peri t*-DPABPEB isomer belongs to the $\mathcal{C}_s$ point group and is associated to an optically inactive state (see table 6.2) which is $1^1A"$. The geometry of the second single-*trans* isomer (*mid t*-DPABPEB) belongs to $\mathcal{C}_{2h}$ point group. The *mid t*-DPABPEB isomer is associated to the equilibrium geometry of the 1^1A_u optically inactive state and is lower in energy (3.652 eV) than the relative energy of the $1^1A"$ minimum (3.687 eV).

For each system, the first optically active state is associated to a cumulenic structure for which the cumulenic isomers have been defined: *c*-DPA, *c*-BPEB and *c*-DPABPEB. We will refer to the energy minimum of the optically active state as the cumulenic energy minimum and the equilibrium geometry as the cumulenic geometry and the cumulenic isomer. The first optically inactive state is associated to a *trans* structure on a single ethynylene group and so the single-*trans* isomers have been defined: *t*-DPA, *t-m*-BPEB, *peri t*-DPABPEB and *mid t*-DPABPEB. We will refer to the energy minimum of the optically inactive state as the single-*trans* energy minimum and the equilibrium geometry as the single-*trans* geometry or the single-*trans* isomer. In the following subsections we are going to define for each system diabatic states which are consistant with the cumulenic structure and with the single-*trans* structure. The potential energy surfaces of the first adiabatic electronic excited states will be investigated.

6.2.2 The bright cumulenic diabatic state

The three systems in the first adiabatic electronic excited state at the FC geometry and at the cumulenic geometry are characterised by a large oscillator strength (see table 6.2). The first

excited state at these two geometries is mainly described by a HOMO/LUMO transition, the weight of the HOMO/LUMO transition is of 0.94. The molecular orbitals at these geometries are much alike, the HOMO/LUMO from the cumulenic geometry of the three systems are gathered in fig. 6.2. The cumulenic geometry is defined by an elongation of the benzenes which have quinoidal shape compared to their shape in the ground state. The four carbons that are between two benzenes are bound to each other by an alternation of single-triple-single bonds (ethynylene group) in the ground state while the four carbons are bound to each other by a sequence of three double bounds (cumulenic group). The geometry variation corresponds to the normal coordinates of a totally symmetric mode and is represented in figure 6.3. Such a modification of the

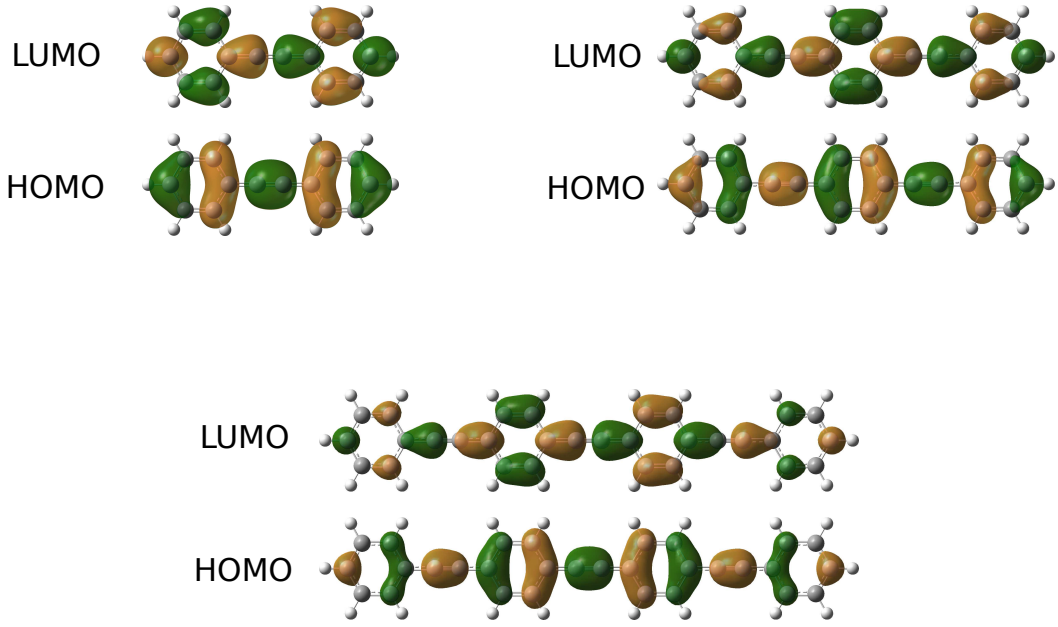

Figure 6.2: HOMO and LUMO representation of DPA, BPEB, and DPABPEB.

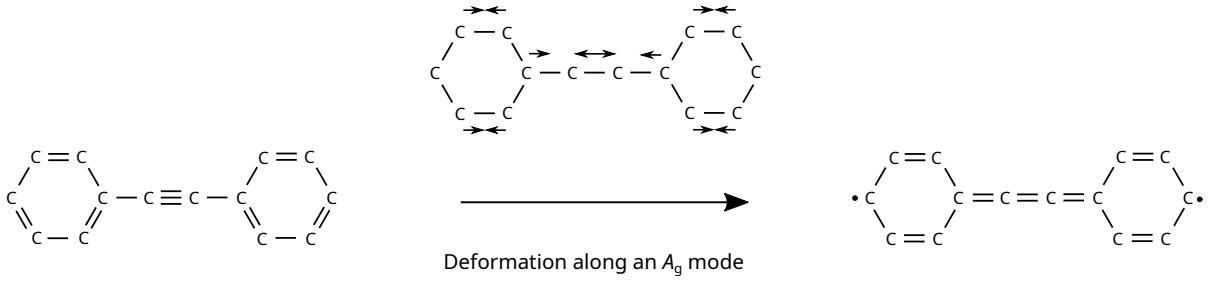

Figure 6.3: Dominant variation of the geometry from the FC geometry to the cumulenic geometry of DPA.

geometry can be explained by the electronic transition within the π system of *o*PE. To understand

the isomerisation of the ethynylene group into a cumulenic structure, the HOMO of DPA are reduced to the molecular orbitals of the ethynylene groups which are defined by the π_x system which is represented in figure 6.4. The two p_x atomic orbitals localised on the triple bond, that are out of the plane of the molecule, bind with each other while they anti-bind with the two p_x atomic orbitals localised on the two benzenes due to an opposite phase. Such a configuration of the p_x atomic orbitals on the carbons is the reason why the equilibrium geometry in the ground state is characterised by an ethynylene group.

The electronic transition from the ground state toward the first optically active electronic state in the $\mathcal{D}_{2h}$ point group is a transition from the π_x molecular orbitals toward the π_x^* molecular orbital. The π_x^* molecular orbital results from a switch of the phase of two p_x atomic orbitals localised on the carbons between two benzenes (see fig. 6.4). Such a switching on the atomic orbital phases allows the molecular system to be characterised by a cumulenic group.

The $\pi_x\pi_x^*$ transition includes in fact all the p_x orbitals of the carbons of the ethynylene groups and also over the benzene rings thus the cumulenic conformation is delocalised over the molecular systems. This leads to the fact that the cumulenic BPEB is lower in energy than the cumulenic DPA and the cumulenic DPABPEB is lower in energy than the cumulenic BPEB (see table 6.1) due to more extended π-conjugation.

On fig. 6.5 the attachment density (in blue) and the detachment density (in red) are gathered

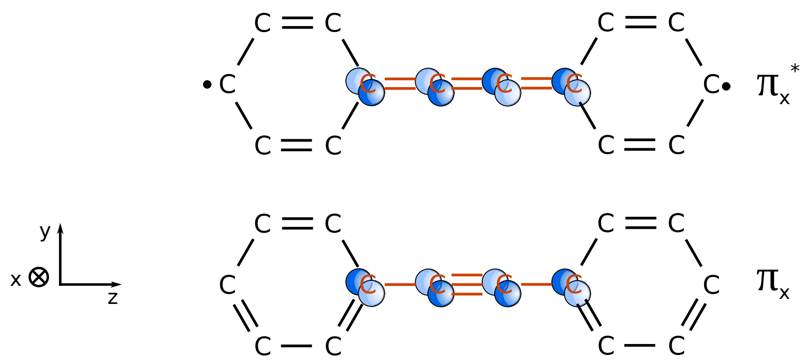

Figure 6.4: Atomic orbitals representation of the π_x and π_x^* molecular orbitals reduced to the ethynylene group involved in the first optically active adiabatic electronic excited state.

for the three molecular systems at the cumulenic geometry in the first adiabatic electronic excited states. First of all, the shape of the attachment and detachment densities are almost identical to the HOMO/LUMO of each molecular system. This means that the electronic transition could be pictured approximately as if an electron of the HOMO were excited to the LUMO. Since the attachment and the detachment densities are delocalised over the system, and so are the

HOMO/LUMO, the overlap descriptor ϕ_S, defined in chapter 3, is equal to 0.86 in the case of DPA, 0.85 for BPEB and for DPABPEB. The three overlap descriptor values are thus almost the same. This can be explained by the fact that the attachment and detachment densities are similar and lie over the whole systems which leads to a high overlap. Finally the descriptor χ gives similar values for the three systems. χ is approximately 0.4 for all case (see fig. 6.5) which means than the net charge involved in the photoexcitation is low. This is due to the fact that in this configuration, the displacement of charge density is delocalised over the system. The attachment and the detachment densities lie on a similar region in space which is noted by a high overlap and a low χ thus this electronic excited state is strongly locally excited.

To conclude this subsection, one can define one excited diabatic state of cumulenic type for

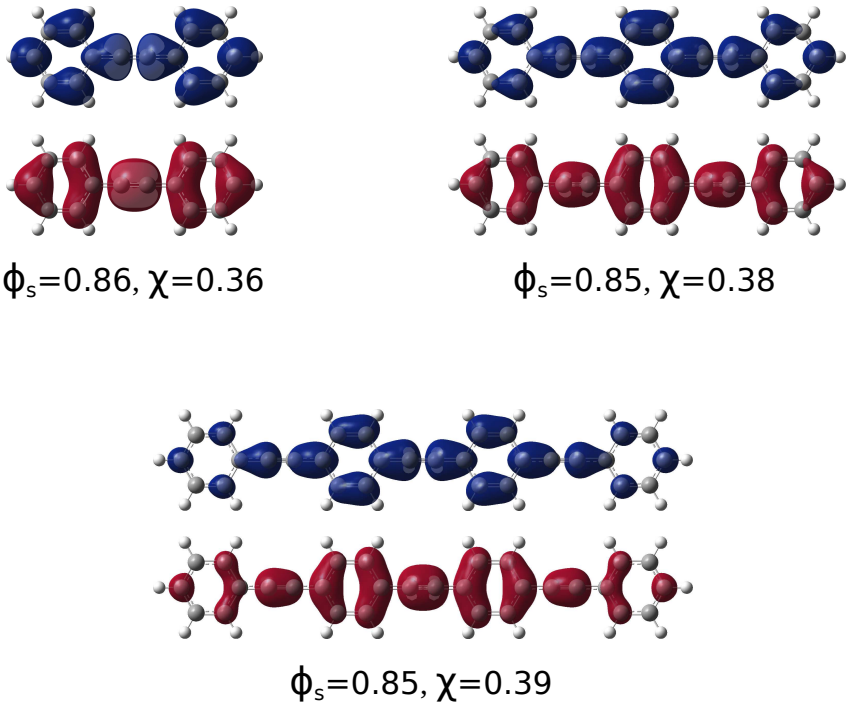

Figure 6.5: Attachment (in blue) and detachment (in red) densities obtained for the three cumulenic isomers of DPA, BPEB and DPABPEB.

each molecular system (DPA, BPEB and DPABPEB). This diabatic state is labelled S_{act} as it involves an electronic transition from the π_x toward the π_x^* molecular orbital of the system. It is a singlet, characterised by a significantly high oscillator strength and is of B_{1u} symmetry in the $\mathcal{D}_{2h}$ point group. The two density based descriptors show that this diabatic state is delocalised over the system. The equilibrium geometry of the energy minimum of this diabatic state implies quinoidal shape for each benzene and cumulenic groups between those benzenes.

6.2.3 The dark single-*trans* diabatic state

The *trans* isomerisation is possible at the ethynylene group that results from an excitation from the π_x molecular orbital to the π_y^* one localised on the carbons of the ethynylene group (see fig. 6.6). The π_y^* molecular orbitals are in the plane (yz) of the molecule and so from a symmetry point of view, the π_y^* might be seen as σ^*. Considering two ethynylene groups of an *o*PE (BPEB and DPABPEB) that can be *trans* isomerised, they can be associated to two additive electronic excitations $\pi_x\pi_y^*$. In the same way, if the three ethynylene groups of DPABPEB have a *trans* conformation, the associated minimum in an adiabatic electronic excited state would be described by three electronic excitations from the π_x to the π_y^* molecular orbitals.

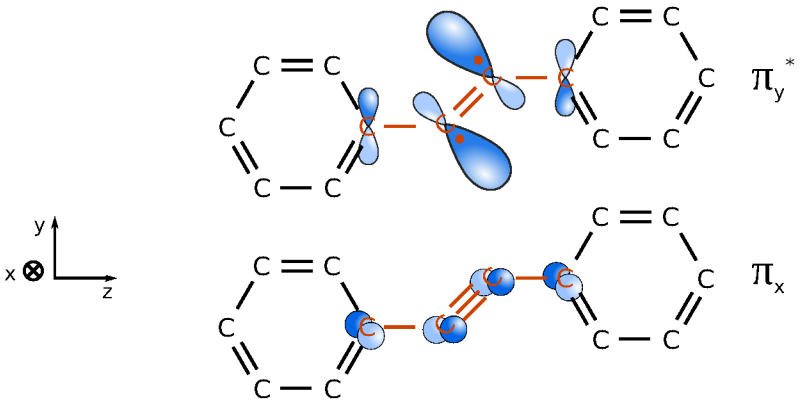

Figure 6.6: Atomic orbitals representation of the π_x and π_y^* molecular orbitals reduced to the ethynylene group involved in the first optically inactive adiabatic electronic excited state.

The equilibrium geometries of the single-*trans* minima are characterised by a HOMO/LUMO pair that differ from the HOMO/LUMO pair of the cumulenic isomer (see fig. 6.7).

Although there is a structural distortion on an ethynylene group due to a *trans* bending, the HOMOs of the *o*PE in the case of the cumulenic structure and single-*trans* structure are similar because the initial state in the electronic excitation is the same. The LUMOs of the cumulenic and *trans* isomers are significantly different since they involve the π_x^* molecular orbital and the π_y^* molecular orbital, respectively. The LUMOs of the single-*trans* isomers are localised on the bent ethynylene group.

The $\pi_x\pi_y^*$ transition is localised on a single ethynylene group for single-*trans* isomers. Thus, this leads to the fact that the minima associated to the four single *trans* isomers are at almost the same energy (see table 6.1). As the minimum energies of the diabatic state S_{act} of the three

*o*PE decrease if the size of the *o*PE increases, only the *trans* isomer of DPA is more stable, than its cumulenic isomer while the *trans* isomers of BPEB and DPABPEB are higher in energy than their cumulenic isomers.

The structure of the *trans*-isomers which are gathered in figure 6.1 shows one electron on each side of the *trans* double bond which is slightly misleading. In fact, it is an orthogonal bi-radical since the two unpaired electrons are in two orthogonal π orbitals. This state is nor a locally excited state nor a charge transfer state, it is an orthogonal bi-radical.

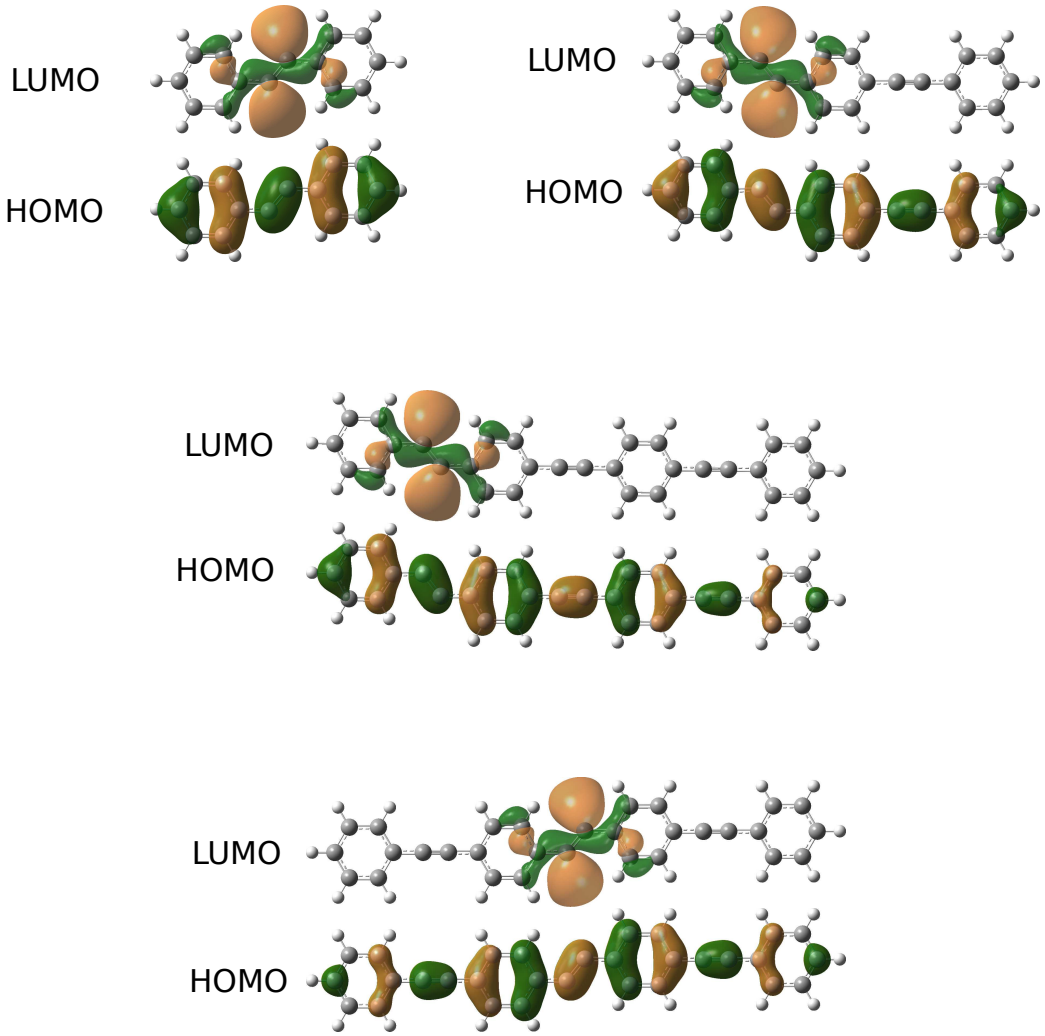

Figure 6.7: HOMO and LUMO representation of DPA, BPEB, and DPABPEB associated to the single-*trans* isomers.

On fig. 6.8 are gathered the attachment and the detachment densities at the single-*trans* geometry. The shape of the attachment and detachment densities are similar to the HOMO/LUMO pairs associated to each *o*PE. The attachment density does not change com-

pared to the LUMOs but the detachment density is localised only on the ethynylene group that is isomerised while the HOMOs are delocalised over the molecular system. Such shapes of the two densities lead to the fact that the overlap descriptor values are lower than those of the cumulenic isomers: $\phi_{\mathrm{S}}(t\mathrm{DPA}) = 0.54$, $\phi_{\mathrm{S}}(t\mathrm{BPEB}) = 0.53$, $\phi_{\mathrm{S}}(p\text{-}t\mathrm{DPABPEB}) = 0.53$, and $\phi_{\mathrm{S}}(m\text{-}t\mathrm{DPABPEB}) = 0.53$ while the χ descriptor shows value around 0.73 which means that almost one electron is transferred in the excitation. Low overlap values and high χ values are typical of a charge-tranfert type state (for which the excitation occurs from one site to another in the same plane) but in our case the excitation occurs from one plane to another and so it is not possible to characterise this electronic excited state as a charge-tranfert state.

The minima associated to a single-*trans* isomer can be viewed as a single excitation toward the π_y^* molecular orbital on an ethynylene group. Since the detachment densities "contract" themselves around the excitation site compared to the HOMOs, one can assume that the electronic transition cannot be reduce to a simple HOMO/LUMO transition otherwise the attachment and detachment densities would have been similar to the HOMOs and LUMOs.

To conclude this subsection, one can define a second diabatic state for each molecular system. This state is a singlet, optically inactive, which results from a $\pi_x\pi_y^*$ single excitation, localised on one ethynylene group of each *o*PE. These diabatic states are labelled S_{trans}.

S_{trans} is of A_{u} symmetry for DPA and DPABPEB when the ethynylene group in the middle has isomerised since they both belong to the $\mathcal{C}_{2h}$ point group and is of A" symmetry for BPEB and DPABPEB when the ethynylene group on the left or on the right has isomerised since they both belong to the $\mathcal{C}_s$ point group.

6.2.4 Potential energy surfaces

In figure 6.9, four rigid scans are gathered. The scans are performed along a γ angle that has been defined such that it is the bending angle on the middle of a cumulenic group. For the scans a) and d), it is a $B_{3\mathrm{g}}$ deformation (from $\mathcal{D}_{2h}$ to $\mathcal{C}_{2h}$) and fo the scans b) and c), it is a $B_{2\mathrm{u}}$ deformation (from $\mathcal{D}_{2h}$ to $\mathcal{C}_s$) to get a single-*trans* conformation for each of the three *o*PE.

The energies have been sorted according to the state symmetry of the systems. The S_{act} state for DPA and DPABPEB is of B_{u} symmetry in $\mathcal{C}_{2h}$ and is of A' symmetry for BPEB and DPABPEB in $\mathcal{C}_s$. Only the energies of the state $1^1B_{1\mathrm{u}}$ is plotted since it has been associated to the S_{act} diabatic state. They are plotted in dashed lines. The optically inactive states of each systems are plotted in plain lines. The color blue is associated to DPA, the color purple is

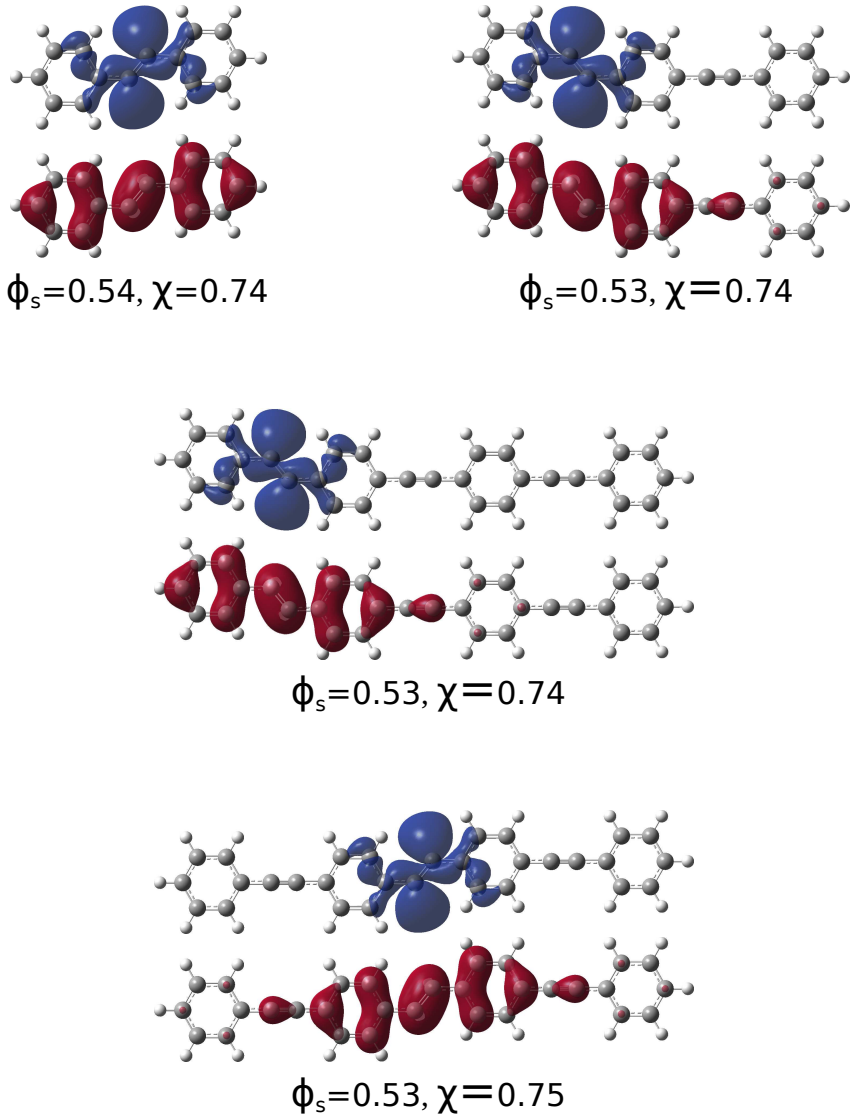

Figure 6.8: Attachment (in blue) and detachment (in red) densities obtained for the four single-*trans* isomers of DPA, BPEB and DPABPEB.

associated to BPEB and the color green is associated to DPABPEB.

We observe in fig. 6.9 that for each rigid scan, the potential energy surface of the first adiabatic excited state actually shows three energy minima. For each *o*PE, at $\gamma = 180°$, the energy minimum is a global minimum and the associated equilibrium geometry is the cumulenic geometry. On the left and on the right of the cumulenic minimum for each scan, there are two minima: they are all located at $\gamma = 133°$ and at $\gamma = 227°$ while the optimisation calculations which gave us the relaxed *trans* isomers are all defined by an angle of $\gamma = 128°$ and $\gamma = 232°$

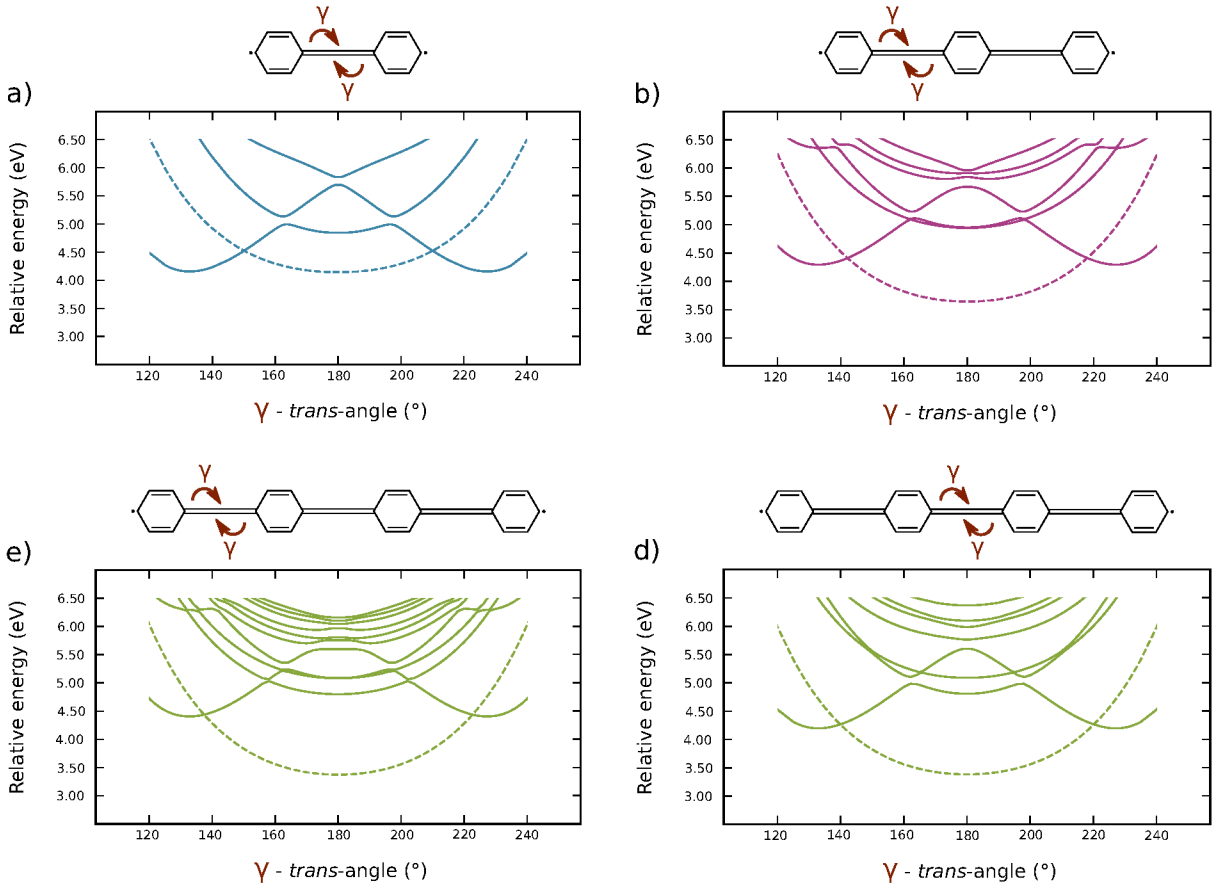

Figure 6.9: Rigid scans along the γ *trans*-bending angle from the equilibrium geometry in the first optically active state.

(the relaxed geometries are the ones presented in table 6.1).

For the scan a) the relative energy of the two minima is 4.155 eV which is higher by 0.439 eV than the relative energy of *t*-DPA. For the scan b) the relative energy of the two minima is 4.276 eV which is higher by 0.591 eV than the relative energy of *t-m*-BPEB. For the scan c) the relative energy of the two minima is 4.406 eV which is higher by 0.719 eV than the relative energy of *peri t*-DPABPEB. For the scan d) the relative energy of the two minima is 4.190 eV which is higher by 0.538 eV than the relative energy of *mid t*-DPABPEB (see table 6.1 and fig. 6.9). The two apparent minima of the rigid scans are associated to two single-*trans* isomers that are equivalent by symmetry. However they are not the global minima associated to the relaxed single-*trans* geometries since they differ a little from the γ values and a lot from the relative energies. The geometry relaxation occurs along totally symmetric coordinates that relax the bond lengths. One can admit that these apparent minima are good approximations to the global

single-*trans* minima.

There are four, equivalent-by-symmetry, single-*trans* isomers considering the molecular system *t*-*m*-BPEB and *peri* *t*-DPABPEB because each of the two ethynylene groups lead to two equivalent *trans* isomers. In the same way, there are two equivalent single-*trans* for *t*-DPA and *m*-*t*-*m*-BPEBDPA since there is only one ethynylene group involved in the *trans* isomerisation. The equivalent single-*trans* isomers of DPA, BPEB and DPABPEB are gathered in figures 6.10 and 6.11.

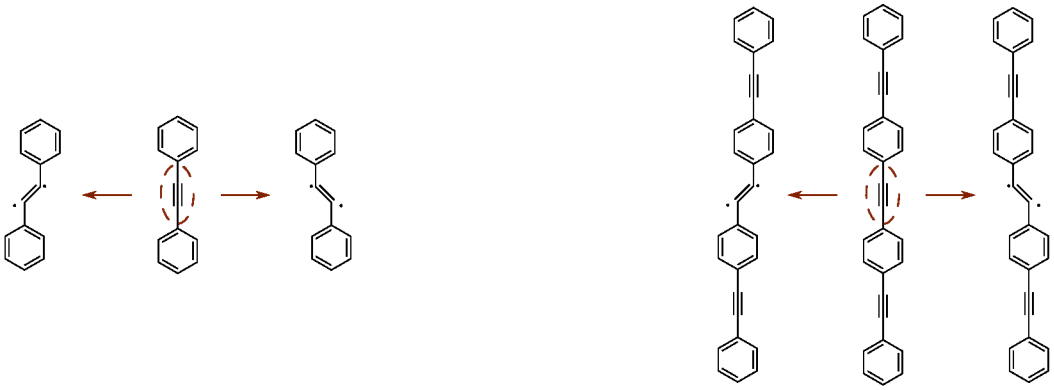

Figure 6.10: Equivalent isomers of DPA and DPABPEB in the $\mathcal{C}_{2h}$ point group.

Due to the many equivalent single *trans* isomers, there are indeed more than one diabatic state S_{trans} for each system. There are as many equivalent S_{trans} states as there are equivalent single-*trans* isomers. There are two S_{trans} states for DPA, BPEB is characterised by four S_{trans} states and DPABPE is actually characterised by six S_{trans} states. Among these six states, four are equivalent with each other and belong to the $\mathcal{C}_{2h}$ point group and two are equivalent, they belon to the $\mathcal{C}_s$ point group. To differenciate the different S_{trans} states of DPABPEB, those associated of the *peri* *t*-DPABPEB are labelled *peri* *t*-S_{trans} and the two associated to the *mid* *t*-DPABPEB are labelled *mid* *t*-S_{trans}

	Rigid scan	Merged algorithm
t-DPA	4.523 - 150°	4.443 - 152°
t-*m*-BPEB	4.393 - 142°	4.189 - 148°
peri *t*-DPABPEB	4.439 - 137°	-
mid *t*-DPABPEB	4.258 - 140°	-

Table 6.3: Relative energies (eV) and γ values of the CoIn between the first and the second adiabatic electronic excited states from the rigid scan and from the minimized CoIn with the merged algorithm.

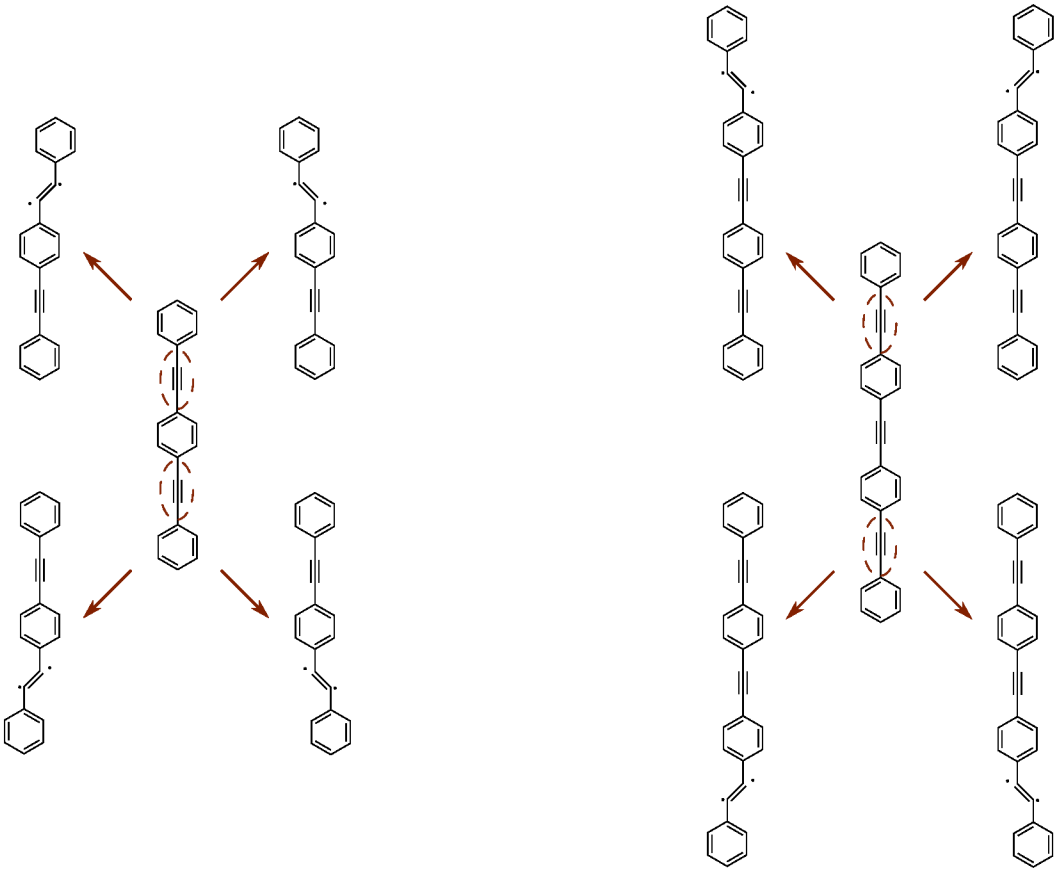

Figure 6.11: Equivalent isomers of BPEB and DPABPEB in the $\mathcal{C}_s$ point group.

We notice for each rigid scan the diabatic states S_{trans} are crossing with the diabatic S_{act} state. The energy values and the γ values of the crossings obtained from the rigid scans and from the optimized CoIn with the merged software are gathered in table 6.3. Considering DPA, this crossing is the one presented in section 5.2 in figs. 5.2 and 5.5.

Either for the rigid scans or for the optimized CoIn, the γ values are very similar. So, the relaxation from the rigid geometries toward the relaxed one is almost along a totally symmetric coordinate that relaxes the lengths of the bonds and to a lower extent, in-plane bending angles. These rigid conical intersections are then good approximations to the optimized ones. However, we know that an increasing size of *o*PE tends to lower in energy the diabatic state S_{act} leading to the fact that the γ values associated to the crossing decrease when the size of an *o*PE increase since the diabatic states S_{trans} are not affected by the size of the systems. Figure 6.12 represents the relative position of the diabatic states S_{act} according the increasing size of the *o*PE.

As it has been explained in this section and in section 5.2 the crossing between the first

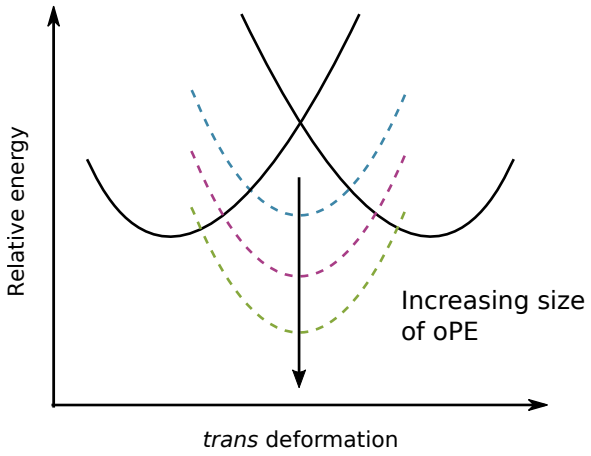

Figure 6.12: Schematic representation of the influence of the size of an *o*PE on the relative position of the S_{act} diabatic states.

and the second adiabatic electronic excited states involves the optically inactive and active diabatic states in the $\mathcal{C}_{2h}$ point group considering DPA and DPABPEB in the case of the *mid* *t*-DPABPEB isomer and in the $\mathcal{C}_s$ point group considering BPEB and DPABPEB in the case of the *peri* *t*-DPABPEB isomer.

The direction that goes from the cumulenic isomer toward the *trans* isomer of the three systems is B_{3g} from a $\mathcal{D}_{2h}$ origin and A' from a $\mathcal{C}_s$ origin. Within the $\mathcal{C}_{2h}$ and the $\mathcal{C}_s$ point group, this direction is totally symmetric. It is chosen as being the gradient difference direction since the two adiabatic electronic excited states swap their symmetries along this direction. The derivative coupling direction ($\overrightarrow{DC}$) is, due to symmetry reasons, orthogonal to the $\overrightarrow{GD}$ vector. For the two CoIn that belong to the $\mathcal{C}_{2h}$ point group, the $\overrightarrow{DC}$ is of B_g symmetry and for the two CoIn that belong to the $\mathcal{C}_s$ point group, it is of A" symmetry. The $\overrightarrow{DC}$ vector involves out-of-plane movements such that the *trans* double bond rotates around the (Oz) axis. Along the B_g or the A" directions, for each *trans* isomer, there are two equivalent transition states that link the cumulenic and the *trans* minima since the *trans* double bond can rotate clockwise or anti-clockwise. The transition states are in the first excited adiabatic state and so it can be determined an adiabatic reaction path in S_1. The transition state of DPA is represented in figure 6.13. Since BPEB, due to symmetry reasons, is characterised by four equivalent *trans* isomers, there are eight transition states. Similarly, there are eight transition states associated to the four equivalent *peri* *t*-DPABPEB isomers.

The transition state of DPA is characterised by a dihedral angle of $\widehat{abde} = 139°$ and a γ value of 156° while the two phenylene groups are in the same molecular plane $\widehat{abfg} = 0°$ (see

figure 6.13). However, it is computationally challenging to determine the transition states of larger system and our calculations have not converged but it is expected that the transition states results from an out-of-plane movement and exist for each *o*PE, due to their close relation with the crossing between similar optically active and forbidden states.

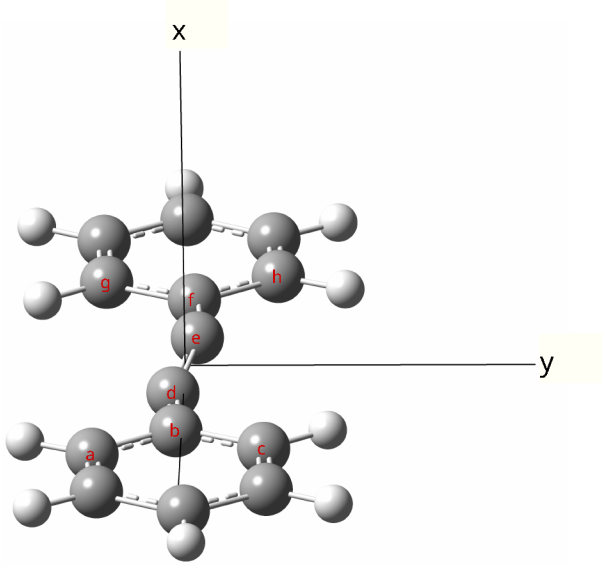

Figure 6.13: Transition state of DPA in the $\mathcal{C}_i$ point group in the first electronic adiabatic excited state. N.B.: The nuclei do not lie within a single plane.

We can notice an avoided crossing at 180° that involves the 2^1A_u and the 3^1A_u states in the rigid scan of DPA. The two states are actually the 5^{th} and the 6^{th} adiabatic electronic excited states and they are, in the $\mathcal{D}_{2h}$ point group, the $1^1B_{3\mathrm{u}}$ and the 2^1A_u states. This avoided crossing leads to a CoIn in the $\mathcal{D}_{2h}$ point group which is located at 5.742 eV. It has been minimized by the use of the merged software. At this CoIn, the vector $\overrightarrow{DC}$ has been chosen such that it is the vector that mixes the two equivalent diabatic states S_{trans} and is of $B_{3\mathrm{g}}$ symmetry. $\overrightarrow{GD}$ is orthogonal to $\overrightarrow{DC}$ due to symmetry reasons, is the one that conserves the total symmetry of the system and so it is of A_g symmetry. The $B_{3\mathrm{g}}$ direction is then the one that mixes the two diabatic states S_{trans} and also the one that allows the first and the second adiabatic electronic excited states to swap their symmetry in the case of the crossing between the diabatic states S_{trans} and S_{act}.

The respective magnitude of the branching space vectors at the CoIn S_5/S_6 are: $0.20\,E_\mathrm{h}a_0^{-1}$ for $\overrightarrow{GD}$ and $0.10\,E_\mathrm{h}a_0^{-1}$ for $\overrightarrow{DC}$. The length of the derivative coupling vector and gradient differ-

ence vector are the same order of magnitude. The coupling between the two adiabatic states is strong such that it can be noticed when studying the coupling between the two adiabatic states at the avoided crossing. We have previously seen that the $1^1A'$ state at the equilibrium geometry of its energy minimum is mainly described by a HOMO/LUMO transition. Their weight of the HOMO/LUMO transition is 0.93. In this case, the first pair of right/left natural transition orbitals (NTO) are similar to the HOMO and to the LUMO. However at the equilibrium geometry of the energy minimum of the 1^1B_{1u} state, the 5^{th} and the 6^{th} excited adiabatic states are described by various single electronic excitations and so these states cannot be reduced to a HOMO/LUMO transition. To characterise the nature of these two electronic excited states, the NTO have been computed. In figure 6.14 the first pair of NTO of DPA of the 5^{th} and the 6^{th} singlet states and those associated to the minima of the two equivalent single-*trans* isomers are depicted.

We see that the ethynylene group is characterised by the π_y^* molecular orbital when considering the left NTO of the 5^{th} singlet state while it is characterised by a totally symmetric Rydberg orbital when considering the left NTO of the 6^{th} singlet state. In figure 6.15 a schematic representation of the sum and of the difference of the molecular orbitals on the ethynylene group of an *o*PE is depicted. We see that either the sum or the difference allows us to localise the molecular orbitals onto the ethynylene group that characterises the two equivalent *trans* isomers. The two equivalent diabatic states S_{trans} can be viewed as the result of a mixing between the pair of right/left NTO of the 5^{th} and the 6^{th} adiabatic electronic excited states. This explains the nature of the two optically inactive states on both sides and why they correspond to clockwise and anticlockwise bent geometries at their minima (see fig. 6.14).

The adiabatic electronic excited states have different symmetries in the $\mathcal{D}_{2h}$ point group, they are the 2^1A_u and the 1^1B_{3u} states and they have very low oscillator strength values. Along the B_{3g} direction (the direction of $\overrightarrow{DC}$) the two states mix together and become both of A_u symmetry. In this case, the study of the density-based descriptors is well suited to understand the coupling between the 5^{th} and the 6^{th} adiabatic electronic excited states since we cannot differenciate them thanks to the symmetry nor their oscillator strength.

Along the derivative coupling and the gradient difference directions, the relative energies,

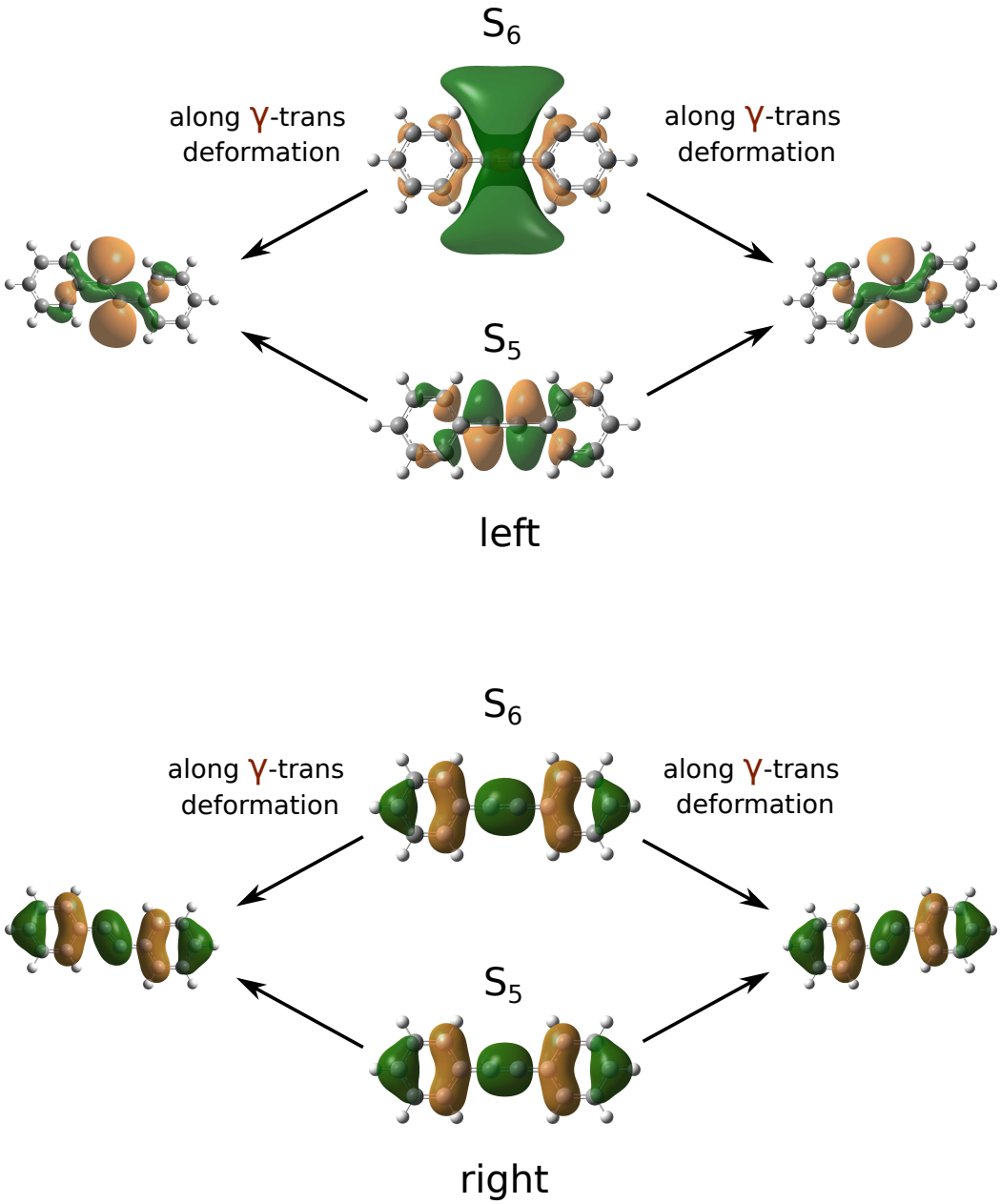

Figure 6.14: Natural transition orbital (NTO) mixing between the 5^{th} and the 6^{th} singlet states at the minimum of 1^1B_{1u} of DPA along the *trans* B_{3g} displacement γ.

the oscillator strength, χ and ϕ_S have been computed and gathered in figure 6.16. The 5^{th} (blue), 6^{th} (orange) and 7^{th} (green) adiabatic electronic excited state energies are plotted in plain lines. The 7^{th} adiabatic electronic excited state is 1^1A_g at the CoIn geometry.

Along the gradient difference direction, we notice in figure 6.16 where the relative energies are plotted that the crossing between the 5^{th} and the 6^{th} singlet states are centered in 0 and there

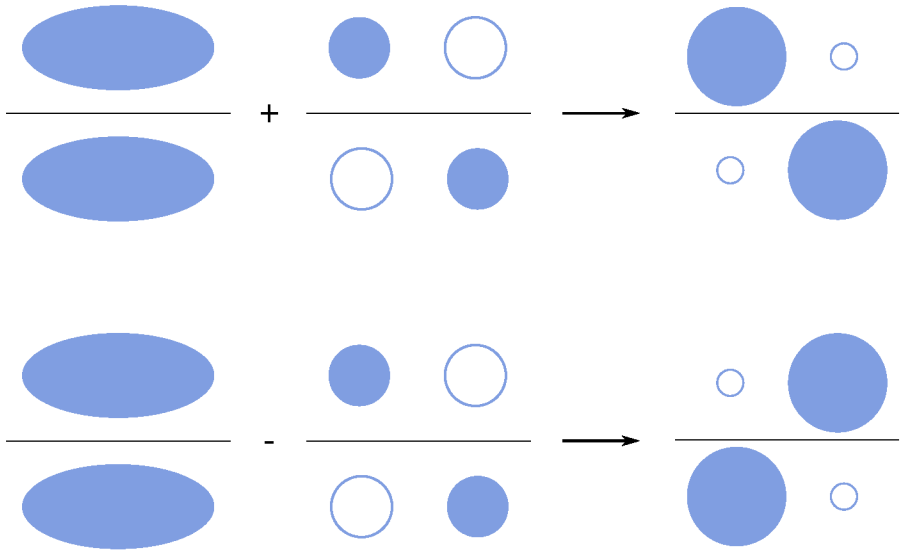

Figure 6.15: Schematic representation of the sum and difference of the frontier molecular orbitals (Rydberg and π_y^* on the ethynylene group.

is an avoided crossing between the 6^{th} and the 7^{th} adiabatic electronic excited states. According to the scan of χ and ϕ_S, this direction is the one that swaps the electronic properties of the two states because we observe a drastic swapping of the density-based descriptor values in the vicinity of the conical intersection at 0. Similar behavior is observed at the avoided crossing between 6^{th} and 7^{th}. Moreover, we observe simultaneously between 5 and 6 on the plots of the two descriptors that the 7^{th} singlet state seems to swap with a higher adiabatic electronic excited state. In subsection 6.2.3 the diabatic states have been associated to optically inactive states but in fact the oscillator strength is not strictly zero, it has value between 0 and $1.50 \cdot 10^{-3}$ and so the swapping of the oscillator strength is observed as well in the vicinity of the conical intersection at 0. However, it is strictly equal to 0 concerning the 7^{th} adiabatic electronic excited state and so no information is given about the avoided crossing between the 6^{th} and the 7^{th} excited state between 1 and 2 nor about the crossing that involves the 7^{th} singlet state and a higher excited state. Moreover, since the oscillator strength is almost zero, even a small variation due to computational error can induce significant variation on the behavior of the oscillator strength. Indeed at 4, the 5^{th} adiabatic electronic excited state seems to swap its oscillator strength with another state but here, this state does not interact either with the 4^{th} nor with the 6^{th} singlet state.

Along the derivative coupling direction, we observe on the plot of the relative energy that there are two crossings between the S_6 and the S_7 adiabatic electronic excited states. According

to the cut along this direction, we observe indeed that the 5^{th} and the 6^{th} couple with each other at 0 and at -4 and 4. This direction is the one that swaps the electronic properties of the descriptors and the oscillator strength. Eventhough the oscillator strength has very small values (between 0.00 and $2.00 \cdot 10^{-3}$) we observe the coupling at 0 and the swapping at -4 and 4.

In figure 6.17 the first left NTO of the 9^{th}, 10^{th}, 12^{th}, and 14^{th} states for BPEB and of the 12^{th} and 14^{th} for DPABPEB are shown. As it has been explained previously, BPEB is characterised by four equivalent S_{trans} diabatic states and we can observe in fig. 6.9 for its rigid scan that there is an avoided crossing between four adiabatic states which are the $3^1A'$, $4^1A'$, $5^1A'$ and the $6^1A'$ states in the $\mathcal{C}_s$ point group. This avoided crossing couples the four adiabatic electronic excited states at the cumulenic isomer geometry of BPEB (1^1B_{2g}, 2^1B_{1g}, 1^1B_{3u} and 2^1A_u) for which the four left NTO are gathered in fig. 6.17. The four right NTO are not shown here as they are similar to the HOMO of the one of *c*-BPEB while the four left NTOs can be related to in-phase and out-of-phase combinations of NTOs shown in fig. 6.14. The four-state conical intersection has not been searched because the program which minimizes the energy of a seam has been developed only for two-state conical intersections. The NTO of the four diabatic states S_{trans} result in equivalent mixing of the first pair of the previous NTO.

Since there are two equivalent *mid t*-DPABPEB, we can notice as well an avoided crossing at 180°. The avoided crossing involves two adiabatic electronic excited states: the 12^{th} and the 14^{th} singlet states. Only the left NTO of these two singlet states are gathered in fig. 6.17 because the right one are also similar to the HOMO of *c*-DPABPEB. We see that the distribution of the NTO at the ethynylene group is similar as the left NTOs in fig. 6.14.

Considering the rigid scan of DPABPEB in which the *trans* bending is performed at one peripheral ethynylene group (see fig. 6.9), it is not possible to determine exactly the adiabatic electronic excited states involved in the avoided crossing at 180° because they are too high in energy and so the adiabatic electronic excited states are too much mixed and entangled (high density of states) with each other. However we still can notice the presence of the avoided crossing.

To conclude this section, two diabatic electronic states have been defined for each *o*PE. The S_{act} diabatic state results from the electronic transition from the π_x to the π_x^* molecular orbitals. It is characterised by a high oscillator strength value and its minimum is associated to

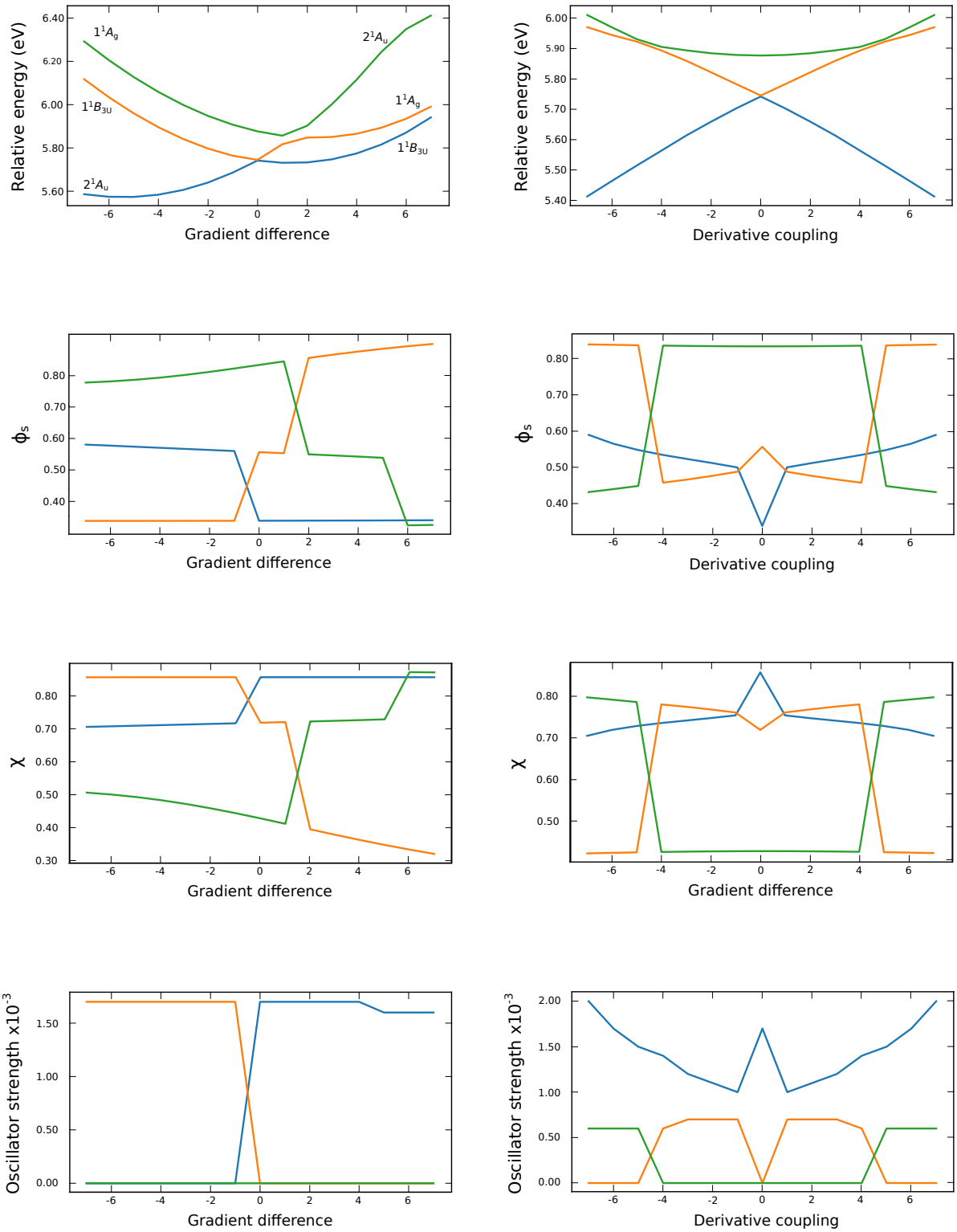

Figure 6.16: Relative energies, oscillator strengths, χ and ϕ_S scans along the branching space directions of the conical intersection S_5/S_6 of DPA.

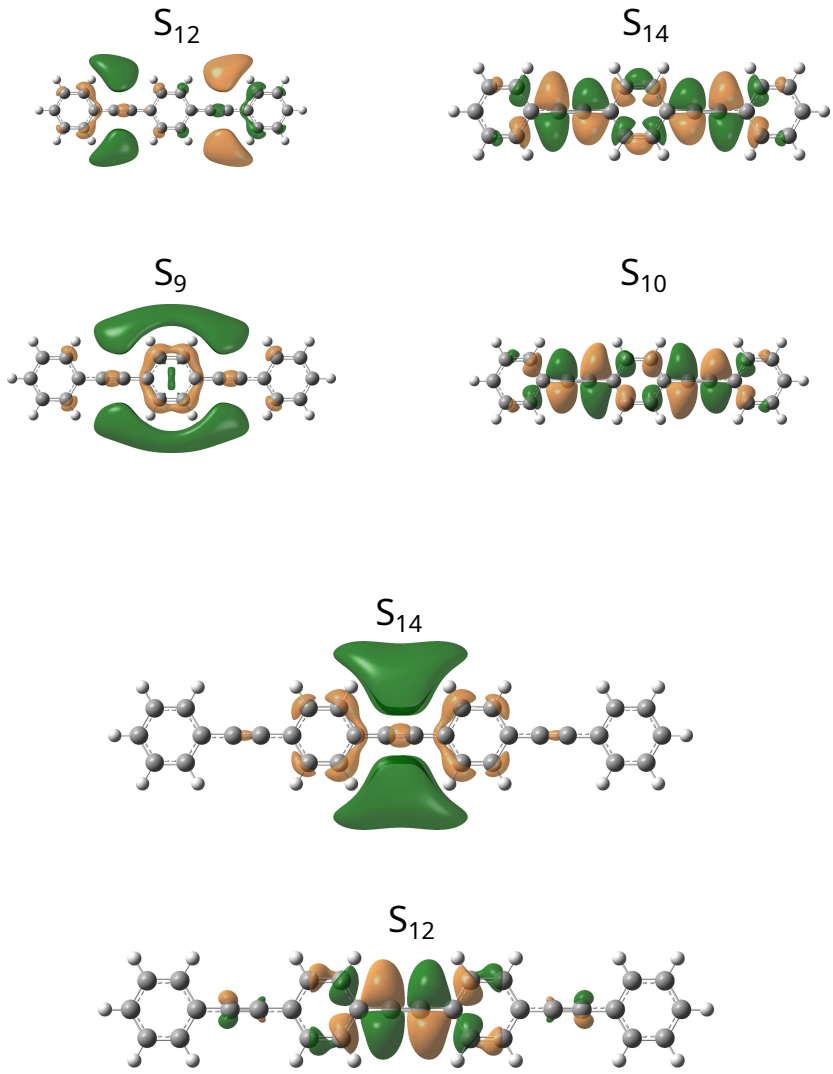

Figure 6.17: Natural transition orbital (NTO) mixing between the 9^{th}, the 10^{th}, the 12^{th} and the 14^{th} singlet states at the minimum of 1^1B_{1u} of BPEB and the NTO between the 12^{th} and the 14^{th} singlet states at the minimum of 1^1B_{1u} of DPABPEB.

the cumulenic isomer of each *o*PE. The second diabatic state is the S_{trans} state. It is defined by the transition between the π_x and the π_y^* molecular orbitals. This state is characterised by a zero oscillator strength and its minimum is associated to a single-*trans* isomer of each *o*PE. This S_{trans} state is not unique: there are actually as many S_{trans} states as there are equivalent single-*trans* isomers for an *o*PE and each ethynylene group allows to get two equivalent single-*trans* isomers. They are mixed with each other and cross which is reflected by the presence of a conical intersection high in energy. As the two states are of the same symmetry in the $\mathcal{C}_{2h}$ and in the $\mathcal{C}_s$ point group. They have very low oscillator strength values, one cannot use them

to characterise the conical intersection and so the density-based descriptors were well suited in this case. In figure 6.18 a schematic representation of the relative position of the diabatic states is shown. The minimum of the S_{act} state is higher in energy than the one of the S_{trans} of DPA while it is the opposite for BPEB and DPABPEB. The electronic delocalization of the cumulenic isomer (π-conjugation) increases when the size of the system increases whereas the single-*trans* diabatic states remain localised on a unique ethynylene group.

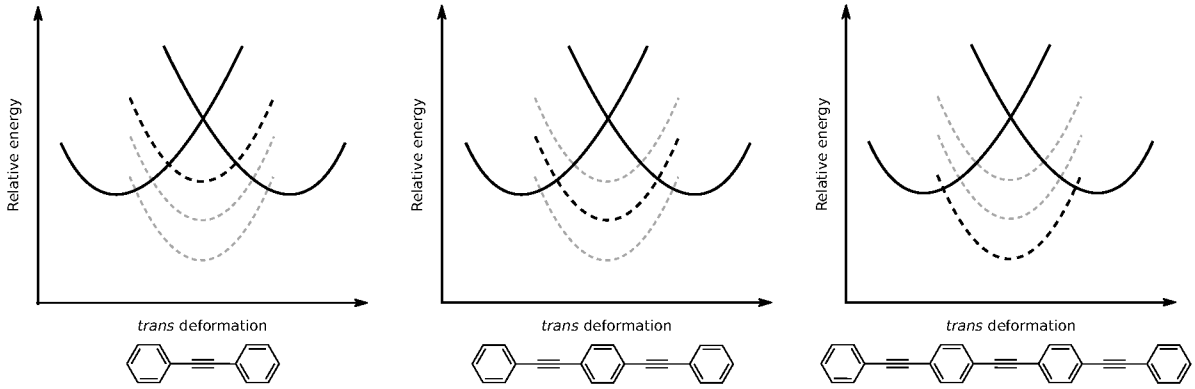

Figure 6.18: Schematic representation of the diabatic states S_{act} and S_{trans} for DPA, BPEB and DPABPEB.

6.3 Solvent effects and steady-state spectroscopy on *o*PE

In this section we now report on the influence of solvents on *o*PE. The polarisable continuum model is used such that only the dielectric contribution is taken into account. We chose five different environments defined by their relative dielectric constant ε_r: acetonitrile ($\varepsilon_r = 35.69$), cyclohexane ($\varepsilon_r = 2.02$), dichloromethane ($\varepsilon_r = 8.93$), hexane ($\varepsilon_r = 1.88$) and *in vacuo* ($\varepsilon_r = 1$). Results *in vacuo* are considered as being the reference. Table 6.4 gathers the relative energetic positions of the ground-state minima according to those *in vacuo*, table 6.5 gathers the relative energetic positions of the minima associated to the cumulenic isomer according to those *in vacuo*, table 6.6 gathers the relative energetic positions of the minima associated to the *trans* isomers according to those *in vacuo* and table 6.7 gathers the adiabatic transition energies (*i.e.* the relative energies between the minimum in the ground-state and those of the first adiabatic electronic excited states).

	in vacuo	acetonitrile	dichloromethane	cyclohexane	hexane
DPA	0.000	-0.156	-0.133	-0.058	-0.052
BPEB	0.000	-0.223	-0.190	-0.083	-0.076
DPABPEB	0.000	-0.290	-0.247	-0.108	-0.098

Table 6.4: Energy shifts in eV between the energy minima of the ground states *in vacuo* and with solvents.

	in vacuo	acetonitrile	dichloromethane	cyclohexane	hexane
c-DPA	4.144	-0.303	-0.267	-0.133	-0.122
c-BPEB	3.624	-0.276	-0.245	-0.127	-0.116
c-DPABPEB	3.376	-0.227	-0.203	-0.107	-0.100

Table 6.5: Adiabatic transition energies in eV of *o*PE *in vacuo* between the ground state energy minima and the first optically active state energy minima, and energy shifts of the adiabatic energies between the ones *in vacuo* and the ones in solvent.

	in vacuo	acetonitrile	dichloromethane	cyclohexane	hexane
t-DPA	3.716	+0.025	+0.021	+0.009	+0.007
t-m-BPEB	3.685	+0.042	+0.036	+0.015	+0.014
peri t-DPABPEB	3.687				
mid t-DPABPEB	3.652	+0.056	+0.047	+0.020	+0.016

Table 6.6: Adiabatic transition energies in eV of *o*PE *in vacuo* between the ground state energy minima and the first optically inactive state energy minima, and energy shifts of the adiabatic energies between the ones *in vacuo* and the ones in solvent.

From tables 6.4, 6.5, and 6.6, we observe that the solvents lower the relative value of the

	in vacuo	acetonitrile	dichloromethane	cyclohexane	hexane
c-DPA	4.144	3.841	3.877	4.011	4.021
c-BPEB	3.624	3.348	3.379	3.497	3.508
c-DPABPEB	3.376	3.149	3.173	3.270	3.276
t-DPA	3.716	3.585	3.604	3.667	3.671
t-m-BPEB	3.685	3.727	3.721	3.700	3.699
peri t-DPABPEB	3.687				
mid t-DPABPEB	3.652	3.708	3.699	3.671	3.668

Table 6.7: Adiabatic transition energies in eV of *o*PE in solvent and *in vacuo* between the ground state energy minima and the first optically active state energy minima (*c*-DPA, *c*-BPEB and *c*-DPABPEB), and between the ground state energy minima and the first optically inactive state energy minima (*t*-DPA, *t-m*-BPEB, *peri t*-DPABPEB and *m-ct*DPABPEB).

ground state minimum energies and the more the size of the system increases the more the system is stabilised. Acetonitrile and dichloromethane have similar stabilisation effect on the *o*PE as they have both high relative dielectric constants and cyclohexane and hexane have as well similar stabilisation effect on *o*PE.

Similarly, the relative energies of the cumulenic isomers is stabilised by the solvent but the *c*-DPA seems to be more stabilised due to the solvent than longer *o*PE.

The relative energies of *trans* isomers in solvent are higher than those *in vacuo*. However, the variation is small: the highest is of +0.056 eV (*m-t*-DPABPE in acetonitrile) and the lowest is +0.007 eV (*t*-DPA in hexane). So we may conclude that the solvent has not significant effect on the relative energy of the *trans* minima.

The adiabatic transition energies of each *o*PE that are gathered in table 6.7 show that the relative energetic position of the minima of each diabatic states is conserved. Concerning DPA, the minimum of S_{act} is always higher in energy than the one of S_{trans} and concerning BPEB and DPABPEB, the S_{act} is always lower in energy than the one of S_{trans}.

The absorption and emission spectra are gathered in appendix in figures 8.1, 8.2, 8.3, 8.4, 8.5, and 8.6. They are the spectra for the three *o*PE in solvent and *in vacuo*. Only absorption and emission spectra between the ground state and the minimum associated to the cumulenic isomer have been computed since the cumulenic isomers belong to optically active states while the *trans* isomers belong to optically inactive states. As the adiabatic energies for each *o*PE are similar between cyclohexane and hexane and between acetonitrile and dichloromethane, the

spectra are gathered in the same plot. Since there are solvent effects on the relative energy of the minima, we note that the first absorption and emission peak is shifted to higher wavelength for an increase of the relative dielectric constant.

	vibrational mode	*in vacuo*	acetonitrile	cyclohexane	dichloromethane	hexane
DPA	n°56	2 185	2 193	2 163	2 194	2 192
BPEB	n°87	2 020	1 986	2 008	1 992	2 010
	n°88	2 268	2 245	2 260	2 249	2 260
DPABPEB	n°118	2 155	2 128	2 145	2 132	2 146
	n°119	2 155	2 134	2 146	2 136	2 147
	n°120	2 290	2 270	2 282	2 273	2 282

Table 6.8: Frequencies in cm^{-1} associated to the stretching vibrational mode of the ethynylene groups of DPA, BPEB and DPABPEB.

No solvent effects are noticed on the vibrational progression for each absorption and emission spectrum and so the ground state and the diabatic state S_{act} are characterised by the same vibrational description. In table 6.8 are gathered the frequencies associated to the stretching vibrational modes on the ethynylene groups of *o*PE. The stretching vibrational modes on the ethynylene groups are the ones that drive the geometric deformation from the FC geometry toward the cumulenic geometry for the three systems. We are then focused on the vibrational mode n°56 for DPA, n°87 and n°88 for BPEB, and n°118, n°119 and n°120 for DPABPEB, they are represented in figure 6.19. We see that the frequencies of these vibrational modes are of the same order of magnitude within the five different environments (*in vacuo*, acetonitrile, cyclohexane, dichloromethane and hexane), see table 6.8.

In conclusion, solvents have indeed effect on the systems, the higher is the dielectric constant, the more stabilised is the cumulenic isomer but solvents seem not to have strong effect on the stabilisation of the *trans* isomers. Moreover, the solvent has no effect on the vibrational progression either in the ground state or in the first electronic adiabatic electronic excited state. In the next sections, theoretical calculations are given *in vacuo*.

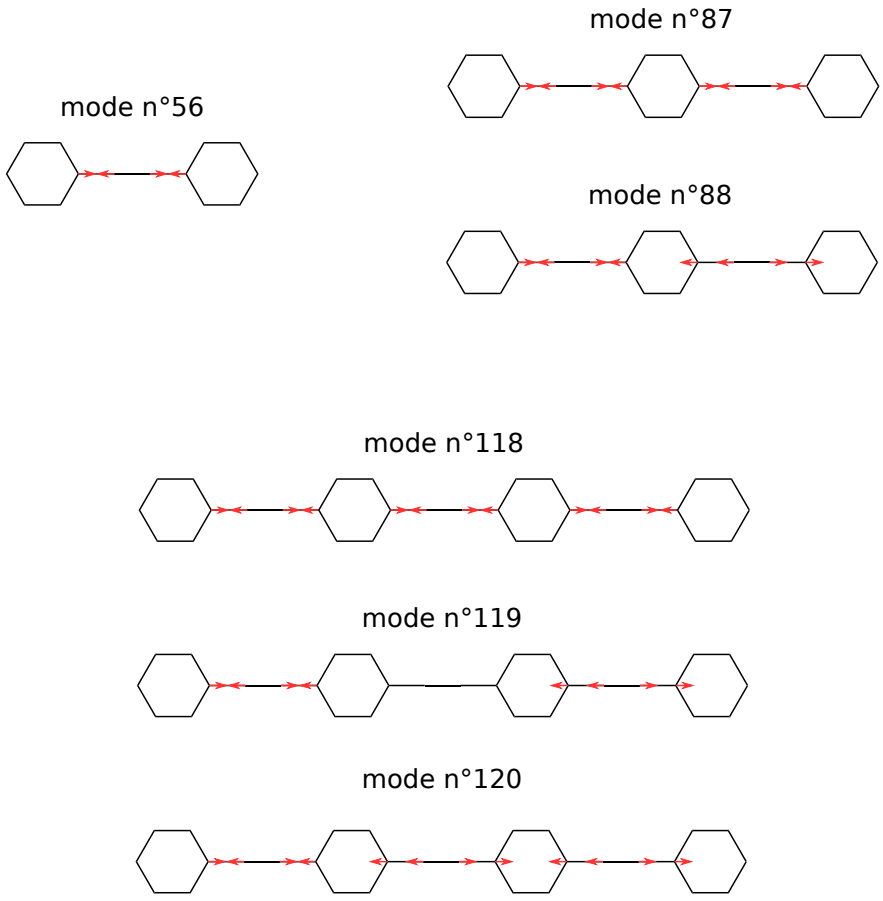

Figure 6.19: Schematic representation of the stretching vibrational modes of DPA, BPEB and of DPABPEB.

6.4 Association of two *oligo*phenylene ethynylenes

In this section, we study how we can provide a rational understanding for the potential energy surfaces of molecular systems that can be described within the pseudofragmentation scheme in which pseudofragments are two similar *o*PE or two *o*PE of different size. We are focused on *m*-BPEB and *m*-DPABPEB, their pseudofragments are two DPA, and one DPA and one BPEB, respectively. The prefix "*m*" for *m*-BPEB and *m*-DPABPEB refered to the *meta* position between the two *o*PE. In a molecular system with two similar pseudofragments, there is no excitation energy transfer (EET) because there is no excitation energy gradient [43] but one can understand how the "localised-on-the-pseudofragment" diabatic states mix with each other. In a molecular system with two different pseudofragments, there are two, non-equivalent by symmetry, equilibrium geometries that are associated to two minima of different energies and belong to two different "localised-on-the-pseudofragment" diabatic states. Since the two diabatic states are not equivalent and so they do not lie at the same energy, *m*-DPABPEB is the smallest molecular entity in which EET can occur due to an excitation energy gradient.

Below, the potential energy surfaces of *m*-BPEB and of *m*-DPABPEB are characterised and studied with the use of the information we have on the potential energy surfaces of DPA and BPEB.

6.4.1 Association of two equivalent *o*PE: the case of *m*-BPEB

m-BPEB has been deeply studied in ref. [43] for which the pseudofragmentation scheme has been explained. The information from ref. [43] on the pseudofragmentation scheme and the potential energy surface are now recalled and expanded. The pseudofragment scheme of *m*-BPEB are represented in figure 6.20

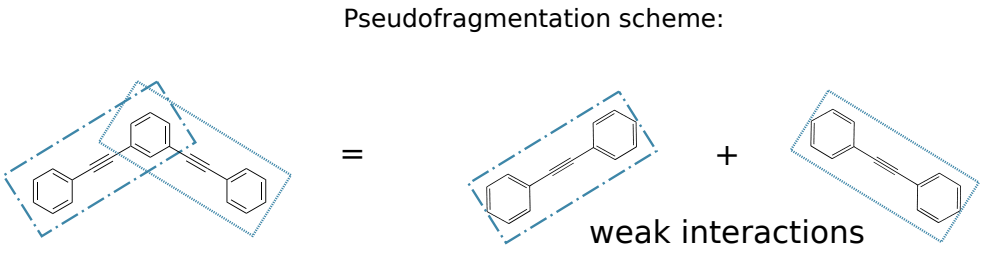

Figure 6.20: Pseudofragmentation scheme of *m*-BPEB into two DPA that are weakly intersecting together.

The first two optically active states of *m*-BPEB in the $\mathcal{C}_{2v}$ point group (1^1B_2 and 1^1A_1)

	m-BPEB	DPA
min S_{act}	$1^1A'$: 4.123	1^1B_{1u} : 4.144
min S_{trans}	$\gamma = 127.90°$ | $\gamma = 232.02°$ 1^1A" : 3.728 | 1^1A" : 3.726	$\gamma = 127.89°$ | $\gamma = 232.11°$ 1^1A_u : 3.716
TS $\mathcal{C}_{2v}$	1^1A_1 : 4.123 1^1B_2 : 4.247	– –
Qx_{pf}^{m-BPEB}	$1^1A_1/1^1B_2$: 4.288	–
$Qx_{cu/tr}^{m-BPEB}$	$\gamma = 151.80°$ | $\gamma = 208.12°$ 1^1A"/$1^1A'$: 4.437 | 1^1A"/$1^1A'$: 4.440	$\gamma = 152.32°$ $1^1B_u/1^1A_u$: 4.444

Table 6.9: Relative energies (in eV), state symmetries and γ values associated to minima (min), 1^{st}-order saddle points (TS) and conical intersections (Qx) of m-BPEB and DPA.

are both delocalised states and they involve electronic excitations between the frontier orbitals and the next pair (HOMO-1, HOMO, LUMO and LUMO+1). We will call them the four frontier orbitals for simplicity. The four near-frontier orbitals are gathered in figure 6.21. At the ground-state equilibrium geometry, 1^1B_2 is the first optically active state and lies at 4.429 eV. Its oscillator strength is $f = 1.71$ and this state is characterised by two electronic transitions (the weight of the electronic excitations are given next within brackets): HOMO→LUMO+1 (0.43) and HOMO-1→LUMO (0.51). The second optically active state ($f = 0.37$) is the 1^1A_1 state and lies at 4.473 eV. This state is mainly characterised by two electronic transitions such that HOMO→LUMO (0.76) and HOMO-1→LUMO+1 (0.16), see figure 6.21. In the $\mathcal{C}_{2v}$ point group, the lowest energy-points of these two states are associated with two respective transition states. The two transition states will be now referenced as TS_{A_1} and TS_{B_2}. They are localised at 4.123 eV and 4.247 eV, respectively (see table 6.9). It can then be defined two diabatic states that match with the 1^1B_2 and the 1^1A_1 states, respectively. They are labelled S_{A_1} and S_{B_2} and they cross at 4.288 eV minimum-energy CoIn in the $\mathcal{C}_{2v}$ point group. The CoIn is labelled Qx_{pf}^{m-BPEB} (see table 6.9). Since these delocalised diabatic states are characteristics of m-BPEB, one cannot find similar diabatic states for the system DPA then table 6.9 shows energy values in the rows "TS $\mathcal{C}_{2v}$" and "Qx_{pf}^{m-BPEB}" for the system m-BPEB only.

At TS_{A_1} and TS_{B_2}, the two density-based descriptors have been calculated, we get: $\phi_S(TS_{B_2}) = 0.86$, $\chi(TS_{B_2}) = 0.36$ and $\phi_S(TS_{A_1}) = 0.87$, $\chi(TS_{A_1}) = 0.35$. Since the two adiabatic electronic excited states are combinations of single excitations among the four frontier orbitals that are

delocalised over the whole system, the overlap density-based descriptor ϕ_S is close to 1 for both states. The net charge density-based descriptor χ is low for both adiabatic electronic excited state because the electronic excitation occurs on the whole system and so the displaced charge is delocalised over the whole molecular system.

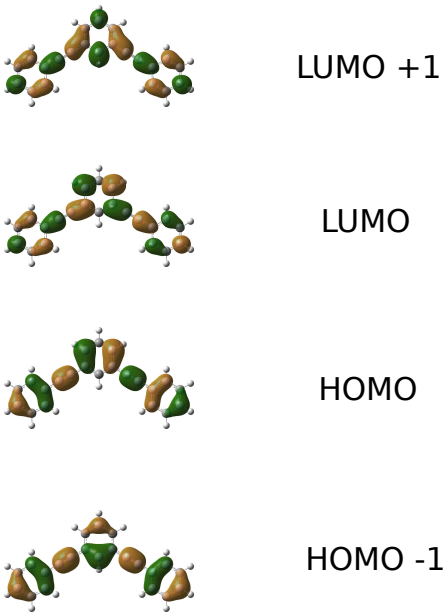

Figure 6.21: The four near-frontier orbitals at the ground state equililbrium geometry for *m*-BPEB.

The conical intersection Qx_{pf}^{m-BPEB} has been characterised in section 5.2. The branching space is defined such that the $\overrightarrow{GD}$ vector preserves the C_{2v} point group. Since the $\overrightarrow{GD}$ vector conserves the group representation, it is totally symmetric (A_1). The direction of the $\overrightarrow{GD}$ vector is the direction that swaps the symmetry between the two adiabatic electronic excited states (1^1A_1 and 1^1B_2). In section 5.2, it has been observed that this direction swaps the oscillator strength and the values of the density-based descriptors as well. The diabatic states S_{A_1} and S_{B_2} conserve then the electronic properties that are associated to the oscillator strength and the density-based descriptors. The $\overrightarrow{DC}$ vector lies in the direction where the two adiabatic electronic excited states couple the most. The derivative coupling direction is the one that breaks the in-plane symmetry of the system and leads to the $\mathcal{C}_s$ point group. In this point group, the first two adiabatic electronic excited states are $1^1A'$ and $2^1A'$. Due to the symmetry of the states, the $\overrightarrow{DC}$ vector is B_2. The first adiabatic electronic excited state is characterised by two equivalent minima where each minimum is associated to locally excited states respectively on the right or on the left of the system. The Lewis structure at the equilibrium geometry of the locally excited

states are such that one of the two ethynylene group of the branches has cumulenic bonds and the two phenyls have quinoidal shape while the ethynylene group on the other branch remains unchanged. The equilibrium geometry of these two equivalent minima are labelled *c*-*m*-BPEB (see figure 6.22).

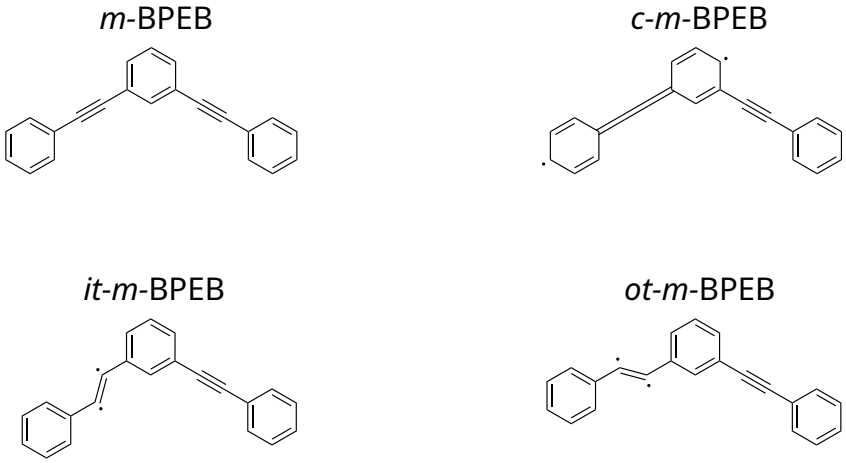

Figure 6.22: Lewis structures at the equilibrium geometry of the ground state (*m*-BPEB) and of the first adiabatic electronic excited state (*c*-*m*-BPEB, *it*-*m*-BPEB and *ot*-*m*-BPEB).

The pseudofragmentation scheme for *m*-BPEB has been explained in ref. [43] and has been developed in the general introduction (see chapter). The sum and the difference of the HOMO-1 and HOMO (LUMO and LUMO+1 respectively) give localised molecular orbitals on either of the two branches of *m*-BPEB. They are similar to the HOMO and LUMO associated to *c*-*m*-BPEB.

The attachment and detachment densities have been computed at the geometries associated to TS_{B_2}, TS_{A_1} and *c*-*m*-BPEB. We see that both of the densities are very alike for the two transition states because they result from a combination of the four near-frontier orbitals that are very similar for the two transition states. Computing the sum and the difference of the attachment and detachment densities would not give us localised sum and difference densities since the attachment and detachment densities are similar up to a phase so it would give an almost vanishing density (for the difference) and a non-zero density (for the sum). However, the attachment and detachment densities for *c*-*m*-BPEB are localised on the branch that has adopted the cumulenic and quinoidal shape concerning the ethynylene group and the two phenyls (see fig. 6.23).

The similarities between the isomers *c*-*m*-BPEB and *c*-DPA are encountered with the shape of the localised HOMO/LUMO on the left or right branch of *m*-BPEB and the HOMO/LUMO

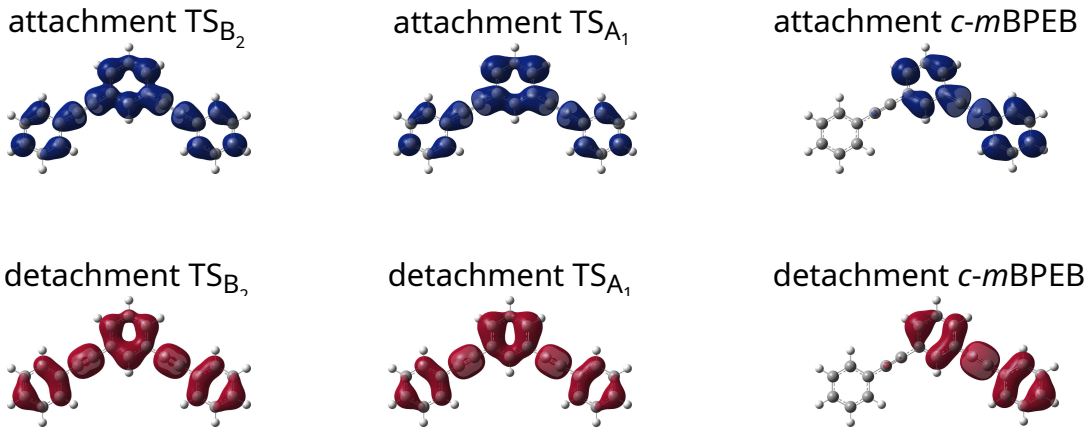

Figure 6.23: Attachment and detachment densities of the transition states TS_{B_2}, TS_{A_1} and of the equilibrium geometry in the first adiabatic electronic excited state in the $\mathcal{C}_s$ point group.

of DPA and with the relative energy values as well. The relative energy of the two equivalent minima lies at 4.123 eV and the cumulenic isomer of DPA is associated to a relative energy of 4.144 eV. *m*-BPEB behaves in fact in the region of the cumulenic equilibrium geometry much as *c*-DPA. The two density-based descriptors computed for *c-m*-BPEB and *c*-DPA give the same value as well: $\phi_S(c\text{BPEB}) = 0.86$, $\chi(c\text{BPEB}) = 0.36$ and $\phi_S(c\text{DPA}) = 0.86$, $\chi(c\text{DPA}) = 0.36$. Since there are two equivalent cumulenic isomers, one can define two equivalent diabatic states which minima correspond to the minima of the $1^1A'$ state and are labelled S_{act} as it has been done in subsection 6.2.2 for DPA, BPEB and DPABPEB. Eventhough *m*-BPEB is composed of 36 atoms which form two ethynylene groups and three phenyls, its cumulenic isomer cannot be compared to the cumulenic isomer of BPEB because the cumulenic bonds are delocalised over the whole system (for BPEB) while it is limited to only one branch of *m*-BPEB due to the *meta* position of the ethynylene group. Such a difference between the two systems leads to the fact that the two cumulenic isomers are associated to the relative energy values: 4.123 eV (*c-m*-BPEB) and 3.624 eV (*c*-BPEB). A schematic representation of the potential energy surface of the first two adiabatic electronic excited states of *m*-BPEB and of the two diabatic states that are localised on the pseudofragments in the $\mathcal{C}_s$ point group is given in figure 6.24.

In figure 6.25 are superimposed the absorption and emission spectra of *m*-BPEB and DPA from the ground state toward the first optically active state. Eventhough there is a small shift toward higher wavelengths according to the spectra of *m*-BPEB, we see that the vibrational progression of the two spectra is conserved and that the first peak associated to the 0-0 transition at 307 nm is present in both spectra. In ref. [152], Chu *et al* have shown that the experimental

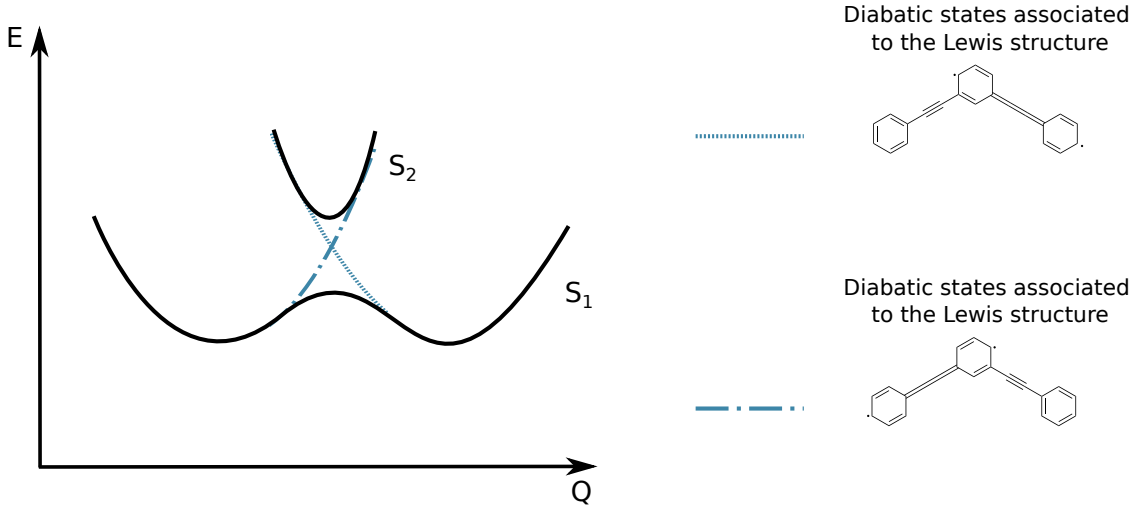

Figure 6.24: Schematic representation of the first two singlet states (S_1 and S_2) and of the two diabatic states localised on the pseudofragments of *m*-BPEB.

absorption and emission spectra do not overlap because the 0-0 transition seems almost forbidden apparently. However the first most intense peak in the experimental absorption spectrum is localised at 301 nm while the first most intense peak in the experimental emission spectrum is at 327 nm. The first intense peak of the absorption spectrum seems to be very similar to the one in our theoretical absorption spectrum which allow us to think that the 0-0 transition is allowed according to the absorption but is forbidden or weakly allowed concerning the emission. Work is in progress to explain such a Stokes-shift between the two spectra.

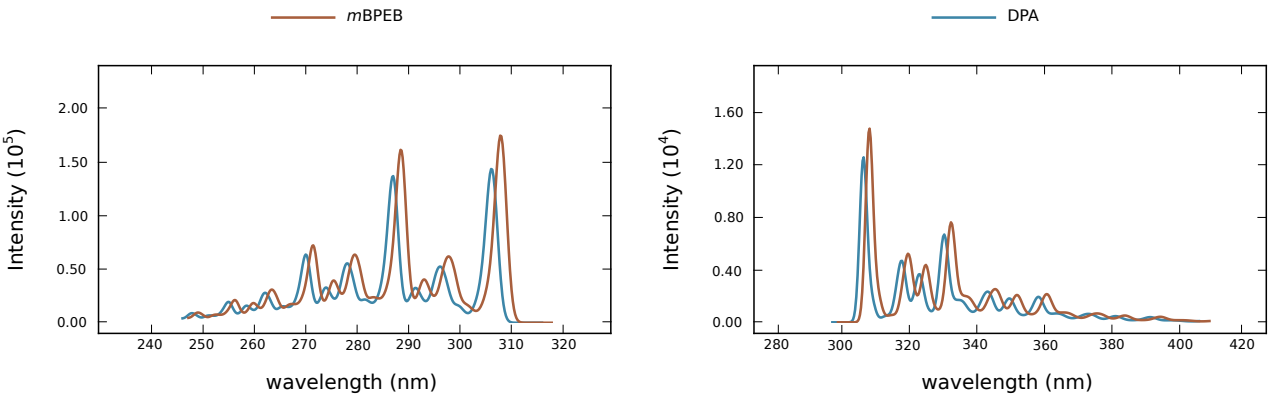

Figure 6.25: Theoretical absorption and emission spectra of *m*-BPEB *in vacuo* within the Franck-Condon and harmonic approximations.

Since *c*-*m*-BPEB behaves as *c*-DPA, there are equilibrium geometries in the first adiabatic electronic excited state that are associated to single-*trans* isomers. Since the two ethynylene groups are equivalent by symmetry, each of them can be *trans*-bent while the second ethynylene

group remains unaltered. However, due to symmetry reasons, the four single-*trans* isomers are not equivalent as it has been explained for BPEB.

An inward single-*trans* bending (leading to the isomer *it*-*m*-BPEB, see fig. 6.26) is different from the outward single-*trans* bending (leading to the isomer *ot*-*m*-BPEB, see fig. 6.26). But an inward (*resp.* outward) single-*trans* bending on the ethynylene group on the left or on the right are equivalent.

The isomer *ot*-*m*-BPEB is located at 3.728 eV with a bending angle of $\gamma = 127.90°$ and the *it*-*m*-BPEB isomer is located at 3.726 eV with a bending angle of $\gamma = 232.60°$. The *trans* isomer of DPA, *t*-DPA, is defined by a relative energy of 3.716 eV and a bending angle of $\gamma = 127.89°$ (see table 6.9). First of all we see that the relative energies of the three different isomers differ from only thousandth of eV. Then the variation of the *trans* bending angle is such that:

- *ot*-*m*-BPEB: $\Delta\gamma = \mid \gamma(c\text{-}m\text{BPEB}) - \gamma(ot\text{-}m\text{BPEB}) \mid = \mid 180.00° - 127.90° \mid = 52.10°$

- *it*-*m*-BPEB: $\Delta\gamma = \mid \gamma(c\text{-}m\text{BPEB}) - \gamma(it\text{-}m\text{BPEB}) \mid = \mid 180.00° - 232.60° \mid = 52.60°$

- *t*-DPA: $\Delta\gamma = \mid \gamma(c\text{DPA}) - \gamma(t\text{DPA}) \mid = \mid 180.00° - 127.89° \mid = 52.11°$

The variation of the *trans*-bending angle from the cumulenic isomer differ from only tenth of degrees. The density-based descriptors of the three single-*trans* isomers are gathered in table 6.10.

	t-DPA	*ot*-*m*-BPEB	*it*-*m*-BPEB
χ	0.73	0.73	0.73
ϕ_S	0.54	0.54	0.54

Table 6.10: Density-based descriptors computed at the equilibrium geometries of the single-*trans* isomers *t*-DPA, *ot*-*m*-BPEB and *it*-*m*-BPEB.

From table 6.10 we see that the three different isomers are described by the same value. Such similarity between the single-*trans* isomers of DPA and *m*-BPEB allows us to define as we did in subsection 6.2.3, diabatic states which minima are associated to the single-*trans* isomers of *m*-BPEB. We define the two diabatic states itS_{trans} and otS_{trans} which respective minima are associated to *it*-*m*-BPEB and *ot*-*m*-BPEB. One has to notice that there are actually two equivalent itS_{trans} and otS_{trans} diabatic states because each of the two ethynylene groups on the left and right branches can be *trans*-bent.

Rigid scans have been performed on *m*-BPEB and are gathered in figure 6.26. Two rigid scans have been performed along the single-*trans* bending angle at one ethynylene group of *m*-BPEB and DPA at their equilibrium geometries in their ground state (scan a) and b) in fig. 6.26) and at their cumulenic equilibrium geometry in their first adiabatic electronic excited state (scan c) and d) in fig. 6.26).

In the scans a) and c), only the 1^1B_u state energy is plotted in blue with dashed line while the three first A_u state energies are plotted in blue with plain line as in fig. 6.9. In the rigid scan a), the geometry at $\gamma = 180°$ corresponds to the equilibrium geometry in the ground state and in the rigid scan c), the geometry at $\gamma = 180°$ corresponds to the equilibrium geometry of the cumulenic isomer *c*-DPA. Both of these geometries belong to $\mathcal{D}_{2h}$ point group. The *trans* bending coordinate γ involves a displacement of B_{3g} symmetry and so all of the geometries obtained, except the two at $\gamma = 180°$, belong to $\mathcal{C}_{2h}$ point group. The 1^1B_u state at $\gamma = 180°$ is then obsviously of B_{1u} symmetry and corresponds to the FC-point in scan a). We know from subsection 6.2.1 that the FC-point of DPA lies at 4.476 eV and the minimum of the 1^1B_{1u} state lies at 4.144 eV. We see in figure 6.26 that the 1^1A_u state crosses the 1^1B_u state at ($\gamma = 152°$, 4.827 eV) in scan a) and at (150°, 4.523 eV) in scan c). The two minima in the rigid scans are located at $\gamma = 133°$, 4.381 eV for scan a) and at ($\gamma = 132°$, 4.155 eV) for scan c). These two minima are actually apparent minima but not global minima associated to the *trans* isomer of DPA, *t*-DPA (see table 6.9). Although the difference of reference geometries for these scans, they look much alike and one can get a qualitative picture of the exact potential energy surface of DPA along the *trans* bending coordinate.

In scans b) and d), the first two optically active states are plotted in brown with dashed line ($1^1A'$ and $2^1A'$ in the $\mathcal{C}_s$ point group and 1^1B_2 and 1^1A_1 in the $\mathcal{C}_{2v}$ point group). The optically inactive states of ^1A" in the $\mathcal{C}_s$ point group are plotted in brown with plain line.

The rigid scan b) is performed with the ground state equilibrium geometry as a reference geometry. The ground state equilibrium geometry belongs to $\mathcal{C}_{2v}$ and so at $\gamma = 180°$ the two optically active states are 1^1B_2 and 1^1A_1. Along the *trans* bending displacement, it appears that there is an avoided crossing between the 1^1B_2 and 1^1A_1 states at $\gamma = 157°$. Since a *trans* bending displacement lower than 180° or higher than 180° leads to two different by symmetry geometries, that is why there is no avoided crossing between the two optically active states for γ values higher than 180°. However we see on the scan b) that there are two crossings between the $1^1A'$ and the 1^1A" states at $\gamma = 152°$ and $\gamma = 209°$ and the two apparent minima of scan b)

are located at ($\gamma = 134°$, 4.395 eV) and at ($\gamma = 229°$, 4.399 eV).

Scan d) is different from b) because all of the geometries used to perform the scan belong to $\mathcal{C}_s$. The reference geometry that is used is the equilibrium geometry associated to the cumulenic isomer: *c-m*-BPEB. The first two optically active states are $1^1A'$ and $2^1A'$ and they correspond to a locally excited state on the cumulenic branch and on the other branch, respectively. The crossings between the $1^1A'$ and the 1^1A" states are located at $\gamma = 150°$ and $\gamma = 211°$, and the apparent minima on the scan d) are located at $\gamma = 134°$, 4.172 eV and $\gamma = 229°$, 4.176 eV. We see that the apparent minima of the two scans are similar according to the γ values and so are the global minima associated to the two single-*trans* isomers. As the scans of DPA, BPEB and DPABPEB, we can consider the rigid scan of *m*-BPEB as a good approximation of the potential energy surfaces.

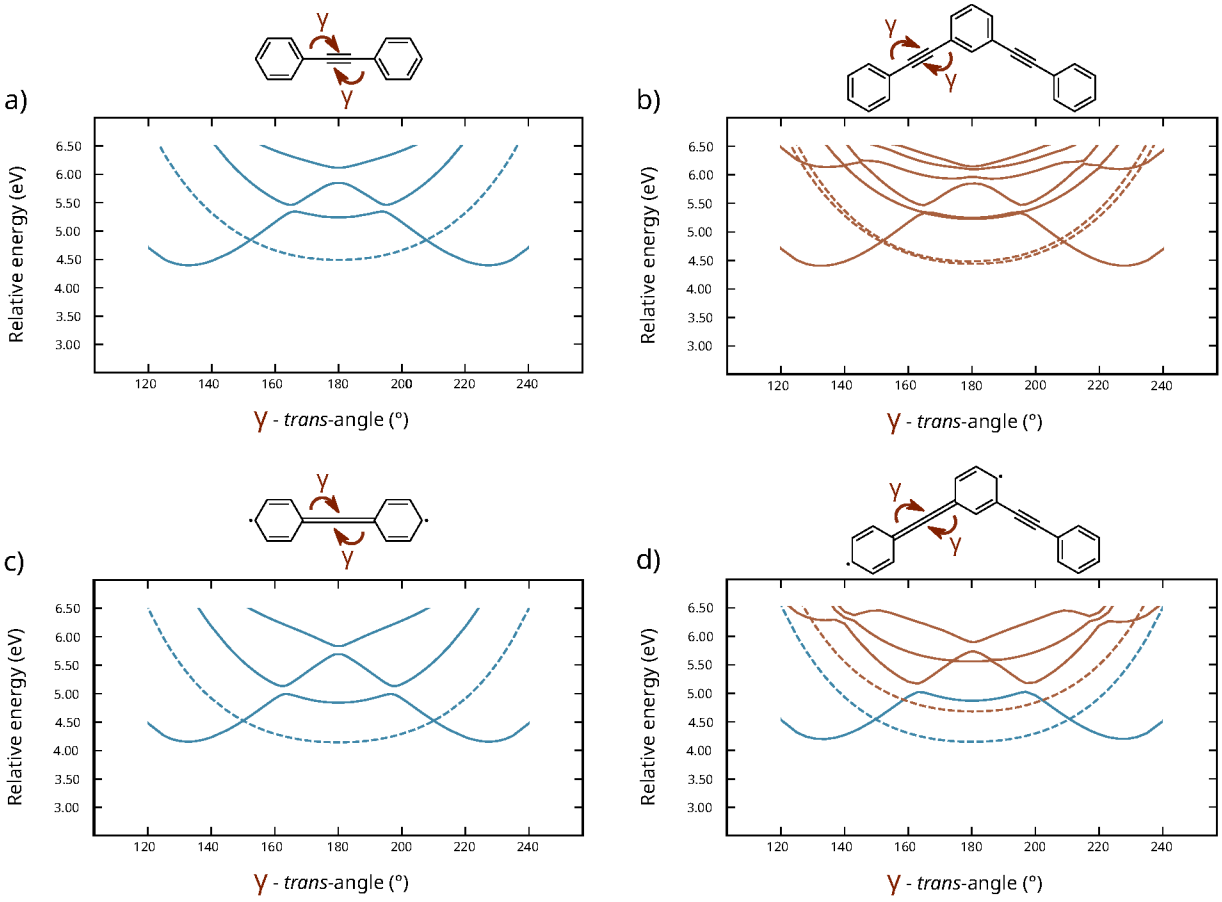

Figure 6.26: Rigid scans along the γ *trans* bending angle from the ground state equilibrium geometry and from the first adiabatic electronic excited state equilibrium geometry of *m*-BPEB and DPA.

Since there are two pairs of different S_{trans} diabatic states and each pair are equivalent

by symmetry, there are actually four equilibrium geometries associated to two equivalent by symmetry *ot*-*m*-BPEB and two equivalent *it*-*m*-BPEB. Figure 6.27 is a two-dimensional rigid scan. The coordinates are the γ *trans*-bending angles on either the branch on the left (γ_1) or on the right (γ_2) of *m*-BPEB. The scan has been performed from the ground state equilibrium geometry. Then the minimum that is observed in the middle of the rigid scan is not the actual global minimum of the $1^1A'$ state (*i.e* the cumulenic isomer). This apparent minimum in the middle is surrounded by four minima which are associated to rigid single-*trans* isomers.

The potential energy surface of the first adiabatic is then composed of at least six energy minima. Two of them are the cumulenic minima, they are related to the equilibrium geometry of the two equivalent cumulenic isomers. The four remaining minima are the *trans* minima, they are associated to the equilibrium geometry of the two equivalent *ot*-*m*-BPEB and the two equivalent *it*-*m*-BPEB isomers. Moreover the two cumulenic minima belong to two equivalent localised excited states that cross in $\mathcal{C}_{2v}$.

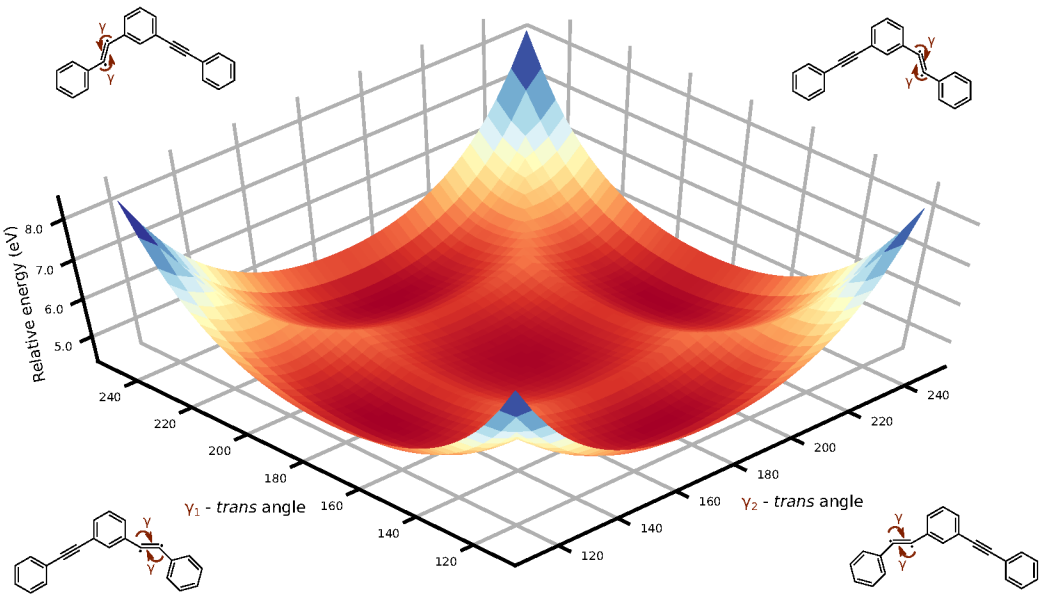

Figure 6.27: Rigid scan along the γ_1 *trans* bending angle (*trans* bending angle on the left branch) and along the γ_2 *trans* bending angle (*trans* bending angle on the right) from the ground state equilibrium geometry.

6.4.2 Association of two different *o*PE: the case of *m*-DPABPEB

The pseudofragmentation scheme

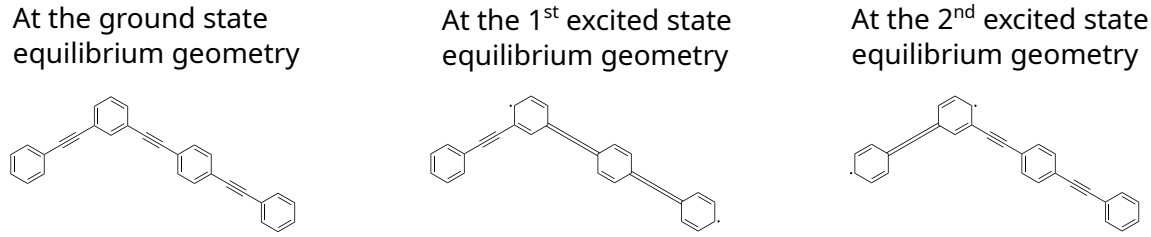

Figure 6.28: Lewis structures at the equilibrium geometries in the ground state, in the first and in the second optically active electronic states.

The system labeled *m*-DPABPEB is an *o*PE and its Lewis structure in the ground state is represented on the left of figure 6.28. This sytem can be pseudofragmented into two smaller *o*PE. The two pseudofragments are DPA and BPEB (see fig. 6.29).

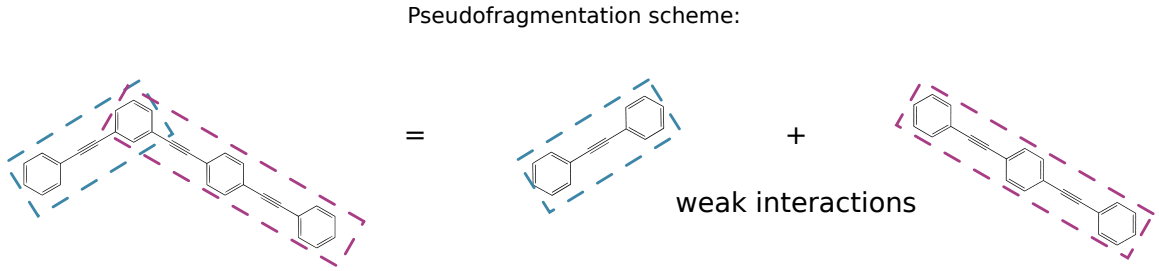

Figure 6.29: Pseudofragmentation scheme of *m*-DPABPEB into DPA and *BPEB* that are weakly interacting together.

	m-DPABPEB	BPEB	DPA
min S_{act}^{DPA}	$2^1A'$: 4.170	–	1^1B_{1u} : 4.123
min S_{act}^{BPEB}	$1^1A'$: 3.606	1^1B_{1u} : 3.624	–
Qx_{pf}	$1^1A'/2^1A'$ 4.293	–	–
min *mid t*-S_{trans}^{BPEB}	$\gamma = 127.73°$ | $\gamma = 232.20°$ 1^1A" : 3.690 | 1^1A" : 3.693	$\gamma = 127.97°$	– –
min *peri t*-S_{trans}^{BPEB}	$\gamma = 127.98°$ | $\gamma = 232.01°$ 1^1A" : 3.690 | 1^1A" : 3.691	1^1A" : 3.685	– –

Table 6.11: Relative energies (in eV), state symmetries and γ values associated to minima (min), 1^{st}-order saddle point (TS) and conical intersections (Qx) of *m*-DPABPEB and DPA.

As it has been developed for m-BPEB, m-DPABBPEB possesses the same characteristics as it pseudofragments. There is an equilibrium geometry in the first adiabatic electronic excited state ($1^1A'$) which is characterised by the Lewis structure that is represented in the middle of fig. 6.28. The system is then characterised by cumulenic groups and quinoidal phenyls on the branch that is associated to the BPEB pseudofragment. This is an optically active state and corresponds to an HOMO/LUMO excitation that is localised on the BPEB pseudofragment (see fig. 6.30). The weight of the HOMO/LUMO excitation is 0.91. One can then define the diabatic state S_{act}^{BPEB} and its minimum lies at 3.606 eV (see table 6.11). It is the same order of magnitude as the minimum of the S_{act} of BPEB (3.624 eV, see table 6.11). The attachment and the detachment densities are computed at the equilibrium geometry of this state and are shown in figure 6.31. We see that the two densities are very alike as those that have been computed at the equilibrium geometry of the S_{act} of BPEB (see fig. 6.5). The first optically active state of m-DPABPEB shows not only similarities according to the transition energies, attachement and detachment densities, HOMO/LUMO transition and Lewis structure with the optically active electronic state of BPEB, it shows similar vibrational progressions according to the theoretical absorption and emission spectra (see 6.32).

Similarly, we can define a second diabatic electronic state S_{act}^{DPA} that is associated to a local excitation at the DPA pseudofragment of m-DPABPEB. The corresponding Lewis structure is represented on the right of figure 6.28. It is characterised by a cumulenic group and two quinoidal phenyls on the DPA pseudofragment branch. Its minimum lies at the same order of magnitude as the one of the S_{act} of DPA (4.170 eV for m-DPABPEB and 4.123 eV for DPA, see table 6.11). However, the equilibrium geometry of a such cumulenic isomer does not exist in the first adiabatic electronic state but it exists in the second adiabatic electronic excited state ($2^1A'$). A schematic representation of the first two adiabatic electronic excited states and of the two diabatic states that are localised on the pseudofragments are shown in figure 6.33.

The equilibrium geometry in the second adiabatic electronic excited states is characterised by transitions between the four frontier orbitals (see fig 6.30): HOMO $-$ 1 $\rightarrow$ LUMO (0.09), HOMO $\rightarrow$ LUMO + 1 (0.10), HOMO $-$ 1 $\rightarrow$ LUMO + 1 (0.30) and HOMO $\rightarrow$ LUMO (0.44). Such mixing between the near orbitals frontiers shows that this state at this equilibrium geometry cannot be characterised by a single HOMO/LUMO excitation onto the DPA pseudofragment branch of m-DPABPEB. However, the NTO of the excitation have been computed and gathered

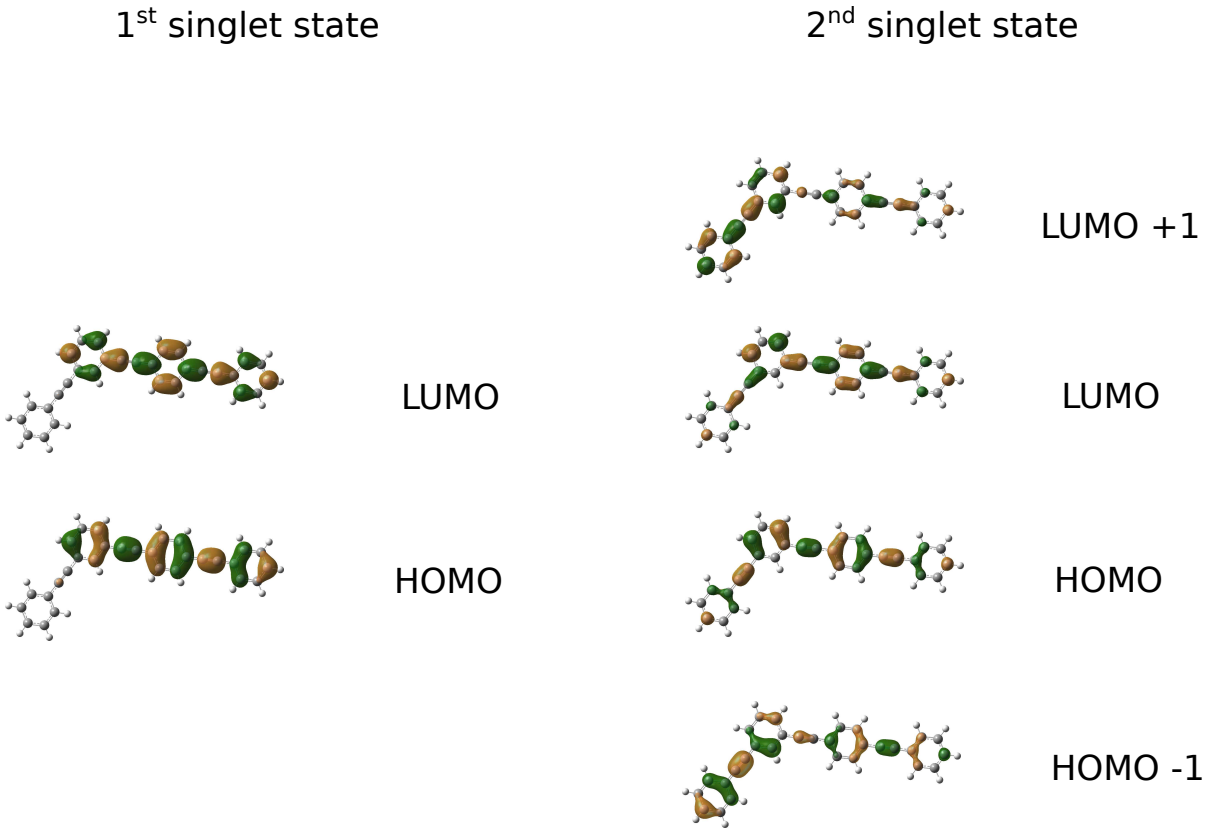

Figure 6.30: Frontier orbitals computed at the equilibrium geometry in the first and in the second optically active electornic state of *m*-DPABPEB.

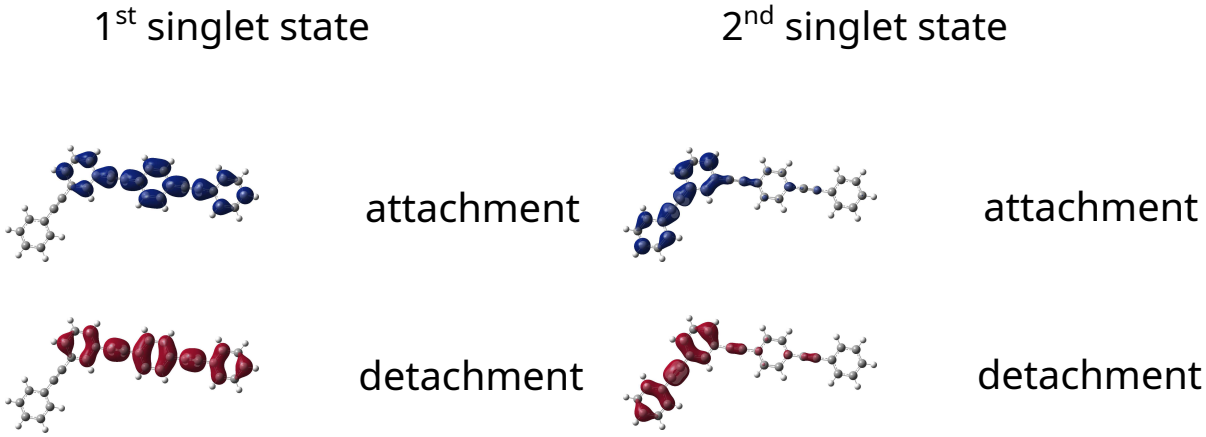

Figure 6.31: Attachment and detachment densities of *m*-DPABPEB computed at the equilibrium geometry of the S_{act}^{BPEB} diabatic state and the S_{act}^{DPA} diabatic state.

on figure 6.34. We see that the first pair of natural orbitals that characterise the electronic excitation are similar to the HOMO/LUMO of DPA (see fig. 6.2). The singular value of the first pair is 0.85 while the singular value of the second pair is 0.1 so we can assume that only the first

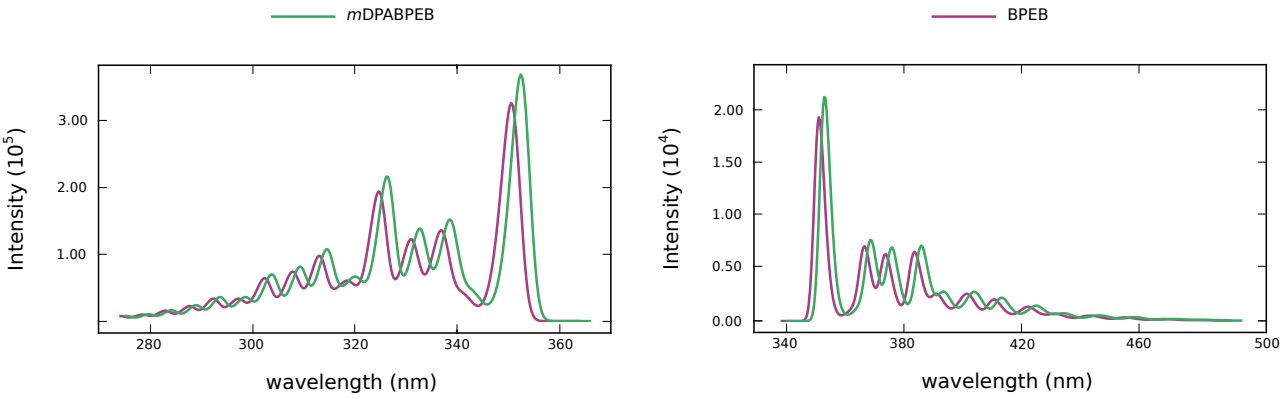

Figure 6.32: Absorption and emission spectra of *m*-DPABPEB between the ground state minimum and the first optically active electronic state.

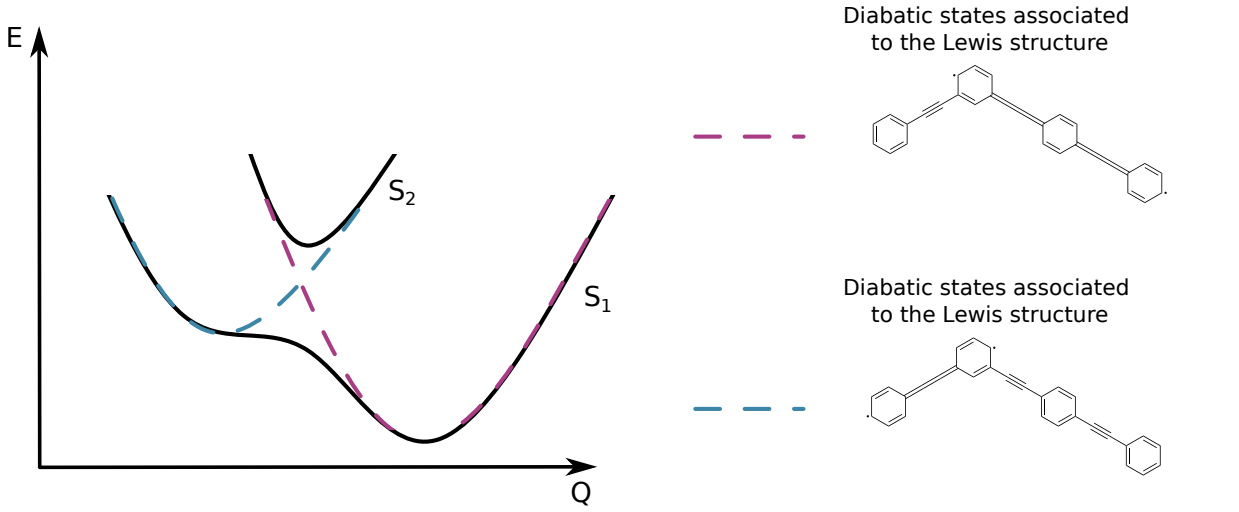

Figure 6.33: Schematic reprensentation of the first two adiabatic electronic excited states ($1^1A'$ and $2^1A'$) of *m*-DPABPEB and of the two diabatic states that are localised on the pseudofragments.

pair of NTO characterise mainly the electronic excitation. The shape of the NTO of the second optically active state are almost identical to the shape of the attachment and the detachment densities (see fig. 6.31).

Figure 6.34: Natural transition orbitals computed at the equilibrium geometry of the second optically active state.

Finaly, we see that the vibrational progression of the second optically active state is similar as well to the vibrational progression of the first optically active state of DPA (see fig. 6.35). However, we see that some transitions are less significant for *m*-DPABPEB than they are for DPA. For instance, the transition at 380 nm for *m*-DPABPEB that corresponds to the transition 119_0^1 and at 387 nm for DPA and it corresponds to the transition 56_0^1. The normal mode n°119 for *m*-DPABPEB and n°56 correspond to a stretching onto the ethynylene groups. They are shown in figure 6.36. Such a decrease of the intensity can be explained by the fact that the second adiabatic electronic excited states is defined by more thant one electronic excitation and so it cannot be explicitly defined as a HOMO/LUMO excitation.

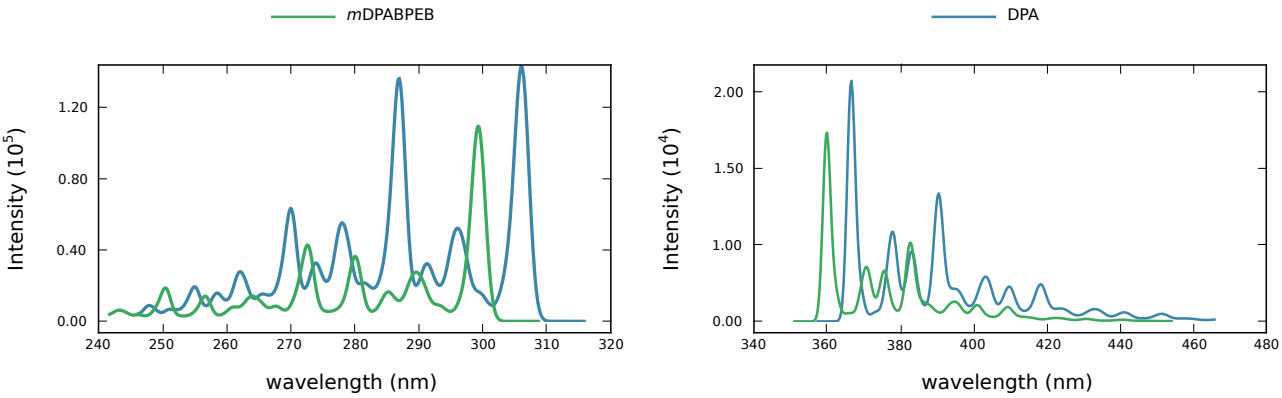

Figure 6.35: Absorption and emission spectra of *m*-DPABPEB between the ground state minimum and the second optically active electronic state.

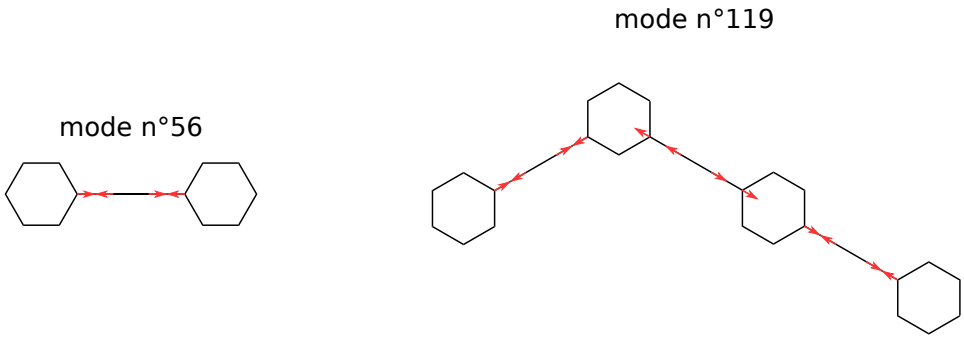

Figure 6.36: Normal mode n°56 of DPA and n°119 of *m*-DPABPEB.

The second adiabatic electronic excited state of *m*-DPABPEB is not described by a single electronic excitation onto the DPA pseudofragment branch but the NTO, the attachment and detachment densities show that contributions onto the DPA pseudofragment branch remain the most significant.

We can then assume that the first two optically active states of *m*-DPABPEB can be defined as

two localised transitions on the BPEB pseudofragment branch and on the DPA pseudofragment branch respectively. We have defined then two diabatic states: S_{act}^{BPEB} and S_{act}^{DPA}. The CoIn between the first and the second adiabatic states lies at 4.293 eV (see table 6.11). Since the $2^1A'$ state results of a mixing of single excitations, we can assume that the two diabatic states are strongly mixed with each other. It is due to the fact that the energy minimum in the $2^1A'$ (at 4.170 eV) state is close to the conical intersection between the two states (see table 6.11).

Single-*trans* isomers of *m*-DPABPEB

According to the pseudofragmentation scheme *m*-DPABPEB behaves as a DPA and a BPEB that are weakly interacting together. We know that there are two equivalent DPA *trans* isomers and four equivalent BPEB single-*trans* isomers. All of the single-*trans* isomers of *m*-DPABPEB are not equivalent by symmetry. *m*-DPABPEB possesses three ethynylene group and so there are six non-equivalent single-*trans* isomers. The Lewis structure associated to the six single-*trans* isomers are gathered in figure 6.37.

No equilibrium geometry has been found in the first and in the second adiabatic electronic excited states associated to *trans* isomer which the DPA pseudofragment branch is *trans*-bent. This may be due to the fact that the diabatic state S_{act}^{DPA} that is localised on the DPA pseudofragment branch does not correspond to a single HOMO/LUMO excitation onto the DPA pseudofragment branch so it is difficult to obtain an equilibrium geometry for which the DPA pseudofragment branch is *trans*-bent. However we still consider two non-equivalent diabatic state S_{trans}^{DPA} which are optically inactive and are defined by the two Lewis structures on the top of figure 6.37.

Four equilibrium geometries associated to the four non-equivalent single-*trans* for which one of the two ethynylene groups of the BPEB pseudofragment branch has been *trans*-bent, have been found. Since the four single-*trans* isomers are non-equivalent the γ *trans*-angle and the relative energies are not the same but yet they are very similar (see table 6.11 and figure 6.37). Four non-equivalent diabatic states are considered S_{trans}^{BPEB}, they are optically inactive and correspond to the four Lewis structures that are in the bottom of figure 6.37.

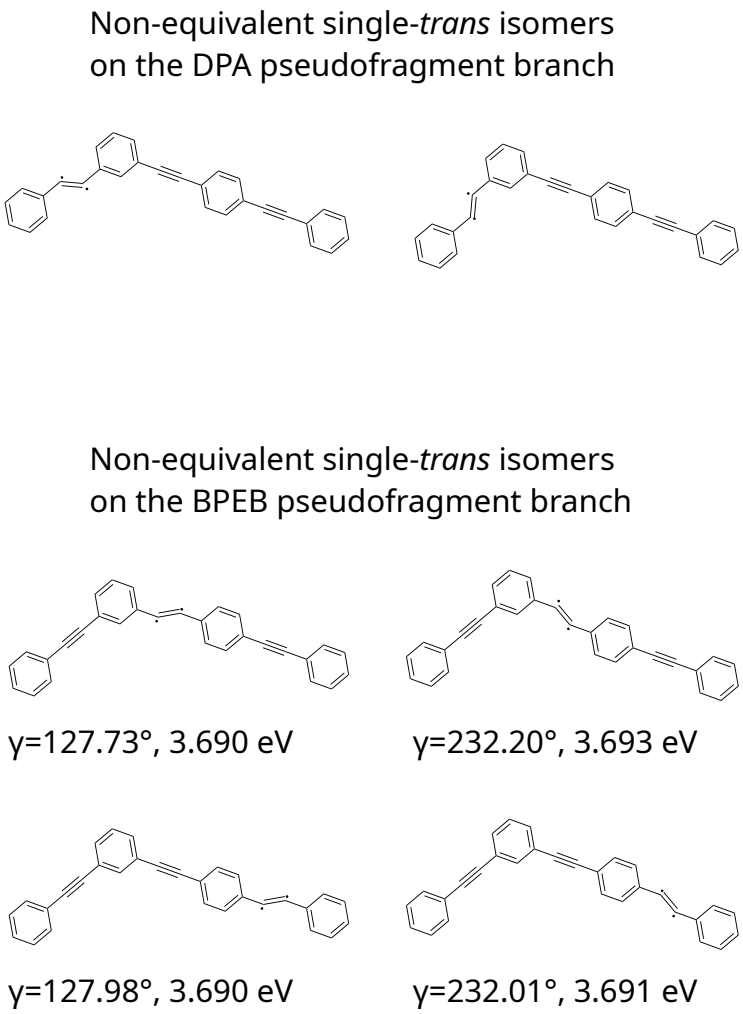

Figure 6.37: Non-equivalent single-*trans* isomers of *m*-DPABPEB

Rigid scans on m-DPABPEB

Rigid scans have been performed for m-DPABPEB and are gathered in figures 6.38 and 6.39. Figure 6.38 gathers the *trans*-bending rigid scans for DPA and m-DPABPEB. The reference geometries are the equilibrium geometries in the S_{act}^{DPA} diabatic state for both systems. Figure 6.39 gathers the *trans*-bending rigid scans for BPEB and m-DPABPEB. The reference geometries are the equilibrium geometries in the S_{act}^{BPEB} diabatic state for both systems. Two rigid scans are perfomed for BPEB peudofragment branches since the two ethynylene groups are not equivalent by symmetry (scans b) and c) in figure 6.39).

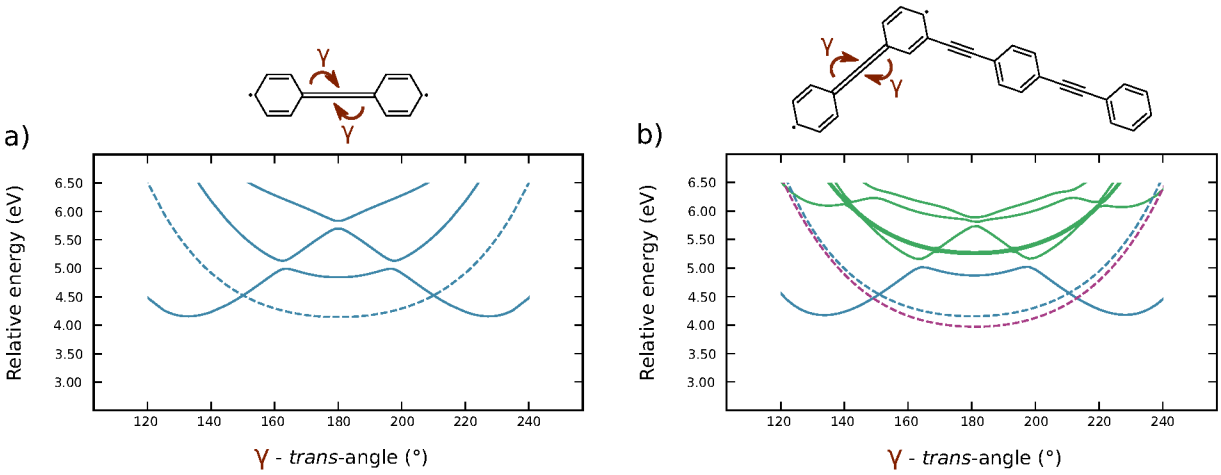

Figure 6.38: Rigid scans along the γ *trans* bending angle at the second adiabatic electronic excited state equilibrium geometry of m-DPABPEB and at the first adiabatic electronic excited state equilibrium geometry of DPA.

The rigid scan a) of fig. 6.38 is the same as the one presented in figure 6.9. The plain blue lines correspond to the optically inactive states of A_u symmetry and the dashed blue line corresponds to the optically active state 1^1B_u. Details on this rigid scan are given in subsection 6.2.4. The potential energy curves of the rigid scan b) are captioned as follow: the dashed red line corresponds to the first optically active state $1^1A'$ that is associated to a local excitation on the BPEB pseudofragment branch, the S_{act}^{BPEB} diabatic state. The dashed blue line corresponds to the second optically active state $2^1A'$ that is associated to a local excitation on the DPA pseudofragment branch, the S_{act}^{DPA} diabatic state. The plain blue line corresponds to the first optically inactive state 1^1A". In the vicinity of the two apparent minima, one can associate this adiabatic state to the two non equivalent diabatic states S_{trans}^{DPA}. Then the green plain lines correspond to higher states of A" symmetry.

Since the reference geometry of the rigid scan is the equilibrium geometry in the $2^1A'$ state, the minimum of the $2^1A'$ state at 180° is indeed the global minimum of this state but the minimum at 180° for the $1^1A'$ state and the two minima at $\gamma = 134°$ and $\gamma = 228°$ are not real minima but they are only apparent minima. The two apparent minima associated to *trans*-bent isomers on the DPA pseudofragment branch are at a relative energy of 4.187 eV and 4.192 eV. The two equivalent apparent *trans* minima of scan a) are localised at 133°, 4.155 eV. So even within the rigid scans, the electronic excited states that are localised on the DPA pseudofragment branch of *m*-DPABPEB behave as the electronic states of DPA.

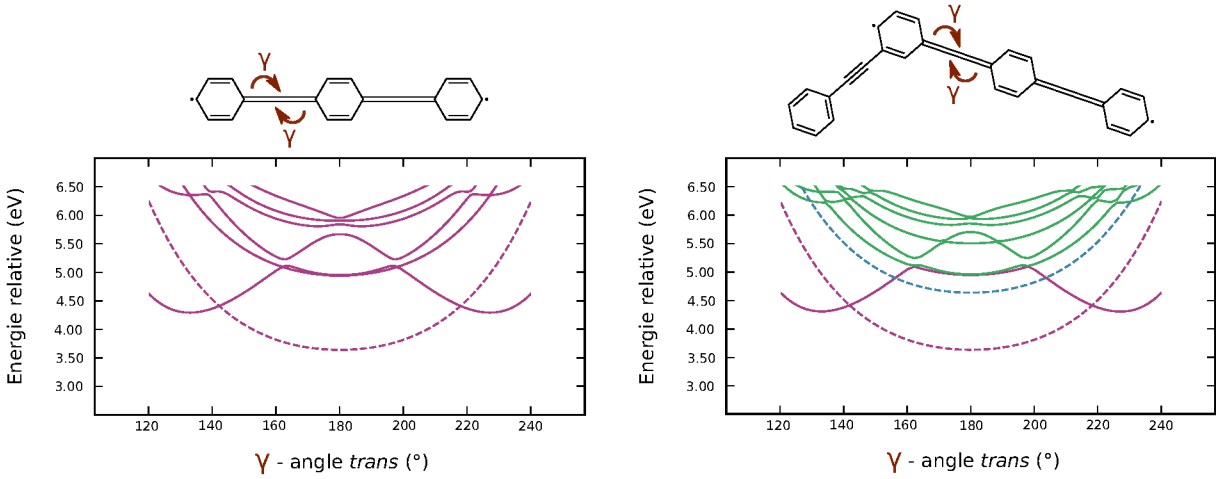

Figure 6.39: Rigid scans along the γ *trans* bending angle from the first adiabatic electronic excited state equilibrium geometry of *m*-DPABPEB and BPEB.

Similarly, the rigid scan of BPEB in fig. 6.39 is the same as the one detailed in fig. 6.9. The plain red lines correspond to the optically inactive states of A_u symmetry and the dashed red line corresponds to the optically active state 1^1B_u. Details on this rigid scan are given in subsection 6.2.4. The scan b) and c) are captioned as the rigid scan of *m*-DPABPEB in fig. 6.38. The reference geometry is the equilibrium geometry at the minimum in the $1^1A'$ state and so the associated relative energy is the one at $\gamma = 180°$ for the $1^1A'$ state in the scan b) and c) in fig. 6.39. All of the other minima in the two rigid scans are then apparent minima. However the apparent minima associated to the single-*trans* isomers (228°, 4.277 eV), (132°, 4.279 eV) in the scan b),and *m*-DPABPEB (228°, 4.290 eV) and (132°, 4.290 eV) in the scan c) are at the same order of magnitude according to the γ angle and the relative energy of the

four equivalent *trans* minima of the rigid scan a) in fig. 6.39 which are localised at 133°, 4.276 eV.

We see that for the rigid scans of *m*-DPABPEB, in both cases of a local excitation on the DPA pseudofragment branch or on the BPEB pseudofragment branch, the diabatic state S_{act}^{DPA} is always higher in energy than the S_{act}^{BPEB} diabatic state. In addition to that we see that both diabatic states (S_{act}^{BPEB} and S_{act}^{DPA}) are crossing the first optically inactive state which minima are associated to the single-*trans* isomers. In the case of a rigid scan which reference geometry is the equilibrium geometry at the 2^1A" state (the DPA pseudofragment branch is characterised by its cumulenic isomer Lewis structure), the optically inactive diabatic states are S_{trans}^{DPA}. In the case of the two rigid scans which reference geometry is the equilibrium geometry at the $1^1A'$ state (the BPEB pseudofragment branch is characterised by its cumulenic isomer Lewis structure), the optically inactive diabatic states are S_{trans}^{BPEB}.

6.5 Association of three *oligo*phenylene ethynylene

The pseudofragmentation of *mb*-DPABPEB

Thanks to the $\mathcal{C}_{2v}$ symmetry this case will be, in fact, simpler than the previous one despite a larger size. In the introduction (chapter), details on the pseudofragmentation scheme of *mb*-DPABPEB are given in fig. 5. For simplicity, this figure is put again in this section (see fig. 6.40). In section 6.4, one has compared the relative energies, the geometries and the potential energy surfaces of *o*PE with their pseudofragments. Here, we are going first to validate the different pseudofragmentation schemes in fig. 6.40, and then an EET mechanism will be suggested.

	mb-DPABPEB	*m*-DPABPEB	*m*-BPEB	BPEB	DPA
S_{act}^{DPA}	$1^1A'$: 4.142	$2^1A'$: 4.170	$1^1A'$: 4.123	-	1^1B_{1u}: 4.144
S_{trans}^{DPA}	1^1A": 3.737 1^1A": 3.736	-	1^1A": 3.726 1^1A": 3.728	-	1^1A_u: 3.716
S_{act}^{BPEB}	1^1A_1: 3.591	$1^1A'$: 3.606	-	1^1B_{1u}: 3.624	-
S_{trans}^{BPEB}	1^1A" : 3.699 1^1A" : 3.694	1^1A" : 3.690 1^1A" : 3.693 1^1A" : 3.690 1^1A" : 3.691	-	1^1A" : 3.685	-

Table 6.12: Relative energies (in eV) and state symmetries of significant features of the potential energy surfaces of *mb*-DPABPEB, *m*-DPABPEB, *m*-BPEB, BPEB and DPA.

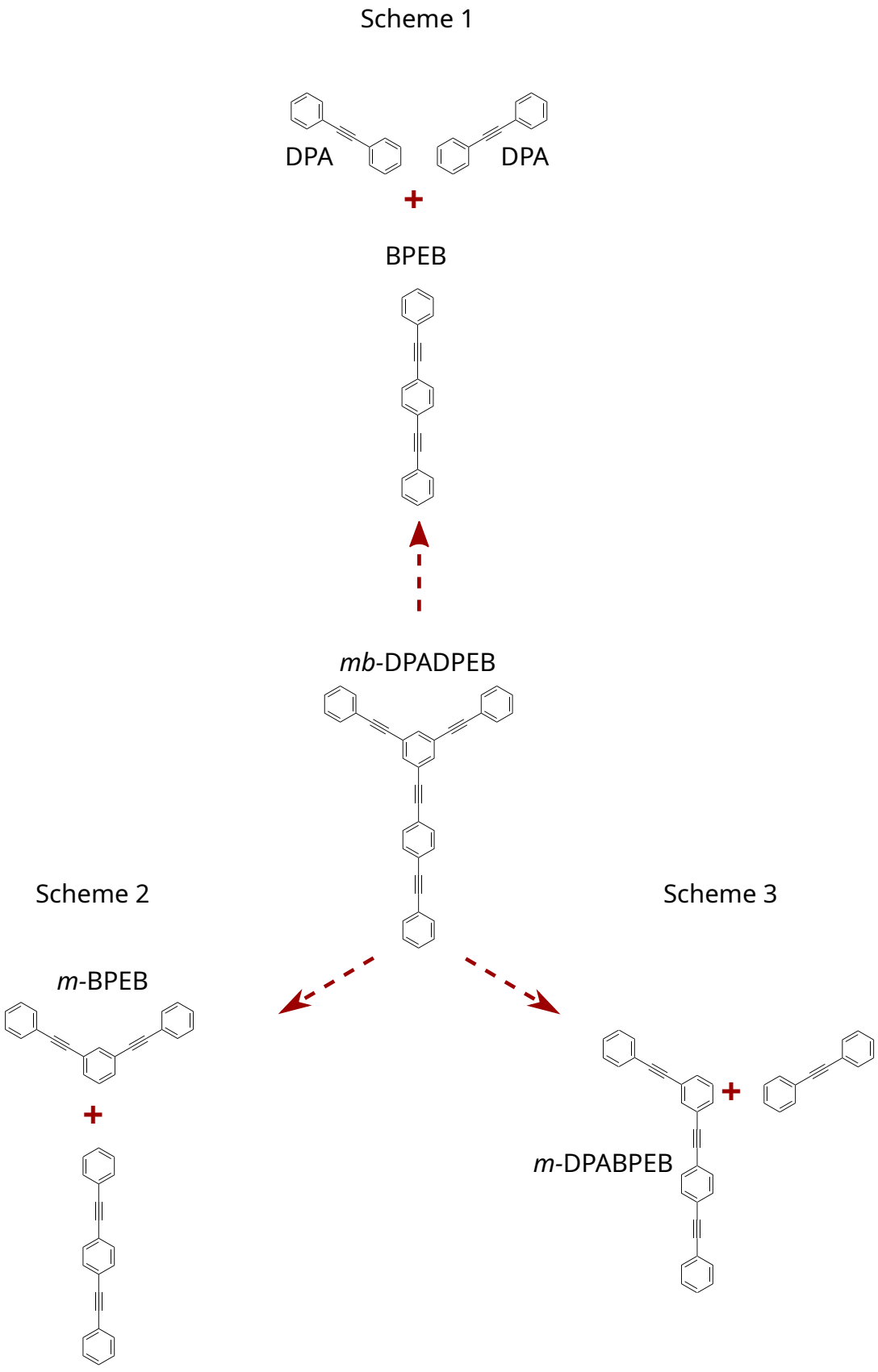

Figure 6.40: The pseudofragmentation schemes of *mb*-DPABPEB.

The ground state equilibrium geometry of *mb*-DPABPEB belongs to the $\mathcal{C}_{2v}$ point group. The equilibrium geometry is associated to the Lewis structure that is represented on the left in figure 6.41.

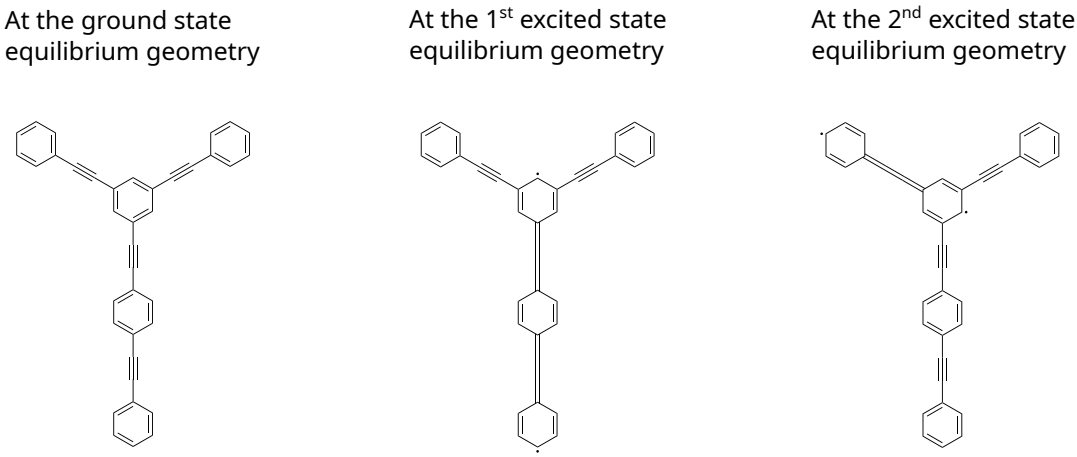

Figure 6.41: Lewis structures at the equilibrium geometries of the ground state, the first and the second optically active electronic states for the molecular system *mb*-DPABPEB.

The first optically active state which minimum exists in the $\mathcal{C}_{2v}$ point group belongs to the 1^1A_1 state and lies at 3.591 eV. This energy minimum is at the same order of magnitude than the energy minima of the first optically active states of *m*-DPABPEB and BPEB: they lie at 3.606 eV and 3.624 eV (see table 6.12). The Lewis structure of the equilibrium geometry at this energy minimum is represented in the middle in figure 6.41. We see that this Lewis structure is composed of two cumulenic groups and three quinoidal phenyls that lie onto the BPEB pseudofragment branch while the structure of the two DPA pseudofragment branches remain similar to their strucures when *mb*-DPABPEB is at the ground state equilibrium geometry. Moreover the two molecular orbitals HOMO/LUMO have been computed at the minimum of the first three optically active states of *mb*-DPABPEB, *m*-DPABPEB and BPEB. They are gathered in figure 6.42. The weight of the HOMO/LUMO excitation are the numbers on the top of each LUMO. We see that the weight of the excitation is high for the three systems and so they are characterised by a HOMO→LUMO excitation that is localised only the BPEB pseudofragment branch (*mb*-DPABPEB and *m*-DPABPEB) and on the whole system (BPEB). As before, we can then define a diabatic state S_{act}^{BPEB} that is associated to a local excitation on the BPEB pseudofragment branch of *mb*-DPABPEB.

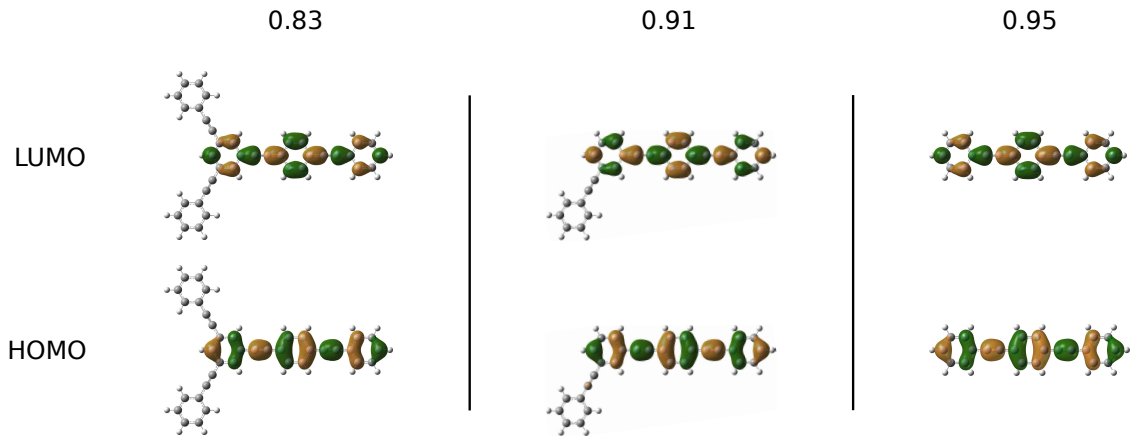

Figure 6.42: HOMO/LUMO of *mb*-DPABPEB (on the left), *m*-DPABPEB (in the middle), and BPEB (on the right) computed at the equilibrium geometry in the first optically active state.

In the $\mathcal{C}_s$ point ground, the second optically active state of *mb*-DPABPEB has an energy minimum that lies at 4.142 eV and belongs to the $1^1A'$ electronic excited state. This energy minimum is at the same order of magnitude as the energy minima of the $2^1A'$ state of *m*-DPABPEB (4.170 eV), the $1^1A'$ state of *m*-BPEB (4.123 eV) and the 1^1A_u state of DPA (4.144 eV), see table 6.12. The Lewis structure associated to the equilibrium geometry of the energy minimum of the $1^1A'$ state of *mb*-DPABPEB is represented on the right in figure 6.41. We see that the structure is defined by a cumulenic group and two quinoidal phenyls on a single DPA pseudofragment branch while the other DPA and the BPEB pseudfragment branches remain similar to their structure at the ground state. The $1^1A'$ state at this equilibrium geometry is characterised by many excitations between the four frontier orbitals (HOMO-1, HOMO, LUMO and HOMO+1). They are gathered on figure 6.43. The main excitations are HOMO $\rightarrow$ LUMO (0.44), HOMO $-1 \rightarrow$ LUMO $+1$ (0.19) and HOMO $-1 \rightarrow$ LUMO (0.16). The number into the brackets are the weight of the excitation. The four frontier orbitals are delocalised over the molecular system but if we compute the NTO (see fig. 6.43), we observe that only the first pair is dominant with a singular value of 0.85. The two NTO are localised only onto the DPA pseudofragment branch which is defined by a cumulenic Lewis structure. In addition to that we see that the detachment and attachment densities are localised only on the same DPA pseudofragment branch. So even if this state cannot be characterised by a single HOMO/LUMO excitation, we still can define as before a second diabatic state S_{act}^{DPA} that is associated to a local excitation on the DPA pseudofragment branch of *mb*-DPABPEB.

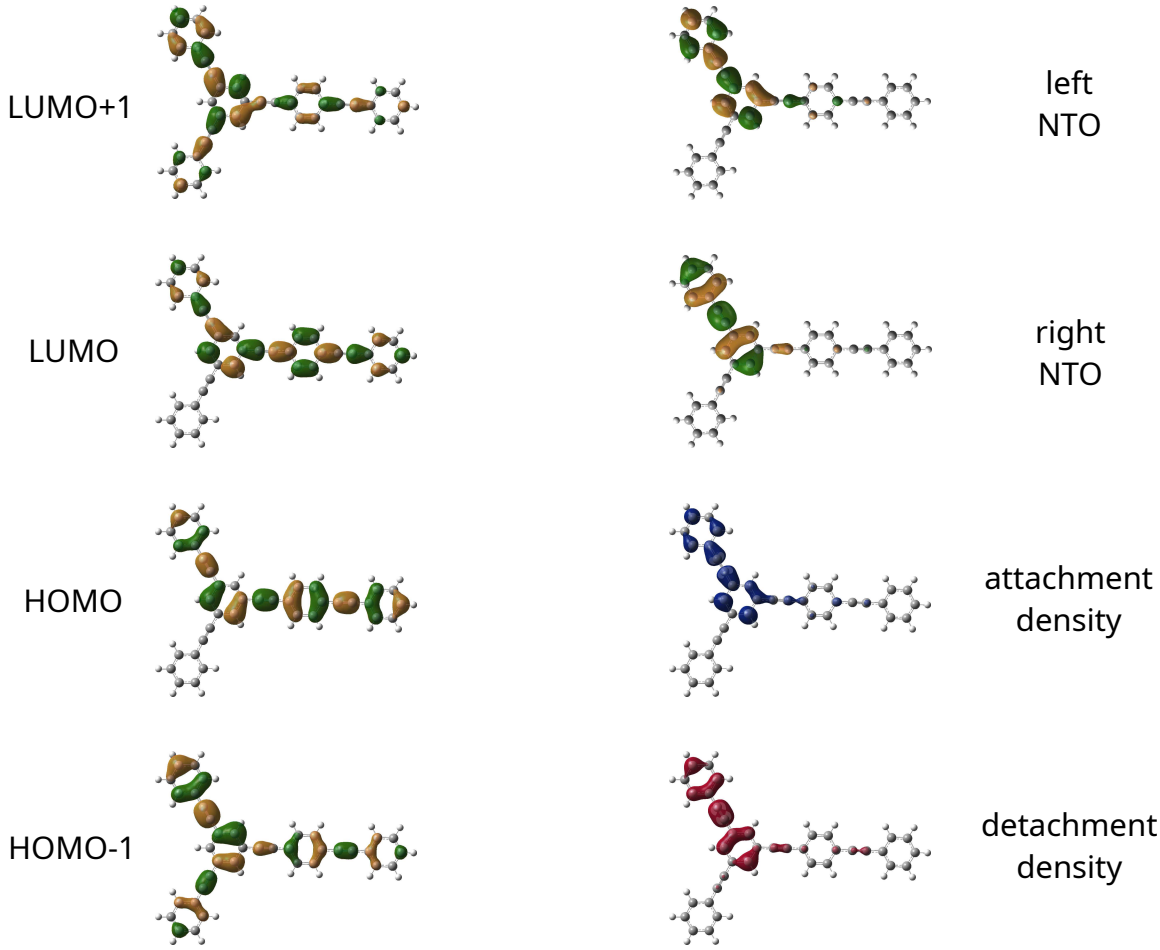

Figure 6.43: The four frontier orbitals (HOMO-1, HOMO, LUMO and LUMO+1), the first pair of NTO, and attachment and detachment densities of *mb*-DPABPEB computed at the equilibrium geometry of the $2^1A'$ state.

A schematic representation of the 1^1A_1, $2^1A'$ and the $3^1A'$ states and the associated diabatic states S_{act}^{DPA} and S_{act}^{BPEB} is shown in figure 6.44. There is a charge transfer state between the second and the fifth adiabatic electronic states in the $\mathcal{C}_s$ and in the $\mathcal{C}_{2v}$ point group. Since charge transfer states are not well described in TDDFT calculations, we have not characterised this charge transfer state.

Scheme 2 shows the possibility to consider *mb*-DPABPEB as BPEB and *m*-BPEB weakly interacting together. In the previous paragraph, we have discussed the fact that *mb*-DPABPEB and *m*-BPEB are both characterised by a diabatic state that is associated to a localised transition onto the DPA pseudofragment branch. However we have studied in subsection 6.4.1 that the first two optically active states in the $\mathcal{C}_{2v}$ point group of *m*-BPEB are two delocalised states and

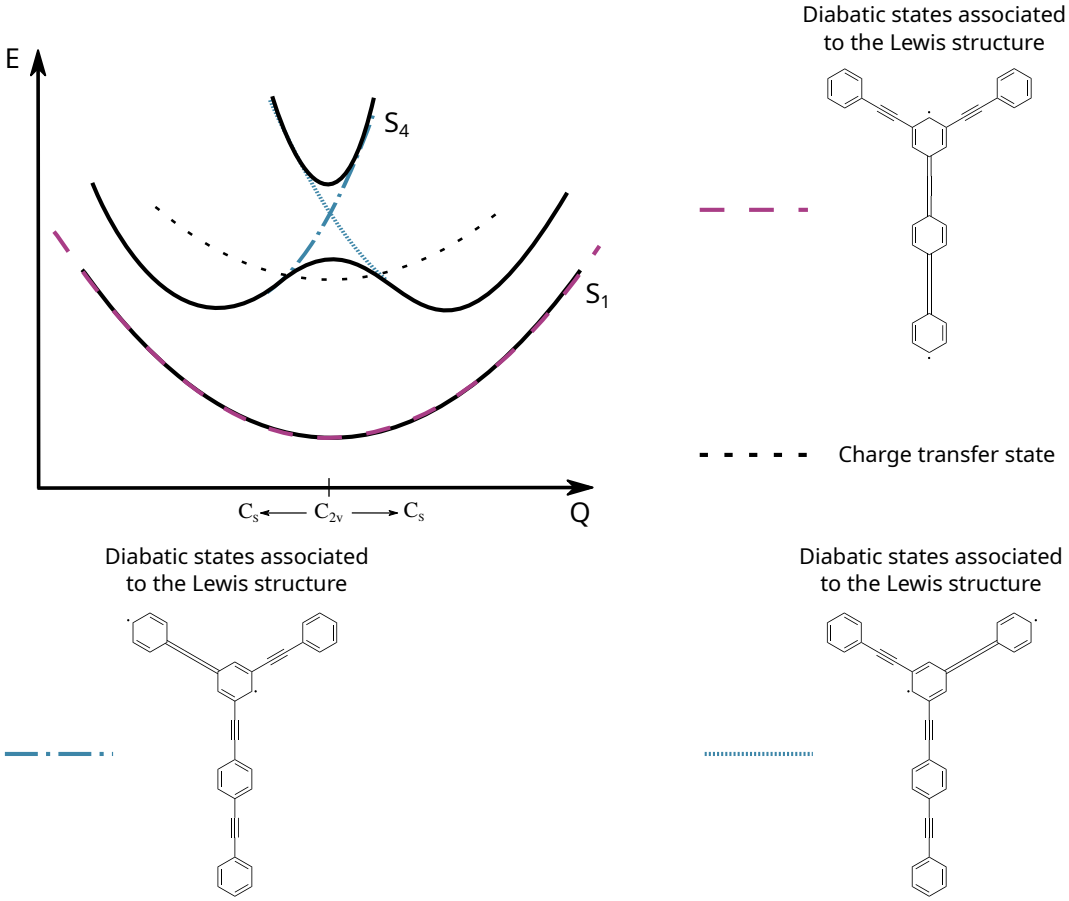

Figure 6.44: Schematic representation of the first adiabatic potential energy surfaces of *mb*-DPABPEB and the diabatic excited states S_{act}^{DPA} and S_{act}^{BPEB}.

are of B_2 and A_1 symmetry. They are characterised by two transition states TS_{A_1} and TS_{B_2} at 4.289 eV and 4.247 eV. Like *m*-BPEB, there are two delocalised adiabatic electronic excited states for *mb*-DPABPEB that correspond to a combinaison of virtual and right NTO that have similar shape than the four orbital frontier of *m*-BPEB (see fig. 6.45). There are the third and the fourth adiabatic electronic excited states and they are of B_2 and A_1 symmetry. As for *m*-BPEB, the B_2 state of *mb*-DPABPEB possesses a transition state that lies at 4.222 eV while the A_1 state possesses an energy minimum at 4.319 eV but it lies at the same order of magnitude than TS_{A_1} of *m*-BPEB.

The schemes are not only valid on the optically active states. Indeed, the various single-*trans* isomers of *mb*-DPABPEB have been investigated. The Lewis structure that characterises the various single-*trans* isomers of *mb*-DPABPEB are gathered in figure 6.46.

There are two non equivalent single-*trans* isomers for which the ethynylene group at the

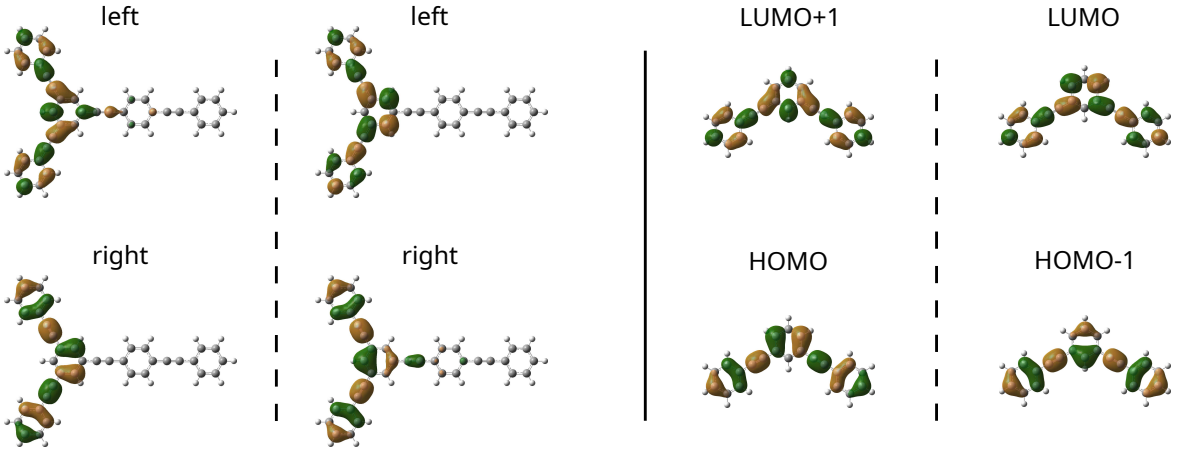

Figure 6.45: The four frontier orbitals of *m*-BPEB and the first two pairs of natural transition orbitals of *mb*-DPABPEB computed at the ground state equilibrium geometry.

DPA pseudofragment branch has been *trans*-bent. We see in table 6.12 that relative energy associated to these two isomers is similar to the one of the isomers of *m*-BPEB and of DPA. and so we can define once again the diabatic states S^{DPA}_{trans} for the system *mb*-DPABPEB.

Considering the single-*trans* isomers for which one ethynylene group of the BEPB pseudofragment branch has been *trans*-bent, there exist two pairs of equivalent single-*trans* isomers. We see in table 6.12 that relative energies associated to these two pairs of equivalent isomers are similar to the one of the isomers of *m*-DPABPEB and of BPEB. and so we can define once again the diabatic states S^{BPEB}_{trans} for the system *mb*-DPABPEB.

To conclude this first part, the three pseudofragmentation schemes in figure 6.40 have been confirmed and so one can expect to detect similar topography between the potential energy surfaces of *mb*-DPABPEB and those of *m*-DPABPEB, BPEB and DPA. We can then draw a Jablonsky diagram of *mb*-DPABPEB which is built with the localised-on-the-pseudofragment diabatic states (see fig. 6.47).

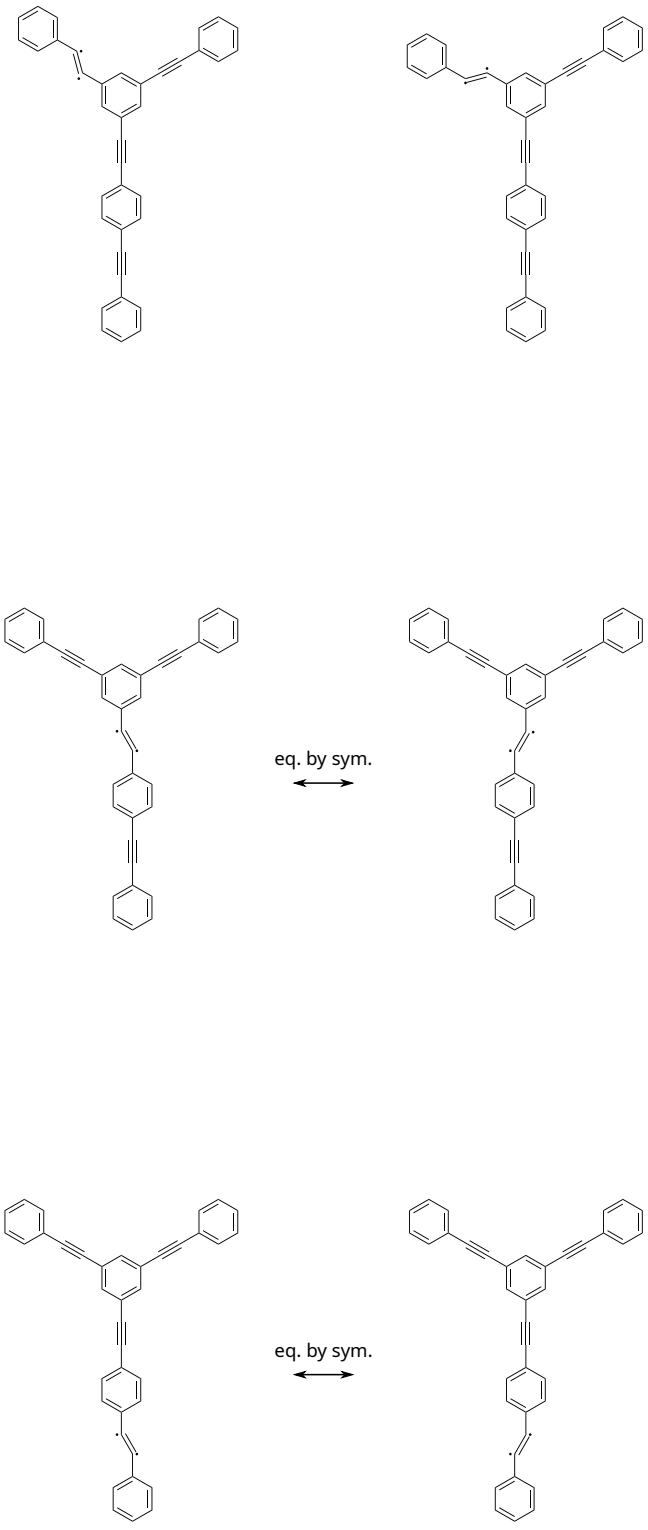

Figure 6.46: Lewis structures at the equilibrium geometries of the first optically inactive electronic states for the molecular system *mb*-DPABPEB.

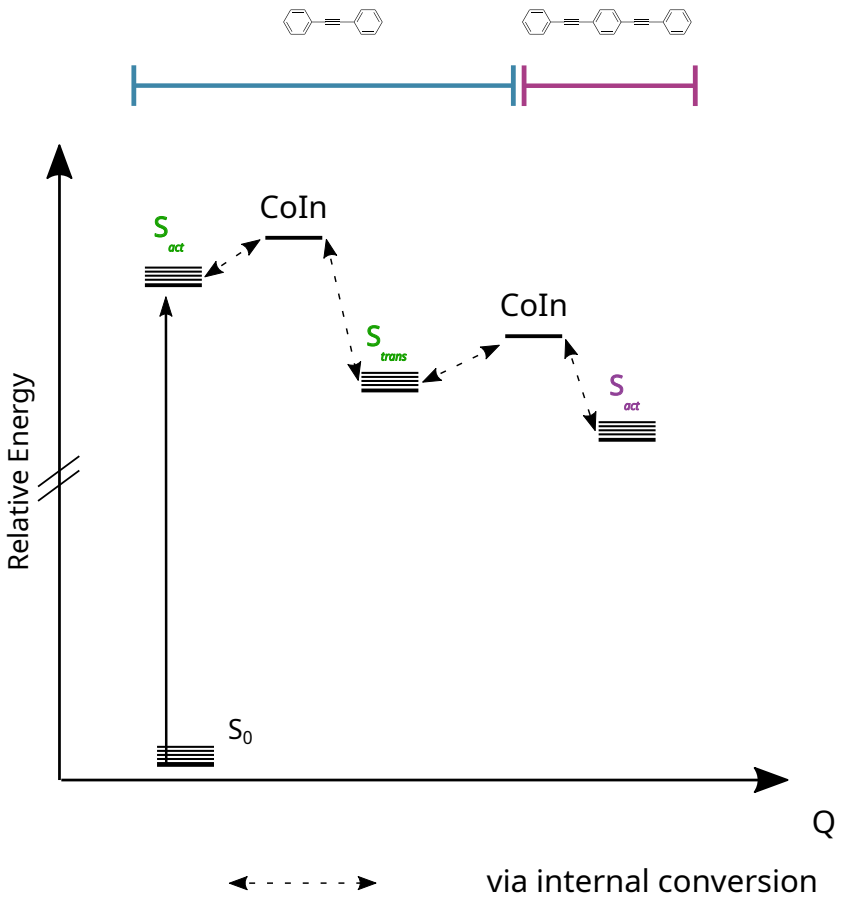

Figure 6.47: Jablonsky diagram of *mb*-DPABPEB that involves the localised-on-the-pseudofragments diabatic states

Rigid scans on *mb*-DPABPEB

The rigid scans in figure 6.48 have been performed from the reference geometries that are the equilibrium geometries of the diabatic states S_{act}^{DPA}. They correspond to a localised excitation on the DPA pseudofragment branch which is defined by a cumulenic structure. The Lewis structures associated to the reference geometries are gathered in the same figure as the rigid scans. The rigid scans a), b) and c) have been already studied in detail in previous subsections 6.2.4, 6.4.1 and 6.4.2. As a reminder: the dotted blue line corresponds for each of the rigid scans to the diabatic states that are associated to the local excitation on the DPA pseudofragment branch. The plain blue lines are optically inactive states for every systems. The two energy minima of the first optically inactive state match with the single-*trans* diabatic states that are local single-*trans*-excitation on the DPA pseudofragment branch. In the case of a *o*PE that can be pseudofragment into at least two DPA (the case of *m*-BPEB and *mb*-DPABPEB) and if the electronic excitation is localised onto one of the two DPA pseudofragment branches, the second optically active state corresponds to a local excitation onto the other DPA pseudofragment branch. This electronic state is labelled in dotted brown line for scan b) and d). The dotted red lines correspond to local excitation onto the BPEB pseudofragment branch. The plain brown, green and dark lines correspond to forbidden states of *m*-BPEB, *m*-DPABPEB and *mb*-DPABPEB, respectively.

We see on the scans a) to d) in fig. 6.48 that each state S_{act}^{DPA} crosses the first optically inactive electronic state. The crossings are actually crossings between the S_{act}^{DPA} state and the S_{trans}^{DPA} state. The γ values of these crossings are gathered on table 6.14. For the systems DPA and *m*-BPEB, the crossings involve the states $1^1A'$ and 1^1A" while for the systems *m*-DPABPEB and *mb*-DPABPEB they involve the states $2^1A'$ and 1^1A". We see that the crossings are localised at the same order of magnitude. In the case of the scan c) and d), the state S_{act}^{BPEB} is the first optically active state for both scans and then lie under the S_{act}^{DPA} state. So it crosses the first optically inactive state for smaller γ values (in the case of $\gamma > 180°$) and for higher γ values (in the case of $\gamma < 180°$).

The energy-minimised conical intersections between the S_{act}^{DPA} and the S_{trans}^{DPA} states are gathered in table 6.13.

To evaluate the mixing between the states S_{act} and S_{trans}, the magnitude of the derivative coupling vector is calculated and compared to the magnitude of the gradient difference vector. In both tables 6.14 and 6.13, the magnitudes of the derivative coupling vector ($|| \overrightarrow{DC} ||$) and of

the gradient difference vector ($||\overrightarrow{GD}||$) for each crossing are gathered in both tables. From the results of the rigid scans and so from table 6.14 we see that for conical intersections between the S_{act}^{DPA} state and the S_{trans}^{DPA} state the magnitude $||\overrightarrow{GD}||$ is 0.09 $E_{\mathrm{h}}a_0^{-1}$ and 0.08 $E_{\mathrm{h}}a_0^{-1}$, and the magnitude $||\overrightarrow{DC}||$ is 0.04 $E_{\mathrm{h}}a_0^{-1}$ and 0.03 $E_{\mathrm{h}}a_0^{-1}$ which give a ratio $\frac{||\overrightarrow{GD}||}{||\overrightarrow{DC}||}$ approximatively equal to 2. Eventhough the magnitude of both vectors are different for the minimised crossings $1^1A'/1^1A$" for DPA and *m*-BPEB in table 6.13, the ratio remains close to 2.

However from the ref. [43], we know that the two states $1^1B_2/1^1A_1$ are strongly coupled with each other and that is proved by the fact that $||\overrightarrow{GD}||= 0.03$ and $||\overrightarrow{DC}||= 0.14$, where the ratio is equal to 0.2.

The coupling between the S_{act}^{DPA} state and the S_{trans}^{DPA} state may be then interpreted such that it is ten times weaker than the coupling between the 1^1B_2 and the 1^1A_1 states. Eventhough it is a weaker coupling, it is a non-zero coupling. Such a weak coupling between these two states can then explain why the cumulenic structure is observed predominantly after a photoexcitation and few picoseconds after, the *trans* structure is observed predominantly in DPA studies [54].

The magnitude of the branching space vectors have been computed as well for the crossings between the S_{trans}^{DPA} and the S_{act}^{BPEB} states (see table 6.14). The magnitude of $||\overrightarrow{GD}||$ increases and the magnitude of $||\overrightarrow{DC}||$ decreases which means that the coupling between the two states decreases. It can be explained by the fact that the two states are associated to two localised states onto two different pseudofragment branches.

Syst.		γ	$\|\|\overrightarrow{GD}\|\|$	$\|\|\overrightarrow{DC}\|\|$
DPA	$1^1A'/1^1A$"	152.00°	0.15	0.08
BPEB	$1^1A'/1^1A$"	148.00°	0.18	0.07
	$1^1B_2/1^1A_1$	-	0.03	0.14
m-BPEB	$1^1A'/1^1A$"	151.88°	0.15	0.08
		208.20°	0.15	0.08

Table 6.13: γ values and magnitudes of the branching space vectors in $E_{\mathrm{h}}a_0^{-1}$ at the conical intersections between the S_{act}^{DPA} state and the S_{trans}^{DPA} that have been minimised in energy by the use of the merged algorithm.

The rigid scans a) to e) in figure 6.49 have been performed for the systems BPEB, *m*-DPABPEB and *mb*-DPABPEB. The reference geometries are the equilibrium geometries in

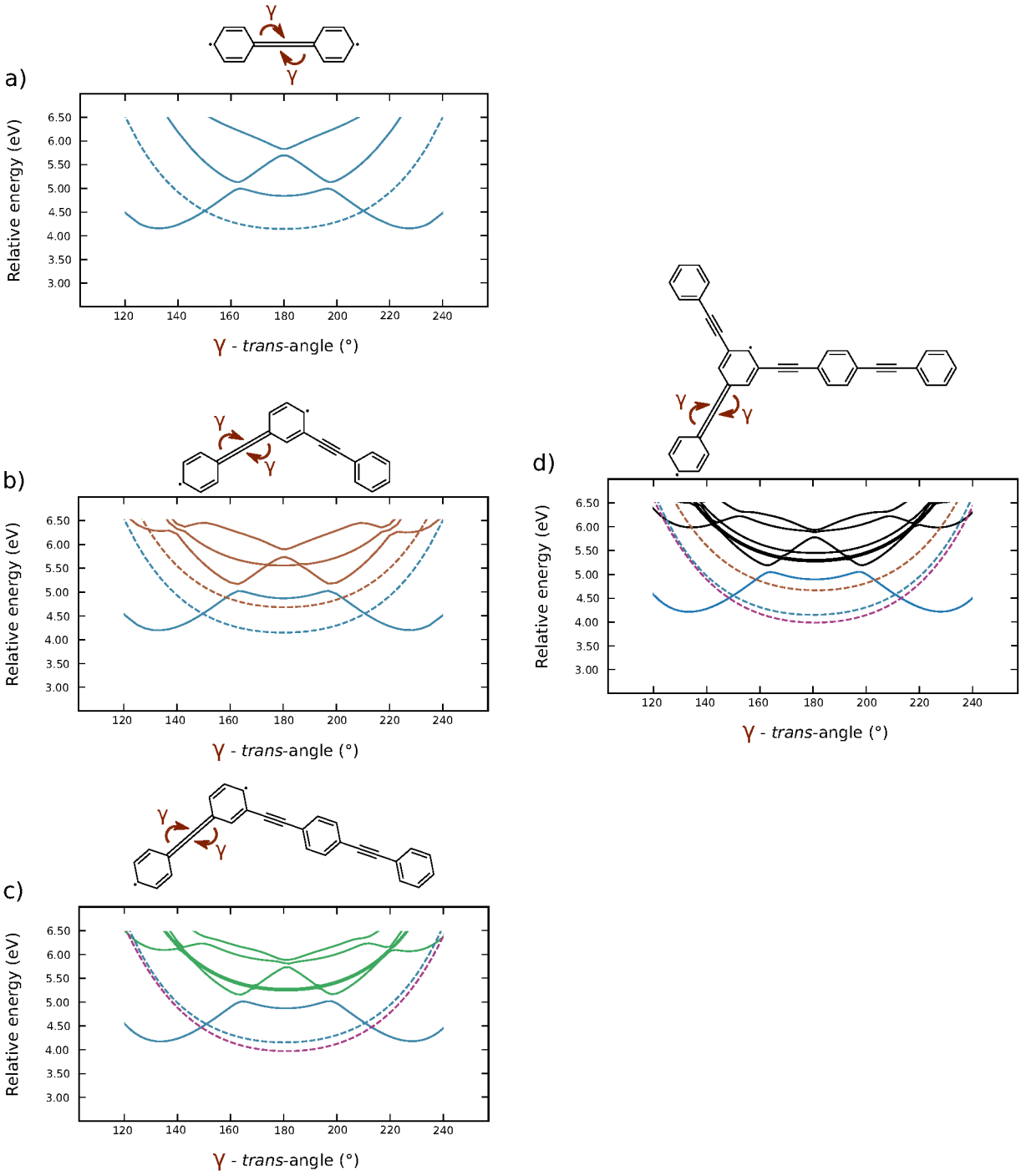

Figure 6.48: Rigid scans of DPA, *m*-BPEB, *m*-DPABPEB and *mb*-DPABPEB at the equilibrium geometry associated to the energy minimum of the diabatic state localised on the DPA pseudofragment branch.

the first adiabatic electronic excited states which is associated to a cumulenic structure onto the BPEB or on the BPEB pseudofragment branch for the systems *m*-DPABPEB and *mb*-

Syst.		γ	$\|\| \overrightarrow{GD} \|\|$	$\|\| \overrightarrow{DC} \|\|$
DPA	$1^1A'/1^1A$"	150.00°	0.09	0.04
m-BPEB	$1^1A'/1^1A$"	149.72°	0.08	0.04
		210.73°	0.08	0.04
m-DPABPEB	$1^1A'/1^1A$"	150.83°	0.09	0.03
		210.48°	0.09	0.03
	$2^1A'/1^1A$"	148.92°	0.13	0.01
		212.96°	0.13	0.02
mb-DPABPEB	$1^1A'/1^1A$"	150.83°	0.09	0.03
	$2^1A'/1^1A$"	150.62°	0.09	0.04
		210.91°	0.09	0.02
	$1^1A'/1^1A$"	148.50°	0.13	0.01
		213.18°	0.13	0.02

Table 6.14: γ values and magnitudes of the branching space vectors in $E_\mathrm{h}a_0^{-1}$ at the conical intersections between the S_{act}^{DPA} state and the S_{trans}^{DPA} on the rigid scans in figure 6.48.

DPABPEB. The plain red line in the scan a) correspond to optically inactive states of BPEB while in scan b) and c) it corresponds to the first optically inactive states of m-DPABPEB where the minima are associated to the rigid equilibrium geometries where the BPEB pseudofragment branch has adopted a single-*trans* structure. The diabatic states associated to the single-*trans* structure is labelled S_{trans}^{BPEB}. The two dotted purple lines in the scans d) and e) are B_2 and the A_1 singlet states in both cases that correspond to delocalised excitation onto the m-BPEB pseudofragment branch on the mb-DPABPEB system. Else, the same caption as the one used in the scans 6.48 is applied.

We see that in the five rigid scans the state S_{act}^{BPEB} is clearly the lowest optically active state for any γ values and cross the S_{trans}^{BPEB} states around $\gamma = 142°$ and $\gamma = 218°$.

The magnitude of the branching space vectors from the conical intersection of the rigid scans are gathered in table 6.15. We see that the magnitude of $\|\| \overrightarrow{GD} \|\|$ is constant for every systems (0.11 $E_\mathrm{h}a_0^{-1}$) and the magnitude of $\|\| \overrightarrow{DC} \|\|$ lie between 0.03 $E_\mathrm{h}a_0^{-1}$ and 0.04 $E_\mathrm{h}a_0^{-1}$ which leads to a ratio equal approximatively to 4. According to the previous study, such value is equivalent to a weak coupling between the S_{trans}^{BPEB} and the S_{act}^{BPEB} states. Due to the weak coupling, since the reference geometry is associated to a cumulenic structure onto the BPEB pseudofragment branch and since the energy associated to these structures are lower than the minimum energy of the single-*trans* structure, one can conclude that if the excitation is localised onto the BPEB

pseudofragment branch, it cannot be transferred onto the DPA pseudofragment branch through a single-*trans* bending onto an ethynylene group on the BPEB pseudofragment.

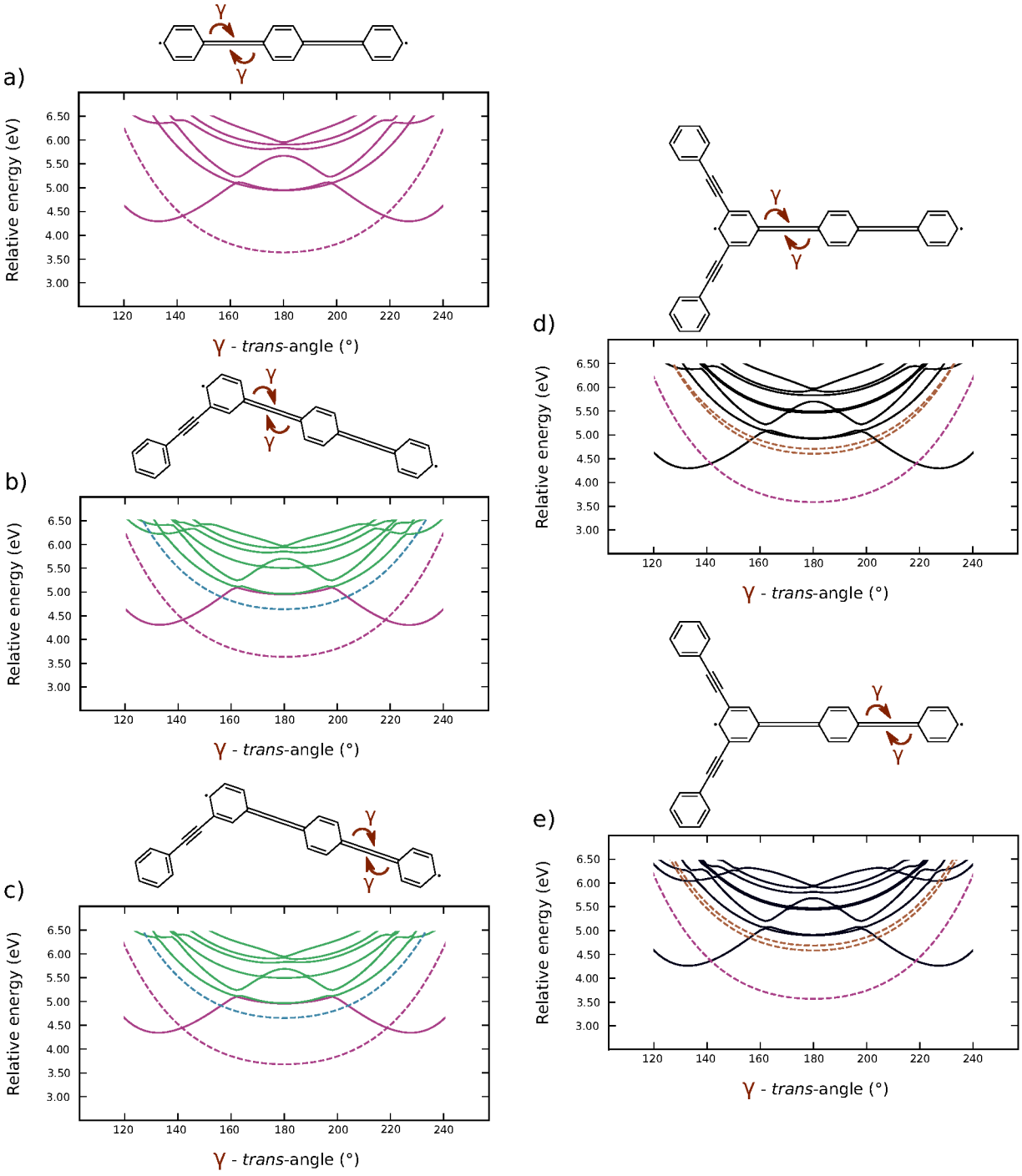

Figure 6.49: Rigid scans of BPEB, *m*-DPABPEB and *mb*-DPABPEB at the equilibrium geometry associated to the energy minimum of the diabatic state localised on the BPEB pseudofragment branch.

Syst.		γ	$\|\| \overrightarrow{GD} \|\|$	$\|\| \overrightarrow{DC} \|\|$
BPEB	$1^1A'/1^1A$"	142.06°	0.11	0.03
Closest ethynylene to the shared phenyl				
m-DPABPEB	$1^1A'/1^1A$"	141.61°	0.11	0.03
		218.12°	0.11	0.03
mb-DPABPEB	$1^1A'/1^1A$"	141.49°	0.11	0.03
Furthest ethynylene to the shared phenyl				
m-DPABPEB	$1^1A'/1^1A$"	141.69°	0.11	0.03
		218.34°	0.11	0.04
mb-DPABPEB	$1^1A'/1^1A$"	141.33°	0.11	0.04

Table 6.15: γ values and magnitudes of the branching space vectors in $E_\mathrm{h}a_0^{-1}$ at the conical intersections between the S_{act}^{DPA} state and the S_{trans}^{BPEB} on the rigid scans in figure 6.49.

Since the coupling between the states $S_{act}^{DPA} - S_{trans}^{DPA}$ and between the states $S_{act}^{DPA} - S_{trans}^{BPEB}$ is non zero, we can suggest a supplementary mechanism to the one that has been already suggested. Indeed, refs. [39–47] suggested that the EET along a PE-D is driven by stretching vibrations on the ethynylene groups of the various pseudofragment of a PE-D. We suggest here that the EET can also be driven by a *trans*-bending motion thanks to the wavepacket that is localised onto the S_{act}^{DPA} diabatic state and can be transferred to the S_{trans}^{DPA} diabatic state. Since the S_{trans}^{DPA} state is optically inactive there cannot be de-excitation through fluorescence. Then the wavepacket can be transferred to the S_{act}^{BPEB} state since it is coupled with the previous optically inactive state.

We thus propose a perhaps more complicated but richer de-activation mechanism involving bright/bright and bright/dark crossings (see fig. 6.50). This awaits confirmation from dynamics calulations.

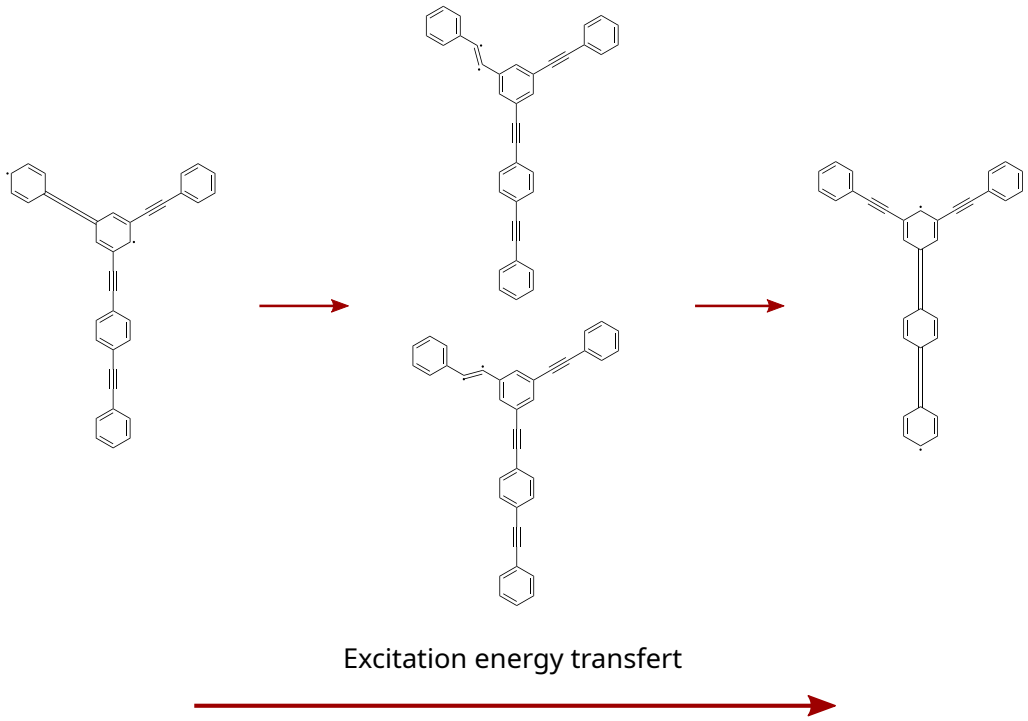

Figure 6.50: New de-activation mechanism that is involved in the TEE of *mb*-DPABPEB.

Chapter 7

Conclusions and outlooks

The opto-electronic properties of phenylene ethynylene dendrimers have raised our attention. The dendritic shape of these systems induces an excitation energy gradient which leads to an excitation energy transfer from the periphery toward its core. A transfer mechanism has been already suggested that would involve stretching of the ethynylene groups of PE-D. Within this thesis, we tried to answer to the questions that are: "Is the stretching motion of the ethynylene groups, the only motion that is involved in the EET?" and "how should we characterise the adiabatic electronic excited states that are involved in the excitation energy transfer ?".

The smallest threefold phenylene ethynylene dendrimer is *mb*DPABPEB. It is the smallest system with a node in which there is an excitation energy gradient. Thus it is an efficient model to determine how the EET can occur along PE-D.

Ho *et al* [43] have suggested a pseudofragmentation scheme for *m*BPEB such that this system behaves as two DPA which are weakly interacting. In the manner of this pseudofragmentation scheme we have studied *mb*DPABPEB according to three pseudofragmentation schemes: *mb*DPABPEB behaves as two DPA and one BPEB which are weakly interacting, one *m*BPEB and one BPEB which are weakly interacting, and one DPA and one *m*DPABPEB which are weakly interacting.

To study *mb*DPABPEB we needed then to study first small *oligo*phenylene ethynylenes and association in *meta* position of two such *oligo*phenylene ethynylenes to determine the validity of the three pseudofragmentation schemes.

Computational tools have been defined to compare *oligo*phenylene ethynylenes with each other and to validate the pseudofragmentation schemes. Two density-based descriptors have been used to characterise the adiabatic electronic excited states of *oligo*phenylene ethynylenes. The two descriptors inform us on the locality of the photoexcitation; there is the density-based

descriptor ϕ_S which determines the overlap between the attachment and the detachment densities and there is the density-based descriptor χ which determines the net charge transferred in the photoexcitation. For conical intersections, a merged algorithm has been written: It combines a seam-energy optimisation algorithm and a software which computes a numerical branching space along the seam. Such a merged algorithm had to be written because conical intersections of some *oligo*phenylene ethynylene involve electronic excited states of same symmetry and we needed to find the geometry of lowest-in-energy conical intersections.

The latter computational tools were used in addition to natural transition orbital determination, oscillator strength determination and symmetry sorting of electronic states. These various tools allow us to define diabatic states for each *oligo*phenylene ethynylene. The $S_{\pi_x\pi_x^*}$ diabatic state which describe a $\pi_x\pi_x^*$ transition onto the ethynylene groups is an optically active state and the energy minimum of this diabatic state is associated to the equilibrium geometry of a cumulenic isomer of *oligo*phenylene ethynylene. The second diabatic state that has been defined is an optically inactive state and is referred to as the $S_{\pi_x\pi_y^*}$ diabatic state. It corresponds to a $\pi_x\pi_y^*$ transition onto a single ethynylene group and its energy minimum is associated to the equilibrium geometry of a *trans* isomer such that the ethynylene group is *trans*-bent. The longer is the *oligo*phenylene ethynylene, the more ethynylene groups there are and so the more possibilities there are to determine *trans* isomers where only one ethynylene group is *trans*-bent, either clockwise or anticlockwise.

We found out that the energy minimum of the $S_{\pi_x\pi_x^*}$ state is lower than the energy minimum of the $S_{\pi_x\pi_y^*}$ state only for DPA. It is the contrary for longer *oligo*phenylene ethynylenes. The ordering of these diabatic states in systems that can be pseudofragmented is conserved according to the pseudofragment, *i.e.* the ordering of the diabatic states in *oligo*phenylene ethynylenes.

So we suggested that in a case where the wave-packet is initially localised onto the diabatic state $S_{\pi_x\pi_x^*}$ that describes the DPA pseudofragment branch of *mb*DPABPEB, a *trans*-bending on the ethynylene group of this branch can occur thanks to a population transfer from the state $S_{\pi_x\pi_x^*}$ toward the state $S_{\pi_x\pi_y^*}$ of the DPA pseudofragment branch. Then a population transfer can occur from this previous $S_{\pi_x\pi_y^*}$ state toward the $S_{\pi_x\pi_x^*}$ state that describes the BPEB pseudofragment branch. Such a population transfer is possible because the magnitude of the derivative coupling vectors are non zero.

Very preliminary adiabatic (only on the first singlet state) quantum dynamics have been performed but they were not very conclusive, they are not presented here in this thesis. However,

non-adiabatic quantum dynamics have not been done to validate the excitation energy transfer mechanism. Dynamical studies could be performed in the case of reduced-systems and would be helpful to validate the suggested mechanism above in further studies.

In the very beginning of the general introduction, we have explained that one of the most promising candidates in opto-electronic devices within the phenylene ethynylene dendrimers is the nanostar. *mb*DPABPEB is only a pseudofragment among others in the pseudofragmentation scheme of the nanostar but it is the first with a threefold node. The complete pseudofragmentation scheme of the nanostar is proposed in figure 7.1. The nanostar can be indeed pseudoframented into: tertiobutyl-DPA, DPA, BPEB, DPABPEB and a perylene group that are all weakly interacting together. However, in this thesis we do not have taken into account the tertiobutyl-DPA that are considered as the antenna of the nanostar and the perylene group that is the energy trap of the nanostar. We expect the tertiobutyl group to have very weak effect on optical properties. Three calculations have been performed in addition the whole study of this thesis to determine the energy minima and the associated equilibrium geometries of the tertiobutyl-DPA and the perylene. At the equilibrium geometry of the ground state of the tertiobutyl-DPA, the energy of the first optically active state lies at 4.482 eV and the minimum energy at the equilibrium geometry in the first optically active state of the perylene group (to which an ethynylene group and a benzene have been added, see fig. 7.1) lies at 2.716 eV. It allows us to draw the schematic representation of a suggested excitation energy transfer mechanism within the nanostar in figure 7.2. We suggest that sixteen tertiobutyl-DPA are locally photo-excited thanks to a specific wavelength that is energetically adequate to such an excitation. The tertiobutyl-DPA are likely to be isomerised into cumulenic isomers and then a population transfer occurs from the $S_{\pi_x\pi_x^*}$ state toward the $S_{\pi_x\pi_y^*}$ state of the antenna. Then the population transfer occur from the previous $S_{\pi_x\pi_y^*}$ state toward the $S_{\pi_x\pi_x^*}$ state of the DPA pseudofragment branch and toward its $S_{\pi_x\pi_y^*}$. After that the DPA can *trans*-bent, the population transfer occurs only between the $S_{\pi_x\pi_x^*}$ states of the various *oligo*phenylene ethynylene pseudofragment branches to reach the lowest diabatic state that is associated to a local excitation onto the perylene group which will then emit. The population transfer that occurs between different diabatic states is done via internal conversion.

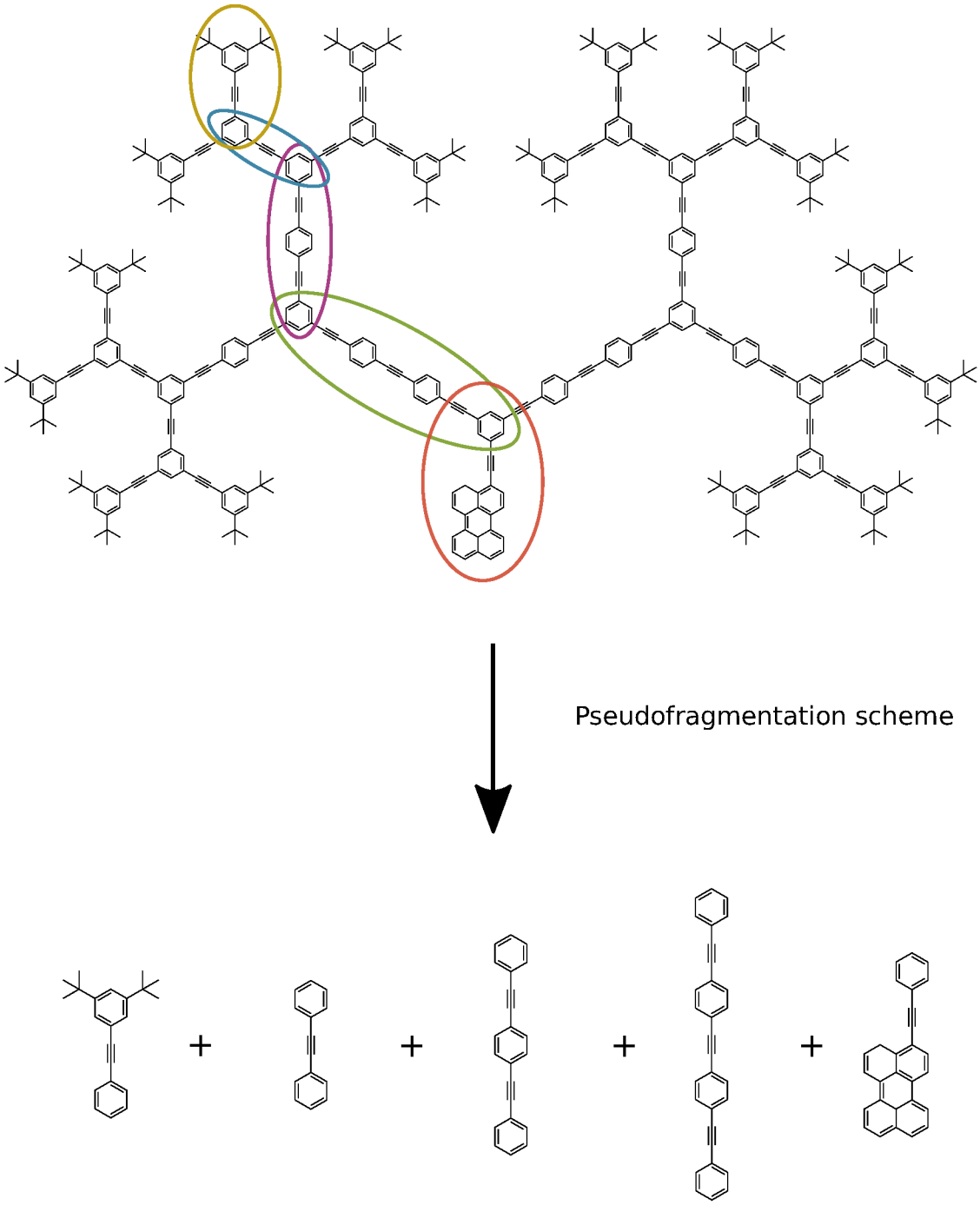

Figure 7.1: Pseudofragmentation scheme of the nanostar.

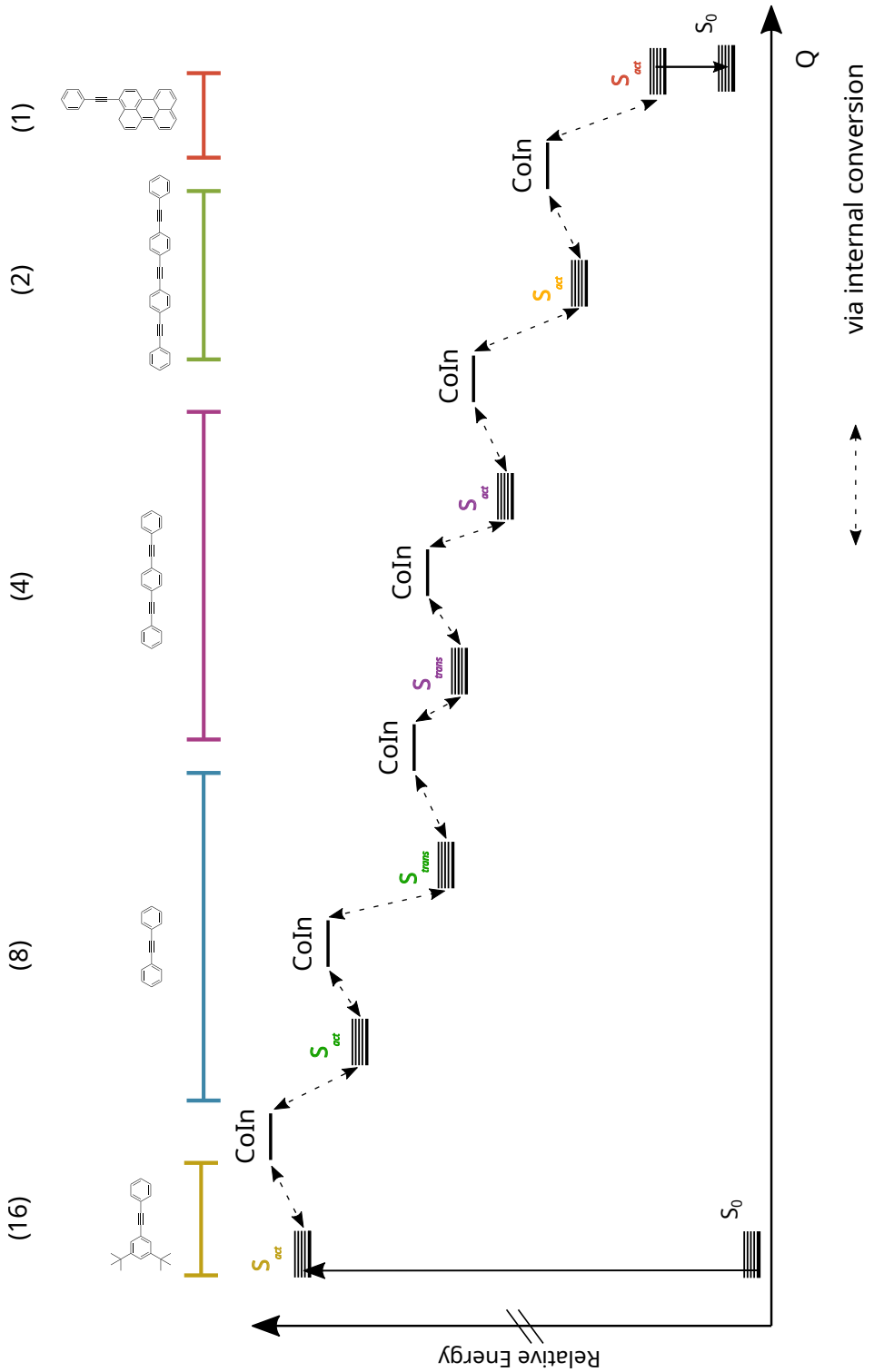

Figure 7.2: Mechanism suggestion of the EET in the nanostar.

Chapter 8

Appendix

8.1 Absorption and emission spectra of *o*PE

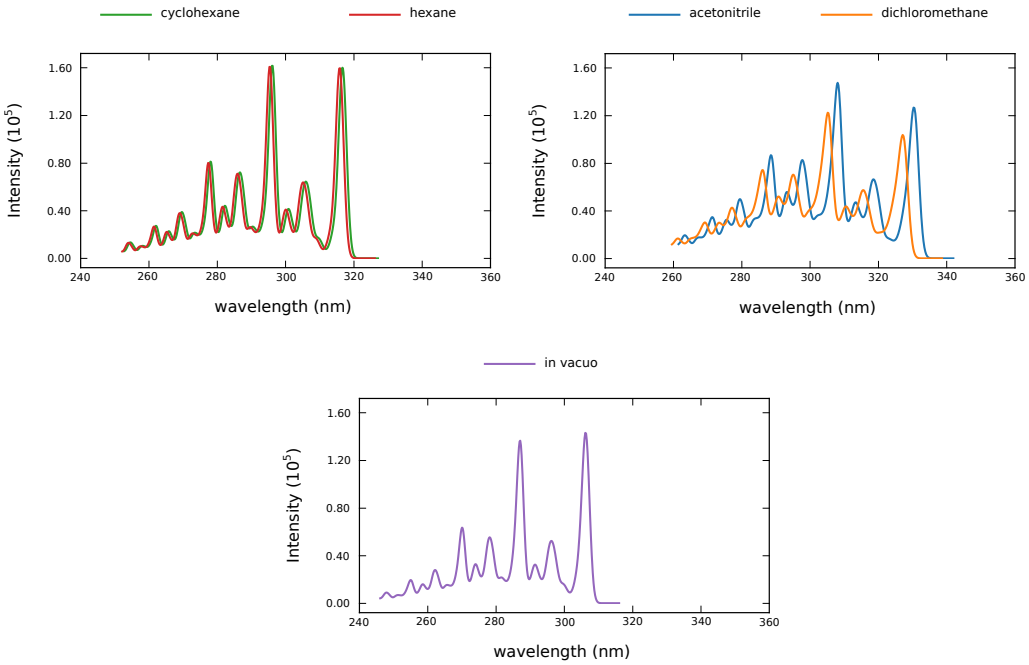

Figure 8.1: Theoretical absorption spectra of DPA in acetonitrile (blue), cyclohexane (orange), dichloromethane (green), hexane (red), and *in vacuo* (purple) within the Franck-Condon and harmonic approximation.

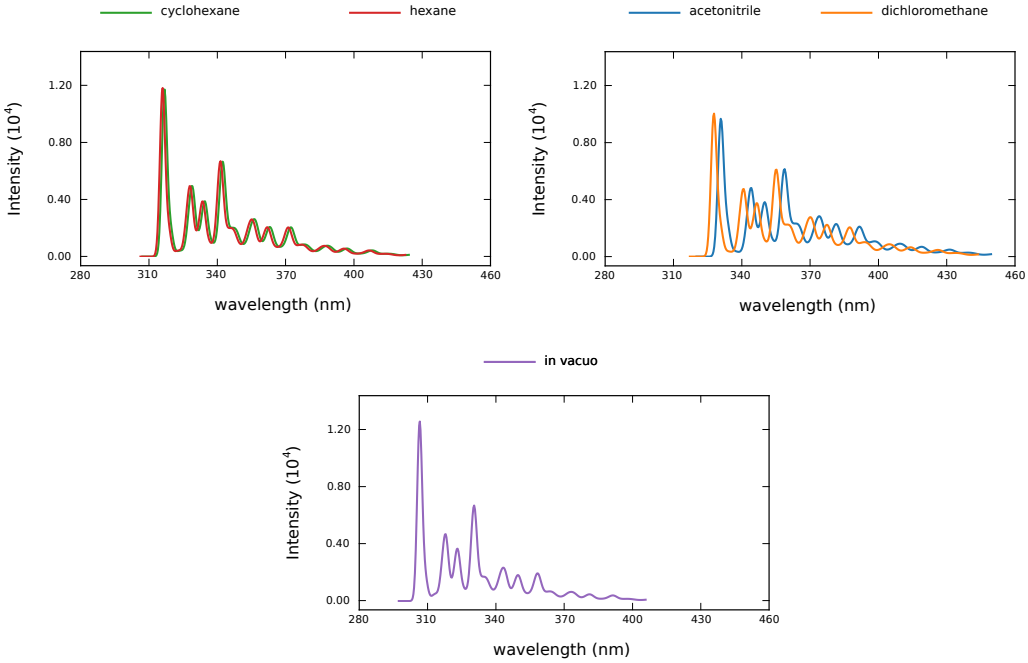

Figure 8.2: Theoretical emission spectra of DPA in acetonitrile (blue), cyclohexane (orange), dichloromethane (green), hexane (red), and *in vacuo* (purple) within the Franck-Condon and harmonic approximation.

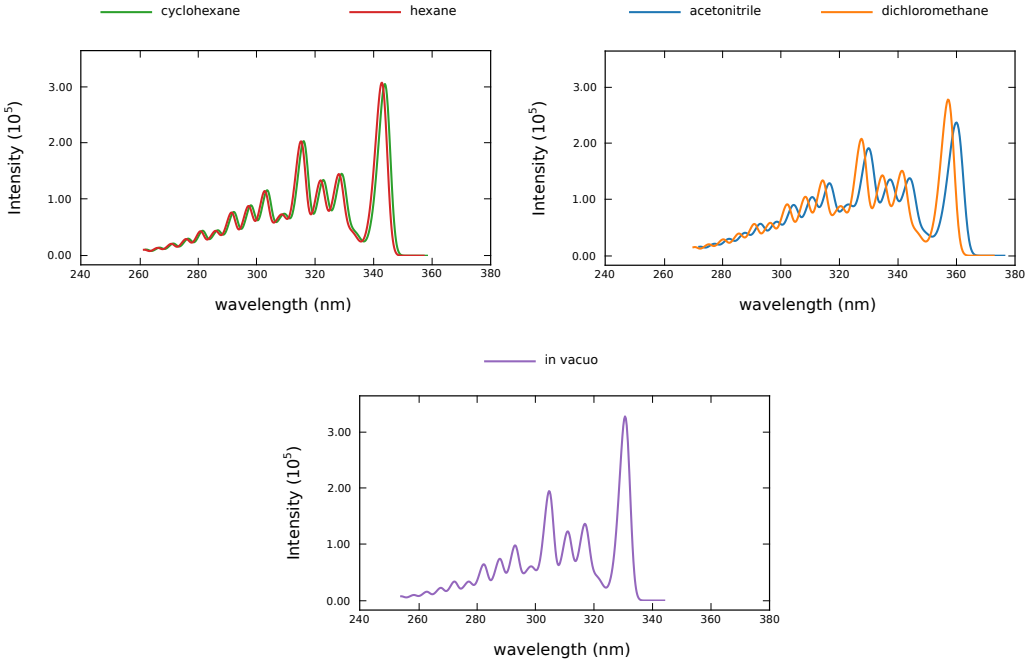

Figure 8.3: Theoretical absorption spectra of BPEB in acetonitrile (blue), cyclohexane (orange), dichloromethane (green), hexane (red), and *in vacuo* (purple) within the Franck-Condon and harmonic approximation.

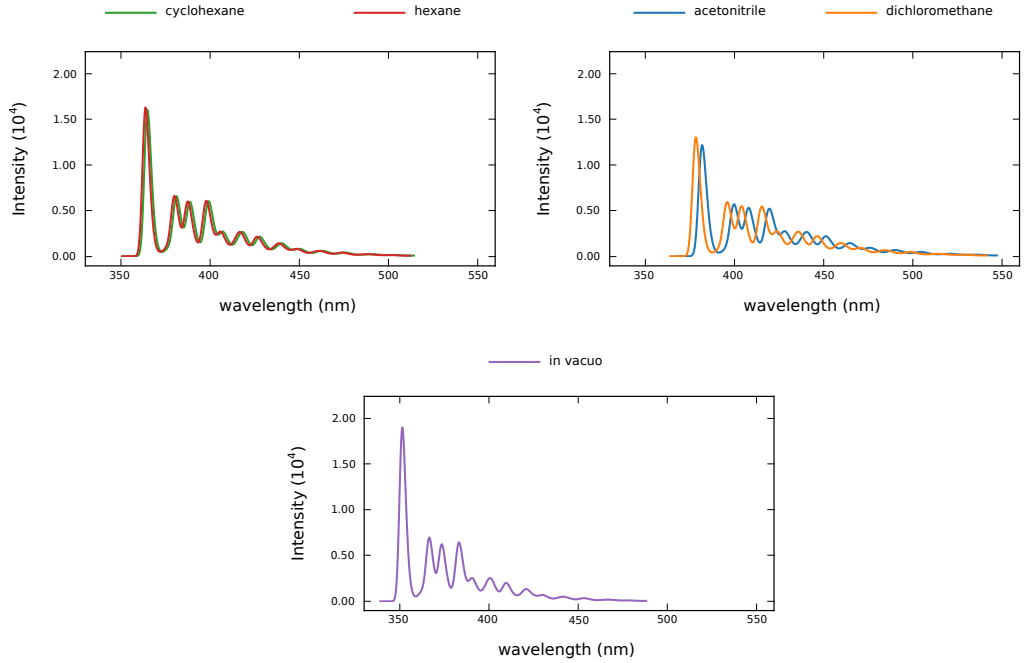

Figure 8.4: Theoretical emission spectra of BPEB in acetonitrile (blue), cyclohexane (orange), dichloromethane (green), hexane (red), and *in vacuo* (purple) within the Franck-Condon and harmonic approximation.

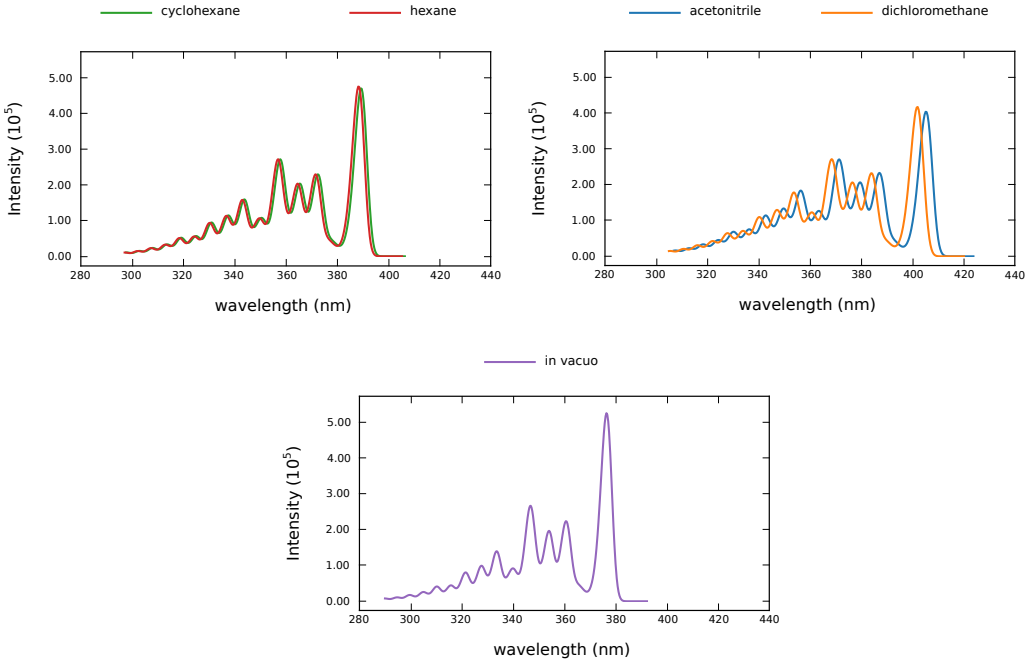

Figure 8.5: Theoretical absorption spectra of DPABPEB in acetonitrile (blue), cyclohexane (orange), dichloromethane (green), hexane (red), and *in vacuo* (purple) within the Franck-Condon and harmonic approximation.

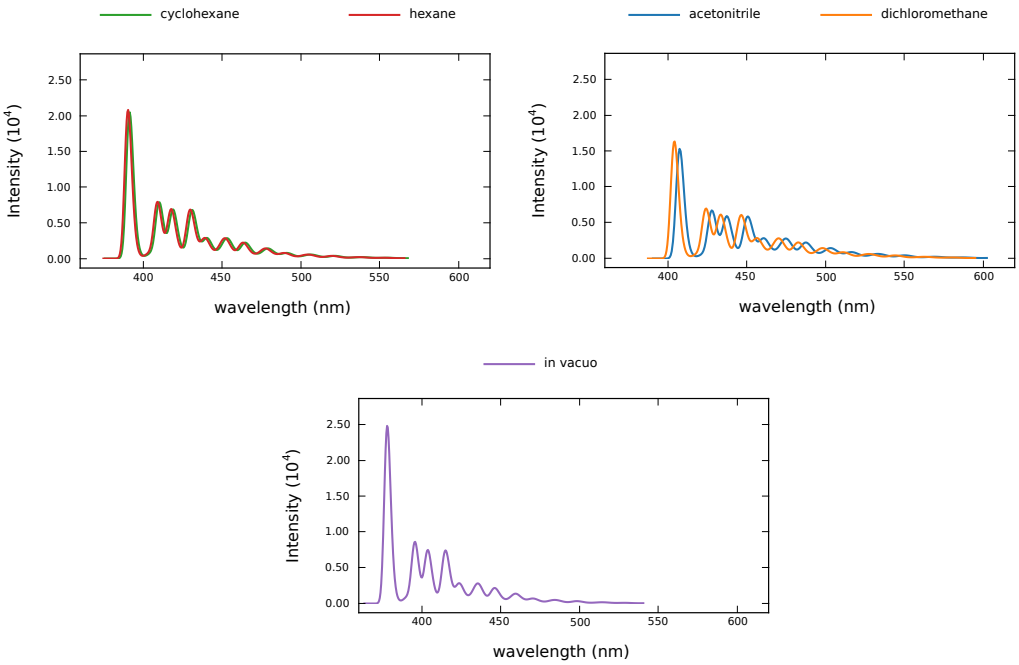

Figure 8.6: Theoretical emission spectra of DPABPEB in acetonitrile (blue), cyclohexane (orange), dichloromethane (green), hexane (red), and *in vacuo* (purple) within the Franck-Condon and harmonic approximation.

Bibliography

[1] G. Breuil, K. Shehu, E. Lognon, S. Pitié, B. Lasorne, and T. Etienne. Diagnosis of two evaluation paths to density-based descriptors of molecular electronic transitions. *Advances in Quantum Chemistry*, 79:289–310, 2019.

[2] J. N. Harvey, , M. Aschi, H. Schwarz, and W. Koch. The singlet and triplet states of phenyl cation. A hybrid approach for locating minimum energy crossing points between non-interacting potential energy surfaces. *Theoretical Chemistry Accounts*, 99(2):95–99, 1998.

[3] M. Cainelli and Y. Tanimura. Exciton transfer in organic photovoltaic cells: A role of local and nonlocal electron–phonon interactions in a donor domain. *J. Chem. Phys.*, 154:034107, 2021.

[4] L. Chen, P. Shenai, F. Zheng, A. Somoza, and Y. Zhao. Optimal energy transfer in light-harvesting systems. *Molecules*, 20:15224–15272, 2015.

[5] C. Creatore, M. A. Parker, S. Emmott, and A. W. Chin. Efficient biologically inspired photocell enhanced by delocalized quantum states. *Phys. Rev. Lett.*, 111:253601, 2013.

[6] J. L. Bredas, E. H. Sargent, and G. D. Scholes. Photovoltaic concepts inspired by coherence effects in photosynthetic systems. *Nature materials*, 16:35–44, 2017.

[7] A. M. van Oijen, M. Ketelaars, J. Köhler, T. J. Aartsma, and J. Schmidt. Unraveling the electronic structure of individual photosynthetic pigment-protein complexes. *Science*, 285(5426):400–402, 1999.

[8] T. Pullerits and V. Sundstrom. Photosynthetic light−harvesting pigment−protein complexes: toward understanding how and why. *Acc. Chem. Res.*, 29:381–389, 1996.

[9] S. Karrasch, P. A. Bullough, and R. Ghosh. The 8.5 a projection map of the light-harvesting complex i from rhodospirillum rubrum reveals a ring composed of 16 subunits. *The EMBO Journal*, 14(4):631–638, 1995.

[10] G. McDermott, S. M. Prince, A. A. Freer., A. M. Hawthornthwaite-Lawless, M. Z. Papiz, R. J. Cogdell, and N. W. Isaacs. Crystal structure of an integral membrane light-harvesting complex from photosynthetic bacteria. *Nature*, 374:517–521, 1995.

[11] W. S. Li and T. Aida. Dendrimers prophyrins and phthalocyanines. *Chem. Rev.*, 109(11):6047–6076, 2009.

[12] Y. Saga, Y. Shibata, and H. Tamiaki. Spectral properties of single light-harvesting complexes in bacterial photosynthesis. *Journal of Photochemistry and Photobiology C*, 11:15–24, 2010.

[13] K. Pan, E. Boulais, L. Yang, and M. Bathe. Structure-based model for light-harvesting properties of nucleic acid nanostructures. *Nucleic Acids Research*, 42:2159–2170, 2014.

[14] M. Ballottari, J. Girardon, L. Dall'Osto, and R. Bassi. Evolution and functional properties of photosystem: light harvesting complexes in eukaryotes. *Biochimica et Biophysica Acta*, 1817:143–157, 2012.

[15] R. Croce and H. van Amerongen. Light-harvesting in photosystem. *Photosynthesis Research*, 116:153–166, 2013.

[16] V. Balzani, S. Campagna, G. Denti, A. Juris, S. Serroni, and M. Venturi. Harvesting sunlight by artificial supramolecular antennae. *Solar Energy Materials and Solar Cells*, 38(4):159–173, 1995.

[17] V. Balzani, P. Ceroni, M. Maestri, and V. Vicinelli. Light-harvesting dendrimers. *Current Opinion in Chemical Biology*, 7:657–665, 2003.

[18] O. Mongin, N. Hoyler, and A. Gossauer. Synthesis and light-harvesting properties of niphaphyrins. *European Journal of Organic Chemistry*, 2000:1193–1197, 2000.

[19] J. Larsen, F. Puntoriero, T. Pascher, N. McClenaghan, S. Campagna, E. Akesson, and V. Sundström. Extending the light-harvesting properties of transition-metal dendrimers. *Chem. Phys. Chem.*, 8:2643–2651, 2007.

[20] A. Adronov and J. M. J. Fréchet. Light-harvesting dendrimers. *Chem. Commun.*, 18(18):1701–1710, 2000.

[21] A. Nantalaksakul, D. R. Reddy, C. J. Bardeen, and S. Thayumanavan. Light-harvesting dendrimers. *Photosynthesis Research*, 87:133–150, 2006.

[22] S. L. Gilat, A. Adronov, and J. M. J. Fréchet. Light harvesting and energy transfer in novel convergently constructed dendrimers. *Angewandte Chemie International Edition*, 38(10):1422–1427, 1999.

[23] G. W. Robinson and R. P. Frosch. Electronic excitation transfer and relaxation. *The Journal of Chemical Physics*, 38:1187–1203, 1963.

[24] F. Caruso, A. W. Chin, A. Datta, S. F. Huelga, and M. B. Plenio. Highly efficient energy excitation transfer in light-harvesting complexes: The fundamental role of noise-assisted transport. *The Journal of Chemical Physics*, 131:105106, 2009.

[25] G. D. Scholes and K. P. Ghiggino. Electronic interactions and interchromophore excitation transfer. *J. Phys. Chem.*, 98:4580–4590, 1994.

[26] J. Saltiel and G. S. Hammond. Mechanisms of photochemical reactions in solution. *cis-trans* isomerization of the stilbenes by excitation transfer from low energy sensitizers. *Journal of the American Chemical Society*, 85:2515–2516, 1963.

[27] A. Asadian, M. Tiersch, G. G. Guerreschi, J. Cai, S. Popescu, and H. J. Briegel. Motional effects on the efficiency of excitation transfer. *New Journal of Physics*, 12:075019, 2010.

[28] H. Dong, D. Z. Xu, J. F. Huang, and C. P. Sun. Coherent excitation transfer via the dark-state channel in a bionic system. *Light: Science and Applications*, 1, 2012.

[29] I. Yamazaki, N. Tamai, and T. Yamazaki. Electronic excitation transfer in organized molecular assemblies. *J. Phys. Chem.*, 94:516–525, 1990.

[30] S. Hess, E. Akesson, R.J. Cogdell, T. Pullerits, and V. Sundström. Energy transfer in spectrally inhomogeneous light-harvesting pigment-protein complexes of purple bacteria. *Biophysical Journal*, 69(6):2211–2225, 1995.

[31] K. Timpmann, F. G. Zhang, A. Freiberg, and V. Sundström. Detrapping of excitation energy from the reaction centre in the photosynthetic purple bacterium rhodospirillum rubrum. *Biochimica et Biophysica Acta (BBA) - Bioenergetics*, 1183(1):185–193, 1993.

[32] W.-D. Jang, N. Nishiyama, and K. Kataoka. Supramolecular assembly of photofunctional dendrimers for biomedical nano-devices. *Supramolecular Chemistry*, 19(4-5):309–314, 2007.

[33] N. Nishiyama, W. D. Jang, and K. Kataoka. Supramolecular nanocarriers integrated with dendrimers encapsulating photosensitizers for effective photodynamic therapy and photochemical gene delivery. *New J. Chem.*, 31:1074–1082, 2007.

[34] S. Kraner, R. Scholz, C. Koerner, and K. Leo. Design proposals for organic materials exhibiting a low exciton binding energy. *The Journal of Physical Chemistry C*, 119(40):22820–22825, 2015.

[35] Alex Adronov and Jean M. J. Fréchet. Light-harvesting dendrimers. *Chem. Commun.*, pages 1701–1710, 2000.

[36] M. Kozaki, S. Suzuki, and K. Okada. Dendritic light-harvesting antennas with excitation energy gradients. *Chemistry Letters*, 42(10):1112–1118, 2013.

[37] D. Astruc. Electron-transfer processes in dendrimers and their implication in biology, catalysis, sensing and nanotechnology. *Nature Chemistry*, 4:255–267, 2012.

[38] C. Supritz, A. Engelmann, and P. Reineker. Optical absorption in compact and extended dendrimers. *Journal of Luminescence*, 111(4):367–381, 2005. Special issue on optical properties of dendrimers.

[39] J. Huang, L. Du, D. Hu, and Z. Lan. Theoretical analysis of excited states and energy transfer mechanism in conjugated dendrimers. *J. Comput. Chem.*, 36(3):151–163, 2015.

[40] V. D. Kleiman, J. S. Melinger, and D. McMorrow. Ultrafast dynamics of electronic excitations in a light-harvesting phenylacetylene dendrimer. *J. Phys. Chem. B*, 105(24):5595–5598, 2001.

[41] J. L. Palma, E. Atas, L. Hardison, T. B. Marder, J. C. Collings, A. Beeby, J. S. Melinger, J. L. Krause, V. D. Kleiman, and A. E. Roitberg. Electronic spectra of the nanostar dendrimer: Theory and experiment. *J. Phys. Chem. C*, 114(48):20702–20712, 2010.

[42] J. F. Galindo, E. Atas, A. Altan, D. G. Kuroda, S. Fernandez-Alberti, S. Tretiak, A. E. Roitberg, and V. D. Kleiman. Dynamics of Energy Transfer in a Conjugated Dendrimer Driven by Ultrafast Localization of Excitations. *J. Am. Chem. Soc.*, 137(36):11637–11644, 2015.

[43] E. K. L. Ho and B. Lasorne. Diabatic pseudofragmentation and nonadiabatic excitation-energy transfer in meta-substituted dendrimer building blocks. *Computational and Theoretical Chemistry*, 1156:25–36, 2019.

[44] J. F. Galindo, S. Fernandez-Alberti, and A. E. Roitberg. Electronic excited state specific IR spectra for phenylene ethynylene dendrimer building blocks. *J. Phys. Chem. C*, 117(50):26517–26528, 2013.

[45] M. A. Soler, A. E. Roitberg, T. Nelson, S. Tretiak, and S. Fernandez-Alberti. Analysis of state-specific vibrations coupled to the unidiectional energy transfer in conjugated dendrimers. *J. Phys. Chem. A*, 116:9802, 2012.

[46] S. Fernandez-Alberti, V. D. Kleiman, S. Tretiak, and A. E. Roitberg. Unidirectional energy transfer in conjugatedmolecules: The crucial role of high-frequency c≡ bonds. . *Phys. Chem. Lett.*, 1:2699, 2010.

[47] S. Fernandez-Alberti, A. E. Roitberg, V. D. Kleiman, J. F. Galindo, T. Nelson, and S. Tretiak. Shishiodoshi unidirectional energy transfer mechanism in phenylene ethynylene dendrimers. *J. Chem. Phys.*, 137:22A526, 2012.

[48] J. Saltiel and V. K. R. Kumar. Photophysics of Diphenylacetylene: Light from the "Dark State". *J. Phys. Chem. A*, 116(43):10548–10558, 2012.

[49] Marek Z. Zgierski and Edward C. Lim. Nature of the 'dark' state in diphenylacetylene and related molecules: state switch from the linear $\pi\pi^*$ state to the bent $\pi\sigma^*$ state. *Chemical Physics Letters*, 387(4-6):352–355, April 2004.

[50] M. Krämer, U. H. F. Bunz, and A. Dreuw. Comprehensive look at the photochemistry of tolane. *The Journal of Physical Chemistry A*, 121(5):946–953, 2017.

[51] C. Robertson and G. A. Worth. Modelling the non-radiative singlet excited state isomerization of diphenyl-acetylene: A vibronic coupling model. *Chemical Physics*, 510:17–29, 2018.

[52] T. Fujiwara, M. Z. Zgierski, and E. C. Lim. Spectroscopy and photophysics of 1,4-Bis(phenylethynyl)benzene: Effects of ring torsion and dark $\pi - \sigma^*$ state. *J. Phys. Chem. A*, 112(21):4736–4741, 2008.

[53] M. Hodecker, A. M. Driscoll, U. H. F. Bunz, and A. Dreuw. Twisting and bending photo-excited phenylethynylbenzenes - a theoretical analysis. *Physical Chemistry Chemical Physics*, 22:9974, 2020.

[54] Y. Hirata, T. Okada, N. Mataga, and T. Nomoto. Picosecond time-resolved absorption spectrum measurements of the higher excited singlet state of diphenylacetylene in the solution phase. *J. Phys. Chem.*, 96(16):6559–6563, 1992.

[55] Y. Tanizaki, H. Inoue, T. Hoshi, and J. Shiraishi. Localized and delocalized electronic transitions in diphenylacetylene, stilbene and diphenylbutadiene. *J. Z. Phys. Chem.*, 74(12):45–58, 1971.

[56] K. Okuyama, T. Hasegawa, M. Ito, and N. Mikami. Electronic spectra of tolane in a supersonic free jet: Large-amplitude torsional motion. *J. Phys. Chem.*, 88:1711–1716, 1984.

[57] Z. Chernia, T. Livneh, I. Pri-Bar, and J.E. Koresh. Mode assignment for linear phenyl acetylene sequence: phenylacetylene, di-phenylacetylene and 1,4-di(phenylethynyl)benzene. *Vibrational Spectroscopy*, 25(2):119–131, 2001.

[58] M. Gutmann, M. Gudipati, P. F. Schoenzart, and G. Hohlneicher. Electronic spectra of matrix-isolated tolan: site selective one- and two-photon spectra. *The Journal of Physical Chemistry*, 96(6):2433–2442, 1992.

[59] D. R. Borst, C. S. Grace, and D. W. Pratt. Identification of the light-absorbing states in tolane with potential relevance to self-similar phenylacetylene dendrimers. *Chemical Physics Letters*, 343(3-4):289–295, 2001.

[60] T. Suzuki, M. Nakamura, T. Isozaki, and T. Ikoma. "dark" excited states of diphenylacetylene studied by nonresonant two-photon excitation optical-probing photoacoustic spectroscopy. *International Journal of Thermophysics*, 33(10):2046–2054, 2012.

[61] E. K. L. Ho, Thibaud Etienne, and Benjamin Lasorne. Vibronic properties of *para* -polyphenylene ethynylenes: TD-DFT insights. *The Journal of Chemical Physics*, 146(16):164303, 2017.

[62] Benjamin G. Levine and Todd J. Martínez. Isomerization through conical intersections. *Annual Review of Physical Chemistry*, 58(1):613–634, 2007.

[63] S. Matsika and P. Krause. Nonadiabatic events and conical intersections. *Annu. Rev. Phys. Chem.*, 62:621–643, 2011.

[64] W. Domcke and D. R. Yarkony. Role of conical intersections in molecular spectroscopy and photoinduced chemical dynamics. *Annu. Rev. Phys. Chem.*, 63:325–352, 2012.

[65] M. Klessinger. Conical intersections and the mechanism of singlet photoreactions. *Angewandte Chemie*, 34:549–551, 1995.

[66] M. A. Robb, F. Bernardi, and M. Olivucci. Conical intersections as a mechanistic feature of organic photochemistry. *Pure and Appl. Chem.*, 67:783–789, 1995.

[67] A. Csehi, M. Kowalewski, G. J. Halasz, and A. Vibok. Ultrafast dynamics in the vicinity of quantum light-induced conical intersections. *New J. Phys.*, 21:093040, 2019.

[68] S. Fernandez-Alberti, V. D. Kleiman, S. Tretiak, and A. E. Roitberg. Nonadiabatic molecular dynamics simulations of the energy transfer between building blocks in a phenylene ethynylene dendrimer. *The Journal of Physical Chemistry A*, 113(26):7535–7542, 2009.

[69] M. J. Bearpark, M. A. Robb, and S. H. Bernhard. A direct method for the location of the lowest energy point on a potential surface crossing. *Chemical Physics Letters*, 223(3):269–274, 1994.

[70] N. Koga and K. Morokuma. Determination of the lowest energy point on the crossing seam between two potential surfaces using the energy gradient. *Chemical Physics Letters*, 119(5):371–374, 1985.

[71] P. J. Kuntz and W. N. Whitton. Conical intersections in h2cl+(1a'). *The Journal of Chemical Physics*, 95(7):5149–5158, 1991.

[72] I. N. Ragazos, M. A. Robb, F. Bernardi, and M. Olivucci. Optimization and characterization of the lowest energy point on a conical intersection using an mc-scf lagrangian. *Chemical Physics Letters*, 197(3):217–223, 1992.

[73] D. R. Yarkony. Systematic determination of intersections of potential energy surfaces using a lagrange multiplier constrained procedure. *Journal of physical chemistry (1952)*, 97:4407–4412, 1993.

[74] M. R. Manaa and D. R. Yarkony. On the intersection of two potential energy surfaces of the same symmetry. Systematic characterization using a Lagrange multiplier constrained procedure. *The Journal of Chemical Physics*, 99(7):5251–5256, 1993.

[75] B. Gonon, A. Perveaux, F. Gatti, D. Lauvergnat, and B. Lasorne. On the applicability of a wavefunction-free, energy-based procedure for generating first-order non-adiabatic couplings around conical intersections. *The Journal of Chemical Physics*, 147(11):114114, 2017.

[76] O. Mülken, V. Bierbaum, and A. Blumen. Coherent exciton transport in dendrimers and continuous-time quantum walks. *The Journal of Chemical Physics*, 124(12):124905, 2006.

[77] E. Y. Poliakov, V. Chernyak, S. Tretiak, and S. Mukamel. Exciton-scaling and optical excitations of self-similar phenylacetylene dendrimers. *The Journal of Chemical Physics*, 110(16):8161–8175, 1999.

[78] S.F. Swallen, R. Kopelman, J.S. Moore, and C. Devadoss. Dendrimer photoantenna supermolecules: energetic funnels, exciton hopping and correlated excimer formation. *Journal of Molecular Structure*, 485-486:585–597, 1999.

[79] S. Olsen. Locally-excited (le) versus charge-transfer (ct) excited state competition in a series of para-substituted neutral green fluorescent protein (gfp) chromophore models. *The Journal of Physical Chemistry B*, 119(6):2566–2575, 2015.

[80] L. G. S. Brooker. Absorption and resonance in dyes. *Rev. Mod. Phys.*, 14:275–293, 1942.

[81] V. Bonačić-Koutecký, J. Koutecký, and J. Michl. Neutral and charged biradicals, zwitterions, funnels in s1, and proton translocation: Their role in photochemistry, photophysics, and vision. *Angewandte Chemie International Edition in English*, 26(3):170–189, 1987.

[82] W. Li, Y. Pan, R. Xiao, Q. Peng, S. Zhang, D. Ma, F. Li, F. Shen, Y. Wang, B. Yang, and Y. Ma. Employing 100% excitons in oleds by utilizing a fluorescent molecule with hybridized local and charge-transfer excited state. *Advanced Functional Materials*, 24(11):1609–1614, 2014.

[83] Z. Lin, R. Kabe, K. Wang, and C. Adachi. Influence of energy gap between charge-transfer and locally excited states on organic long persistence luminescence. *Nature Communications*, 11(191), 2020.

[84] C. A. Guido, P. Cortona, and C. Adamo. Effective electron displacements: A tool for time-dependent density functional theory computational spectroscopy. *The Journal of Chemical Physics*, 140(10):104101, 2014.

[85] F. Plasser, M. Wormit, and A. Dreuw. New tools for the systematic analysis and visualization of electronic excitations. formalism. *The Journal of Chemical Physics*, 141(2):024106, 2014.

[86] F. Plasser, S. A. Bäppler, M. Wormit, and A. Dreuw. New tools for the systematic analysis and visualization of electronic excitations. applications. *The Journal of Chemical Physics*, 141(2):024107, 2014.

[87] F. Plasser and H. Lischka. Analysis of excitonic and charge transfer interactions from quantum chemical calculations. *Journal of Chemical Theory and Computation*, 8(8):2777–2789, 2012.

[88] F. Plasser, B. Thomitzni, S. A. Bäppler, J. Wenzel, D. R. Rehn, M. Wormit, and A. Dreuw. Statistical analysis of electronic excitation processes: Spatial location, compactness, charge transfer, and electron-hole correlation. *Journal of Computational Chemistry*, 36:1609–1620, 2015.

[89] T. Le Bahers, C. Adamo, and I. Ciofini. A qualitative index of spatial extennt in charge-trabsfer excitations. *Journal of Chemical Theory and Computation*, 7:2498–2506, 2011.

[90] M. Campetella, F. Maschietto, M. J. Frisch, G. Scalmani, I. Ciofini, and C. Adamo. Charge transfer excitations in tddft: A ghost-hunter index. *Journal of Computational Chemistry*, 38:2151–2156, 2017.

[91] I. Ciofini, T. Le Bahers, C. Adamo, F. Odobel, and D. Jacquemin. Through-space charge transfer in rod-like molecules: Lessons from theory. *The Journal of Physical Chemistry C*, 116:11946–11955, 2012.

[92] L. Huet, A. Perfetto, F. Muniz-Miranda, M. Campetella, C. Adamo, and I. Ciofini. General density-based index to analyze charge transfer phenomena: From models to butterfly molecules. *Journal of Chemical Theory and Computation*, 16(7):4543–4553, 2020.

[93] F. Gatti, B. Lasorne, H. D. Meyer, and A. Nauts. Vibronic Couplings. In *Applications of Quantum Dynamics in Chemistry*, Lecture Notes in Chemistry, pages 81–109. Springer International Publishing, Cham, 2017.

[94] X. Yang and K. Liu. *Modern Trends in Chemical Reaction Dynamics: Part I: Experiment and Theory*, volume 14 of *Advanced Series in Physical Chemistry*. World Scientific, 2004.

[95] Wolfgang Domcke, David R Yarkony, and Horst Köppel. *Conical Intersections: Electronic Structure, Dynamics and Spectroscopy*, volume 15 of *Advanced Series in Physical Chemistry*. WORLD SCIENTIFIC, July 2004.

[96] D. H. Waldeck. Photoisomerization dynamics of stilbenes. *Chem. Rev.*, 91:415–436, 1991.

[97] F. Jensen. *Introduction to computational chemistry*. John Wiley & Sons Ltd, Odense, Denmark, wiley edition, 1999.

[98] C. Eckart. Some Studies Concerning Rotating Axes and Polyatomic Molecules. *Physical Review*, 47(7):552–558, 1935.

[99] Roberto Improta, Giovanni Scalmani, Michael J. Frisch, and Vincenzo Barone. Toward effective and reliable fluorescence energies in solution by a new state specific polarizable continuum model time dependent density functional theory approach. *The Journal of Chemical Physics*, 127(7):074504, August 2007.

[100] B. Mennucci and J. Tomasi. Continuum solvation models: A new approach to the problem of solute's charge distribution and cavity boundaries. *The Journal of Chemical Physics*, 106:5151–5158, 1997.

[101] V. Barone, M. Cossi, and J. Tomasi. A new definition of cavities for the computation of solvation free energies by the polarizable continuum mode. *The Journal of Chemical Physics*, 107:3210–3221, 1997.

[102] R. Improta, V. Barone, G. Scalmani, and M. J. Frisch. A state-specific polarizable continuum model time dependent density functional theory method for excited state calculations in solution. *The Journal of Chemical Physics*, 125:054103, 2003.

[103] D. R. Yarkony. *Modern Electronic Structure Theory: (In 2 Parts)*, volume 2 of *Advanced Series in Physical Chemistry*. World Scientific Publishing Company, 1995.

[104] H. Köppel. Diabatic representation: methods for the construction of diabatic electronic states. In *Advanced Series in Physical Chemistry*, volume 15, pages 175–204. World Scientiiic, 2004.

[105] H. Koppel, W. Domcke, and L. S. Cederbaum. Multimode molecular dynamics beyond the born-oppenheimer approximation. *Advance in Chemical Physics*, 57:59–246, 1984.

[106] Y. Zhou, S. Wang, and Y. Zhang. Catalytic Reaction Mechanism of Acetylcholinesterase Determined by Born Oppenheimer Ab Initio QM MM Molecular Dynamics Simulations. *J. Phys. Chem. B*, 114(26):8817–8825, 2010.

[107] P. Pechukas. Transition State Theory. *Annu. Rev. Phys. Chem.*, 32(1):159–177, 1981.

[108] International Union of Pure and Applied Chemistry. *IUPAC Compendium of Chemical Terminology – The Gold Book*. 1987.

[109] D. C. Clary. Fast Chemical Reactions: Theory Challenges Experiment. *Annual Review of Physical Chemistry*, 41(1):61–90, 1990.

[110] A. M. Wodtke, J. C. Tully, and D. J. Auerbach. Electronically non-adiabatic interactions of molecules at metal surfaces: Can we trust the Born–Oppenheimer approximation for surface chemistry? *International Reviews in Physical Chemistry*, 23(4):513–539, 2004.

[111] I. Bersuker. *The Jahn-Teller Effect*. Cambridge University Press, Cambridge, 2006.

[112] L. Åsbrink, E. Lindholm, and O. Edqvist. Jahn-Teller effect in the vibrational structure of the photoelectron spectrum of benzene. *Chemical Physics Letters*, 5(9):609–612, June 1970.

[113] N. Matsunaga and D. R. Yarkony. Energies and derivative couplings in the vicinity of a conical intersection. II. CH2 $2^3a''$,$3^3a''$ and H2S $1^1a''$,$2^1a''$, unexpected results in an ostensibly standard case. *J. Chem. Phys.*, 107(19):7825–7838, 1997.

[114] P. O. Löwdin. Quantum Theory of Many-Particle Systems. I. Physical Interpretations by Means of Density Matrices, Natural Spin-Orbitals, and Convergence Problems in the Method of Configurational Interaction. 97(6):1474–1489, 1955.

[115] R. McWeeny. Some Recent Advances in Density Matrix Theory. *Reviews of Modern Physics*, 32(2):335–369, 1960.

[116] D. Ter Haar. Theory and applications of the density matrix. *Reports on progress in Physics*, 24(1):304–362, 1961.

[117] P. A. M. Dirac. Note on the interpretation of the density matrix in the many-electron problem. *Mathematical Proceedings of the Cambridge Philosophical Society*, 27(2):240–243, 1931.

[118] W. Koch and M. C. Holthausen. *A Chemist's Guide to Density Functional Theory*. Wiley-VCH, Germany, wiley-vch edition, 2000.

[119] L. B. Da Silva, Jr. Barbee, T. W., R. Cauble, P. Celliers, D. Ciarlo, S. Libby, R. A. London, D. Matthews, S. Mrowka, J. C. Moreno, D. Ress, J. E. Trebes, A. S. Wan, and F. Weber. Electron Density Measurements of High Density Plasmas Using Soft X-Ray Laser Interferometry. *Phys. Rev. Lett.*, 74(20):3991–3994, 1995. American Physical Society.

[120] S. S. Harilal, C. V. Bindhu, Riju C. Issac, V. P. N. Nampoori, and C. P. G. Vallabhan. Electron density and temperature measurements in a laser produced carbon plasma. *Journal of Applied Physics*, 82(5):2140–2146, 1997. American Institute of Physics.

[121] M. Torikoshi, T. Tsunoo, M. Sasaki, M. Endo, Y. Noda, Y. Ohno, T. Kohno, K. Hyodo, K. Uesugi, and N. Yagi. Electron density measurement with dual-energy x-ray CT using synchrotron radiation. *Phys. Med. Biol.*, 48(5):673–685, 2003. IOP Publishing.

[122] P. Coppens. Electron density from X-ray diffraction. *Annual Review of Physical Chemistry*, 43(1):663–692, 1992.

[123] M. A. L. Marques, C. A. Ullrich, F. Nogueira, A. Rubio, K. Burke, and E. K. U. Gross. *Time-Dependent Density Functional Theory*. Lecture Notes in Physics. Springer Berlin Heidelberg, 2006.

[124] Mark E. Casida. Time-dependent density-functional theory for molecules and molecular solids. *Journal of Molecular Structure*, 914(1):3–18, 2009. Time-dependent density-functional theory for molecules and molecular solids.

[125] P. Hohenberg and W. Kohn. Inhomogeneous Electron Gas. *Physical review*, 136(3B):B864–B871, 1964.

[126] E. Runge and E. K. U. Gross. Density-functional theory for time-dependent systems. *Phys. Rev. Lett.*, 52:997–1000, 1984.

[127] R. van Leeuwen. Mapping from densities to potentials in time-dependent density-functional theory. *Phys. Rev. Lett.*, 82:3863–3866, 1999.

[128] T. Etienne. A comprehensive, self-contained derivation of the one-body density matrices fril single-reference excited-state calculation methods using the equation-of-motion formalism. *International Journal of Quantum Chemistry*, 120(5):e26110, 2020.

[129] T. Yanai, D. P. Tew, and N. C. Handy. A new hybrid exchange-correlation functional using the Coulomb-attenuating method (CAM-B3LYP). *Chemical Physics Letters*, 393:51–57, 2004.

[130] C. Adamo and D. Jacquemin. The calculations of excited-state properties with Time-Dependent Density Functional Theory. *Chem. Soc. Rev.*, 42(3):845–856, 2013.

[131] M. J. Frisch, G. W. Trucks, H. B. Schlegel, G. E. Scuseria, M. A. Robb, J. R. Cheeseman, G. Scalmani, V. Barone, G. A. Petersson, H. Nakatsuji, X. Li, M. Caricato, A. V. Marenich, J. Bloino, B. G. Janesko, R. Gomperts, B. Mennucci, H. P. Hratchian, J. V. Ortiz, A. F. Izmaylov, J. L. Sonnenberg, D. Williams-Young, F. Ding, F. Lipparini, F. Egidi, J. Goings, B. Peng, A. Petrone, T. Henderson, D. Ranasinghe, V. G. Zakrzewski, J. Gao, N. Rega, G. Zheng, W. Liang, M. Hada, M. Ehara, K. Toyota, R. Fukuda, J. Hasegawa, M. Ishida, T. Nakajima, Y. Honda, O. Kitao, H. Nakai, T. Vreven, K. Throssell, J. A. Montgomery, Jr., J. E. Peralta, F. Ogliaro, M. J. Bearpark, J. J. Heyd, E. N. Brothers, K. N. Kudin, V. N. Staroverov, T. A. Keith, R. Kobayashi, J. Normand, K. Raghavachari, A. P. Rendell, J. C. Burant, S. S. Iyengar, J. Tomasi, M. Cossi, J. M. Millam, M. Klene, C. Adamo, R. Cammi, J. W. Ochterski, R. L. Martin, K. Morokuma, O. Farkas, J. B. Foresman, and D. J. Fox. Gaussian~16 Revision C.01, 2016. Gaussian Inc. Wallingford CT.

[132] Mesra. `https://mesrasoftware.wordpress.com/`.

[133] Fabrizio Santoro, Alessandro Lami, Roberto Improta, Julien Bloino, and Vincenzo Barone. Effective method for the computation of optical spectra of large molecules at finite temperature including the Duschinsky and Herzberg–Teller effect: The Qx band of porphyrin as a case study. *The Journal of Chemical Physics*, 128(22):224311, 2008.

[134] T. Etienne. Probing the locality of excited states with linear algebra. *Journal of Chemical Theory and Computation*, 11(4):1692–1699, 2015.

[135] M. J. G. Peach, P. Benfield, T. Helgaker, and D. J. Tozer. Excitation energies in density functional theory: An evaluation and a diagnostic test. *The Journal of Chemical Physics*, 128(4):044118, 2008.

[136] W. Ortiz, B. P. Krueger, V. D. Kleiman, J. L. Krause, and A. E. Roitberg. Energy transfer in the nanostar: The role of coulombic coupling and dynamics. *J. Phys. Chem. B*, 109(23):11512–11519, 2005.

[137] M. R. Shortreed, S. F. Swallen, Z. Y. Shi, W. Tan, Z. Xu, C. Devadoss, J. S. Moore, and R. Kopelman. Directed energy transfer funnels in dendrimeric antenna supermolecules. *J. Phys. Chem. B*, 101:6318, 1997.

[138] T. Tada, D. Nozaki, M. Kondo, and K. Yoshizawa. Molecular orbital interactions in the nanostar dendrimer. *J. Phys. Chem. B*, 107:14204, 2003.

[139] S. Fernandez-Alberti, Adrian E. Roitberg, Valeria D. Kleiman, T. Nelson, and S. Tretiak. Shishi-odoshi unidirectional energy transfer mechanism in phenylene ethynylene dendrimers. *The Journal of Chemical Physics*, 137(22):22A526, 2012.

[140] T. Minami, S. Tretiak, V. Chernyak, and S. Mukamel. Frenkel-exciton Hamiltonian for dendrimeric nanostar. *Journal of Luminescence*, 87-89:115–118, May 2000.

[141] Stephen F. Swallen, Zhengguo Zhu, Jeffrey S. Moore, and Raoul Kopelman. Correlated excimer formation and molecular rotational dynamics in phenylacetylenedendrimers. *J. Phys. Chem. B*, 104:3988, 2000.

[142] D. Ondarse-Alvarez, N. Oldani, A. E. Roitberg, V. Kleiman, S. Tretiak, and S. Fernandez-Alberti. Energy transfer and spatial scrambling of an exciton in a conjugated dendrimer. *Phys. Chem. Chem. Phys.*, 20:29648, 2018.

[143] J. C. Kirkwood, C. Scheurer, V. Chernyak, and S. Mukamel. Simulations of energy funneling and time-and frequency-gated fluorescence indendrimers. *J. Chem. Phys.*, 114:2419, 2001.

[144] M. C. Aguilera, S. Fernandez-Alberti A. E. Roitberg, V. D. Kleiman, and J. F. Galindo. Unraveling direct and indirect energy transfer pathways in a light-harvesting dendrimer. *J. Phys. Chem. C*, 124:22383, 2020.

[145] V. M. Freixas, D. Ondarse-Alvarez, S. Tretiak, D. V. Makhov, D. V. Shalashilin, and S. Fernandez-Alberti. Photoinduced non-adiabatic energytransfer pathways in dendrimer buildingblocks. *J. Chem. Phys.*, 150:124301, 2019.

[146] M. Flock, L. Bosse, D. Kaiser, B. Engels, and I. Fischer. Ultrafast dynamics in the vicinity of quantum light-induced conical intersections. *Phys. Chem. Chem. Phys.*, 21:13157–13164, 2019.

[147] M. Wierzbicka, I. Bylinska, C. Czaplewski, and W. Wiczk. Experimental and theoretical studies of the spectroscopic properties of simple symmetrically substituted diphenylacetylene derivatives. *RSC Adv.*, 5:29294–29303, 2015.

[148] M. Szyszkowska, I. Bylińska, and W. Wiczk. Variable-temperature absorption and emission properties of 1,2-diphenylacetylene and 1,4-diphenylbuta-1,3-diyne derivatives. *Journal of Photochemistry and Photobiology A: Chemistry*, 348:47–56, 2017.

[149] S. Menning, M. Krämer, A. Duckworth, F. Rominger, A. Beeby, A. Dreuw, and U. H. F. Bunz. Bridged Tolanes: A Twisted Tale. *J. Org. Chem.*, 79(14):6571–6578, 2014.

[150] Y. Amatsu and M. Hosokawa. Theoretical study on the photochemical behavior of diphenylacetylene in the low-lying excited states. *The Journal of Physical Chemistry A*, 108:10238–10244, 2004.

[151] C. Ferrante, U. Kensy, and B. Dick. Does diphenylacetylene (tolan) fluoresce from its second excited singlet state? semiempirical mo calculations and fluorescence quantum yield measurements. *The Journal of Physical Chemistry*, 97:13457–13463, 1993.

[152] Q. Chu and Y. Pang. Vibronic structures in the electronic spectra of oligo(phenylene ethynylene): effect of m-phenylene to the optical properties of poly(m-phenylene ethynylene). *Spectrochimica Acta Part A: Molecular and Biomolecular Spectroscopy*, 60(7):1459–1467, 2004.